Electronic Supplementary Information

Acid-base-induced *fac*→*mer* isomerization of luminescent iridium(III) complexes

Anastasia Yu. Gitlina,[a] Farzaneh Fadaei-Tirani,[a] Albert Ruggi,[b] Carolina Plaice,[a] and Kay Severin[a]*

[a] Institut des Sciences et Ingénierie Chimiques, École Polytechnique Fédérale de Lausanne (EPFL), 1015 Lausanne, Switzerland
[b] Département de Chimie, Université de Fribourg, 1700 Fribourg, Switzerland

Table of Contents

Materials and methods

All reactions were carried out under an atmosphere of dry N_2 using Schlenk or Glovebox techniques unless otherwise mentioned. All reagents and solvents were purchased from chemical suppliers (Precious Metals Online, Sigma Aldrich, Fluorochem, TCI, Apollo) and used as received without additional purification. Dry solvents were obtained from a solvent purification system possessing activated aluminum oxide columns (Innovative Technology, Inc.).

Reactions accelerated with microwave irradiation were performed in an Initiator+ microwave synthesizer (Biotage) using glass microwave reaction vials (10–20 mL) equipped with stirring bars and sealed by caps with septa.

Solution ^{1}H, 2D ^{1}H–^{1}H COSY, ^{13}C {^{1}H} and ^{19}F {^{1}H} and variable-temperature NMR spectra were recorded at indicated temperatures on a Bruker Avance 400 MHz spectrometer. All chemical shifts are reported in ppm and aligned with respect to the residual signal of corresponding deuterated solvent.[1]

Electrospray ionization (ESI) and nanochip-ESI HRMS data were obtained from a Q-ToF XEVO G2-XS mass spectrometer (Waters) and Linear Trap Quadrupole (LTQ) Orbitrap Elite ETD mass spectrometer (Thermo Fisher), respectively, operated in positive mode.

Elemental analyses were performed on an organic elemental analyzer Flash 2000 (Thermo Scientific).

UV-Vis spectra were recorded on a Cary 60 Spectrophotometer (Aglient Technologies). Emission and excitation spectra were recorded on a Cary Eclipse fluorescence spectrometer (Varian). Quartz Suprasil cuvette and its Schlenk modification (10×10 mm) were used for solution photophysical measurements.

Flash chromatography was performed using commercial silica gel 230–400 mesh (Silicycle, Inc.). Preparative chiral HPLC was performed on a 1260 Infinity system (Aglient Technologies) operated in manual mode. Analytical chiral HPLC was performed on an automatic ultra-fast liquid chromatograph (Shimadzu) Prominence UFLC XR operating with LC-AD XR solvent delivery unit, SIL-20A XR autosampler, CMB-20A system controller, CTO-20A column oven, SPD-20A UV-Vis detector, RF-20A XS fluorescence detector, and Chromeleon software. Chiral columns Chiralpak IA, IB, IC ID, IF (4.6×250 mm) were used for screening in analytical HPLC.

Circular dichroism (CD) spectra were measured on a Chirascan V100 spectrometer (Applied Photophysics) in dichloromethane at 50 nm·min^{-1} scan speed with 1 nm resolution and response time of 1 s, sample temperature 22.5 °C, cuvette length 1 mm. The unit in CD spectra were transformed from ellipticity (θ, mdeg) into molar extinction coefficient ($\Delta\varepsilon$, M^{-1}·cm^{-1}) by using the following equation: $\Delta\varepsilon$ (M^{-1}·cm^{-1}) = θ (mdeg) / [32980 × b (cm) × c (M)], where b is the length of the light path and c is the molar concentration of the sample solution.

Synthesis of the facial isomers of $Ir(ppy)_3$, $Ir(tpy)_3$, $Ir(meppy)_3$, $Ir(buppy)_3$, $Ir(fppy)_3$ and $Ir(dfppy)_3$

Facial isomers of the iridium(III) complexes $Ir(ppy)_3$, $Ir(tpy)_3$, $Ir(meppy)_3$, $Ir(buppy)_3$ $Ir(fppy)_3$ and $Ir(dfppy)_3$, where ppy = 2-phenylpyridine, tpy = 2-(4-methylphenyl)pyridine, meppy = 2-(4-methoxyphenyl)pyridine, buppy = 2-(4-*tert*-butylphenyl)pyridine, fppy = 2-(4-fluorophenyl)pyridine, dfppy = 2-(2,4-difluorophenyl)pyridine, were prepared according to the procedure described by H. Konno and Y. Sasaki for ***fac*-Ir(ppy)$_3$** and ***fac*-Ir(tpy)$_3$** with some modifications.[2] The modified procedure was used for the synthesis of ***fac*-Ir(meppy)$_3$**, ***fac*-Ir(buppy)$_3$**, ***fac*-Ir(fppy)$_3$**, ***fac*-Ir(dfppy)$_3$**. Furthermore, we report a method for the recovery of the ligand, which is used in excess during the reaction (Scheme S1).

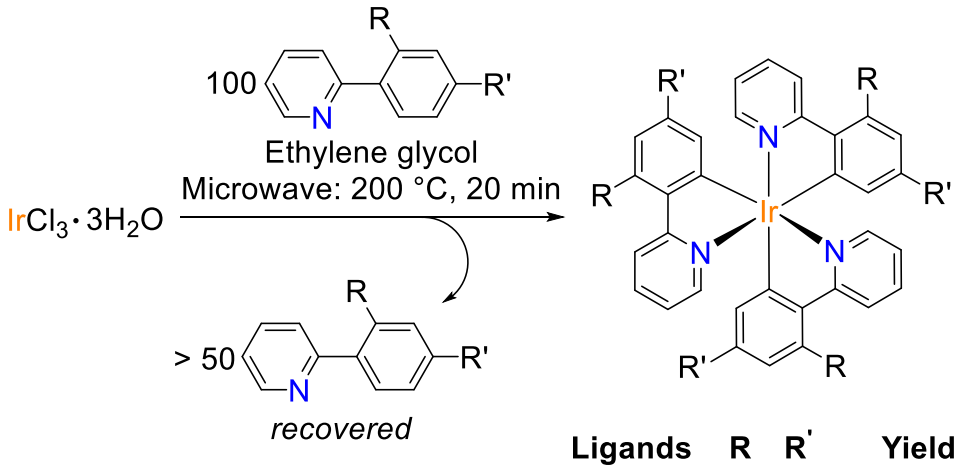

Ligands	R	R'	Yield
ppy	H	H	92%
tpy	H	Me	89%
meppy	H	OMe	95%
buppy	H	*t*Bu	86%
fppy	H	F	90%
dfppy	F	F	91%

Scheme S1. Synthesis of the facial isomers of $Ir(ppy)_3$, $Ir(tpy)_3$, $Ir(meppy)_3$, $Ir(buppy)_3$, $Ir(fppy)_3$ and $Ir(dfppy)_3$.

Ethylene glycol (10 mL) was added to a microwave reaction vial containing a stirring bar, $IrCl_3 \cdot 3H_2O$ (50.0 mg, 0.14 mmol, 1.00 equiv.), and the respective arylpyridine ligand (14.2 mmol, 100 equiv.). The vial was sealed by a cap with a septum and degassed by multiple vacuum-N_2 purging cycles. The vial was placed in the microwave synthesizer and the mixture was heated to 200 °C for 20–40 min. The resulting crystalline precipitate was isolated by centrifugation, washed with methanol (2×15 mL) and diethyl ether (2×15 mL), and dried under vacuum.

***fac*-Ir(ppy)$_3$**. Obtained from $IrCl_3 \cdot 3H_2O$ and Hppy (2.20 g, 14.2 mmol) with the reaction time of 20 min. Yellow crystals, 84 mg (92%). **^{1}H NMR** (400 MHz, CD_2Cl_2, 298 K) δ 7.92 (d, J = 8.2 Hz, 1H), 7.68–7.63 (m, 2H), 7.57 (m, 1H), 6.94–6.87 (m, 2H), 6.81–6.74 (m, 2H). **^{13}C {^{1}H} NMR** (101 MHz, CD_2Cl_2, 298 K) δ 167.0, 161.6, 147.8, 144.4,

137.3, 136.8, 130.2, 124.6, 122.7, 120.4, 119.4. The NMR spectra are in agreement with those reported in the literature.[3]

***fac*-Ir(tpy)$_3$**. Obtained from $IrCl_3 \cdot 3H_2O$ and Htpy (2.40 g, 14.2 mmol) with the reaction time of 20 min. Yellow crystals, 87 mg (89%). **^{1}H NMR** (400 MHz, CD_2Cl_2, 298 K) δ 7.87 (d, *J* = 8.2 Hz, 1H), 7.63–7.55 (m, 2H), 7.48 (d, *J* = 5.4 Hz, 1H), 6.85 (t, *J* = 6.5 Hz, 1H), 6.71 (d, *J* = 7.9 Hz, 1H), 6.61 (s, 1H), 2.10 (s, 3H). **^{13}C {^{1}H} NMR** (101 MHz, CD_2Cl_2, 298 K) δ 167.1, 162.0, 147.5, 141.8, 139.9, 137.9, 136.5, 124.5, 122.0, 121.6, 119.0, 22.0. The NMR spectra are in agreement with those reported in the literature.[3]

***fac*-Ir(meppy)$_3$**. Obtained from $IrCl_3 \cdot 3H_2O$ and Hmeppy (2.62 g, 14.2 mmol) with the reaction time of 40 min. Yellow crystals, 99 mg (95%). **^{1}H NMR** (400 MHz, CD_2Cl_2, 298 K) δ 7.79 (d, *J* = 8.2 Hz, 1H), 7.69–7.45 (m, 3H), 6.94–6.77 (m, 1H), 6.47 (dd, *J* = 8.6, 2.7 Hz, 1H), 6.31 (d, *J* = 2.7 Hz, 1H), 3.55 (s, 3H). **^{13}C {^{1}H} NMR** (101 MHz, CD_2Cl_2, 298 K) δ 166.7, 164.1, 161.4, 147.6, 137.6, 136.5, 125.9, 121.6, 121.4, 118.7, 106.3, 55.0. The NMR spectra are in agreement with those reported in the literature.[4]

***fac*-Ir(buppy)$_3$**. Obtained from $IrCl_3 \cdot 3H_2O$ and Hbuppy (2.99 g, 14.2 mmol) with the reaction time of 40 min. Yellow crystals, 100 mg (86%). **^{1}H NMR** (400 MHz, CD_2Cl_2, 298 K) δ 7.90–7.81 (m, 1H), 7.71–7.49 (m, 3H), 6.91 (m, 3H), 1.07 (s, 9H). The NMR spectrum is in agreement with that reported in the literature.[5]

***fac*-Ir(fppy)$_3$**. Obtained from $IrCl_3 \cdot 3H_2O$ and Hfppy (2.45 g, 14.2 mmol) with the reaction time of 40 min. Yellow crystals, 91 mg (90%). **^{1}H NMR** (400 MHz, CD_2Cl_2, 298 K) δ 7.87 (d, *J* = 8.2 Hz, 1H), 7.74–7.64 (m, 2H), 7.52 (dq, *J* = 5.5, 1.6, 0.8 Hz, 1H), 6.94 (ddd, *J* = 7.1, 5.6, 1.3 Hz, 1H), 6.62 (td, *J* = 8.7, 2.7 Hz, 1H), 6.39 (dd, *J* = 10.3, 2.7 Hz, 1H). **^{19}F {^{1}H} NMR** (376 MHz, CD_2Cl_2, 298 K) δ –112.33 (s). The NMR spectra are in agreement with those reported in the literature.[5]

***fac*-Ir(dfppy)$_3$**. Obtained from $IrCl_3 \cdot 3H_2O$ and Hppy (2.71 g, 14.2 mmol). Light yellow crystals, 97 mg (91%). **^{1}H NMR** (400 MHz, CD_2Cl_2, 298 K) δ 8.31 (d, *J* = 8.6 Hz, 1H), 7.73 (t, *J* = 7.9 Hz, 1H), 7.51 (d, *J* = 4.8 Hz, 1H), 6.98 (t, *J* = 6.5 Hz, 1H), 6.48–6.34 (m, 1H), 6.24 (dd, *J* = 9.2, 2.4 Hz, 1H). **^{19}F {^{1}H} NMR** (376 MHz, CD_2Cl_2, 298 K) δ –109.67 (d, *J* = 9.8 Hz), –110.86 (d, *J* = 10.3 Hz). The NMR spectra are in agreement with those reported in the literature.[3]

The excess of ligand remaining in the ethylene glycol solution after centrifugation of the iridium complex was extracted with 2 M H_2SO_4 (aq., 50 mL) by shaking the mixture in a separating funnel for 5 min. Subsequently, $KHCO_3$ (sat. aq., 100 mL) was added to the mixture and the ligand was extracted with ethyl acetate (3×50 mL). The organic layer was washed with distilled water (2×50 mL), brine (2×50 mL), and dried over anhydrous $MgSO_4$. The solvent was evaporated to give more than 50 equiv. of regenerated ligand. Flash column chromatography using a mixture of dichloromethane/hexane (1:5 v/v) can be used for the purification of the ligand, if needed.

Synthesis of the complexes *mer*-Ir(tppy)$_3$ and *fac*-Ir(tppy)$_3$

The ligand 2-([1,1':4',1''-terphenyl]-4-yl)pyridine (**Htppy**) was synthesized by a Suzuki–Miyaura cross-coupling reaction (Scheme S2).

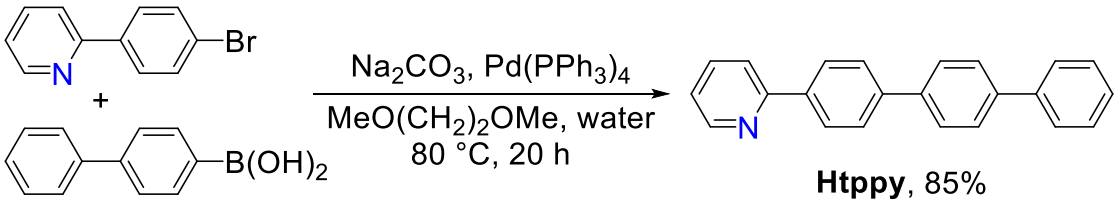

Scheme S2. Synthesis of the ligand **Htppy**.

A mixture of 2-(4-bromophenyl)pyridine (871 mg, 3.72 mmol, 1.0 equiv.), 4-biphenylboronic acid (810 mg, 4.09 mmol, 1.1 equiv.), Na_2CO_3 (1.18 g, 11.1 mmol, 3.0 equiv.) and $Pd(PPh_3)_4$ (215 mg, 0.19 mmol, 5 mol. %) was placed in a 100 mL Schlenk flask equipped with a stirring bar and degassed. Subsequently, a degassed mixture of 1,2-dimethoxyethane-water (4:1 v/v, 50 mL) was added to the solids. The mixture was stirred under an atmosphere of N_2 at 80 °C for 20 h. After cooling down to room temperature, the mixture was poured into NH_4Cl (sat. aq., 100 mL) and the product was extracted with dichloromethane (3×100 mL). The organic layer was washed with brine, dried over $MgSO_4$, and concentrated *in vacuo*. The residue was purified from triphenylphosphine oxide by chromatography on silica and the product was eluted with dichloromethane (R_f = 0.47) to give a pale-yellow precipitate after solvent evaporation. The precipitate was rinsed with diethyl ether (2×7 mL) and dried under vacuum to give **Htppy** (971 mg, 85%) as a white crystalline solid. **^{1}H NMR** (400 MHz, CD_2Cl_2, 298 K) δ 8.70 (m, 1H), 8.14 (m, 2H), 7.85–7.77 (m, 6H), 7.73 (m, 2H), 7.68 (m, 2H), 7.48 (m, 2H), 7.38 (m, 1H), 7.27 (m, 1H). **^{13}C {^{1}H} NMR** (101 MHz, $CDCl_3$, 298 K) δ 157.0, 149.6, 141.5, 140.8, 140.6, 139.5, 138.1, 137.2, 129.0, 127.7, 127.6, 127.6, 127.5, 127.2, 122.4, 120.8. **HRMS** (ESI/QTOF) m/z: $[M+H]^+$ calcd. for $C_{23}H_{18}N^+$ 308.1434; found 308.1431. **Elem. anal.** calcd. for $C_{23}H_{17}N$: C, 89.87; H, 5.57; N, 4.56; found: C, 89.59; H, 5.36; N, 4.48. Single crystals of **Htppy** were obtained by slow diffusion of hexane into dichloromethane solution of **Htppy** at room temperature. The compound was described in the literature without full characterization.[6]

The chloro-bridged dimer **[Ir(tppy)$_2$(μ-Cl)]$_2$** was obtained following the procedure described by B. Orwat and co-workers for the synthesis of the complexes [Ir(ppy)$_2$(μ-Cl)]$_2$ and [Ir(dfppy)$_2$(μ-Cl)]$_2$ with some modifications.[7]

[Ir(tppy)$_2$(μ-Cl)]$_2$. A mixture of 2-ethoxyethanol-water (3:1 v/v, 20 mL) was added to a microwave reaction vial equipped with a stirring bar and containing $IrCl_3 \cdot 3H_2O$ (705 mg, 2.00 mmol, 1.0 equiv.) and **Htppy** (1355 mg, 4.371 mmol, 2.2 equiv.). The vial was sealed by a cap with a septum and degassed by multiple vacuum-N_2 purging cycles. The vial was placed in the microwave synthesizer and the reaction mixture was heated to 150 °C for 20 min. The resulting precipitate was isolated by centrifugation, washed with methanol (2×15 mL) and diethyl ether (2×15 mL), and dried under

vacuum to give **[Ir(tppy)$_2$(μ-Cl)]$_2$** (1378 mg, 82%) as an orange amorphous powder. **^{1}H NMR** (400 MHz, CD_2Cl_2, 298 K) δ 9.42 (d, *J* = 5.0 Hz, 1H), 8.02 (d, *J* = 8.0 Hz, 1H), 7.91–7.83 (m, 1H), 7.67 (d, *J* = 8.2 Hz, 1H), 7.59–7.55 (m, 2H), 7.50 (d, *J* = 8.4 Hz, 2H), 7.41 (d, *J* = 7.8 Hz, 2H), 7.34–7.30 (m, 3H), 7.15 (dd, *J* = 8.1, 1.8 Hz, 1H), 6.98–6.90 (m, 1H), 6.23 (d, *J* = 1.7 Hz, 1H).

The facial isomer of the homoleptic iridium(III) complex Ir(tppy)$_3$ was synthesized from its meridional isomer by thermal *mer*-to-*fac* isomerization using the conditions described by A. R. McDonald and co-workers.[8] The complex ***mer*-Ir(tppy)$_3$** was obtained following the standard conditions for the synthesis of facial isomers of homoleptic iridium(III) complexes from the corresponding chloro-bridged dimers in glycerol.[3]

***mer*-Ir(tppy)$_3$**. A mixture of **[Ir(tppy)$_2$(μ-Cl)]$_2$** (200 mg, 0.12 mmol, 1.0 equiv.), **Htppy** (91 mg, 0.3 mmol, 2.5 equiv.) and K_2CO_3 (164 mg, 1.19 mmol, 10 equiv.) was placed in a 100 mL Schlenk flask equipped with stirring bar and degassed. Subsequently, glycerol (20 mL) was added to the solids. The mixture was stirred under an atmosphere of N_2 at 200 °C for 22 h (*the utilization of a heating block instead of an oil bath is convenient*). After cooling down to room temperature, the mixture was poured into water (20 mL). The brown precipitate was isolated by centrifugation, washed with methanol (3×15 mL) and diethyl ether (2×15 mL) and dried under high vacuum. The residue was purified by flash chromatography on silica and the product was eluted with dichloromethane to give ***mer*-Ir(tppy)$_3$** (177 mg, 67%) as an orange amorphous solid. **^{1}H NMR** (400 MHz, CD_2Cl_2, 298 K) δ 8.30 (dd, *J* = 5.9, 1.0 Hz, 1H), 8.10 (d, *J* = 4.6 Hz, 1H), 8.04 (d, *J* = 8.2 Hz, 1H), 7.96–7.22 (m, 40H), 7.01–6.93 (m, 2H), 6.85 (m, 3H). **^{13}C {^{1}H} NMR** (101 MHz, CD_2Cl_2, 298 K) δ 155.5, 153.9, 148.6, 145.8, 141.9, 141.8, 141.2, 137.4, 136.9, 136.5, 136.4, 135.6, 135.1, 131.2, 129.4, 129.3, 129.3, 129.3, 129.2, 129.2, 128.1, 128.0, 127.9, 127.8, 127.7, 127.7, 127.6, 127.4, 127.4, 125.2, 125.2, 125.1, 123.1, 122.9, 122.2, 120.9, 120.8, 119.9, 119.7, 119.6, 119.4, 119.0. **HRMS** (ESI/QTOF) m/z: $[M+H]^+$ calcd. for $C_{69}H_{49}{}^{193}IrN_3^+$ 1112.3550; found 1112.3551. **Elem. anal.** calcd. for $C_{69}H_{48}IrN_3$: C, 74.57; H, 4.35; N, 3.78; found: C, 74.54; H, 4.38; N, 3.60. Single crystals of ***mer*-Ir(tppy)$_3$** were obtained by slow gas phase diffusion of hexane into a solution of ***mer*-Ir(tppy)$_3$** in dichloromethane at room temperature.

***fac*-Ir(tppy)$_3$**. ***mer*-Ir(tppy)$_3$** (170 mg, 0.15 mmol) and phenol (3 g) were added to a microwave reaction vial equipped with a stirring bar. The vial was sealed by a cap with a septum and degassed by multiple vacuum-N_2 purging cycles. The vial was placed in a heating block and the mixture was stirred at refluxing temperature of phenol (185 °C) for 20 h. After cooling to room temperature, the brown solution was transferred to a 25 mL round-bottom flask, and phenol was completely removed by sublimation on a water-cooled condenser (47 °C). The brownish-yellow precipitate was purified by chromatography on silica and the product was eluted with dichloromethane to give ***fac*-Ir(tppy)$_3$** (170 mg, quant.) as an orange crystalline solid. **^{1}H NMR** (400 MHz, CD_2Cl_2, 298 K) δ 7.99 (d, *J* = 8.2 Hz, 1H), 7.79 (d, *J* = 8.2 Hz, 1H), 7.69 (m, 2H), 7.62–7.44 (m, 6H), 7.38 (t, *J* = 7.6 Hz, 2H), 7.28 (m, 3H), 6.99 (t, *J* = 6.4 Hz, 1H). **^{13}C {^{1}H} NMR** (101 MHz, CD_2Cl_2, 298 K) δ 166.8, 161.9, 147.9, 144.2, 141.6, 141.6, 141.3,

139.9, 136.9, 135.6, 129.2, 127.9, 127.6, 127.6, 127.4, 125.0, 122.7, 119.7, 119.6. **HRMS** (ESI/QTOF) m/z: $[M+H]^+$ calcd. for $C_{69}H_{49}{}^{193}IrN_3{}^+$ 1112.3550; found 1112.3548. **Elem. anal.** calcd. for $C_{69}H_{48}IrN_3$: C, 74.57; H, 4.35; N, 3.78; found: C, 74.51; H, 4.34; N, 3.60. Single crystals of ***fac*-Ir(tppy)$_3$** were obtained by slow gas phase diffusion of diethyl ether into a solution of ***fac*-Ir(tppy)$_3$** in dichloromethane at room temperature.

Synthesis of the heteroleptic complex *fac*-Ir(dfppy)$_2$(tpy)

The chloro-bridged dimer **[Ir(dfppy)$_2$(μ-Cl)]$_2$** was synthesized analogously to **[Ir(tppy)$_2$(μ-Cl)]$_2$** from $IrCl_3 \cdot 3H_2O$ (705 mg, 2.00 mmol, 1.0 equiv.) and **Hdfppy** (841 mg, 4.40 mmol, 2.2 equiv.). The complex was isolated as light-yellow powder (1039 mg, 85%). **^{1}H NMR** (400 MHz, CD_2Cl_2, 298 K) δ 9.12 (dd, J = 5.8, 0.9 Hz, 1H), 8.33 (d, J = 8.4 Hz, 1H), 7.95–7.78 (m, 1H), 6.87 (ddd, J = 7.3, 5.9, 1.3 Hz, 1H), 6.38 (ddd, J = 12.4, 9.2, 2.3 Hz, 1H), 5.29 (dd, J = 9.1, 2.3 Hz, 1H). **^{19}F {^{1}H} NMR** (376 MHz, CD_2Cl_2, 298 K) δ –108.42 (d, J = 9.6 Hz), –110.61 (d, J = 10.1 Hz). The NMR data are in agreement with those reported in the literature.[9]

The heteroleptic iridium(III) complex ***fac*-Ir(dfppy)$_2$(tpy)** was obtained from **[Ir(dfppy)$_2$(μ-Cl)]$_2$** and **Htpy** as described by A. Kazama and co-workers[10] (Scheme S3) with modifications regarding the purification.

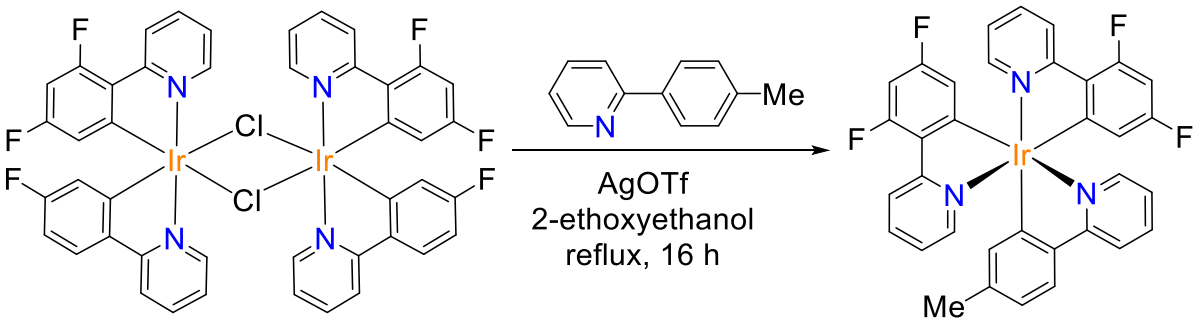

***fac*-Ir(dfppy)$_2$(tpy)**, 73%

Scheme S3. Synthesis of the heteroleptic iridium(III) complex ***fac*-Ir(dfppy)$_2$(tpy)**.

***fac*-Ir(dfppy)$_2$(tpy)**. A mixture of **[Ir(dfppy)$_2$(μ-Cl)]$_2$** (455 mg, 0.37 mmol, 1.0 equiv.), **Htpy** (190 mg, 1.12 mmol, 3.0 equiv.) and AgOTf (201 mg, 0.79 mmol, 2.1 equiv.) was placed in a 50 mL Schlenk flask equipped with stirring bar and degassed. Subsequently, 2-ethoxyethanol (12 mL) was added to the solids. The mixture was stirred under N_2 atmosphere at refluxing temperature (135 °C) for 16 h. After cooling down to room temperature, the mixture was poured into water (20 mL). The yellow precipitate was isolated by centrifugation and suspended in dichloromethane (150 mL). The organic layer was washed with water (2×50 mL), brine (50 mL), dried over $MgSO_4$, filtered, and concentrated *in vacuo*. The product was purified by column chromatography on silica and eluted with hexane/ethyl acetate (2:1, v/v) with R_f = 0.27 to give a yellow powder after solvent evaporation. The powder was recrystallized by slow diffusion of methanol into a solution of the product in dichloromethane at room temperature to give ***fac*-Ir(dfppy)$_2$(tpy)** as yellow crystalline needles (405 mg, 73%). **^{1}H NMR** (400 MHz, CD_2Cl_2, 298 K) δ 8.30 (d, J = 8.5 Hz, 2H), 7.89 (d, J = 8.2 Hz, 1H), 7.76–7.62 (m, 3H), 7.62–7.49 (m, 3H), 7.43 (d, J = 5.3 Hz, 1H), 6.93 (m, 3H), 6.77 (d, J = 7.9 Hz, 1H), 6.56 (s, 1H), 6.48–6.31 (m, 2H), 6.31–6.19 (m, 2H), 2.13 (s, 3H). **^{19}F {^{1}H} NMR** (376 MHz, CD_2Cl_2, 298 K) δ –109.06 (d, J = 10.2 Hz), –109.47 (d, J = 9.8 Hz), –111.01 (d, J = 9.7 Hz), –111.23 (d, J = 9.8 Hz). **^{13}C {^{1}H} NMR** (126 MHz, CD_2Cl_2, 298 K) δ 166.78 (s), 166.44 (dd, J = 34.4, 6.3 Hz), 165.36–165.07 (m), 163.62–163.05 (m), 161.28 (d, J = 12.5 Hz), 159.34 (s), 147.75 (d, J = 5.5 Hz), 147.48 (s), 141.57 (s),

140.70 (s), 137.63 (s), 137.47 (s), 137.30 (s), 128.26 (m), 124.72 (s), 123.65 (dd, *J* = 21.2, 7.9 Hz), 122.79 (d, *J* = 6.9 Hz), 122.44 (d, *J* = 20.9 Hz), 119.43 (s), 118.37 (ddd, *J* = 15.7, 10.1, 2.6 Hz), 96.94–96.27 (m), 21.95 (s). **HRMS** (ESI/QTOF) m/z: $[M+H]^+$ calcd. for $C_{34}H_{23}F_4{}^{193}IrN_3{}^+$ 742.1452; found 742.1451. **Elem. anal.** calcd. for $C_{34}H_{22}F_4IrN_3$: C, 55.13; H, 2.99; N, 5.67; found: C, 55.13; H, 2.98; N, 5.67. The NMR spectra of ***fac*-Ir(dfppy)$_2$(tpy)** obtained are in agreement with those reported in the literature.[10,11]

General procedure for the reversible *fac*↔*mer* isomerization

The *fac*↔*mer* isomerizations for the complexes $Ir(ppy)_3$, $Ir(tpy)_3$, $Ir(meppy)_3$, $Ir(buppy)_3$, $Ir(fppy)_3$, $Ir(dfppy)_3$, $Ir(tppy)_3$ and $Ir(dfppy)_2(tpy)$ were performed in NMR scale following the General Procedure optimized for each complex (Scheme S4). The *mer*→*fac* isomerization of $Ir(tppy)_3$ was achieved thermally and not by light irradiation.

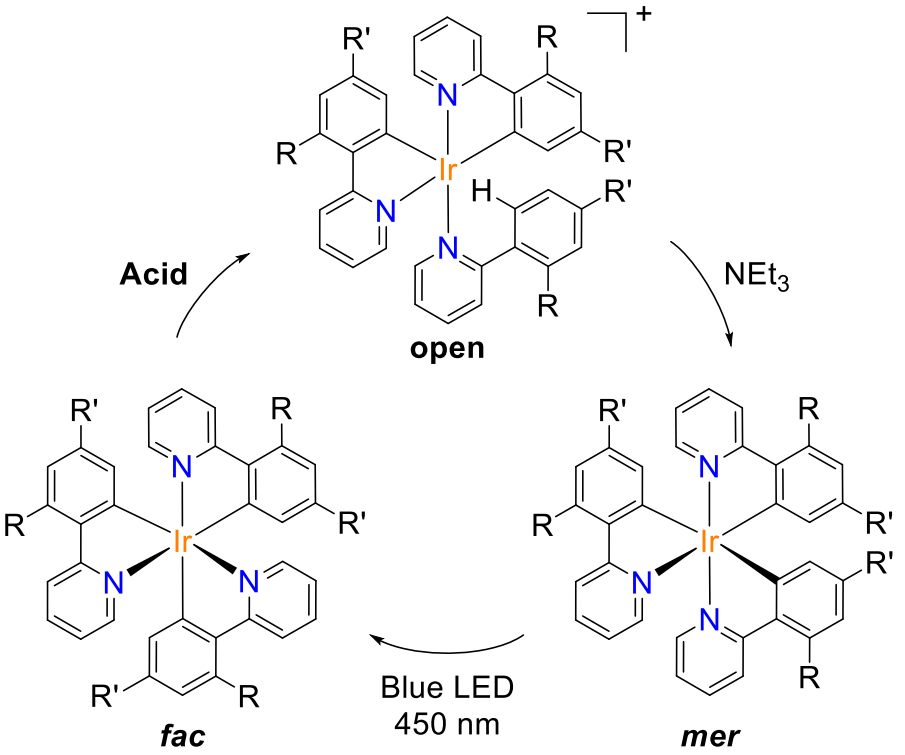

Ligands	R	R'	Acid (equiv.)	NEt_3, equiv.	Light, h
ppy	H	H	TFA (10)	10.5	3
tpy	H	Me	TFA (10)	10.5	1
meppy	H	OMe	TFA (10)	10.5	1
buppy	H	*t*Bu	TFA (5)	5.5	2.5
fppy	H	F	$HNTf_2$ (2)	2.5	2
dfppy	F	F	$HNTf_2$ (5)	5.5	2
tppy	H	*p*-C_6H_4Ph	TFA (10)	10.5	✖
$(dfppy)_2(tpy)$			TFA (100)	105	2

Scheme S4. General Procedure for the *fac*↔*mer* isomerizations of $Ir(C^N)_3$ complexes.

Stock solutions of trifluoroacetic acid (TFA, 0.5 M), bistriflimidic acid ($HNTf_2$, 0.2 M), and triethylamine (NEt_3, 0.5 M) were prepared in CD_2Cl_2. The **facial isomer** of $Ir(C^N)_3$ complex (1–5 mg, 1 equiv.) was placed in a 5 mL vial equipped with a stirring bar and dissolved in 0.5 mL of CD_2Cl_2 resulting in a yellow solution. Subsequently, the corresponding acid (5, 10 or 100 molar equiv.) was added in one portion under vigorous stirring (1400 rpm). The reaction was accompanied by a change of color to greenish-yellow and emission quenching. After 1 min of stirring at room temperature,

the solution was transferred to an NMR tube, and a spectrum of the protonated complex ('**open form**') was recorded.

Subsequently, the solution of the **open form** was transferred back to the vial, and an aliquot of the NEt_3 stock solution (5.5, 10.5 or 105 molar equiv.) was added slowly dropwise under vigorous stirring (1400 rpm). The reaction was accompanied by a change of color back to yellow and by an increased emission intensity. After 1 min of stirring at room temperature, the solution was transferred to an NMR tube, and a spectrum of the **meridional isomer** was recorded.

Subsequently, the NMR tube containing the solution of the meridional isomer was exposed to the blue light of a Kessil LED lamp (λ_{em} = 450 nm, 90 W, A360W E-series tuna blue https://kessil.com/aquarium/saltwater_A360.php) at room temperature for 1–3 h. Finally, a spectrum of the **facial isomer** was recorded.

Visualization of a simplified version of the General Procedure (under air, without stirring) for the isomerization of $Ir(ppy)_3$ is shown in Figure S1.

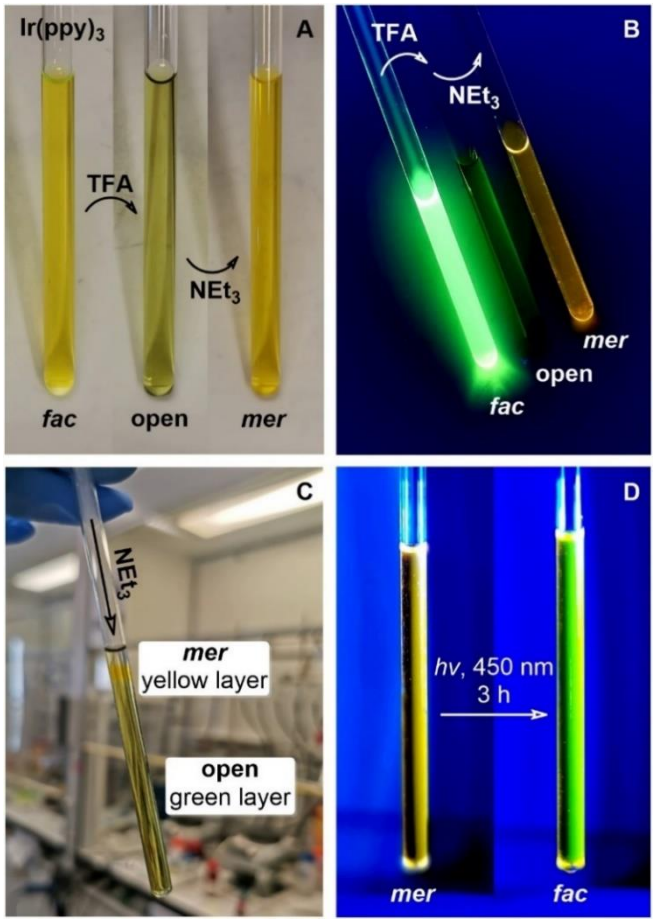

Figure S1. Photos of NMR tubes during the *fac*→*mer*→*fac* isomerization of $Ir(ppy)_3$. Acid-base *fac*→*mer* isomerization of $Ir(ppy)_3$ under daylight (A) and upon irradiation at 366 nm (B). Formation of a layer of the *mer* isomer upon addition of NEt_3 to the solution of the open form (C). Photochemical *mer*→*fac* isomerization of $Ir(ppy)_3$ (D).

[Ir(ppy)$_2$(Hppy)](O$_2$CCF$_3$). A solution of the open form (greenish-yellow, weak green emission) was obtained upon addition of an aliquot of a stock solution of TFA in CD_2Cl_2

(0.5 M, 76.3 µL, 38.2 µmol, 10.0 equiv.) to a solution of ***fac*-Ir(ppy)$_3$** (2.5 mg, 3.8 µmol, 1.0 equiv.) in 0.5 mL of CD_2Cl_2 (yellow, intensive green emission). **^{1}H NMR** (400 MHz, CD_2Cl_2, 298 K) δ 8.17 (d, *J* = 5.8 Hz, 1H), 8.01 (ddd, *J* = 8.2, 6.4, 2.4 Hz, 2H), 7.94–7.73 (m, 8H), 7.56 (dd, *J* = 7.8, 1.4 Hz, 1H), 7.40–7.22 (m, 6H), 7.07–6.97 (m, 2H), 6.94–6.85 (m, 3H), 6.45 (dd, *J* = 7.9, 1.0 Hz, 1H), 6.14 (d, *J* = 5.5 Hz, 1H). **^{19}F {^{1}H} NMR** (376 MHz, CD_2Cl_2, 253 K) δ –76.03 (s). **^{13}C {^{1}H} NMR** (101 MHz, CD_2Cl_2, 253 K) δ 168.6, 162.5, 161.8, 152.7, 149.9, 149.1, 147.2, 146.6, 145.6, 142.6, 139.4, 139.4, 139.2, 136.5, 134.2, 134.1, 134.0, 133.0, 131.4, 131.2, 126.5, 125.6, 125.5, 125.0, 124.8, 124.7, 124.6, 123.5, 120.2, 120.1. **HRMS** (nanochip-ESI/LTQ-Orbitrap) m/z: $[M]^+$ calcd. for $C_{33}H_{25}IrN_3^+$ 656.1672; found 656.1679. Single crystals of **[Ir(ppy)$_2$(Hppy)](NTf$_2$)** were obtained by slow gas phase diffusion of hexane into a solution of the mixture of ***fac*-Ir(ppy)$_3$** (20 mg, 1.0 equiv.) and $HNTf_2$ (43 mg, 5.0 equiv.) in dichloromethane at room temperature.

***mer*-Ir(ppy)$_3$**. A solution of the *mer* isomer (yellow, yellow emission) was obtained upon addition of an aliquot of a stock solution of NEt_3 in CD_2Cl_2 (0.5 M, 80.2 µL, 40.1 µmol, 10.5 equiv.) to the solution of **[Ir(ppy)$_2$(Hppy)](O$_2$CCF$_3$)**. **^{1}H NMR** (400 MHz, CD_2Cl_2, 298 K) δ 8.09 (d, *J* = 5.0 Hz, 1H), 8.00–7.90 (m, 2H), 7.84 (d, *J* = 8.1 Hz, 2H), 7.78 (d, *J* = 7.3 Hz, 1H), 7.72 (d, *J* = 7.3 Hz, 1H), 7.69–7.60 (m, 3H), 7.60–7.50 (m, 2H), 7.03–6.73 (m, 10H), 6.59 (dd, *J* = 7.1, 1.1 Hz, 1H), 6.42 (d, *J* = 7.5 Hz, 1H). **^{13}C {^{1}H} NMR** (101 MHz, CD_2Cl_2, 298 K) δ 177.8, 175.6, 171.0, 168.9, 168.3, 160.1, 153.7, 151.8, 148.5, 146.1, 145.5, 143.0, 138.2, 137.3, 136.3, 134.9, 133.2, 131.1, 130.4, 130.4, 130.1, 124.9, 124.8, 124.5, 123.0, 122.7, 122.0, 121.9, 121.5, 119.7, 119.4, 119.3, 119.0. The NMR spectra of ***mer*-Ir(ppy)$_3$** obtained *in situ* are in agreement with those reported in the literature.[3]

[Ir(tpy)$_2$(Htpy)](O$_2$CCF$_3$). A solution of the open form (greenish-yellow, weak green emission) was obtained upon addition of an aliquot of a stock solution of TFA in CD_2Cl_2 (0.5 M, 57.5 µL, 28.7 µmol, 10.0 eqiuv.) to a solution of ***fac*-Ir(tpy)$_3$** (2.0 mg, 2.9 µmol, 1.0 equiv.) in 0.5 mL of CD_2Cl_2 (yellow, intensive green emission). **^{1}H NMR** (400 MHz, CD_2Cl_2, 298 K) δ 8.17 (d, *J* = 5.9 Hz, 1H), 7.97 (ddd, *J* = 21.8, 11.0, 4.9 Hz, 2H), 7.87–7.69 (m, 5H), 7.57 (d, *J* = 7.3 Hz, 2H), 7.43 (d, *J* = 7.9 Hz, 1H), 7.32–7.09 (m, 5H), 7.02–6.94 (m, 1H), 6.90–6.76 (m, 2H), 6.68 (s, 1H), 6.27 (s, 1H), 6.16 (d, *J* = 5.7 Hz, 1H), 2.50 (s, 3H), 2.31 (s, 3H), 2.12 (s, 3H). **^{19}F {^{1}H} NMR** (376 MHz, CD_2Cl_2, 273 K) δ –75.95 (s). **^{13}C {^{1}H} NMR** (101 MHz, CD_2Cl_2, 273 K) δ 169.1, 162.9, 162.2, 152.8, 149.9, 149.3, 147.5, 145.2, 143.8, 143.0, 142.1, 142.0, 139.9, 139.3, 139.2, 137.0, 134.9, 134.4, 133.9, 126.2, 125.9, 125.7, 125.7, 125.3, 125.0, 124.2, 122.9, 119.9, 119.8, 22.1, 21.9, 21.6.

***mer*-Ir(tpy)$_3$**. A solution of the *mer* isomer (yellow, yellow emission) was obtained upon addition of an aliquot of a stock solution of NEt_3 in CD_2Cl_2 (0.5 M, 60.3 µL, 30.1 µmol, 10.5 equiv.) to the solution of **[Ir(tpy)$_2$(Htpy)](O$_2$CCF$_3$)**. **^{1}H NMR** (400 MHz, CD_2Cl_2, 298 K) δ 8.06 (d, *J* = 5.0 Hz, 1H), 7.87 (dd, *J* = 10.0, 4.5 Hz, 2H), 7.77 (dd, *J* = 8.0, 3.4 Hz, 2H), 7.56 (m, 7H), 6.88–6.82 (m, 1H), 6.82–6.66 (m, 6H), 6.36 (s, 1H), 6.21 (s, 1H), 2.12 (s, 6H), 2.10 (s, 3H). The NMR spectrum of ***mer*-Ir(tpy)$_3$** obtained *in situ* are in agreement those reported in the literature for individual compound.[3]

[Ir(meppy)$_2$(Hmeppy)](O$_2$CCF$_3$). A solution of the open form (greenish-yellow, weak cyan emission) was obtained upon addition of an aliquot of a stock solution of TFA in CD_2Cl_2 (0.5 M, 134.4 µL, 67.2 µmol, 10.0 eqiuv.) to a solution of ***fac*-Ir(meppy)$_3$** (5.0 mg, 6.7 µmol, 1.0 equiv.) in 0.5 mL of CD_2Cl_2 (yellow, intensive green emission). **^{1}H NMR** (400 MHz, CD_2Cl_2, 293 K) δ 8.16 (d, *J* = 5.2 Hz, 1H), 7.95 (td, *J* = 7.9, 1.5 Hz, 1H), 7.87 (d, *J* = 8.7 Hz, 2H), 7.81–7.67 (m, 4H), 7.50 (d, *J* = 8.7 Hz, 1H), 7.37–7.19 (m, 4H), 7.16 (d, *J* = 8.2 Hz, 2H), 6.98 (ddd, *J* = 7.2, 5.8, 1.4 Hz, 1H), 6.89 (dd, *J* = 8.6, 2.5 Hz, 1H), 6.86–6.78 (m, 1H), 6.59 (dd, *J* = 8.6, 2.5 Hz, 1H), 6.41 (d, *J* = 2.5 Hz, 1H), 6.29 (d, *J* = 5.5 Hz, 1H), 5.95 (d, *J* = 2.5 Hz, 1H), 3.87 (s, 3H), 3.78 (s, 3H), 3.62 (s, 3H). **^{19}F {^{1}H} NMR** (376 MHz, CD_2Cl_2, 273 K) δ –76.13 (s). **^{13}C {^{1}H} NMR** (101 MHz, CD_2Cl_2, 273 K) δ 168.5, 164.2, 162.5, 162.0, 161.3, 160.3, 152.4, 149.9, 149.8, 149.2, 139.4, 139.3, 139.3, 139.1, 138.8, 135.7, 135.6, 127.5, 126.6, 125.8, 125.1, 123.7, 122.5, 121.5, 119.7, 119.6, 119.5, 119.1, 109.7, 109.3, 56.5, 55.6, 55.5.

***mer*-Ir(meppy)$_3$**. A solution of the *mer* isomer (yellow, intensive green emission) was obtained upon addition of an aliquot of a stock solution of NEt_3 in CD_2Cl_2 (0.5 M, 141.1 µL, 70.6 µmol, 10.5 equiv.) to the solution of **[Ir(meppy)$_2$(Hmeppy)](O$_2$CCF$_3$)**. **^{1}H NMR** (400 MHz, CD_2Cl_2, 298 K) δ 8.05 (dd, *J* = 5.9, 0.9 Hz, 1H), 7.90 (dd, *J* = 5.6, 0.9 Hz, 1H), 7.82 (d, *J* = 8.2 Hz, 1H), 7.69 (dd, *J* = 15.3, 8.6 Hz, 4H), 7.63–7.45 (m, 5H), 6.83 (m, 1H), 6.69 (m, 2H), 6.57–6.46 (m, 3H), 6.40 (d, *J* = 2.7 Hz, 1H), 6.09 (d, *J* = 2.6 Hz, 1H), 5.89 (d, *J* = 2.6 Hz, 1H), 3.59 (s, 6H), 3.55 (s, 3H). The NMR spectrum of ***mer*-Ir(meppy)$_3$** obtained *in situ* are analogous to those for ***mer*-Ir(tpy)$_3$** reported in the literature.[4]

[Ir(buppy)$_2$(Hbuppy)](O$_2$CCF$_3$). A solution of the open form (greenish-yellow, weak green emission) was obtained upon addition of an aliquot of a stock solution of TFA in CD_2Cl_2 (0.5 M, 27.9 µL, 14.0 µmol, 5.0 eqiuv.) to a solution of ***fac*-Ir(buppy)$_3$** (2.3 mg, 2.8 µmol, 1.0 equiv.) in 0.5 mL of CD_2Cl_2 (yellow, intensive green emission). **^{1}H NMR** (400 MHz, CD_2Cl_2, 293 K) δ 8.09 (d, *J* = 5.8 Hz, 1H), 8.01 (td, *J* = 7.9, 1.4 Hz, 1H), 7.93 (d, *J* = 8.0 Hz, 1H), 7.87 (m, 2H), 7.83–7.69 (m, 5H), 7.45 (d, *J* = 8.2 Hz, 1H), 7.34 (m, 4H), 7.26 (ddd, *J* = 7.4, 5.9, 1.4 Hz, 1H), 7.08–6.95 (m, 2H), 6.94–6.82 (m, 2H), 6.36 (d, *J* = 1.8 Hz, 1H), 6.25 (d, *J* = 5.6 Hz, 1H), 1.33 (s, 9H), 1.22 (s, 9H), 1.03 (s, 9H).

***mer*-Ir(buppy)$_3$**. A solution of the *mer* isomer (yellow, yellow emission) was obtained upon addition of an aliquot of a stock solution of NEt_3 in CD_2Cl_2 (0.5 M, 30.7 µL, 15.4 µmol, 5.5 equiv.) to the solution of **[Ir(buppy)$_2$(buppy)](O$_2$CCF$_3$)**. **^{1}H NMR** (400 MHz, CD_2Cl_2, 298 K) δ 8.07 (d, *J* = 5.0 Hz, 1H), 7.89 (dd, *J* = 5.6, 3.4 Hz, 2H), 7.76 (d, *J* = 8.3 Hz, 2H), 7.71–7.48 (m, 7H), 7.03 (dd, *J* = 8.2, 2.1 Hz, 1H), 7.00–6.91 (m, 3H), 6.91–6.84 (m, 1H), 6.82–6.70 (m, 2H), 6.67 (d, *J* = 2.0 Hz, 1H), 6.53 (d, *J* = 1.9 Hz, 1H), 1.14–1.13 (m, 18H), 1.08 (s, 9H).

[Ir(fppy)$_2$(Hfppy)](NTf$_2$). A solution of the open form (yellow, weak cyan emission) was obtained upon addition of an aliquot of a stock solution of $HNTf_2$ in CD_2Cl_2 (0.2 M, 35.7 µL, 7.1 µmol, 2.0 eqiuv.) to a solution of ***fac*-Ir(fppy)$_3$** (2.5 mg, 3.6 µmol, 1.0 equiv.) in 0.5 mL CD_2Cl_2 (light-yellow, cyan emission). **^{1}H NMR** (400 MHz, CD_2Cl_2, 293 K) δ 8.16–8.00 (m, 2H), 7.96–7.85 (m, 5H), 7.84–7.75 (m, 1H), 7.61 (dt, *J* = 16.3, 8.1 Hz, 1H), 7.58–7.47 (m, 2H), 7.42–7.25 (m, 4H), 7.18 (ddd, *J* = 7.2, 5.7, 1.5 Hz,

1H), 7.04 (td, *J* = 8.7, 2.5 Hz, 1H), 6.95 (ddd, *J* = 7.4, 5.9, 1.4 Hz, 1H), 6.79 (td, *J* = 8.5, 2.5 Hz, 1H), 6.51 (dd, *J* = 9.1, 2.6 Hz, 2H), 6.08 (dd, *J* = 9.7, 2.5 Hz, 1H). **^{19}F {^{1}H} NMR** (376 MHz, CD_2Cl_2, 293 K) δ –104.33 (s), –107.09 (s), –107.73 (s).

***mer*-Ir(fppy)$_3$**. A solution of the *mer* isomer (yellow, intensive cyan emission) was obtained upon addition of an aliquot of a stock solution of NEt_3 in CD_2Cl_2 (44.6 µL, 8.9 µmol, 2.5 equiv.) to the solution of **[Ir(fppy)$_2$(Hfppy)](NTf$_2$)**. **^{1}H NMR** (400 MHz, CD_2Cl_2, 298 K) δ 8.01 (dd, *J* = 5.9, 0.9 Hz, 1H), 7.93–7.85 (m, 2H), 7.82–7.72 (m, 4H), 7.72–7.65 (m, 2H), 7.64–7.53 (m, 3H), 6.93 (m, 1H), 6.80 (m, 2H), 6.67 (m, 3H), 6.50 (dd, *J* = 9.0, 2.8 Hz, 1H), 6.22 (dd, *J* = 8.8, 2.7 Hz, 1H), 6.02 (dd, *J* = 10.2, 2.6 Hz, 1H). **^{19}F {^{1}H} NMR** (376 MHz, CD_2Cl_2, 298 K) δ –111.99 (s), –112.32 (s), –112.75 (s).

[Ir(dfppy)$_2$(Hdfppy)](NTf$_2$). A solution of the open form (yellow, weak cyan emission) was obtained upon addition of an aliquot of a stock solution of $HNTf_2$ in CD_2Cl_2 (0.2 M, 32.8 µL, 6.6 µmol, 5.0 eqiuv.) to a solution of ***fac*-Ir(dfppy)$_3$** (1.0 mg, 1.3 µmol, 1.0 equiv.) in 0.5 mL CD_2Cl_2 (light-yellow, intensive cyan emission). **^{1}H NMR** (400 MHz, CD_2Cl_2, 293 K) δ 8.37 (m, 2H), 8.10 (td, *J* = 7.8, 1.5 Hz, 1H), 8.05–7.93 (m, 3H), 7.86 (m, 1H), 7.52–7.45 (m, 1H), 7.44–7.34 (m, 3H), 7.12 (m, 2H), 7.06–6.97 (m, 1H), 6.92–6.76 (m, 2H), 6.66 (ddd, *J* = 12.5, 8.8, 2.4 Hz, 1H), 6.20 (dd, *J* = 8.1, 2.3 Hz, 1H), 5.98–5.88 (m, 1H). **^{19}F {^{1}H} NMR** (376 MHz, CD_2Cl_2, 293 K) δ –99.30 (s), –104.05 (d, *J* = 11.2 Hz), –104.36 (d, *J* = 11.8 Hz), –106.16 (d, *J* = 10.9 Hz), –107.09 (d, *J* = 11.9 Hz), –109.14 (d, *J* = 11.2 Hz).

***mer*-Ir(dfppy)$_3$**. A solution of the *mer* isomer (yellow, intensive cyan emission) was obtained upon addition of an aliquot of a stock solution of NEt_3 in CD_2Cl_2 (14.4 µL, 7.2 µmol, 5.5 equiv.) to the solution of **[Ir(dfppy)$_2$(Hdfppy)](NTf$_2$)**. **^{1}H NMR** (400 MHz, CD_2Cl_2, 298 K) δ 8.34 (d, *J* = 9.9 Hz, 1H), 8.23 (d, *J* = 6.9 Hz, 2H), 8.03 (d, *J* = 5.8 Hz, 1H), 7.93 (d, *J* = 5.6 Hz, 1H), 7.74 (t, *J* = 8.8 Hz, 1H), 7.70–7.60 (m, 2H), 7.54 (d, *J* = 5.8 Hz, 1H), 7.01–6.96 (m, 1H), 6.85 (t, *J* = 6.6 Hz, 2H), 6.51–6.32 (m, 4H), 5.98 (dd, *J* = 7.6, 2.4 Hz, 1H), 5.79 (dd, *J* = 9.1, 2.4 Hz, 1H). **^{19}F {^{1}H} NMR** (376 MHz, CD_2Cl_2, 298 K) δ –109.33 (d, *J* = 10.0 Hz), –109.48 (d, *J* = 10.5 Hz), –109.70 (d, *J* = 9.7 Hz), –109.77 (d, *J* = 9.5 Hz), –110.22 (d, *J* = 9.6 Hz), –111.43 (m). The NMR spectra of ***mer*-Ir(dfppy)$_3$** obtained *in situ* are in agreement with those reported in the literature.[3]

[Ir(tppy)$_2$(Htppy)](O$_2$CCF$_3$). A solution of the open form (greenish-yellow, weak white emission) was obtained upon addition of an aliquot of a stock solution of TFA in CD_2Cl_2 (0.5 M, 36.0 µL, 18.0 µmol, 10.0 eqiuv.) to a solution of ***fac*-Ir(tppy)$_3$** (2.0 mg, 1.8 µmol, 1.0 equiv.) in 0.5 mL CD_2Cl_2 (yellow, greenish-yellow emission). **^{1}H NMR** (400 MHz, CD_2Cl_2, 298 K) δ 8.37 (d, *J* = 5.0 Hz, 1H), 8.09 (m, 5H), 7.98 (t, *J* = 7.9 Hz, 2H), 7.87–7.77 (m, 4H), 7.73–7.58 (m, 16H), 7.50–7.35 (m, 16H), 7.26 (d, *J* = 1.7 Hz, 1H), 7.11 (m, 1H), 6.95 (m, 2H), 6.87 (d, *J* = 1.8 Hz, 1H), 6.55 (d, *J* = 4.8 Hz, 1H). **^{19}F {^{1}H} NMR** (376 MHz, CD_2Cl_2, 298 K) δ –75.87 (s).

***mer*-Ir(tppy)$_3$**. A solution of the *mer* isomer (yellow, yellow emission) was obtained upon addition of an aliquot of a stock solution of NEt_3 in CD_2Cl_2 (37.8 µL, 18.9 µmol, 10.5 equiv.) to the solution of **[Ir(tppy)$_2$(Htppy)](O$_2$CCF$_3$)**. The spectroscopic data of ***mer*-Ir(tppy)$_3$** obtained *in situ* are in agreement with those presented above.

[Ir(dfppy)$_2$(Htpy)](O$_2$CCF$_3$). A solution of the open form (greenish-yellow, green emission) was obtained upon addition of an aliquot of a stock solution of TFA in CD_2Cl_2 (0.5 M, 25.8 µL, 337 µmol, 100 equiv.) to a solution of ***fac*-Ir(dfppy)$_2$(tpy)** (2.5 mg, 3.4 µmol, 1.0 equiv.) in 0.5 mL CD_2Cl_2 (yellow, intensive green emission). **^{1}H NMR** (400 MHz, CD_2Cl_2, 298 K) δ 8.39 (d, *J* = 8.9 Hz, 1H), 8.29 (m, 1H), 8.05 (m, 2H), 7.91–7.82 (m, 3H), 7.63 (d, *J* = 7.3 Hz, 2H), 7.42–7.32 (m, 2H), 7.10 (m, 3H), 6.98 (m, 1H), 6.89–6.81 (m, 1H), 6.69–6.56 (m, 1H), 6.36 (dd, *J* = 8.2, 2.3 Hz, 1H), 6.23 (m, 1H), 6.03 (dd, *J* = 8.9, 1.7 Hz, 1H), 2.51 (s, 3H). **^{19}F {^{1}H} NMR** (376 MHz, CD_2Cl_2, 298 K) δ –76.23 (s), –104.64 (d, *J* = 11.0 Hz), –104.86 (d, *J* = 11.7 Hz), –106.85 (d, *J* = 11.0 Hz), –107.45 (d, *J* = 11.1 Hz).

***mer*-Ir(dfppy)$_2$(tpy)**. A solution of the *mer* isomer (yellow, cyan emission) was obtained upon addition of an aliquot of a stock solution of NEt_3 in CD_2Cl_2 (49.3 µL, 335 µmol, 105 equiv.) to the solution of **[Ir(dfppy)$_2$(Htpy)](O$_2$CCF$_3$)**. **^{1}H NMR** (400 MHz, CD_2Cl_2, 298 K) δ 8.30 (m, 1H), 8.19 (m, 1H), 7.93 (m, 2H), 7.80 (d, *J* = 8.0 Hz, 1H), 7.68 (t, *J* = 8.3 Hz, 1H), 7.59 (m, 4H), 6.92 (m, 1H), 6.79 (m, 3H), 6.47–6.32 (m, 3H), 6.29 (s, 1H), 5.83 (dd, *J* = 9.2, 2.4 Hz, 1H), 2.13 (s, 3H). **^{19}F {^{1}H} NMR** (376 MHz, CD_2Cl_2, 298 K) δ –110.00 (t, *J* = 9.6 Hz), –110.26 (d, *J* = 9.2 Hz), –111.91 (d, *J* = 9.8 Hz). **^{13}C {^{1}H} NMR** (126 MHz, CD_2Cl_2, 298 K) δ 184.09–183.85 (m), 172.53 (s), 170.54 (s), 165.66 (d, *J* = 10.5 Hz), 165.47–165.21 (m), 164.99 (d, *J* = 7.2 Hz), 164.51 (d, *J* = 6.2 Hz), 164.10 (d, *J* = 11.0 Hz), 163.60 (d, *J* = 10.5 Hz), 163.33 (m), 162.01 (d, *J* = 10.9 Hz), 161.25 (d, *J* = 13.0 Hz), 153.14 (s), 151.80 (s), 148.55 (s), 142.52 (s), 140.70 (s), 137.99 (s), 137.00 (s), 135.88 (s), 133.80 (s), 129.17 (m), 127.19 (m), 124.90 (s), 123.86 (d, *J* = 21.8 Hz), 123.35 (s), 123.06 (m), 122.61 (s), 122.17 (s), 119.38 (s), 118.79 (dd, *J* = 13.7, 2.7 Hz), 112.45 (dd, *J* = 16.3, 2.6 Hz), 98.01 (t, *J* = 27.3 Hz), 95.60 (t, *J* = 27.2 Hz), 22.06 (s). The spectroscopic data of a different isomer of ***mer*-Ir(dfppy)$_2$(tpy)** have been reported in the literature.[12]

NMR control of repetitive *fac*↔*mer* isomerization

The General Procedure (Scheme S4) was used for multiple *fac*→*mer*→*fac* isomerizations of the complexes $Ir(ppy)_3$, $Ir(tpy)_3$, $Ir(meppy)_3$, and $Ir(dfppy)_3$. Three cycles for each compound were performed. ^1H (400 MHz) and ^{19}F (376 MHz) NMR measurements were performed in CD_2Cl_2 at 298 K. Each new cycle was started by the addition of acid to the solution from the previous cycle without purification steps.

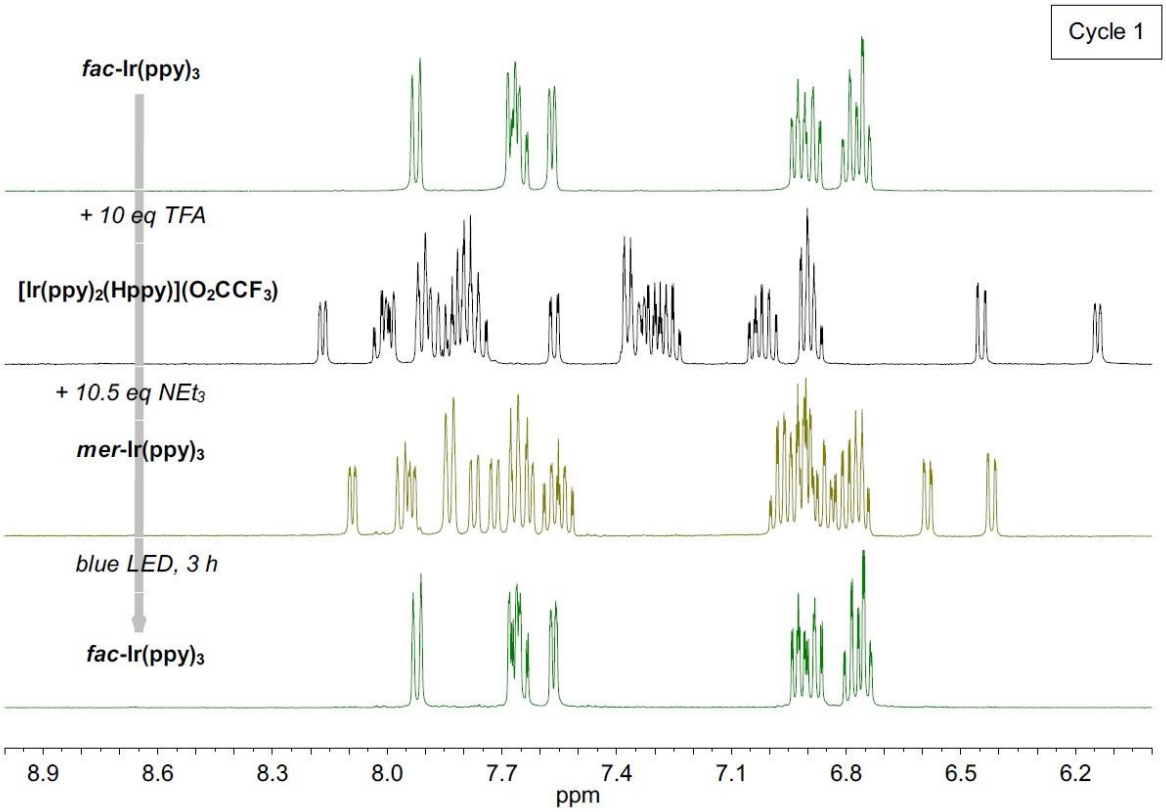

Figure S2. ^1H NMR spectra of Cycle 1 *fac*→*mer*→*fac* for $Ir(ppy)_3$.

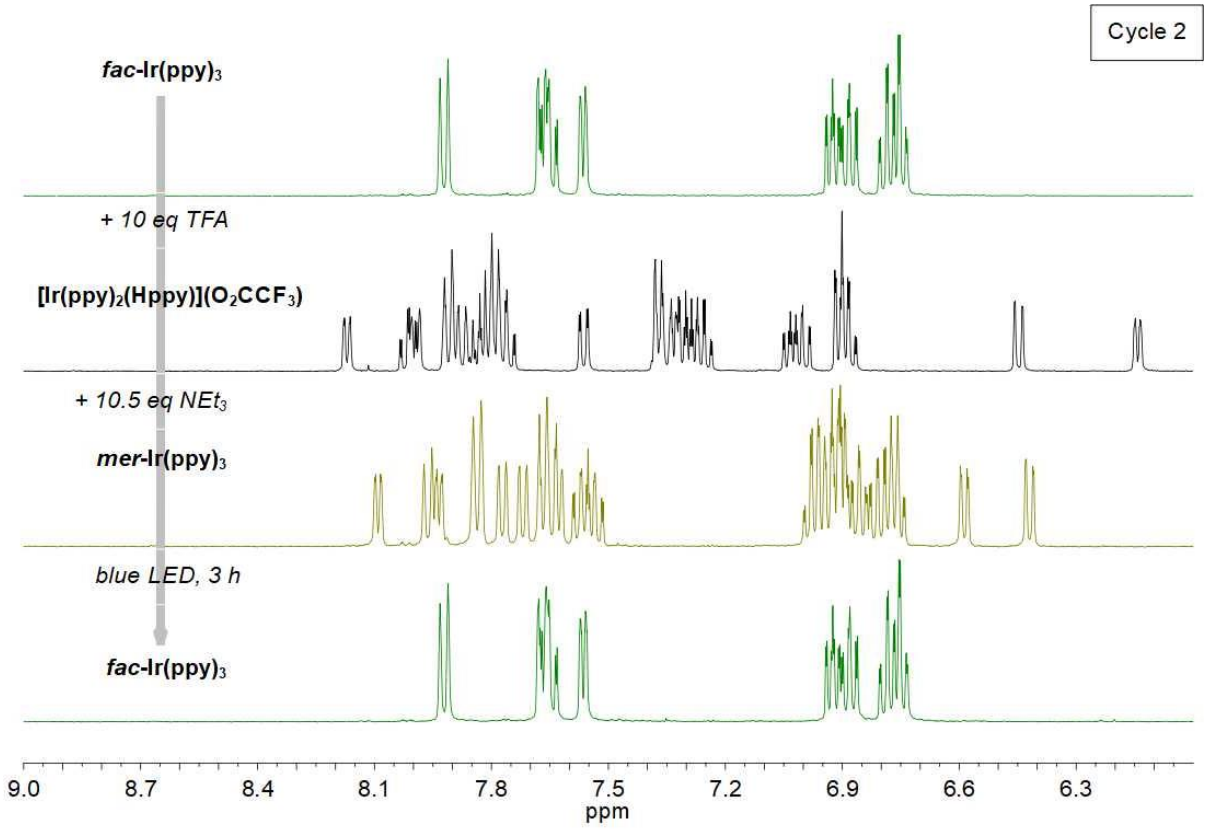

Figure S3. ^{1}H NMR spectra of Cycle 2 *fac*→*mer*→*fac* for Ir(ppy)$_3$.

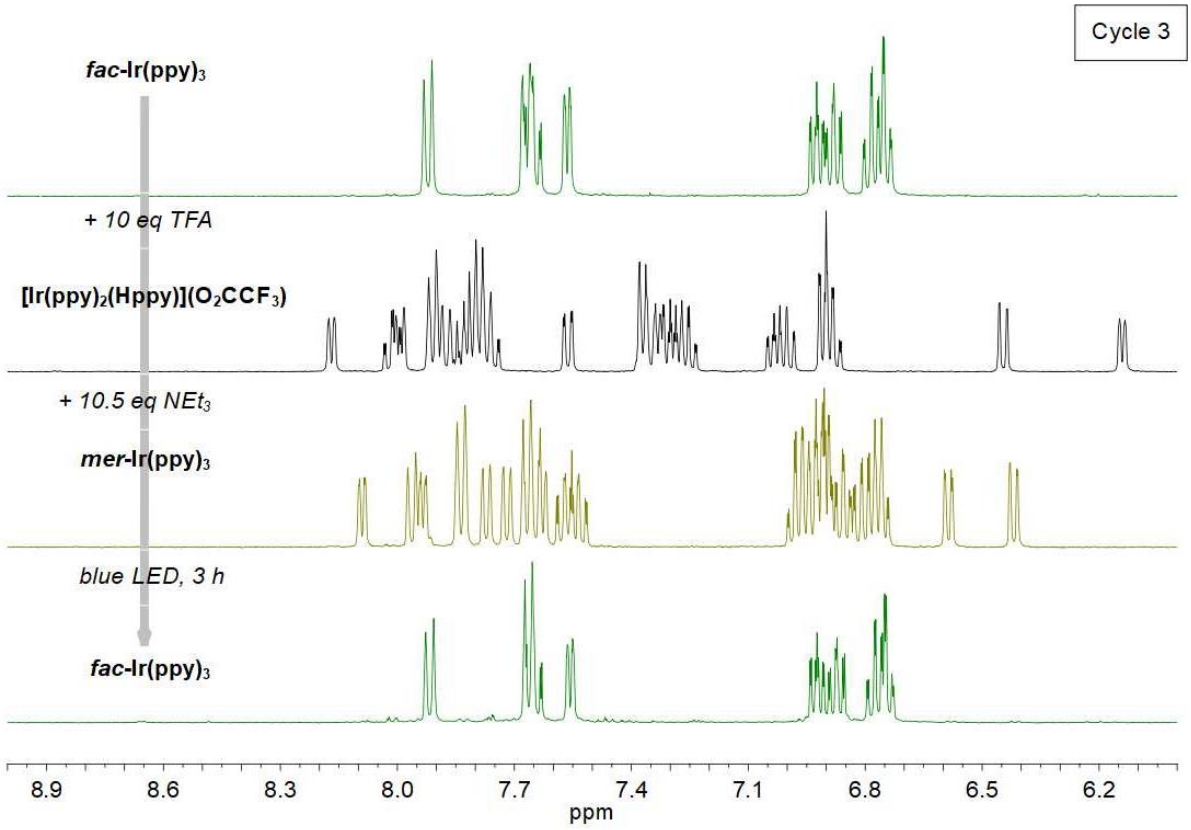

Figure S4. ^{1}H NMR spectra of Cycle 3 *fac*→*mer*→*fac* for Ir(ppy)$_3$.

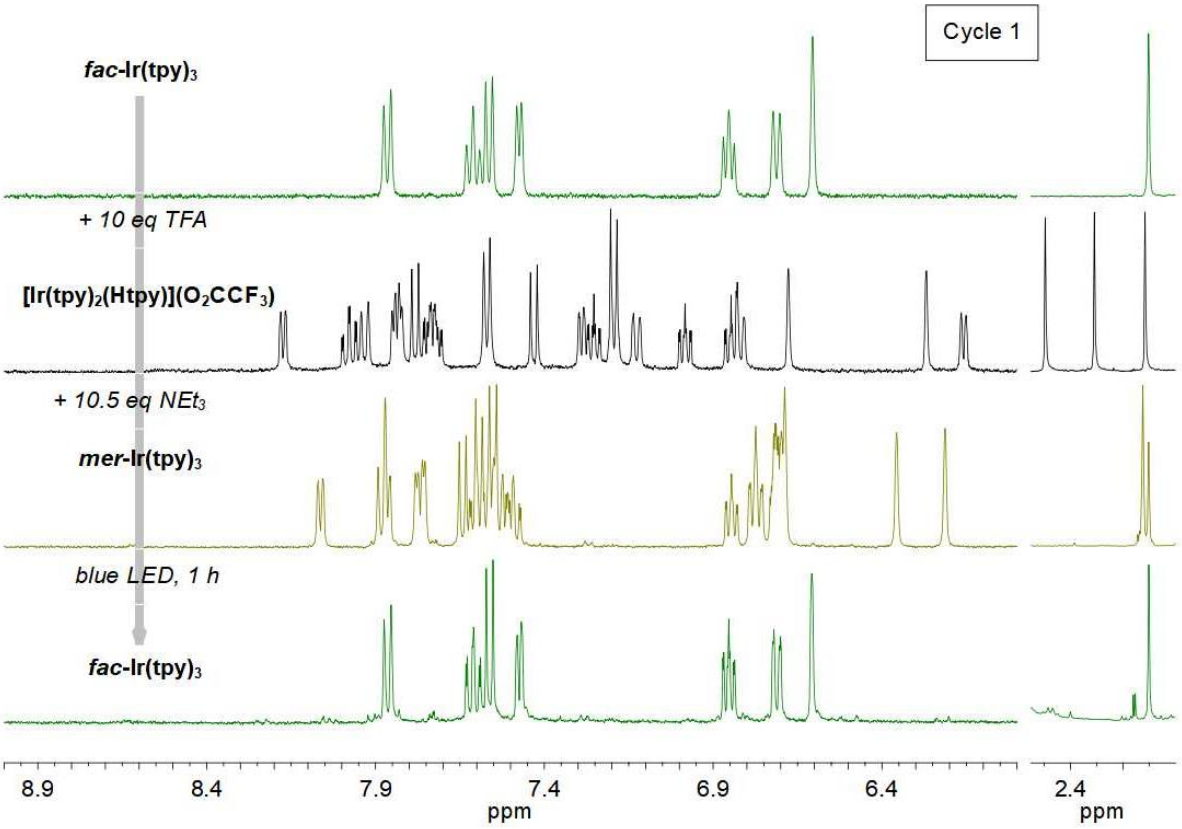

Figure S5. ^{1}H NMR spectra of Cycle 1 *fac*→*mer*→*fac* for Ir(tpy)$_3$.

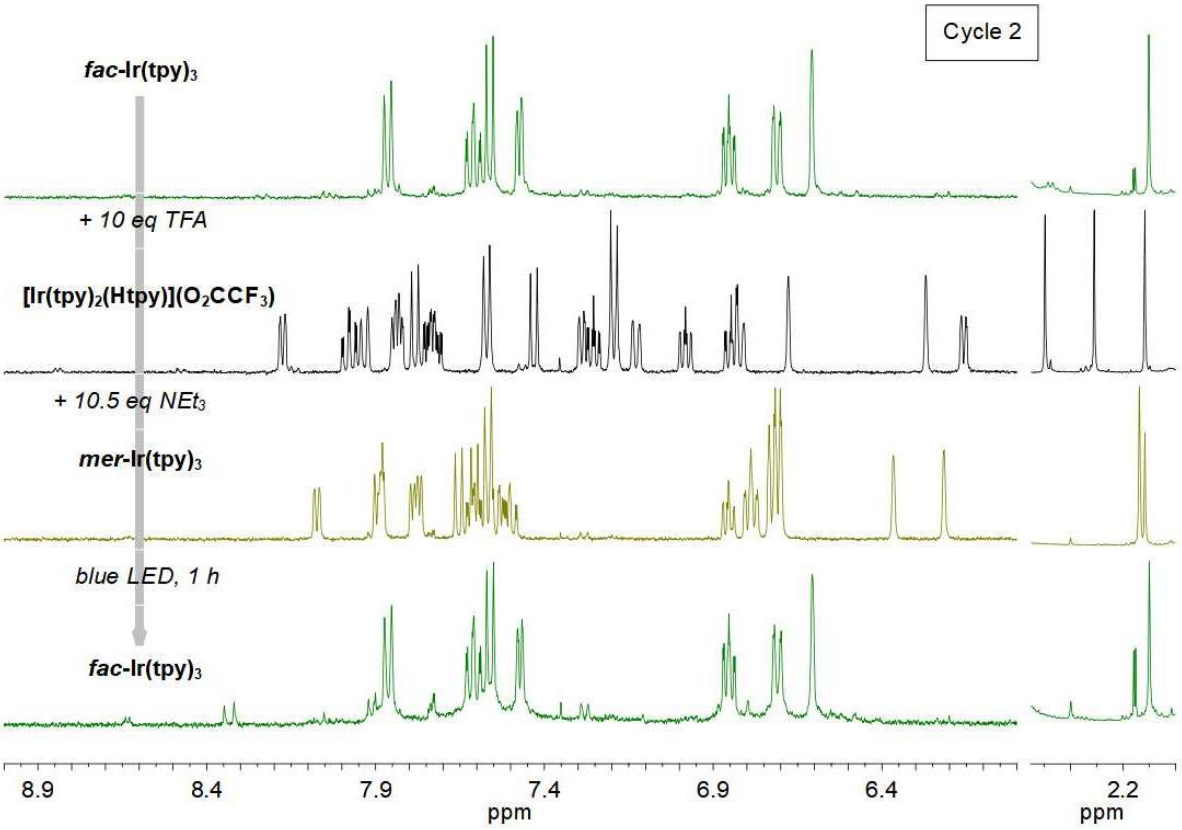

Figure S6. ^{1}H NMR spectra of Cycle 2 *fac*→*mer*→*fac* for Ir(tpy)$_3$.

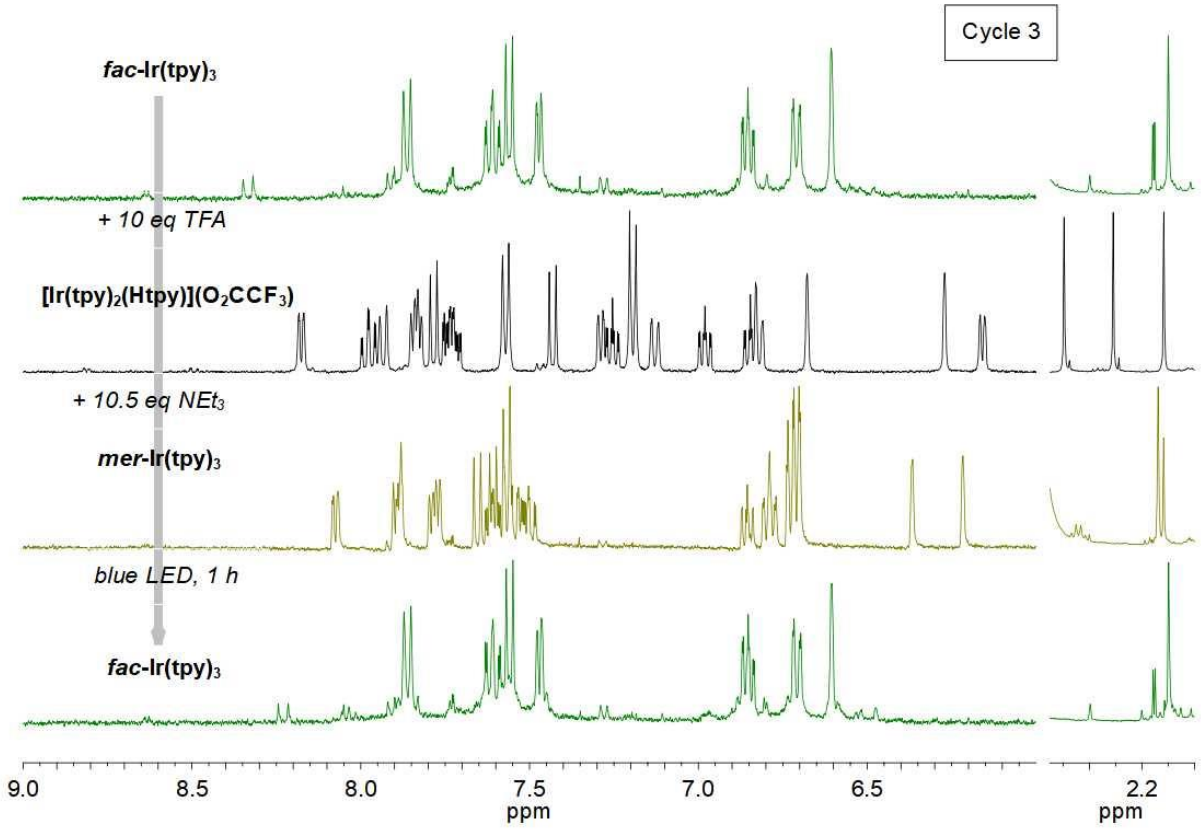

Figure S7. ^{1}H NMR spectra of Cycle 3 *fac*→*mer*→*fac* for Ir(tpy)$_3$.

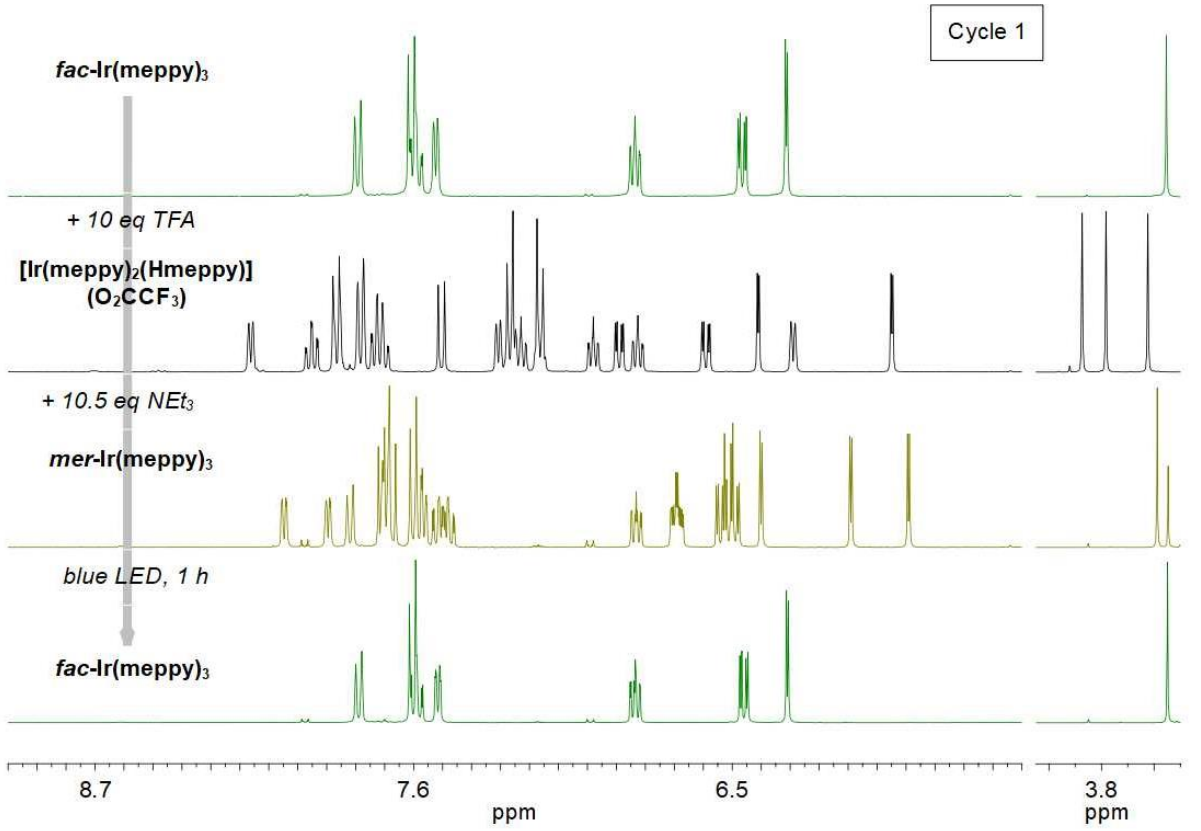

Figure S8. ^{1}H NMR spectra of Cycle 1 *fac*→*mer*→*fac* for Ir(meppy)$_3$.

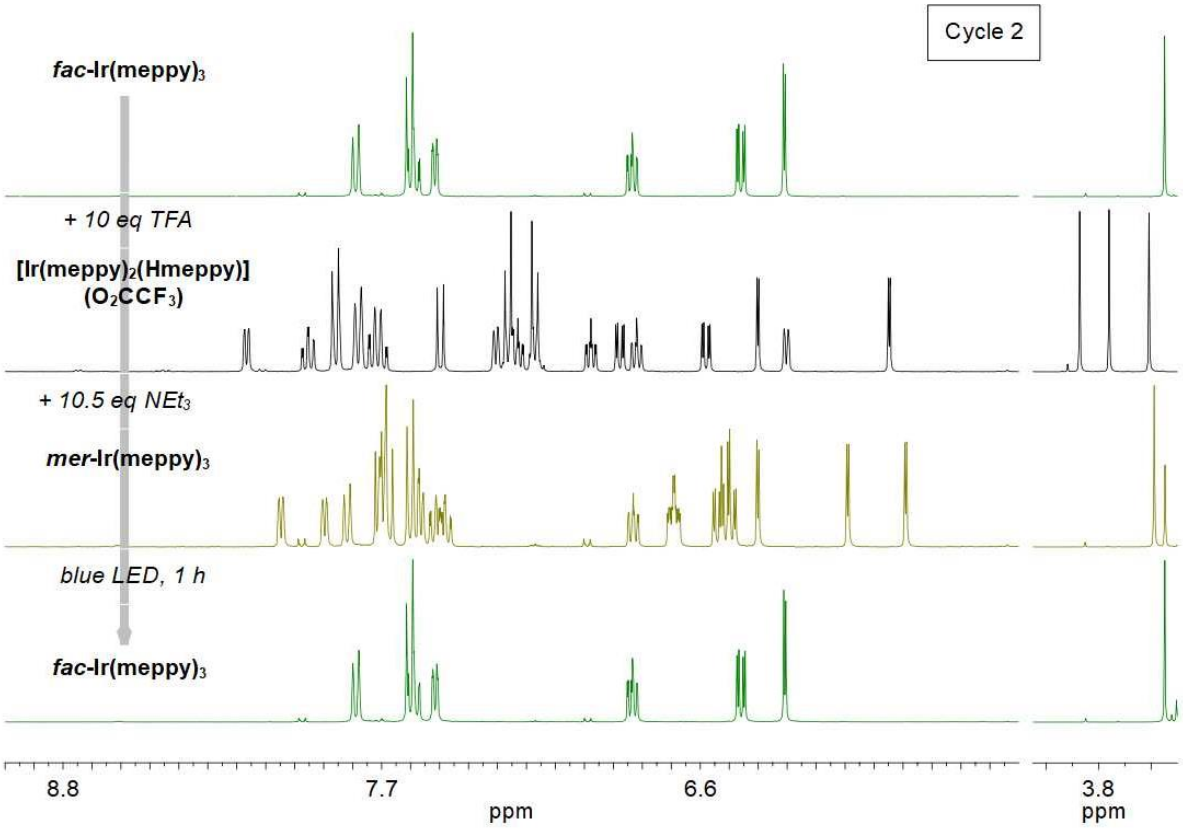

Figure S9. ^{1}H NMR spectra of Cycle 2 *fac*→*mer*→*fac* for Ir(meppy)$_3$.

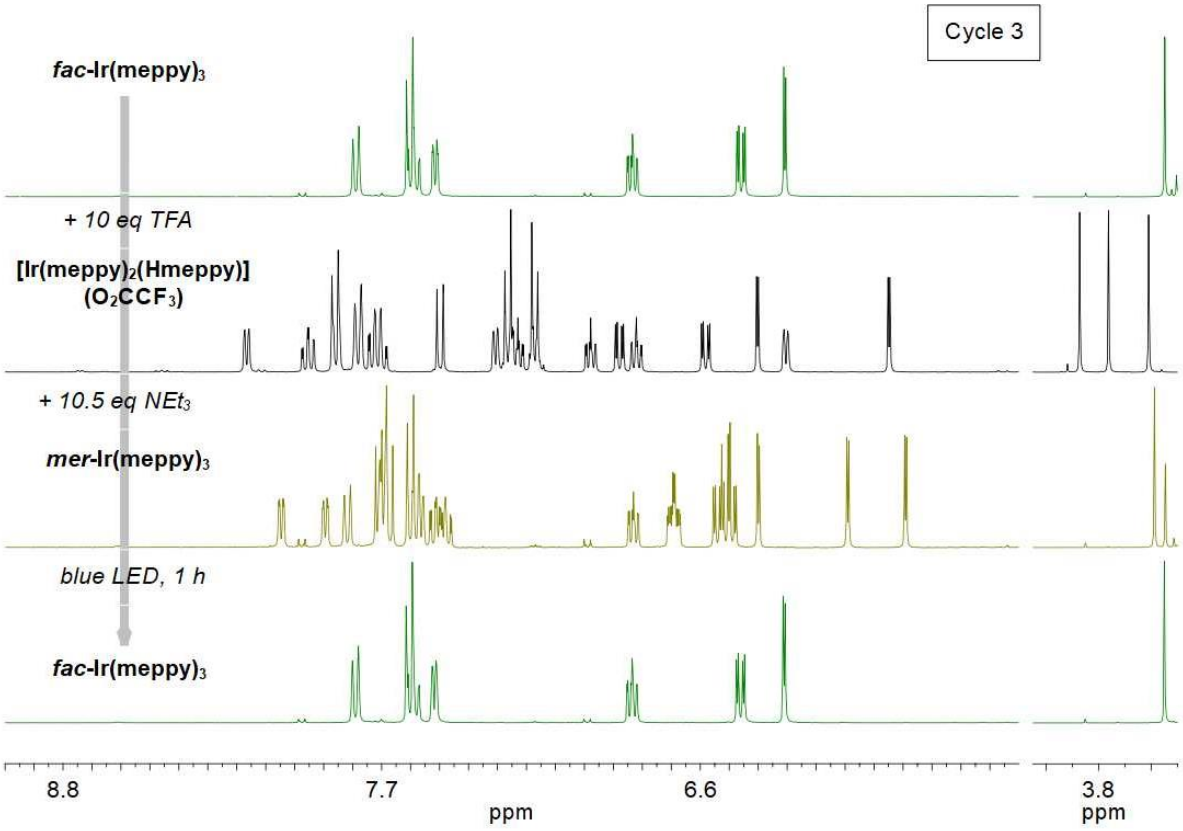

Figure S10. ^{1}H NMR spectra of Cycle 3 *fac*→*mer*→*fac* for Ir(meppy)$_3$.

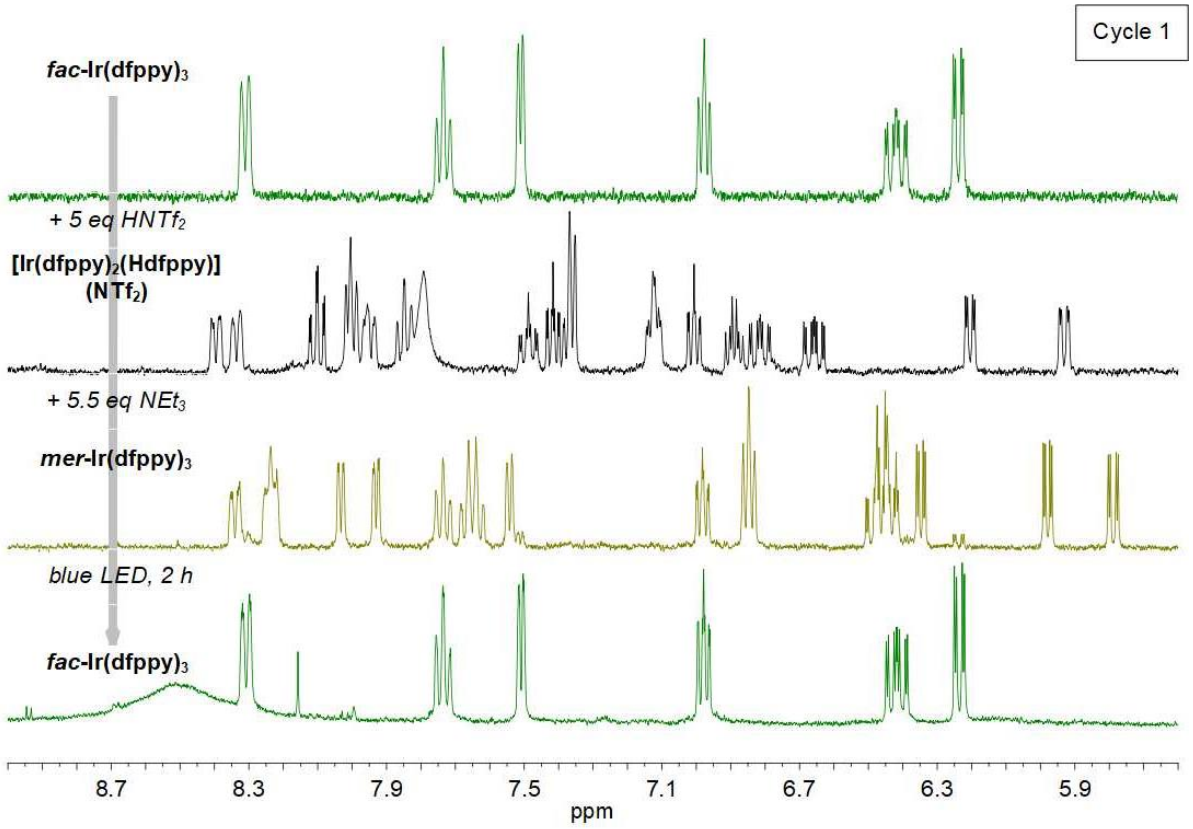

Figure S11. ^{1}H NMR spectra of Cycle 1 *fac*→*mer*→*fac* for Ir(dfppy)$_3$.

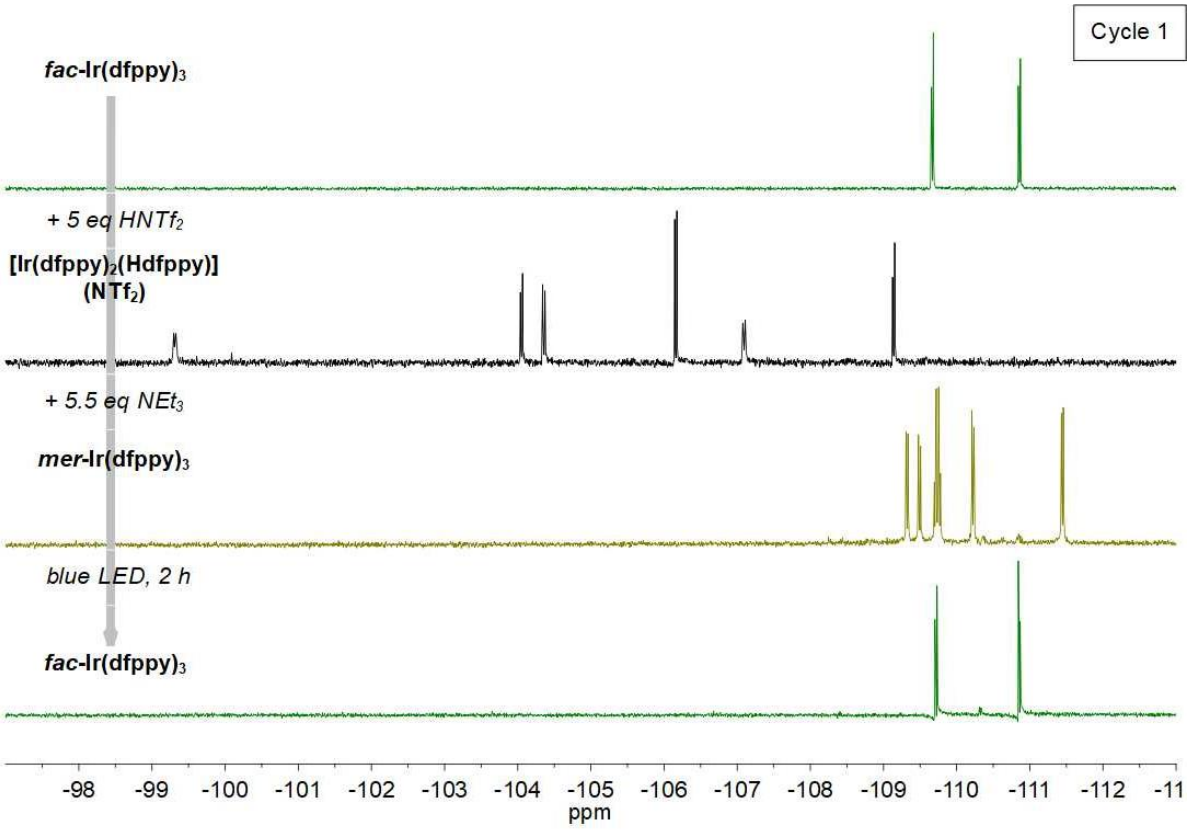

Figure S12. ^{19}F NMR spectra of Cycle 1 *fac*→*mer*→*fac* for Ir(dfppy)$_3$.

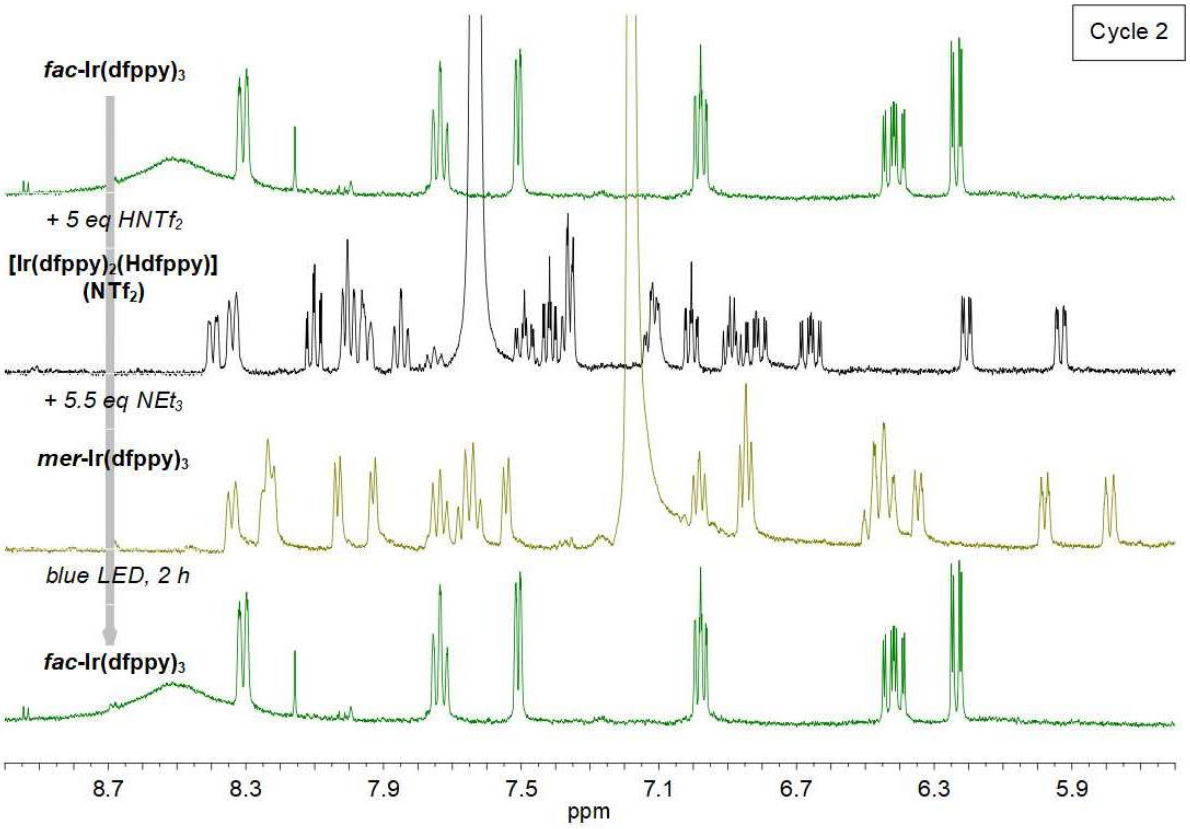

Figure S13. ^{1}H NMR spectra of Cycle 2 *fac*→*mer*→*fac* for Ir(dfppy)$_3$.

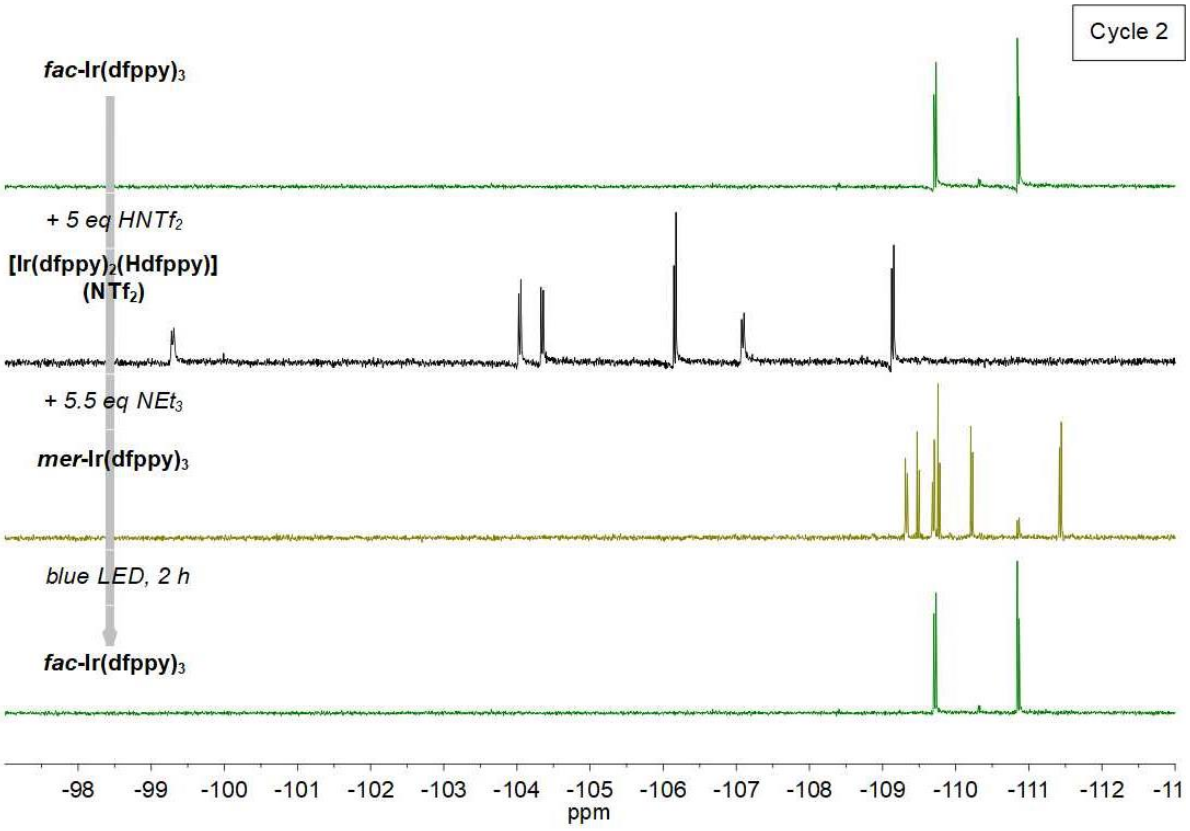

Figure S14. ^{19}F NMR spectra of Cycle 2 *fac*→*mer*→*fac* for Ir(dfppy)$_3$.

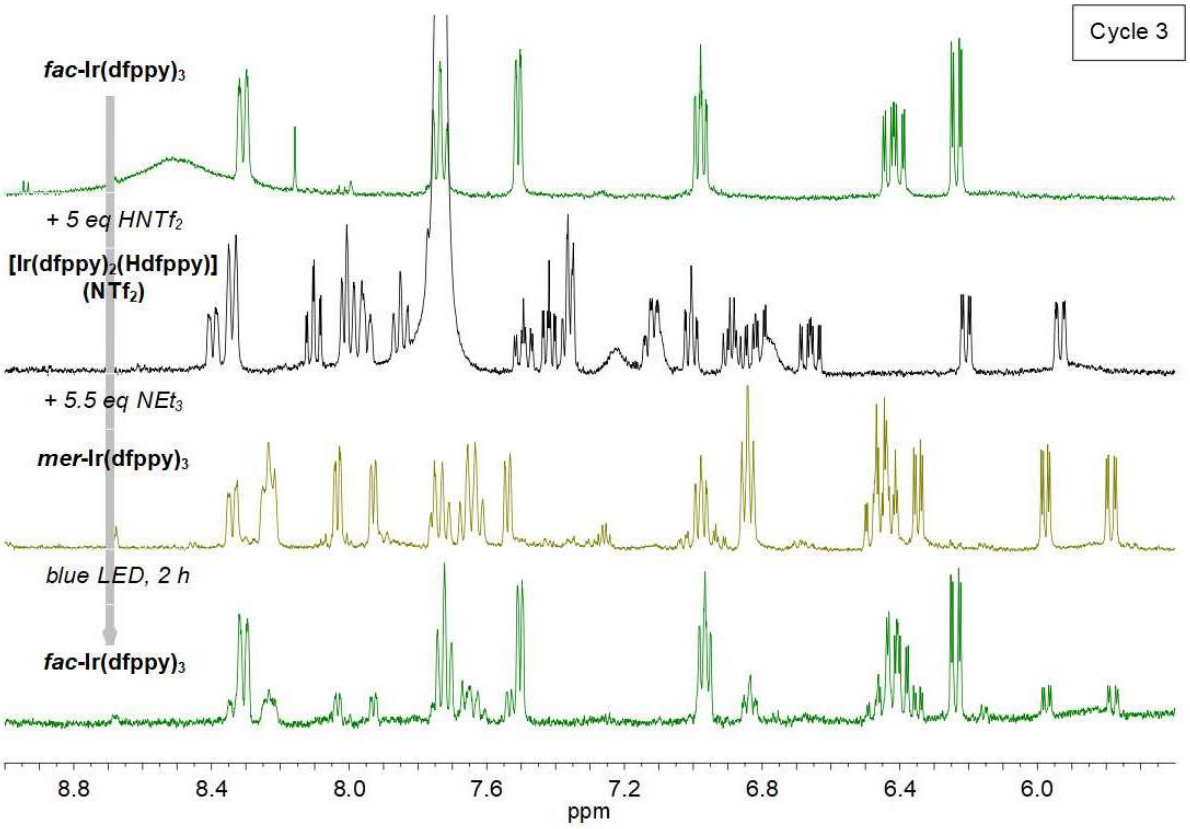

Figure S15. ^{1}H NMR spectra of Cycle 3 *fac*→*mer*→*fac* for Ir(dfppy)$_3$.

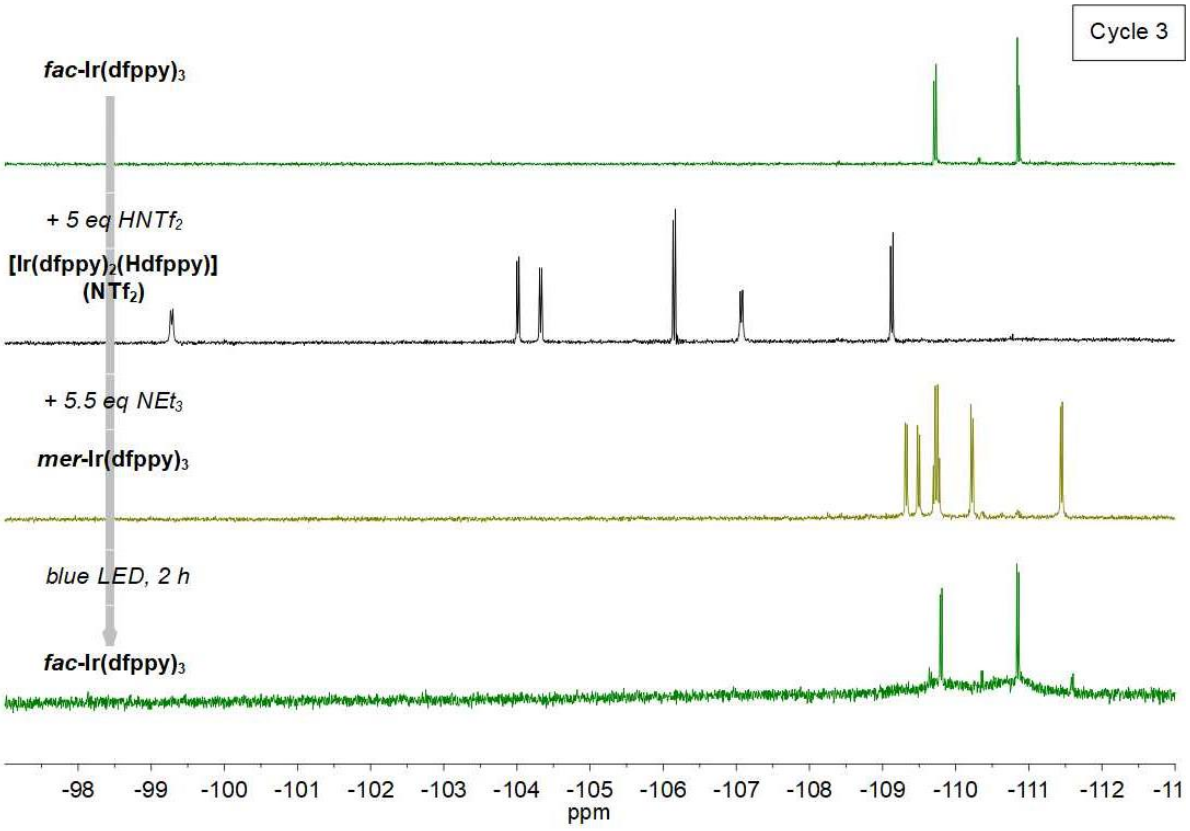

Figure S16. ^{19}F NMR spectra of Cycle 3 *fac*→*mer*→*fac* for Ir(dfppy)$_3$.

A single *fac*→*mer*→*fac* isomerization was performed for the complexes Ir(buppy)$_3$, Ir(fppy)$_3$, Ir(tppy)$_3$ and Ir(dfppy)$_2$(tpy) using the General Procedure. The cycles were monitored by ^{1}H (400 MHz) and ^{19}F (376 MHz) NMR spectroscopy (CD_2Cl_2, 298 K).

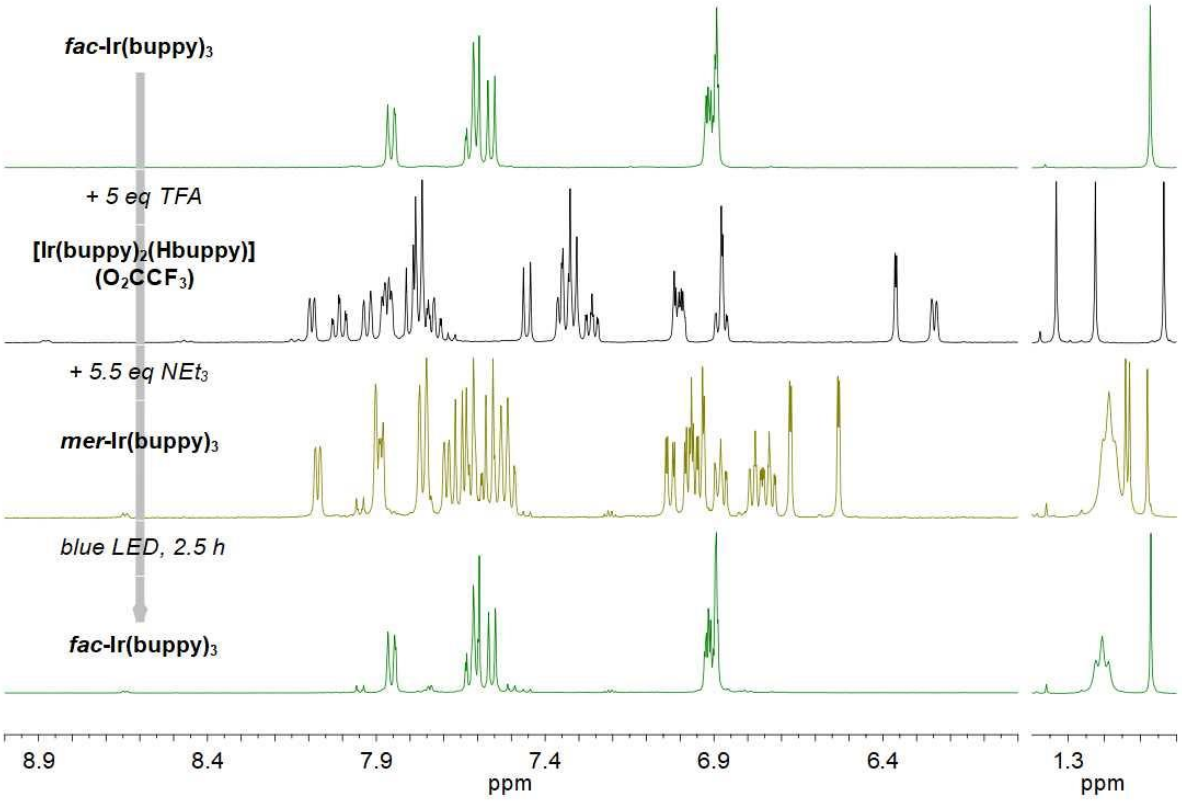

Figure S17. ^{1}H NMR spectra of cycle *fac*→*mer*→*fac* for Ir(buppy)$_3$.

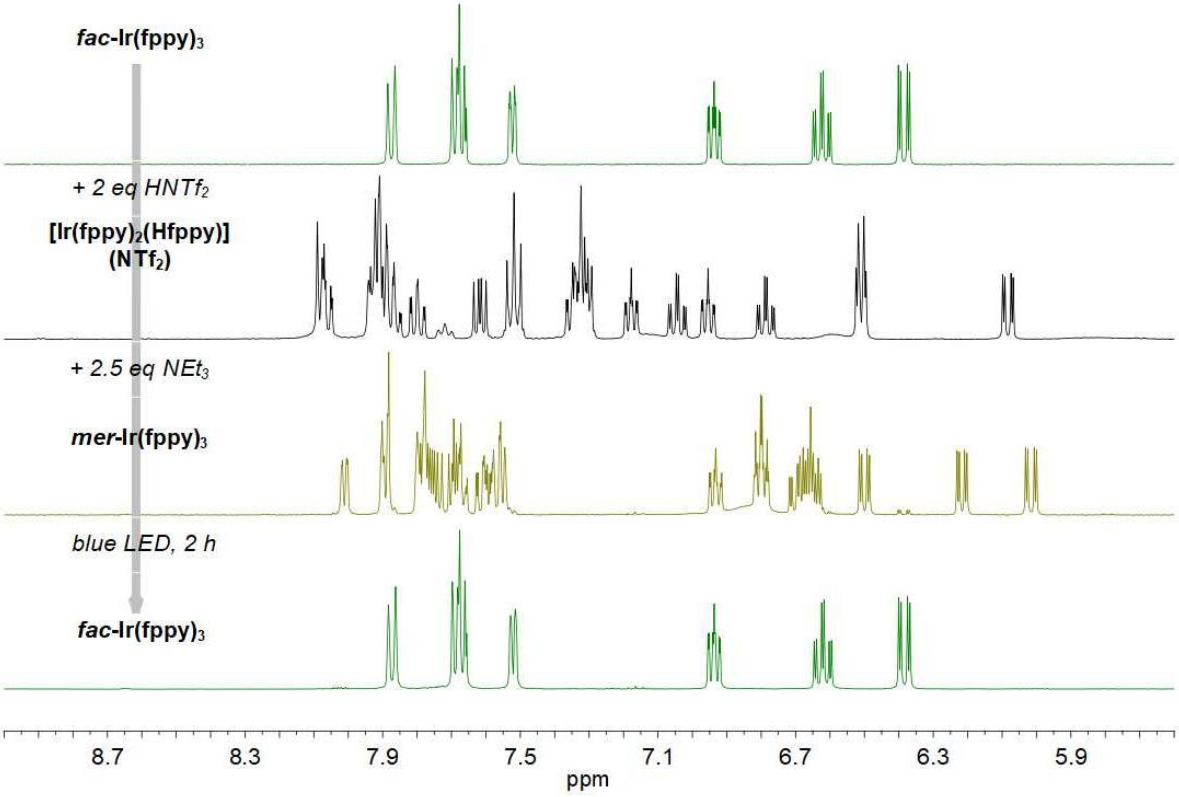

Figure S18. ^{1}H NMR spectra of cycle *fac*→*mer*→*fac* for Ir(fppy)$_3$.

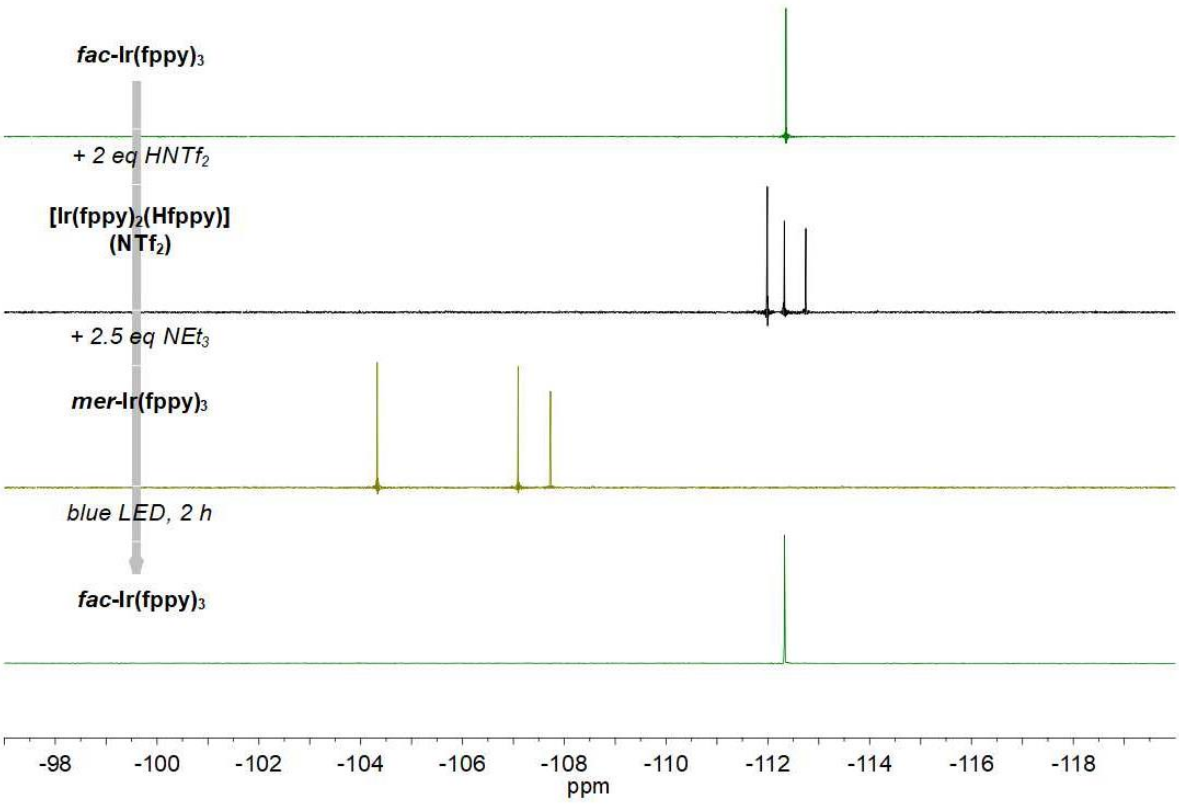

Figure S19. ^{19}F NMR spectra of cycle *fac*→*mer*→*fac* for Ir(fppy)$_3$.

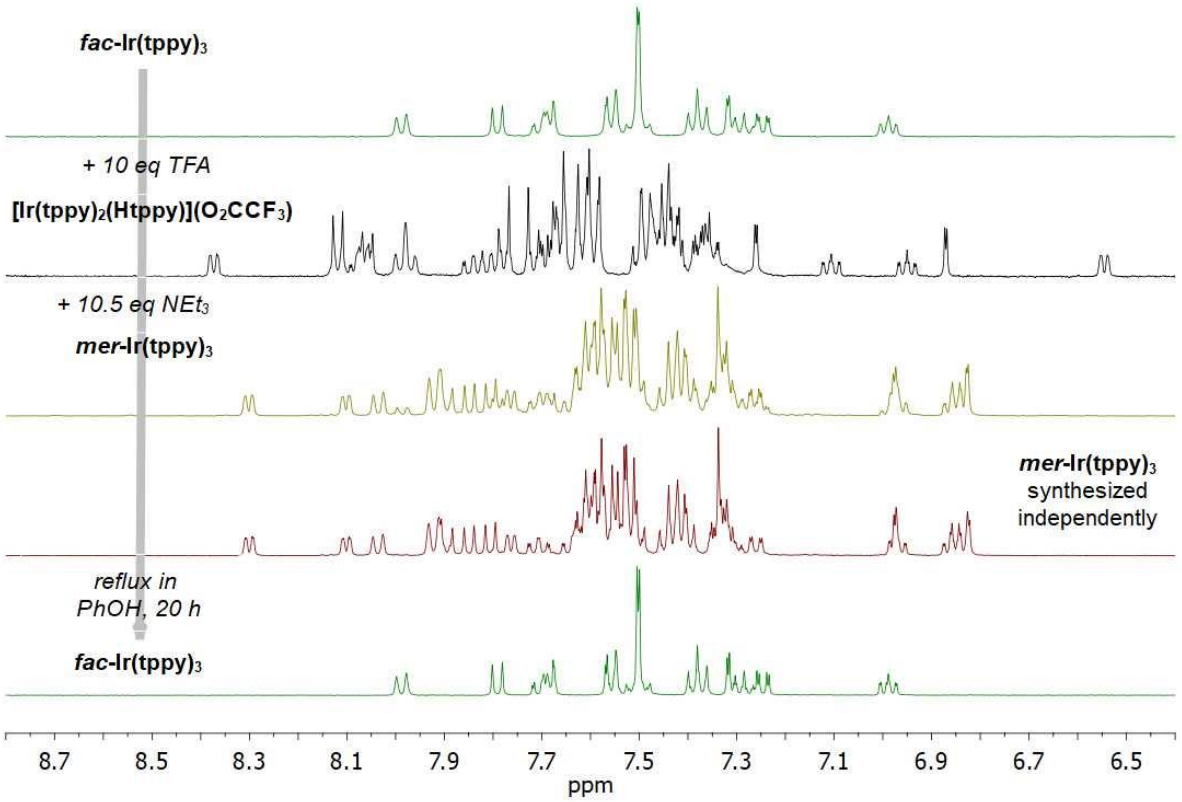

Figure S20. ^{1}H NMR spectra of cycle *fac*→*mer*→*fac* for Ir(tppy)$_3$.

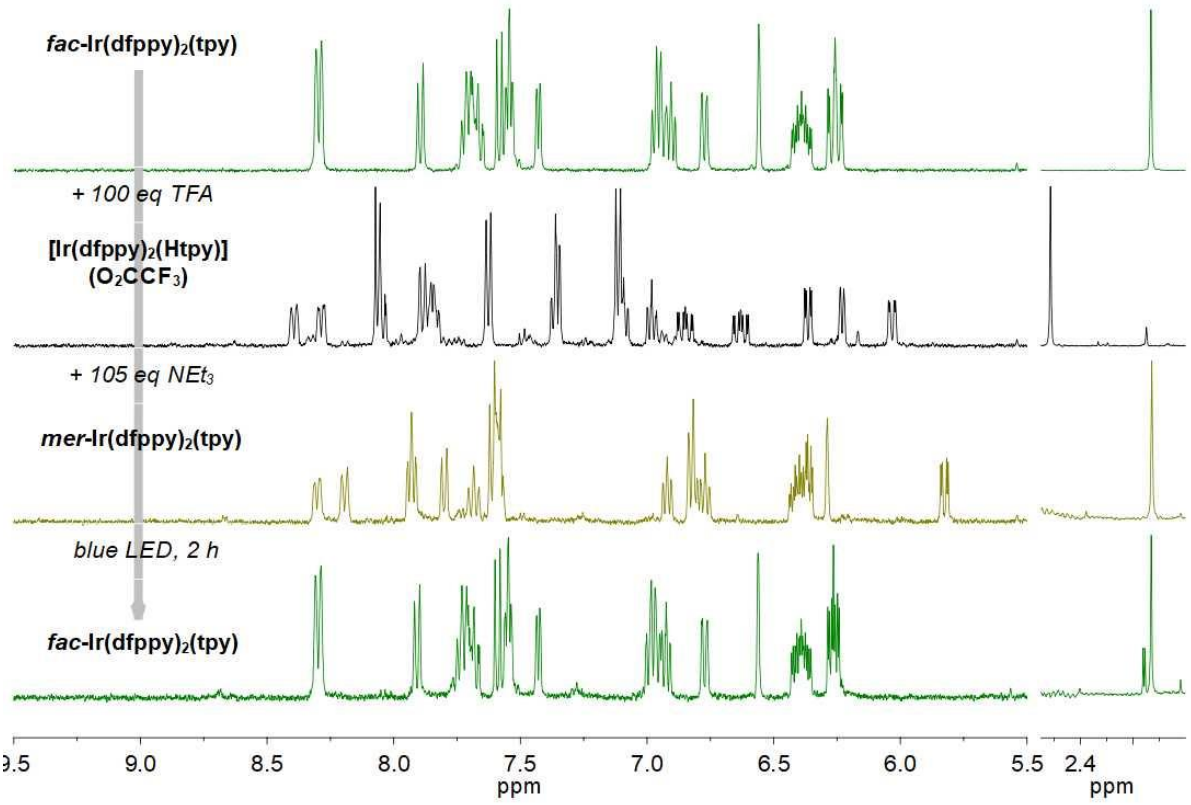

Figure S21. ^{1}H NMR spectra of cycle *fac*→*mer*→*fac* for Ir(dfppy)$_2$(tpy).

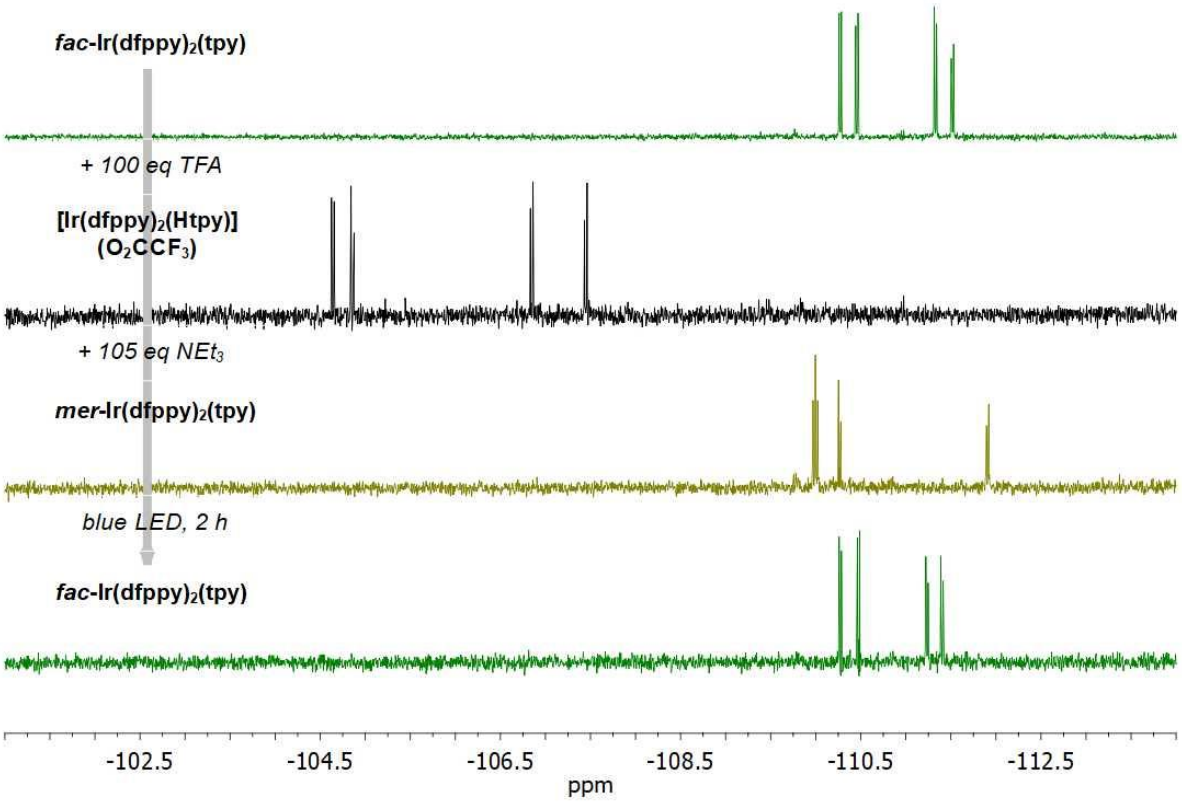

Figure S22. ^{19}F NMR spectra of cycle *fac*→*mer*→*fac* for Ir(dfppy)$_2$(tpy).

Photophysical properties

The photophysical properties of the *fac* and the *mer* isomers of the complexes $Ir(ppy)_3$, $Ir(tpy)_3$, $Ir(meppy)_3$, $Ir(buppy)_3$, $Ir(fppy)_3$ and $Ir(dfppy)_3$ are reported in the literature.[3–5]

Photophysical measurements for the ligand Htppy and the complexes $Ir(tppy)_3$ and $Ir(dfppy)_2(tpy)$ were performed on aerated optically diluted (A < 0.1) solutions of spectrophotometric grade dichloromethane (for Htppy) and THF (for Ir(III) complexes). Absorption spectra were performed on a Perkin Elmer Lambda 40 spectrometer. Steady state fluorescence measurements were performed with an Edinburgh FS5 fluorometer using a Xe light source. Photoluminescence lifetimes (τ) were measured on a time-correlated single photon counting Edinburgh LifeSpec II spectrometer using an Edinburgh Picosecond pulsed diode laser (λ_{exc} = 405 nm) as excitation source. The fitting of the emission decays was performed by using Fluoracle software. The quality of the fitting was evaluated *via* the analysis of the χ^2 parameter and of the residual distribution.

Solid state quantum yields (Φ_{solid}) were measured with an integrating sphere module of the Edinburgh FS5, and quantum yield values were calculated with Fluoracle software. Quantum yields of solutions (Φ_{sol}) were measured by using the relative method. A solution of fluorescein (Acros) in aqueous NaOH (0.1 M) was used as a reference (Φ_r = 0.92). Optically diluted solutions were excited at an isoabsorptive wavelengths and quantum yields were calculated according to the equation:

$$\Phi = \Phi_r \frac{A_r}{A} \frac{I}{I_r} \left(\frac{n}{n_r}\right)^2$$

where I and I_r – the values of the integrated areas below the emission spectra of the Ir(III) complexes and reference, respectively, A and A_r – the absorbances at the excitation wavelength of the Ir(III) complexes and reference, respectively, n and n_r – the refractive indexes of the solvents used for Ir(III) complexes and reference, respectively.[13]

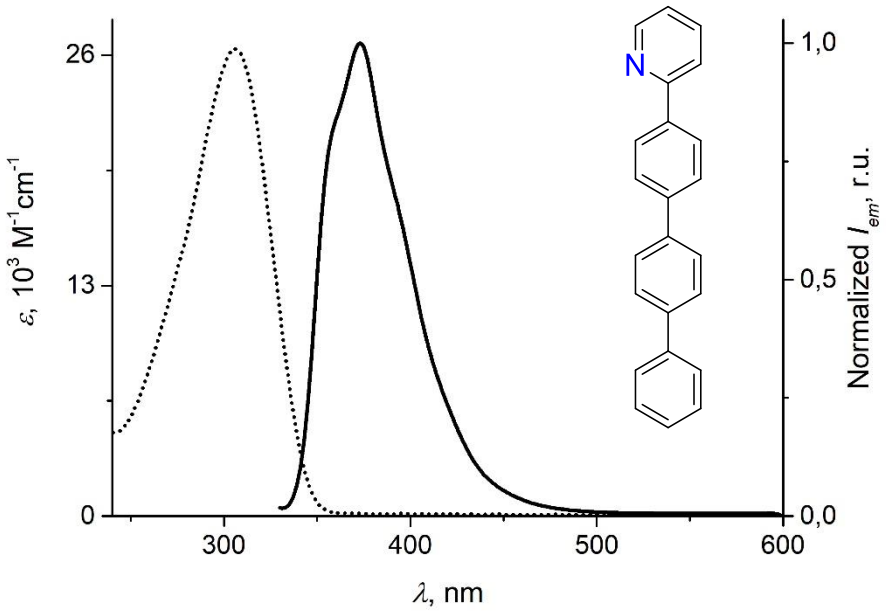

Figure S23. UV-Vis (dotted) and emission spectra (solid, @315) of **Htppy** in DCM.

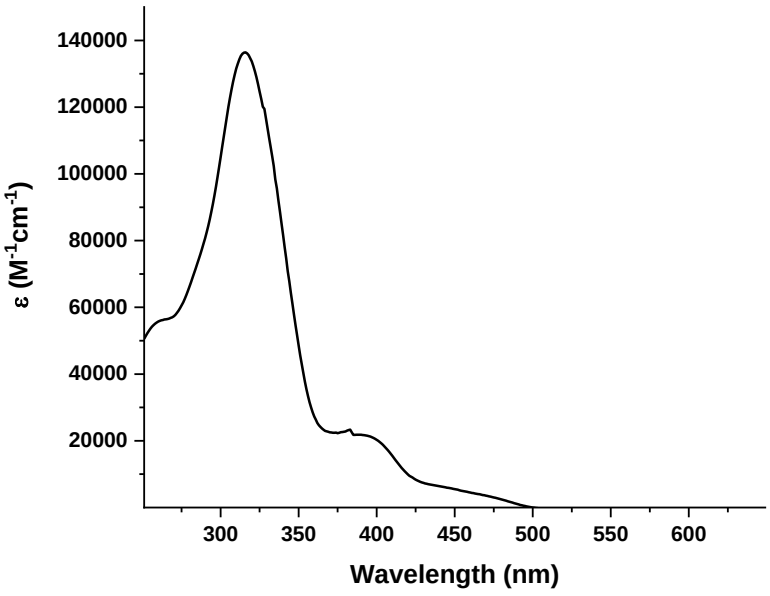

Figure S24. UV-Vis spectrum of ***fac*-Ir(tppy)$_3$** in THF.

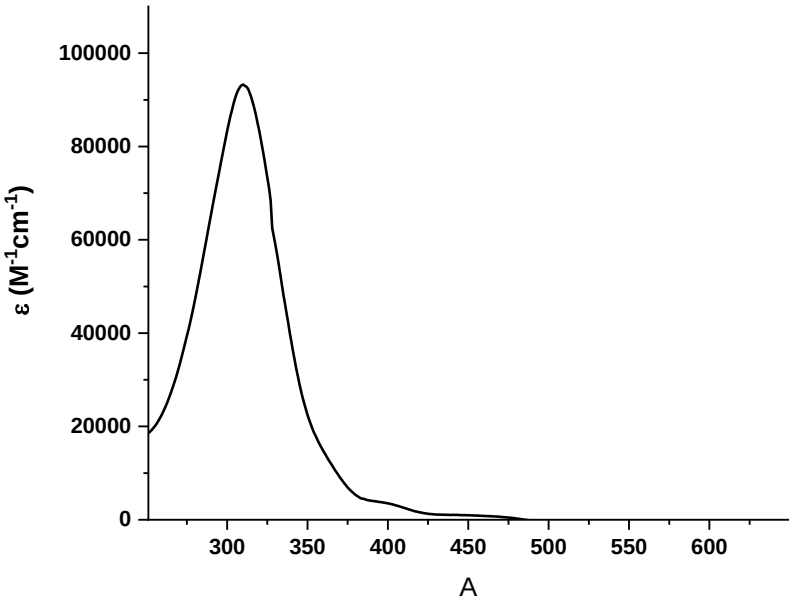

Figure S25. UV-Vis spectrum of ***mer*-Ir(tppy)$_3$** in THF.

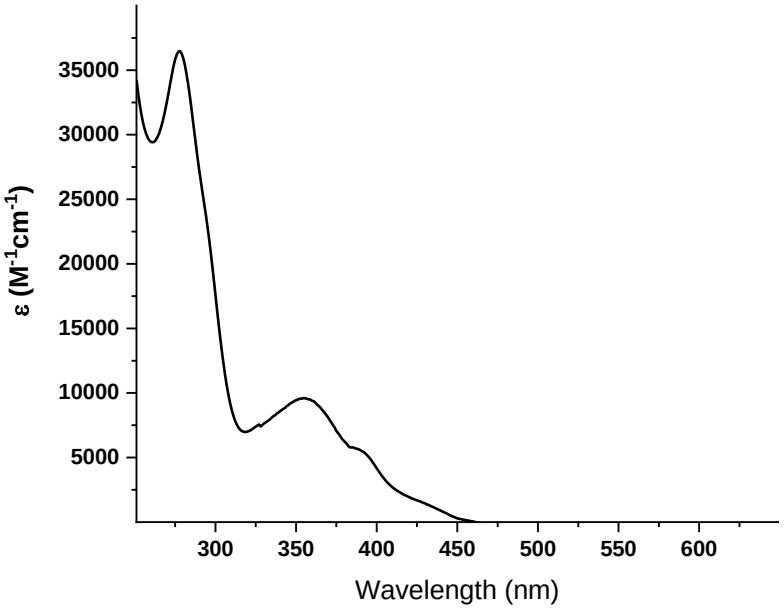

Figure S26. UV-Vis spectrum of ***fac*-Ir(dfppy)$_2$(tpy)** in THF.

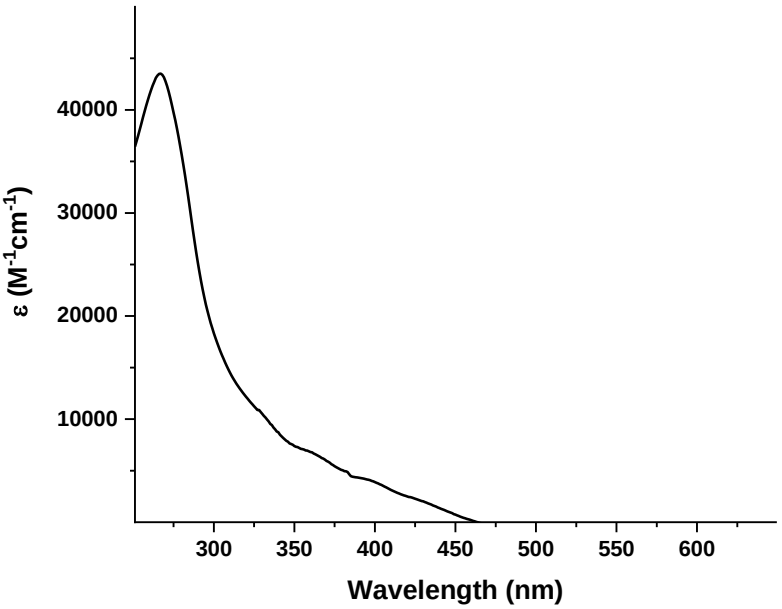

Figure S27. UV-Vis spectrum of ***mer*-Ir(dfppy)$_2$(tpy)** in THF.

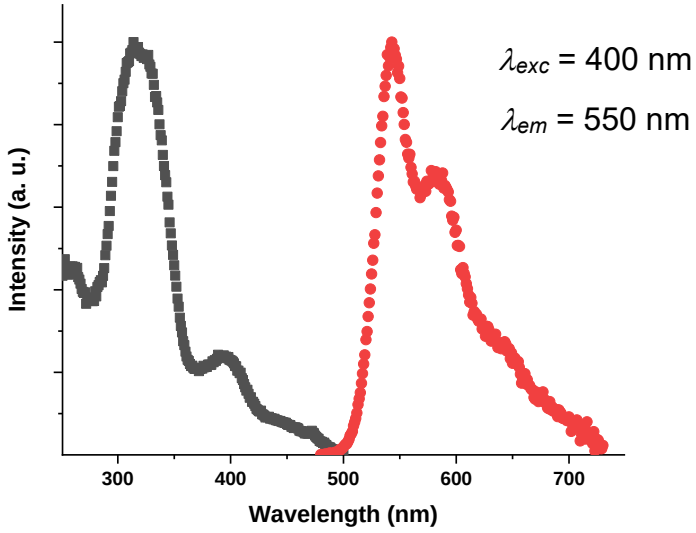

Figure S28. Excitation (black, λ_{em}) and emission (red, λ_{exc}) spectra of ***fac*-Ir(tppy)$_3$** in THF.

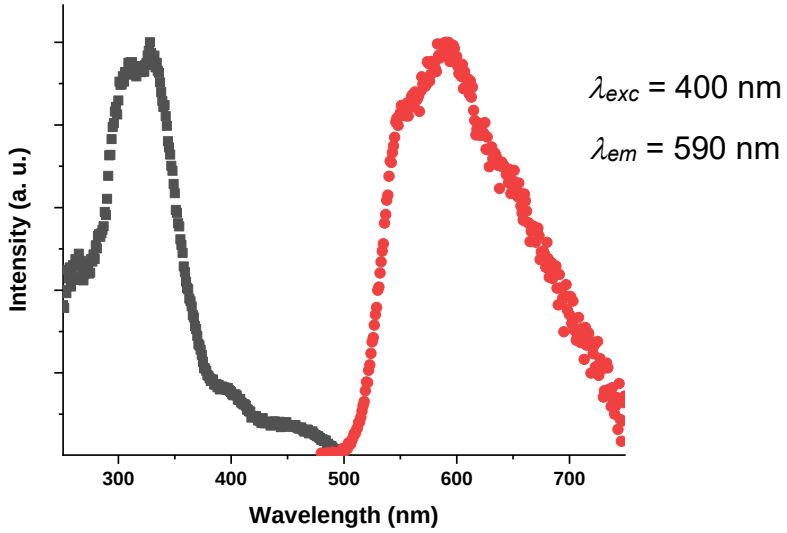

Figure S29. Excitation (black, λ_{em}) and emission (red, λ_{exc}) spectra of ***mer*-Ir(tppy)$_3$** in THF.

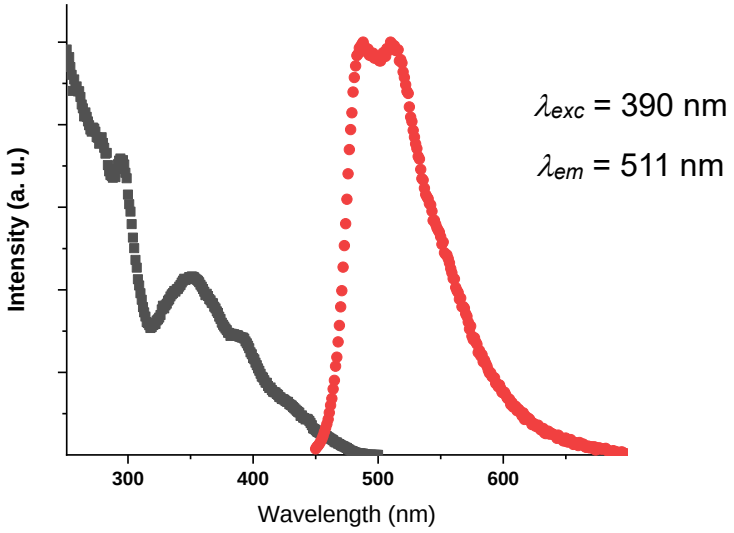

Figure S30. Excitation (black, λ_{em}) and emission (red, λ_{exc}) spectra of ***fac*-Ir(dfppy)$_2$(tpy)** in THF.

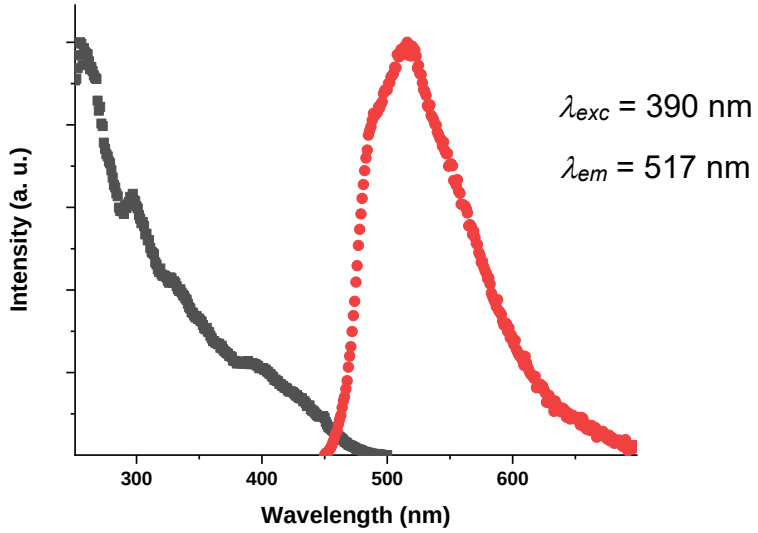

Figure S31. Excitation (black, λ_{em}) and emission (red, λ_{exc}) spectra of ***mer*-Ir(dfppy)$_2$(tpy)** in THF.

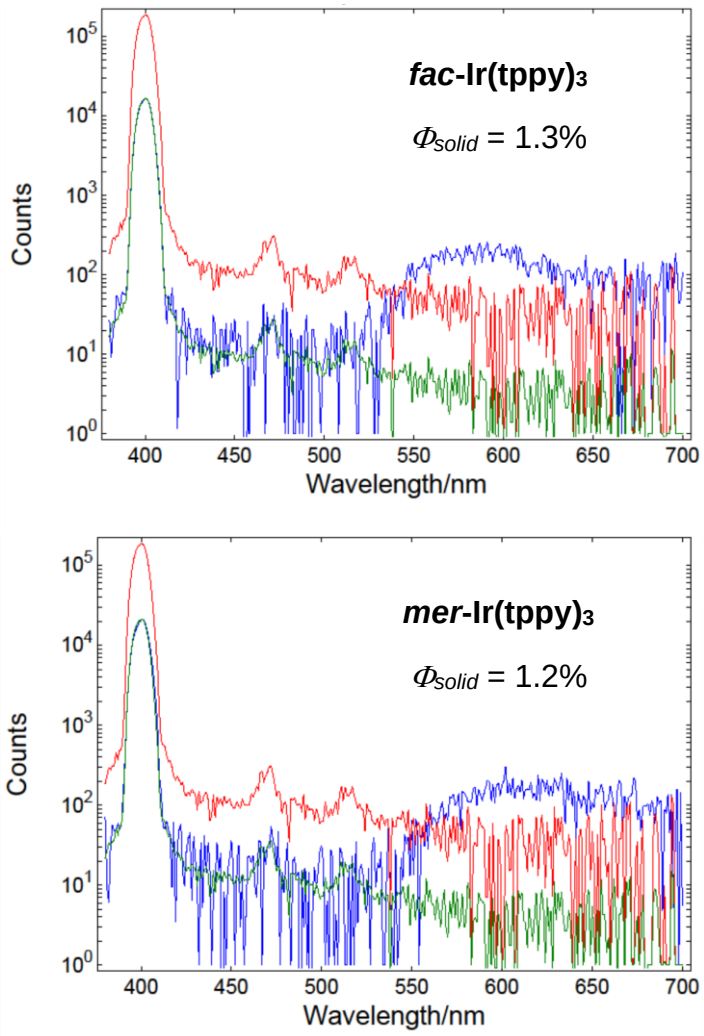

Figure S32. Solid state photon counting spectra of the complexes Ir(tppy)$_3$ (λ_{exc} = 405 nm).

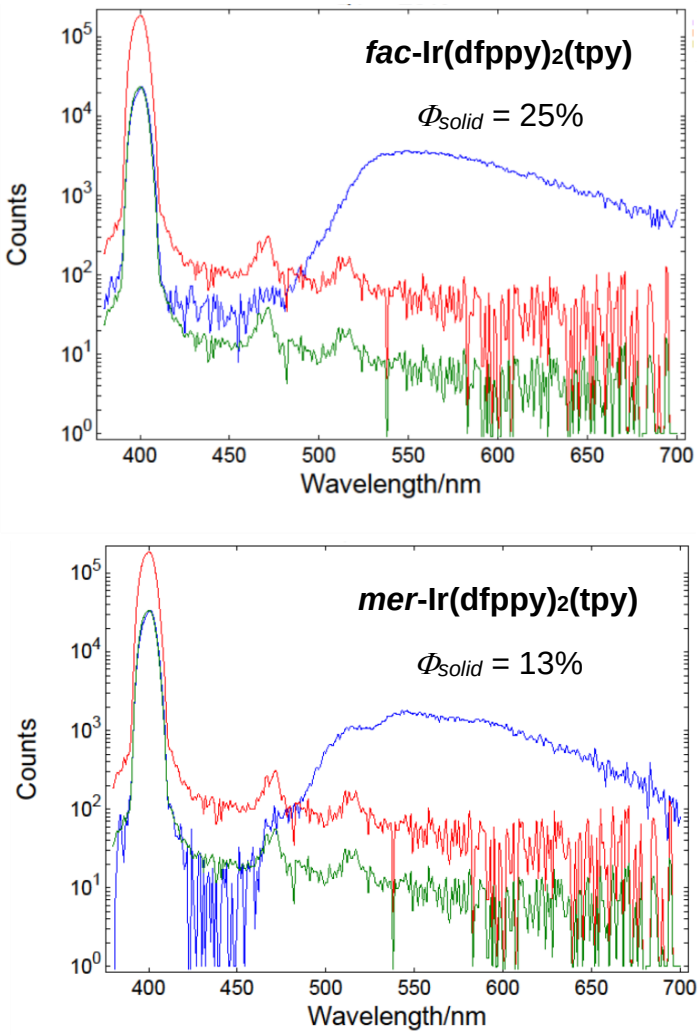

Figure S33. Solid state photon counting spectra of the complexes Ir(dfppy)$_2$(tpy) (λ_{exc} = 405 nm).

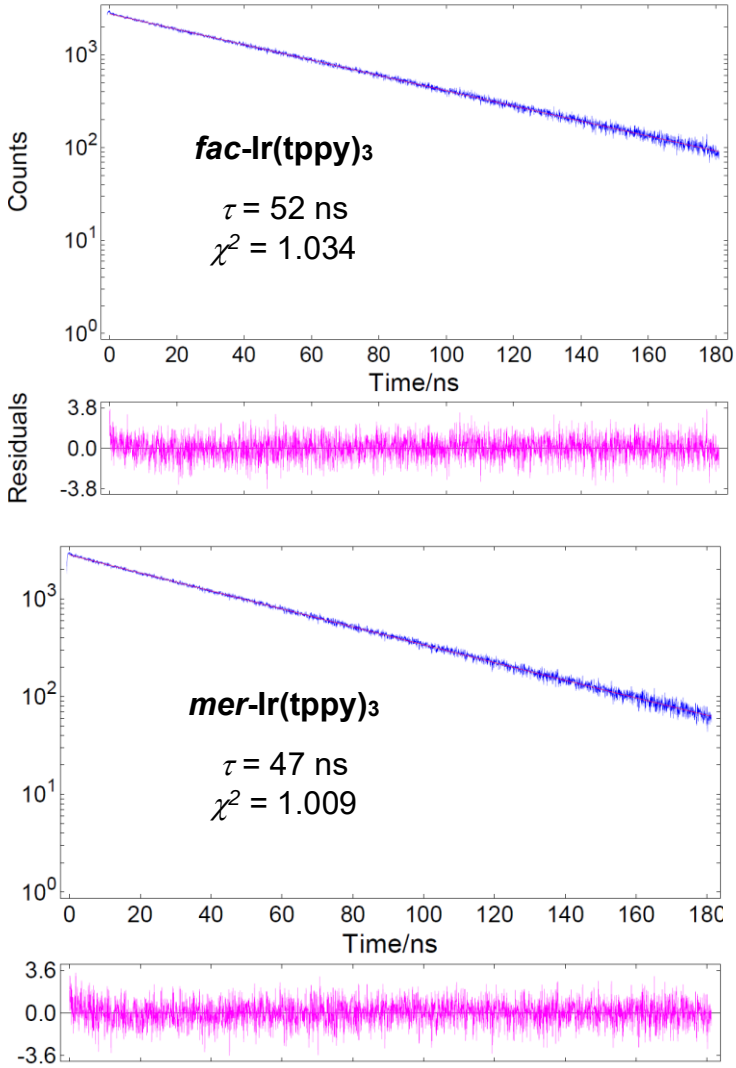

Figure S34. Photoluminescence decay curves of the Ir(tppy)$_3$ isomers recorded by time-correlated single photon counting (λ_{exc} = 405 nm, THF).

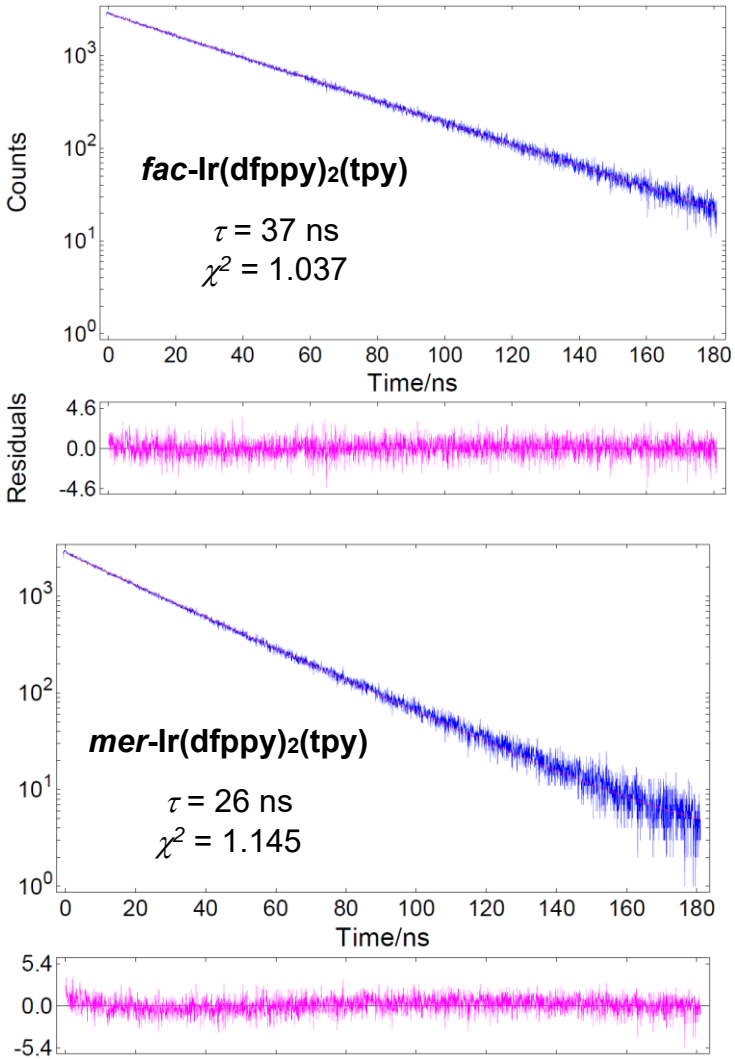

Figure S35. Photoluminescence decay curves of the Ir(dfppy)$_2$(tpy) isomers recorded by time-correlated single photon counting (λ_{exc} = 405 nm, THF).

Table S1. Optical properties of the compounds.

Compound	λ_{abs}, nm (ε, 10^4 $M^{-1}\cdot cm^{-1}$)	λ_{em}, nm (@λ_{exc})
Htppy	306 (26)	373 (@315)
***fac*-Ir(tppy)$_3$**	314 (13.7), 391 (2.2), 454 (0.51)	543, 584, 642sh
***mer*-Ir(tppy)$_3$**	310 (9.3), 393 (0.39)	552, 590
***fac*-Ir(dfppy)$_2$(tpy)**	278 (3.6), 354 (0.96), 389 (0.56), 425 (0.17)	488, 511,545sh
***mer*-Ir(dfppy)$_2$(tpy)**	266 (4.3), 325 (1.1)	487, 515, 552sh

Table S2. Photoluminescence quantum yields and lifetimes of Ir(III) complexes.

Compound	Φ_{solid}, %[a]	Φ_{sol}, %[b]	τ, ns[c]
***fac*-Ir(tppy)$_3$**	1.3	1.5	52
***mer*-Ir(tppy)$_3$**	1.2	1.3	47
***fac*-Ir(dfppy)$_2$(tpy)**	25	2.4	37
***mer*-Ir(dfppy)$_2$(tpy)**	13	1.4	26

[a] Absolute photoluminescence quantum yields in solid state measured using integrating sphere. [b] Relative photoluminescence quantum yields in THF solution measured referring to the solution of fluorescein in aqueous 0.1 M NaOH (Φ_r = 0.92). [c] Photoluminescence lifetime measured by time-correlated single photon counting in THF solution.

Spectroscopic monitoring of the acid-base *fac*→*mer* isomerization

To demonstrate reversibility of the ***fac***↔***mer*** isomerizations, 10 cycles were performed for Ir(ppy)$_3$ using the General Procedure. The excitation and emission spectra of *fac*-Ir(ppy)$_3$ and *mer*-Ir(ppy)$_3$ during the 1st cycle are presented in Figure S36. The emission intensity at λ = 514 nm was recorded after each isomerization (Fig. S37). The solutions for the measurements were prepared in dichloromethane by dilution to *ca.* 10^{-5} M.

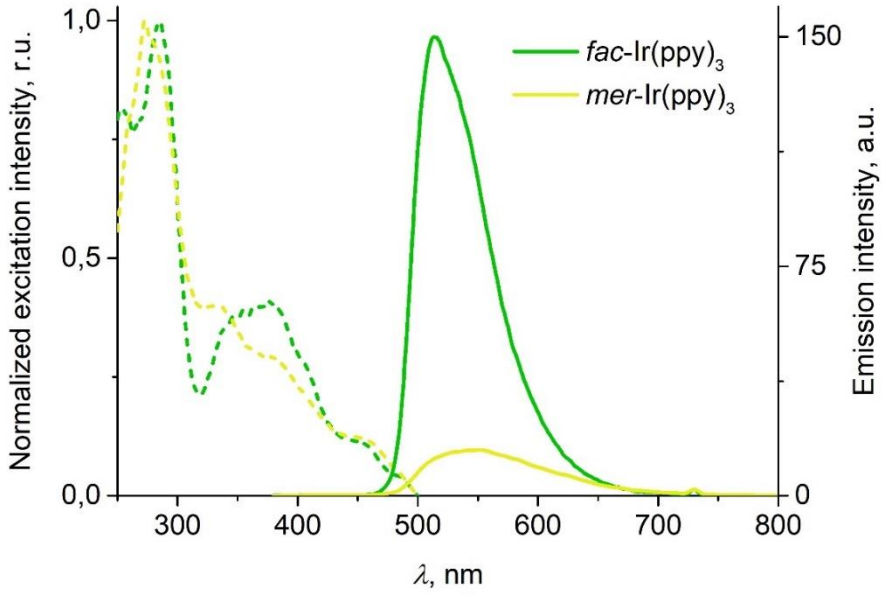

Figure S36. Excitation (dashed lines, @λ_{em}) and emission spectra (solid lines, @365) of Ir(ppy)$_3$ solution during the isomerization from *fac* to *mer*.

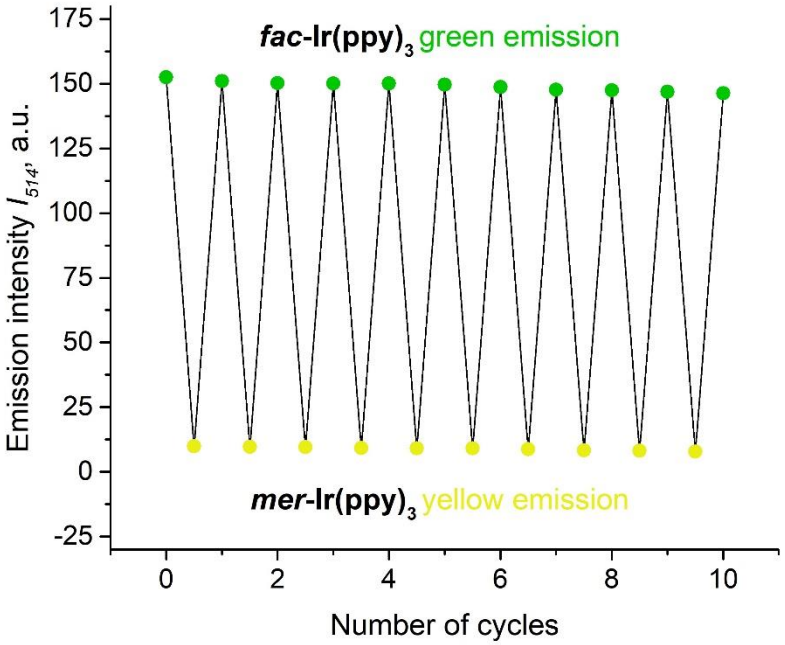

Figure S37. The luminescence intensity at 514 nm of a solution containing Ir(ppy)$_3$ during *fac*↔*mer* isomerization cycles (λ_{ex} = 365 nm).

A simple rewritable data storage device based on $Ir(ppy)_3$

To demonstrate the possibility of using $Ir(C^N)_3$ complexes for rewritable data storage devices, a simple luminescent display based on $Ir(ppy)_3$ was constructed.

A Microseal 384-well black-colored polypropylene-based PCR plate (Bio-Rad Laboratories, Inc.) was used as a matrix. The *fac* isomer of $Ir(ppy)_3$ was dissolved in *o*-dichlorobenzene (1.5 mg/mL) and aliquots of the solutions were pipetted into each well (20 µL per well) (Fig. S38 A). Then, the word “Iridium” was written using a pipette “pen” with TFA (3 µL per well) as the black “ink” (Fig. S38 B). The addition of NEt_3 to the ‘Iridium wells’ (7 µL per well) resulted in an orange emission (Fig. S38 C). Finally, the word was erased by exposure to blue light for 7 h (Fig. S38 D).

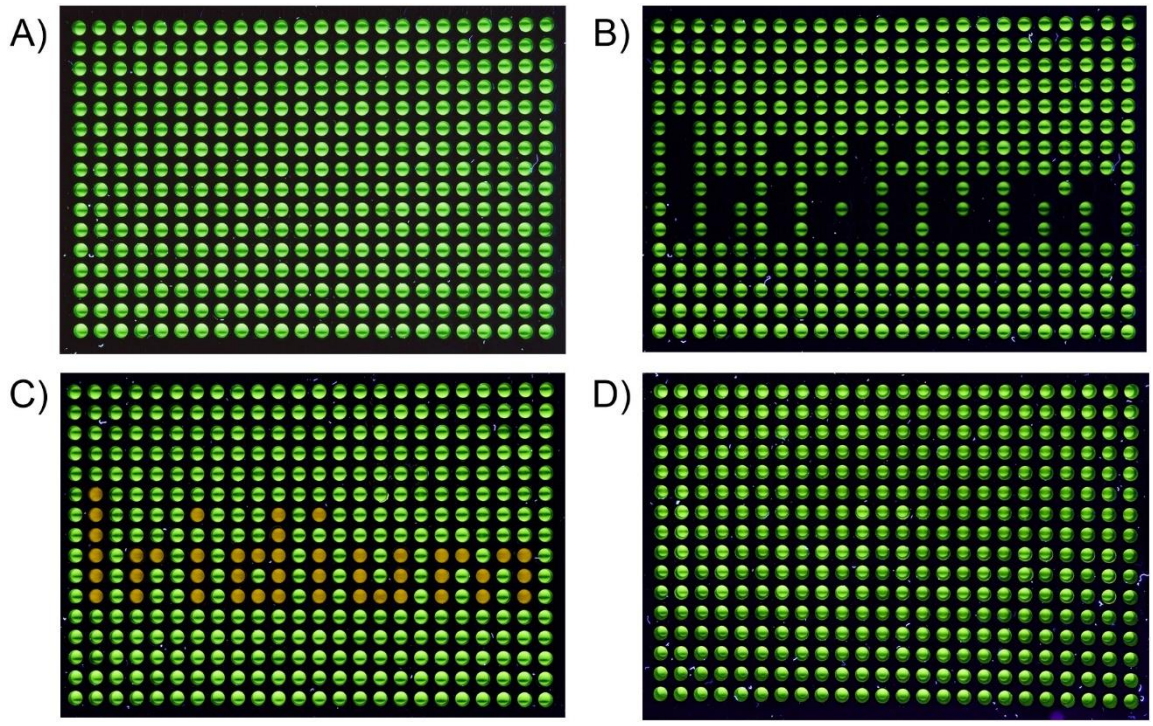

Figure S38. A rewritable luminescent display based on *fac*↔*mer* $Ir(ppy)_3$ isomerization.

A short video showing the isomerization from *fac*- to *mer*-$Ir(ppy)_3$ in the well plate is given as a supporting material.

Ligand exchange control experiment

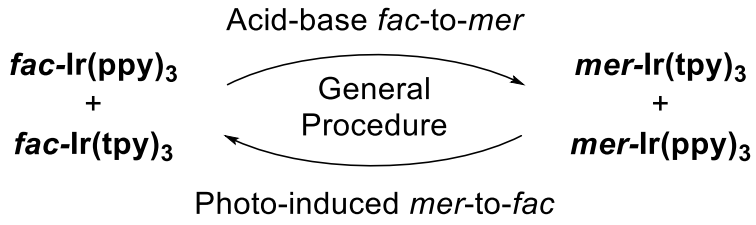

Scheme S5. A *fac*→*mer*→*fac* isomerization of a mixture of ***fac*-Ir(ppy)$_3$** and ***fac*-Ir(tpy)$_3$** using the General Procedure.

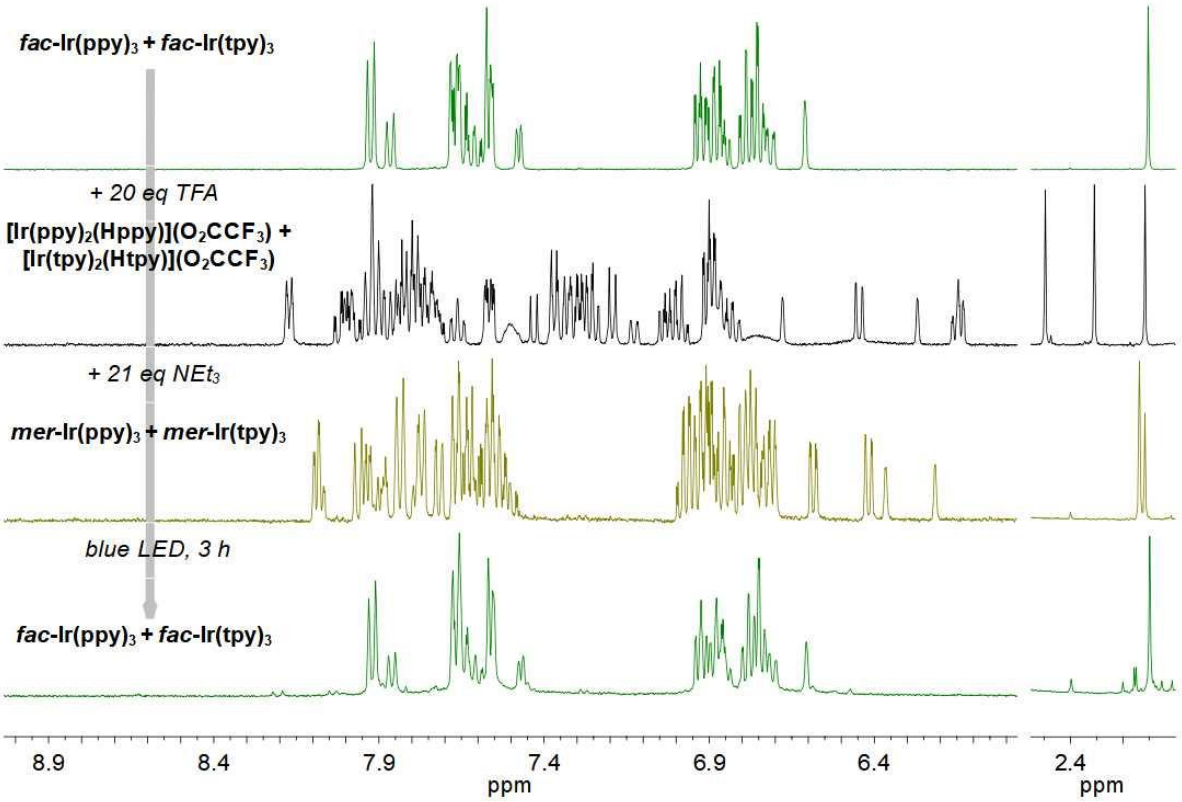

Figure S39. ^{1}H NMR (CD_2Cl_2, 298 K) spectra for the reaction shown in Scheme S5.

The NMR spectrum obtained after irradiation (Fig. S39, bottom) is nearly identical to that of the starting mixture (Figure S39, top), indicating that ligand scrambling during isomerization is negligible.

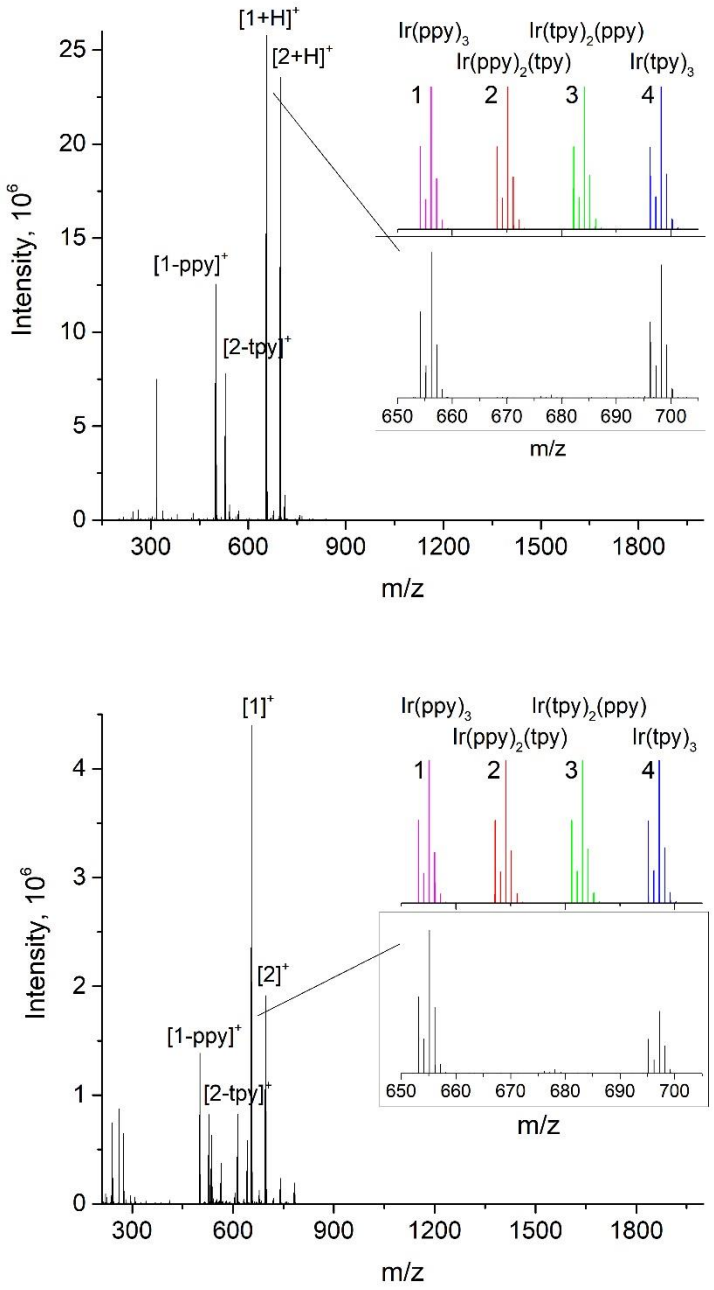

Figure S40. HRMS of the product mixture after the *fac*→*mer* isomerization (ESI$^+$, top), and after the photochemical *mer*→*fac* isomerization (APPI$^+$, bottom). Simulated spectra of the hypothetical heteroleptic complexes are shown in color.

Table S3. HRMS data.

Compound	Formula	*fac*→*mer* (ESI$^+$)		*mer*→*fac* (APPI$^+$)	
		Calcd. $[M+H]^+$	Found	Calcd. $[M]^+$	Found
^{193}Ir(ppy)$_3$	$C_{33}H_{24}IrN_3$	656.1672	656.1687	655.1594	655.1603
^{193}Ir(ppy)$_2$(tpy)	$C_{34}H_{26}IrN_3$	670.1829	*n.f.*	669.1750	*n.f.*
^{193}Ir(tpy)$_2$(ppy)	$C_{35}H_{28}IrN_3$	684.1985	*n.f.*	683.1907	*n.f.*
^{193}Ir(tpy)$_3$	$C_{36}H_{30}IrN_3$	698.2142	698.2153	697.2063	697.2064

Chiral HPLC resolution of Δ and Λ isomers and stereoselectivity of the acid-base *fac*→*mer* and the photochemical *mer*→*fac* isomerizations

The conditions for optical resolution of racemic ***fac*-Ir(ppy)$_3$** and ***mer*-Ir(ppy)$_3$** into their Δ and Λ isomers were found using analytical chiral HPLC by screening the column type (Chiralpak IA, IB, IC, ID, IF) and the ratio of the solvents (hexane/*i*-PrOH from 80:20 to 98:2, v/v). The following conditions were chosen and used for further *ee* analyses: column Chiralpak IA (size 4.6×250 mm, temperature 35 °C), eluent hexane/*i*-PrOH 95:5, injection volume 10 µL, flow 1 mL/min, detection at 254 nm, run time 30 min, sample solution: 2.5 mg/mL in dichloromethane. The HPLC profiles of the racemic ***fac*-Ir(ppy)$_3$** and ***mer*-Ir(ppy)$_3$** are shown in Fig. S41 and Fig. S42, respectively.

For the stereoselectivity studies, racemic ***fac*-Ir(ppy)$_3$** was separated into two enantiomerically enriched samples using preparative chiral HPLC. The following conditions were employed: column Chiralpak IA (size 20×250 mm, temperature 25 °C), eluent hexane/*i*-PrOH 95:5, injection volume 0.5 mL (6 times successively), flow 18 mL/min, detection at 254 nm, run time 45 min, sample solution: 2.5 mg/mL in dichloromethane. The HPLC profiles of the samples are shown in Fig. S43 and Fig. S46. The assignment of the peaks in the chromatogram of the *fac* isomer was made based on the work of X. Chen and co-workers.[14] The 1st eluted enantiomer is ***Δ*-*fac*-Ir(ppy)$_3$** and the 2nd eluted enantiomer is ***Λ*-*fac*-Ir(ppy)$_3$**.

1st eluted: ***Δ*-*fac*-Ir(ppy)$_3$**. 3.4 mg (45%), Δ:Λ = 83:17 (*ee* = 66%), $\tau_{\Delta\text{-}fac} \approx 8.9$ min.

2nd eluted: ***Λ*-*fac*-Ir(ppy)$_3$**. 2.8 mg (37%), Δ:Λ = 30:70 (*ee* = 40%), $\tau_{\Lambda\text{-}fac} \approx 11.3$ min.

The assignment of the peaks in the chromatogram of the *mer* isomer was made based on X-ray crystallography and CD spectroscopy. The 1st eluted enantiomer (96:4, *ee* = 92%) was obtained using preparative chiral HPLC following the conditions described above. Its HPLC profile and CD spectrum are given in Fig. S49 and Fig. S50, respectively. Single crystals of this enantiomer were obtained by slow gas phase diffusion of pentane into a solution of the complex in dichloromethane at room temperature. The absolute configuration was determined by X-ray crystallography as ***Δ*-*mer*-Ir(ppy)$_3$** (Fig. S51, inset). The CD spectra of the measured crystal (Fig. S51) and the whole sample with *ee* = 92% (Fig. S50) showed the same absolute configuration. Thus, the 1st eluted enantiomer was assigned as ***Δ*-*mer*-Ir(ppy)$_3$**, and the 2nd eluted enantiomer was assigned as ***Λ*-*mer*-Ir(ppy)$_3$**.

1st eluted: ***Δ*-*mer*-Ir(ppy)$_3$**. $\tau_{\Delta\text{-}mer} \approx 6.4$ min.

2nd eluted: ***Λ*-*mer*-Ir(ppy)$_3$**. $\tau_{\Lambda\text{-}mer} \approx 8.5$ min.

The enantiomerically enriched samples of ***Δ*-*fac*-Ir(ppy)$_3$** (Δ:Λ = 83:17, *ee* = 66%) and ***Λ*-*fac*-Ir(ppy)$_3$** (Δ:Λ = 30:70, *ee* = 40%) were isomerized to *mer* following the General Procedure. Subsequently, the *mer* isomers were isomerized back to *fac* isomers photochemically. The reactions were followed by analytical chiral HPLC (Fig. S43–48) and CD spectroscopy (Fig S52–54).

It was found that the *fac*→*mer* isomerization proceeds stereoselectively with the same ratio Δ:Λ = 83:17 (Fig. S43 and Fig. S44) for the first sample and Δ:Λ = 30:70 (Fig. S46 and Fig. S47) for the second sample. In turn, the photochemical *mer*→*fac* isomerization proceeds with racemization in both cases (Fig. S45 and Fig. S48). The summary of these results is shown in Scheme S6.

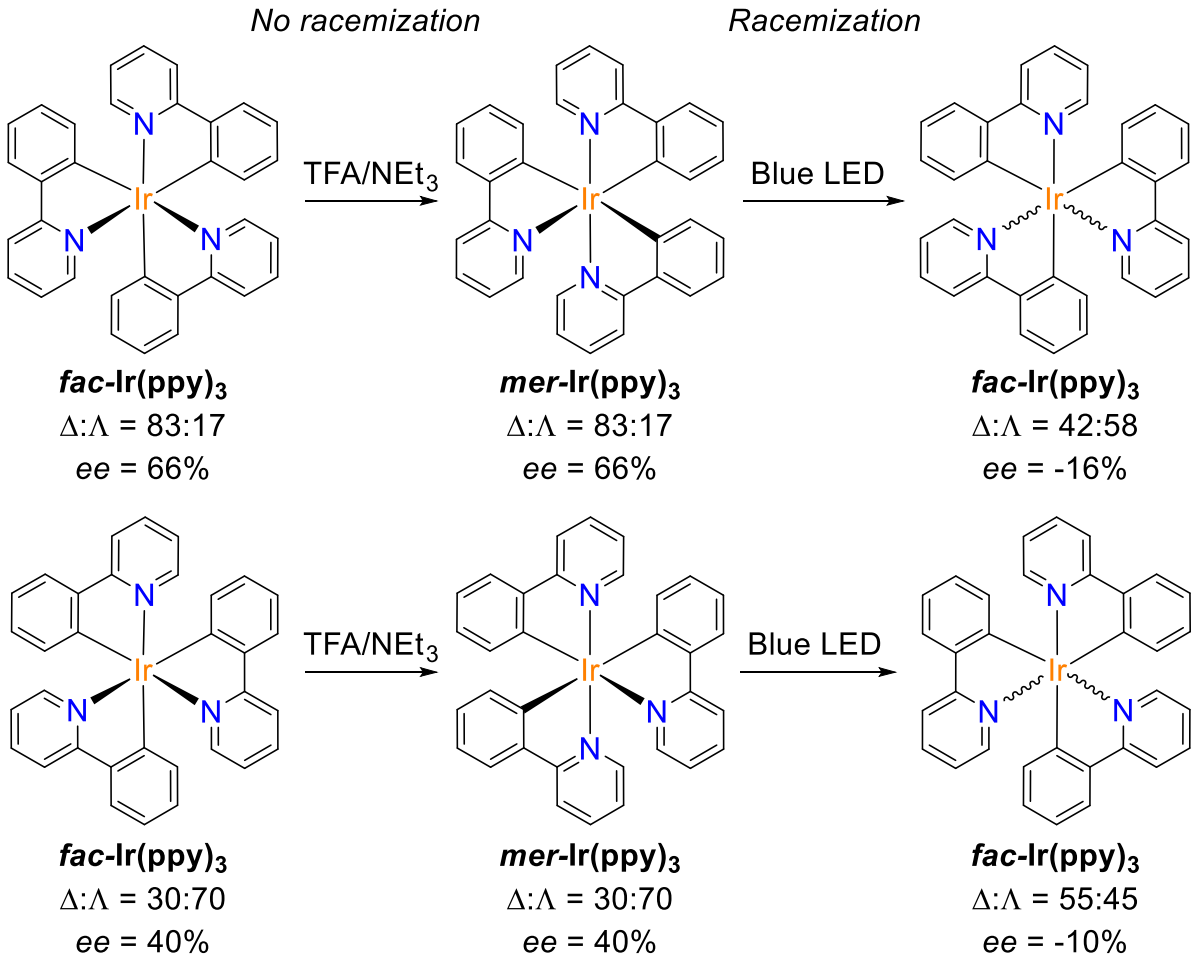

Scheme S6. *fac*→*mer*→*fac* isomerization of two enantiomerically enriched samples of ***fac*-Ir(ppy)$_3$**.

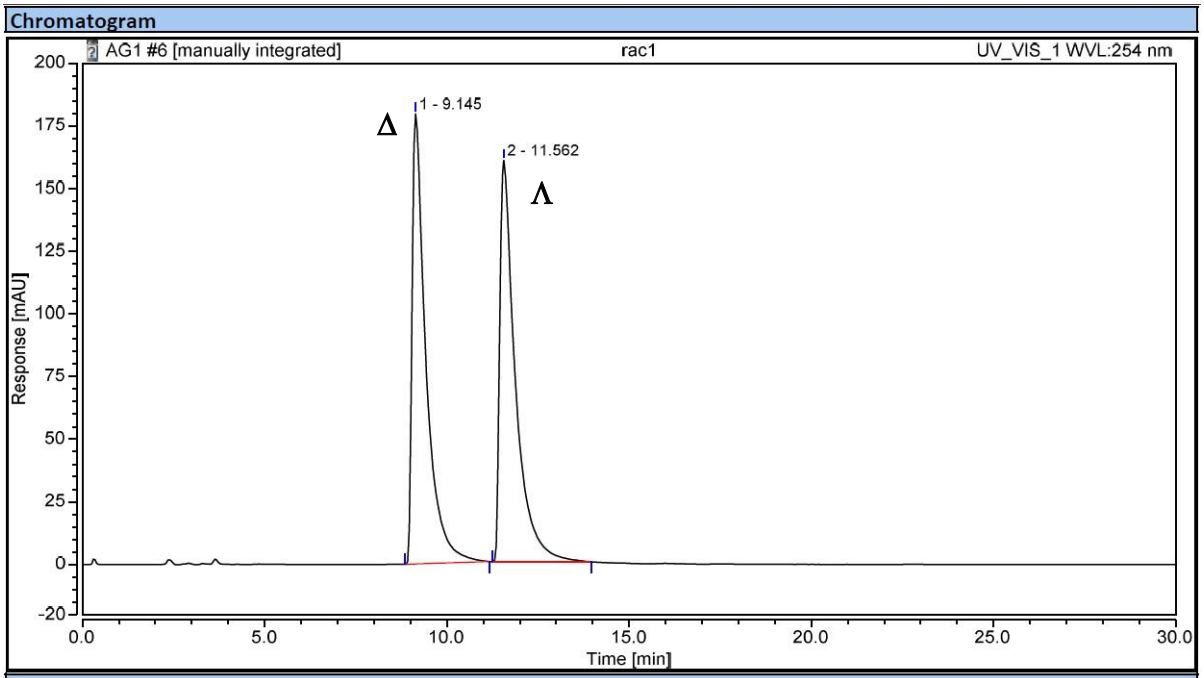

Integration Results

No.	Peak Name	Retention Time min	Area mAU*min	Height mAU	Relative Area %	Relative Height %	Amount n.a.
1		9.145	79.494	179.585	49.99	52.86	n.a.
2		11.562	79.531	160.170	50.01	47.14	n.a.
Total:			**159.025**	**339.755**	**100.00**	**100.00**	

Figure S41. HPLC profile of the racemic ***fac*-Ir(ppy)$_3$**.

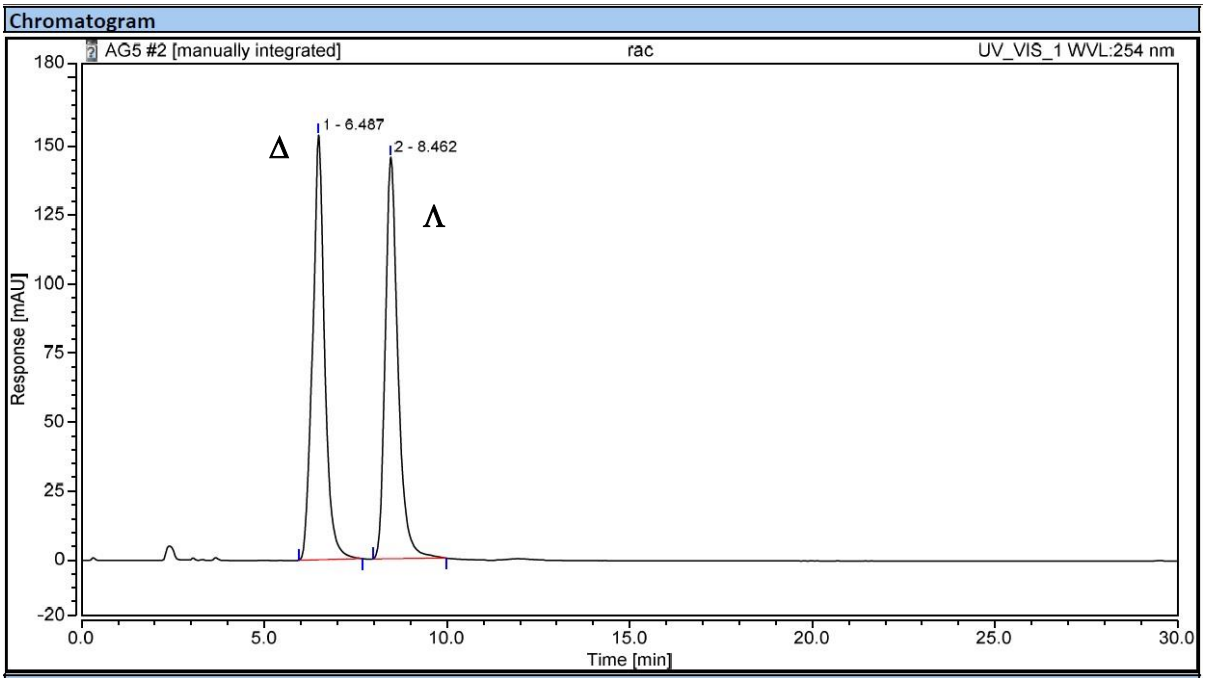

Integration Results

No.	Peak Name	Retention Time min	Area mAU*min	Height mAU	Relative Area %	Relative Height %	Amount n.a.
1		6.487	58.731	153.847	50.01	51.39	n.a.
2		8.462	58.712	145.524	49.99	48.61	n.a.
Total:			**117.443**	**299.372**	**100.00**	**100.00**	

Figure S42. HPLC profile of the racemic ***mer*-Ir(ppy)$_3$**.

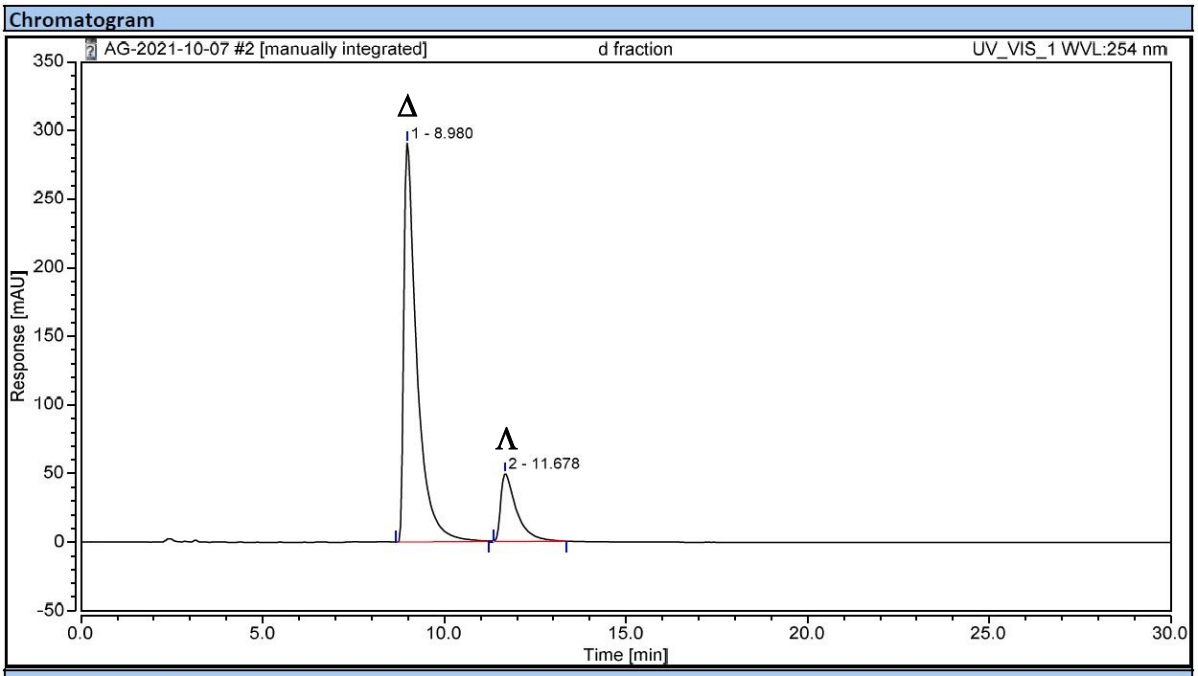

Integration Results

No.	Peak Name	Retention Time min	Area mAU*min	Height mAU	Relative Area %	Relative Height %	Amount n.a.
1		8.980	122.220	290.633	83.11	85.49	n.a.
2		11.678	24.842	49.335	16.89	14.51	n.a.
Total:			**147.062**	**339.968**	**100.00**	**100.00**	

Figure S43. HPLC profile of enantioenriched ***Δ-fac*-Ir(ppy)$_3$** before the *fac*→*mer* isomerization.

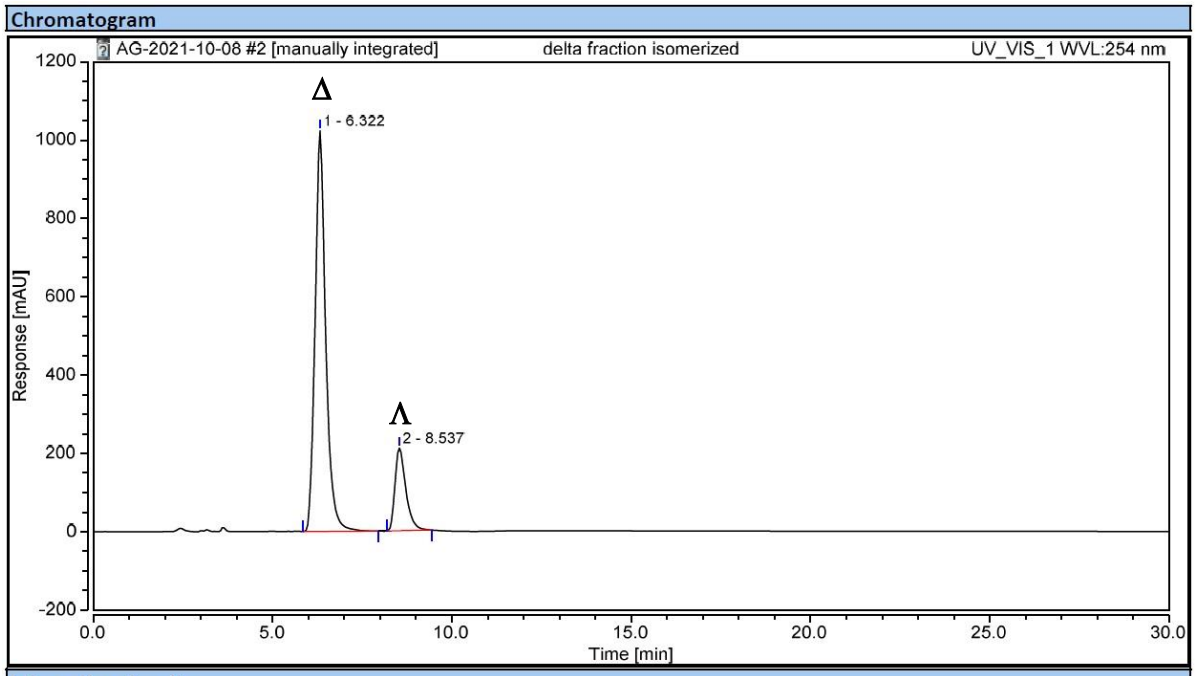

Integration Results

No.	Peak Name	Retention Time min	Area mAU*min	Height mAU	Relative Area %	Relative Height %	Amount n.a.
1		6.322	350.955	1022.611	82.55	82.90	n.a.
2		8.537	74.212	210.960	17.45	17.10	n.a.
Total:			**425.167**	**1233.570**	**100.00**	**100.00**	

Figure S44. HPLC profile of enantioenriched ***Δ-mer*-Ir(ppy)$_3$** obtained in the acid-base *fac*→*mer* isomerization.

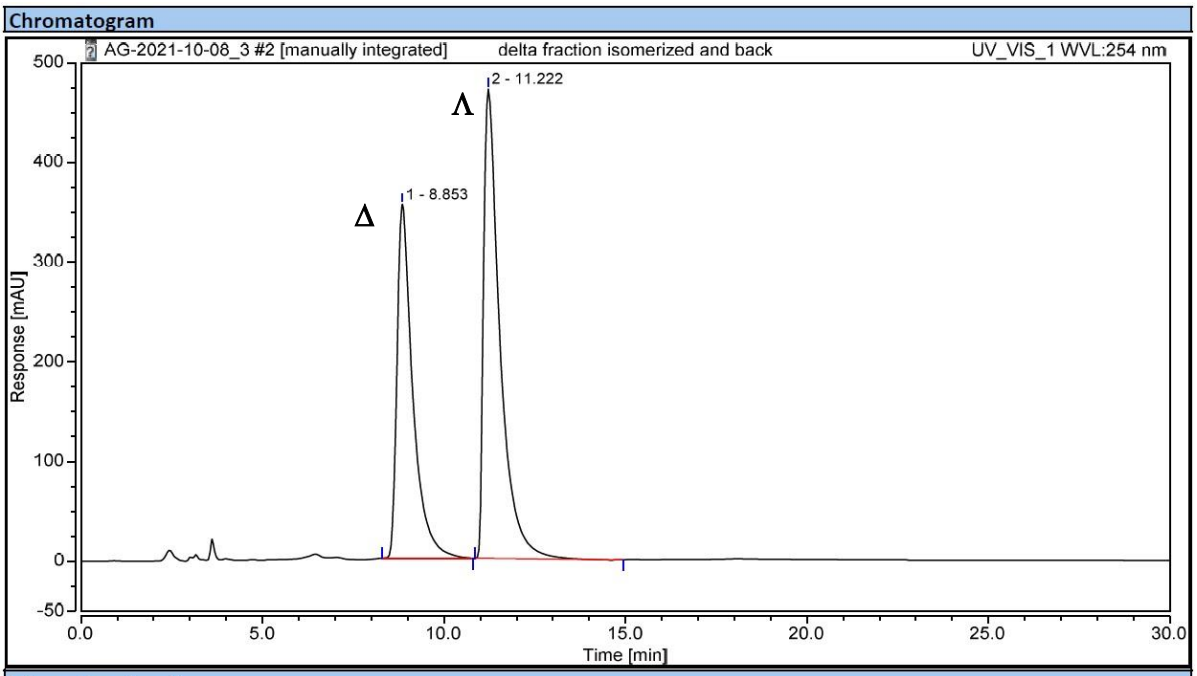

Integration Results

No.	Peak Name	Retention Time min	Area mAU*min	Height mAU	Relative Area %	Relative Height %	Amount n.a.
1		8.853	178.847	354.989	42.02	42.98	n.a.
2		11.222	246.752	470.918	57.98	57.02	n.a.
Total:			**425.599**	**825.907**	**100.00**	**100.00**	

Figure S45. HPLC profile of the mixture after photochemical *mer→fac* isomerization.

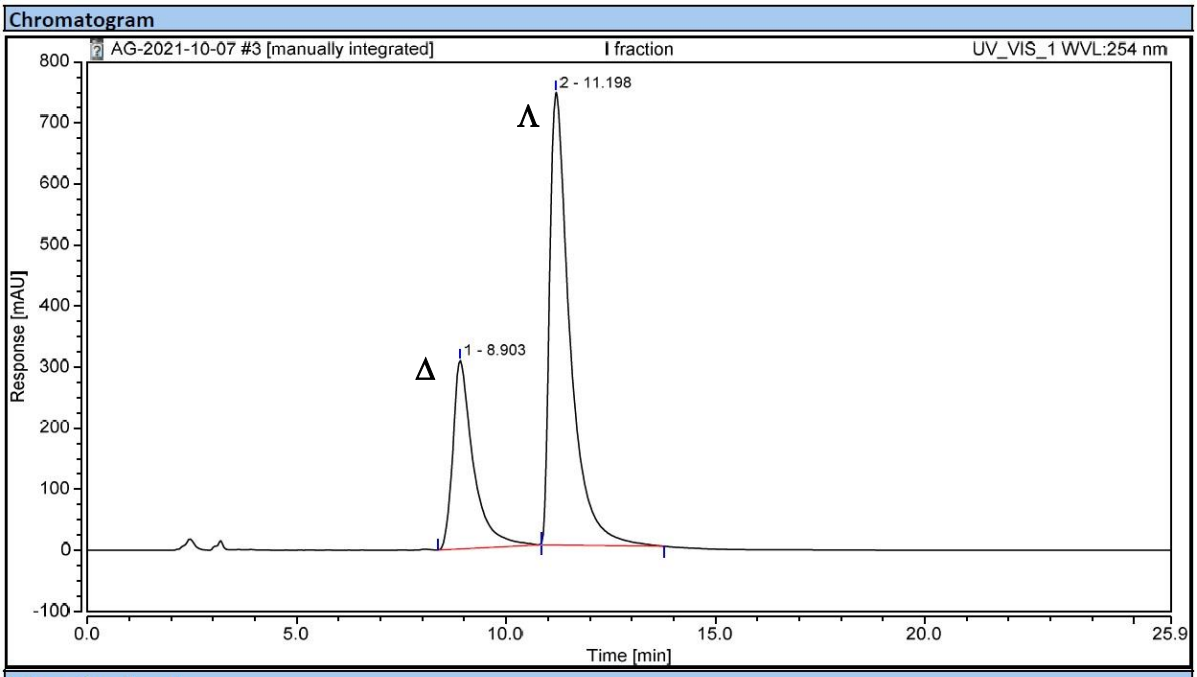

Integration Results

No.	Peak Name	Retention Time min	Area mAU*min	Height mAU	Relative Area %	Relative Height %	Amount n.a.
1		8.903	175.249	308.665	29.52	29.40	n.a.
2		11.198	418.421	741.238	70.48	70.60	n.a.
Total:			**593.671**	**1049.903**	**100.00**	**100.00**	

Figure S46. HPLC profile of enantioenriched ***Λ*-*fac*-Ir(ppy)$_3$** before the *fac→mer* isomerization.

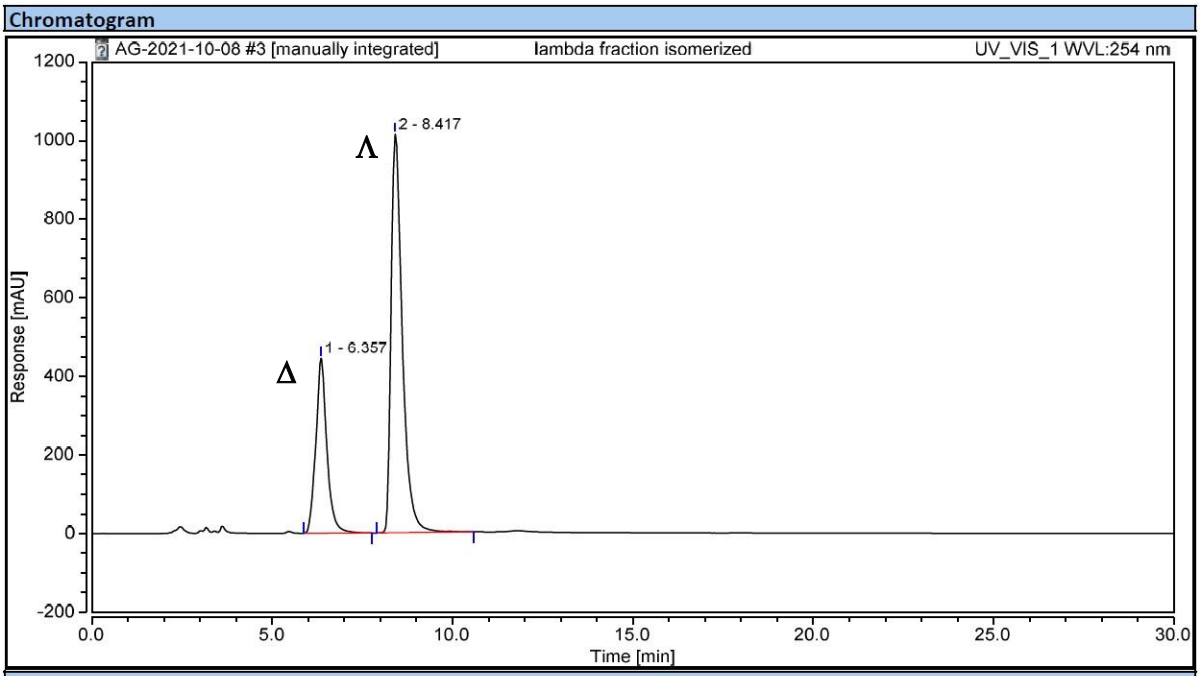

Integration Results

No.	Peak Name	Retention Time min	Area mAU*min	Height mAU	Relative Area %	Relative Height %	Amount n.a.
1		6.357	158.378	445.786	30.20	30.52	n.a.
2		8.417	366.000	1014.711	69.80	69.48	n.a.
Total:			**524.378**	**1460.497**	**100.00**	**100.00**	

Figure S47. HPLC profile of enantioenriched ***Λ-mer*-Ir(ppy)$_3$** obtained in the acid-base *fac*→*mer* isomerization.

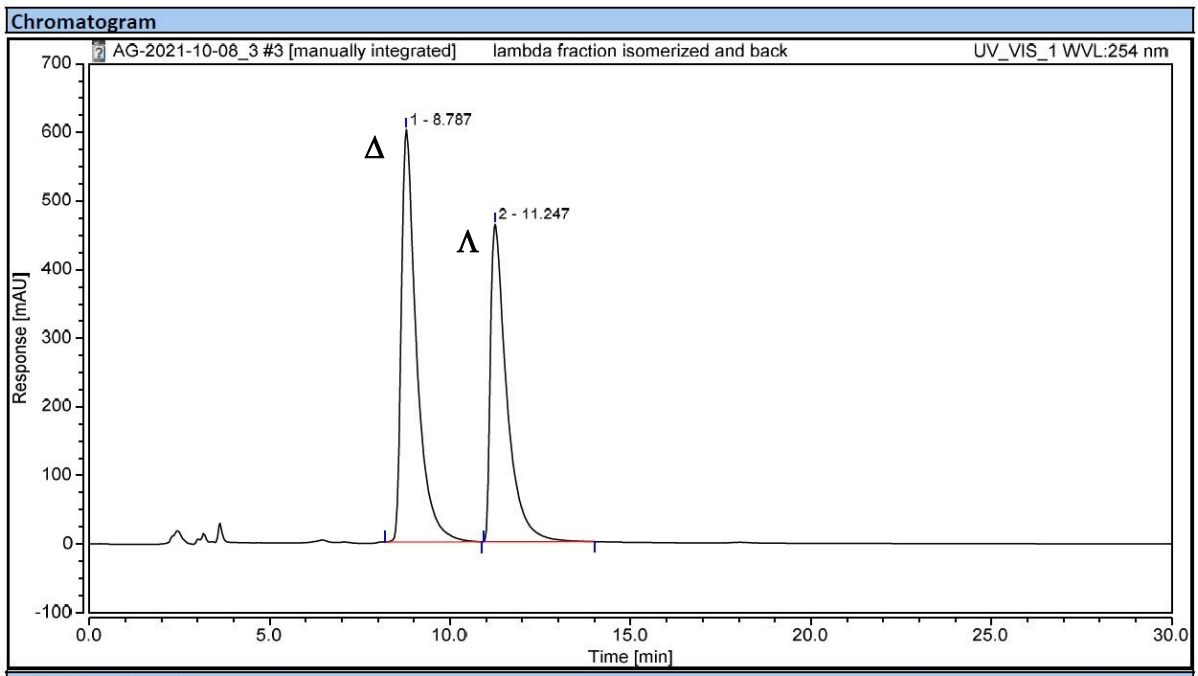

Integration Results

No.	Peak Name	Retention Time min	Area mAU*min	Height mAU	Relative Area %	Relative Height %	Amount n.a.
1		8.787	295.063	601.396	54.86	56.51	n.a.
2		11.247	242.826	462.831	45.14	43.49	n.a.
Total:			**537.889**	**1064.226**	**100.00**	**100.00**	

Figure S48. HPLC profile of the mixture after photochemical *mer*→*fac* isomerization.

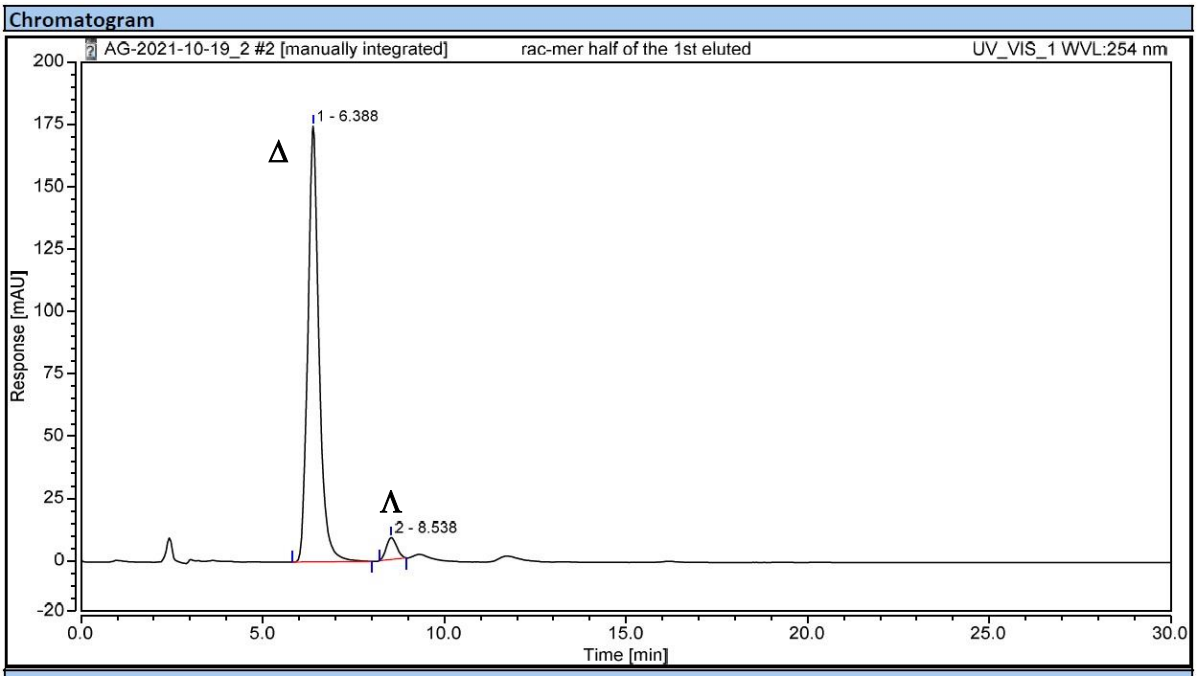

Integration Results

No.	Peak Name	Retention Time min	Area mAU*min	Height mAU	Relative Area %	Relative Height %	Amount n.a.
1		6.388	62.276	174.674	95.56	95.22	n.a.
2		8.538	2.892	8.761	4.44	4.78	n.a.
Total:			**65.168**	**183.435**	**100.00**	**100.00**	

Figure S49. HPLC profile of the 1st eluted enantiomer of ***mer*-Ir(ppy)$_3$**.

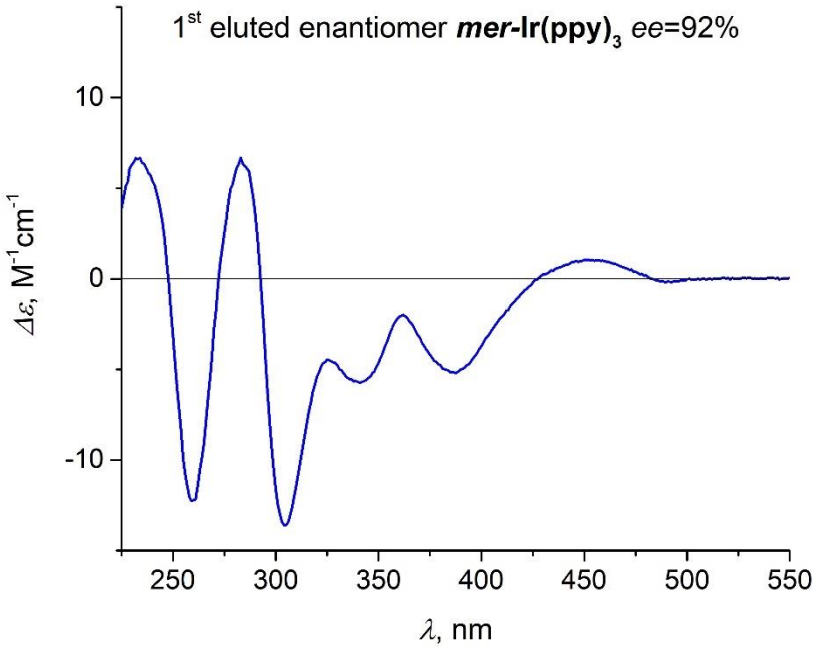

Figure S50. CD spectrum of the 1st eluted enantiomer of ***mer*-Ir(ppy)$_3$**.

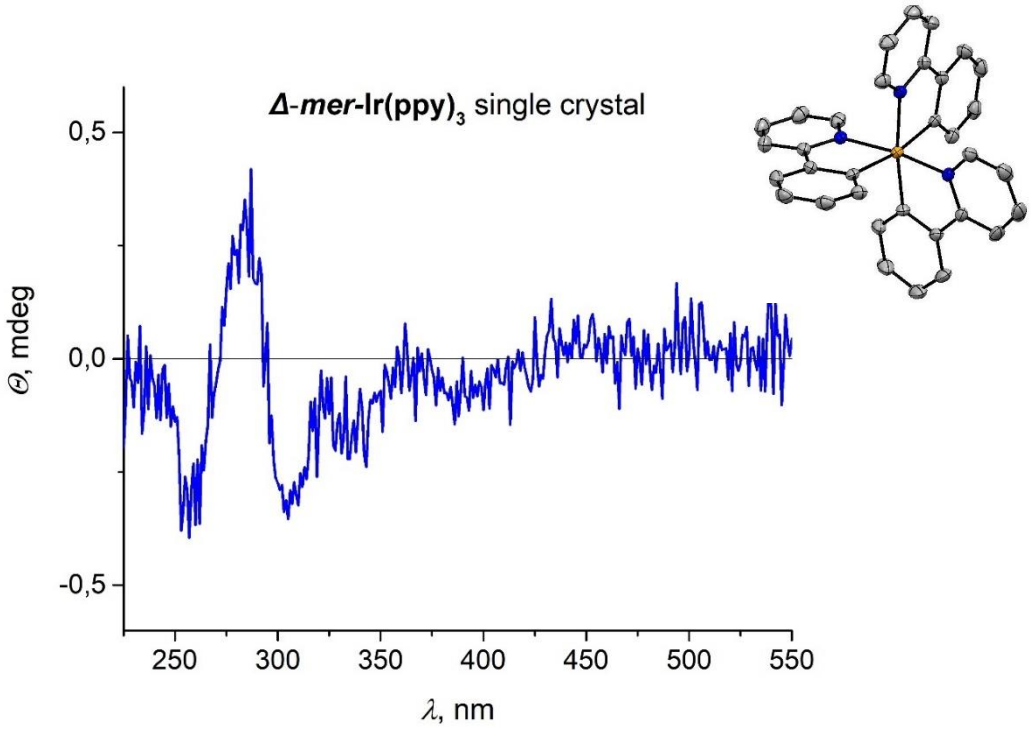

Figure S51. CD spectrum of a solution of the single crystal obtained after crystallization of the 1st eluted enantiomer of ***mer*-Ir(ppy)$_3$** (inset: ORTEP view with 50% probability. Hydrogen atoms are not shown for clarity).

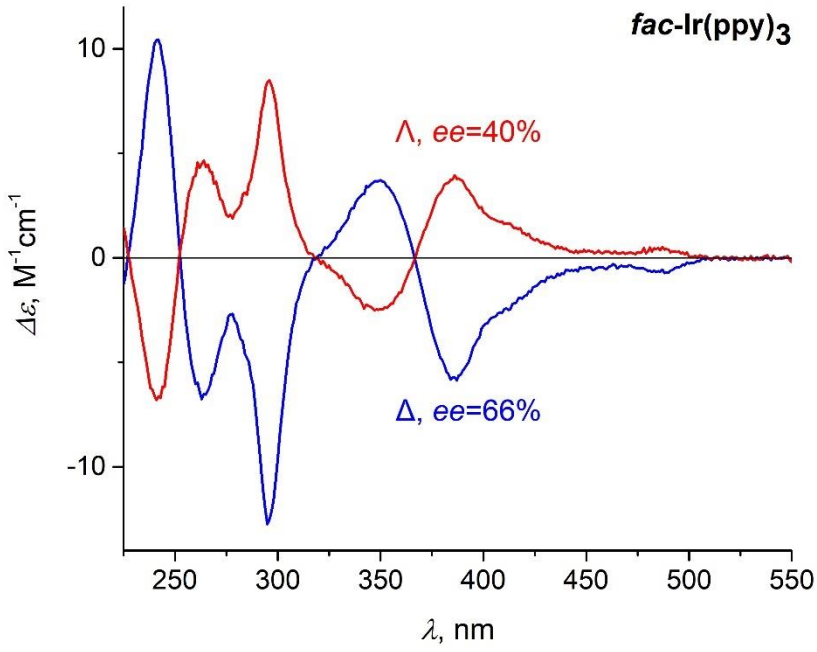

Figure S52. CD spectra of enantioenriched ***Δ*-*fac*-Ir(ppy)$_3$** (blue line) and ***Λ*-*fac*-Ir(ppy)$_3$** (red line) before the *fac*→*mer* isomerization.

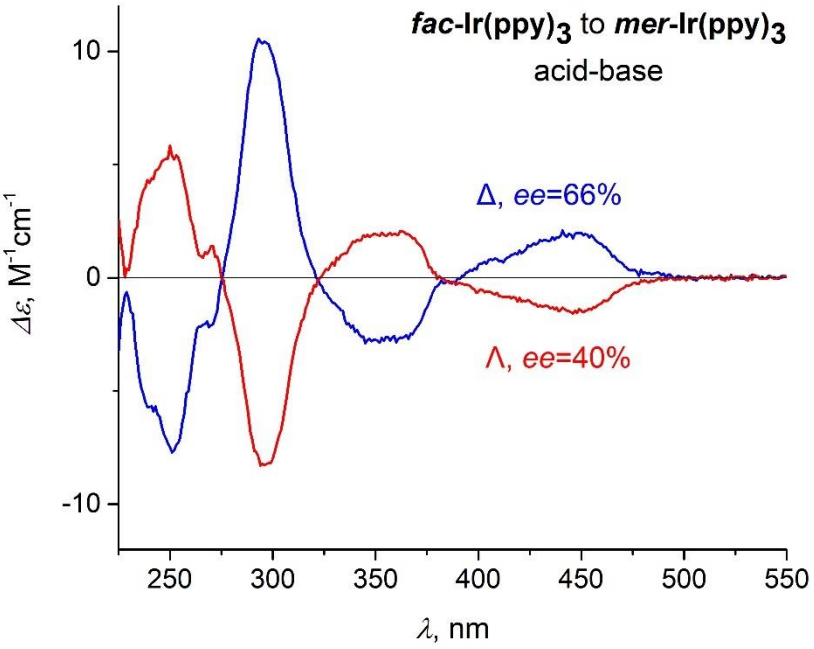

Figure S53. CD spectra of enantioenriched ***Δ*-*mer*-Ir(ppy)$_3$** (blue line) and ***Λ*-*mer*-Ir(ppy)$_3$** (red line) after the *fac*→*mer* isomerization.

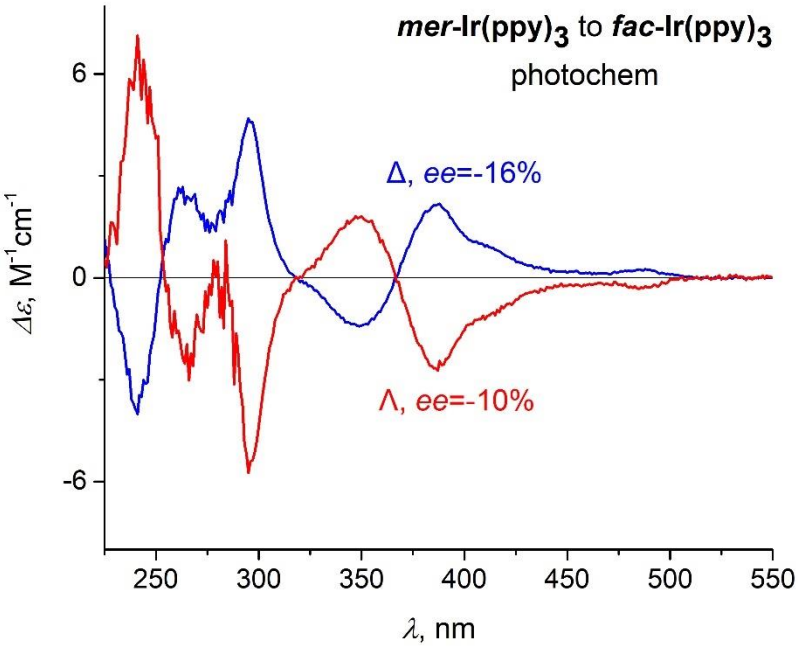

Figure S54. CD spectra of enantioenriched ***Δ*-*fac*-Ir(ppy)$_3$** (blue line) and ***Λ*-*fac*-Ir(ppy)$_3$** (red line) after the photochemical *mer*→*fac* isomerization.

Large-scale synthesis of *mer*-Ir(ppy)$_3$ from *fac*-Ir(ppy)$_3$

***fac*-Ir(ppy)$_3$** (50 mg, 76 µmol) was placed in a 100 mL Schlenk flask equipped with a stirring bar and dissolved under stirring in 20 mL of dichloromethane (*yellow solution with green luminescence when irradiated at 365 nm,* Fig. S55 A). Subsequently, pure TFA (0.5 mL) was added in one portion under mild stirring (350 rpm). The reaction was accompanied by a change of color to greenish-yellow and quenching of the emission (Fig. S55 B). After 1 min of stirring at room temperature, NEt_3 (1 mL) was added dropwise under fast stirring (650 rpm). The reaction was accompanied by a color change back to yellow and a turn-on of the emission (Fig. S55 C). After 1 min of stirring at room temperature, the solvent and the excess of NEt_3 were removed under vacuum. The resulting yellow crystalline precipitate was rinsed with methanol (2×15 mL) and diethyl ether (1×15 mL) to wash away the salt $HNEt_3(O_2CCF_3)$ and dried under vacuum to give ***mer*-Ir(ppy)$_3$** (50 mg, quant.). This procedure can be used for all other complexes mentioned in this work.

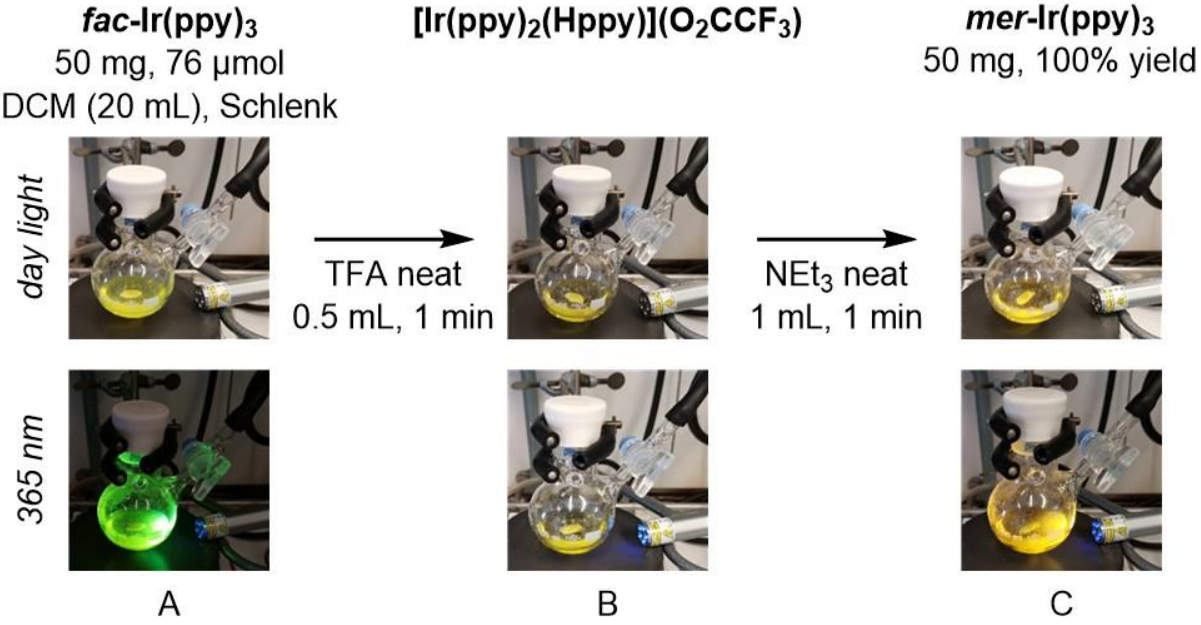

Figure S55. Stepwise visualization of the 50 mg synthesis of ***mer*-Ir(ppy)$_3$** from ***fac*-Ir(ppy)$_3$** through the open form**.** The solution of ***fac*-Ir(ppy)$_3$** in dichloromethane before the addition of TFA (A), the mixture after the addition of TFA (B), and the mixture after the addition of NEt_3 (C).

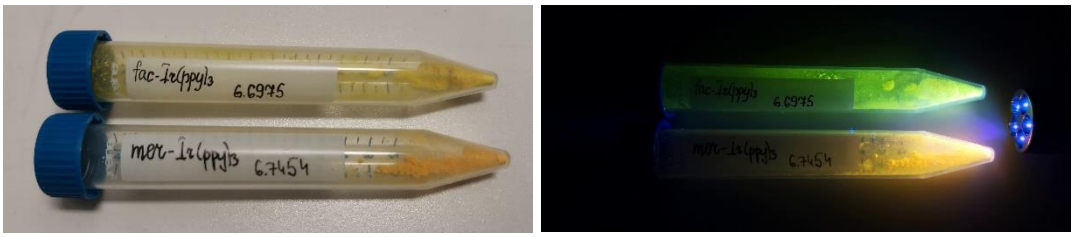

Figure S56. Photo images of starting material ***fac*-Ir(ppy)$_3$** and the product ***mer*-Ir(ppy)$_3$** under daylight (left) and under irradiation at 365 nm (right).

Crystallographic data

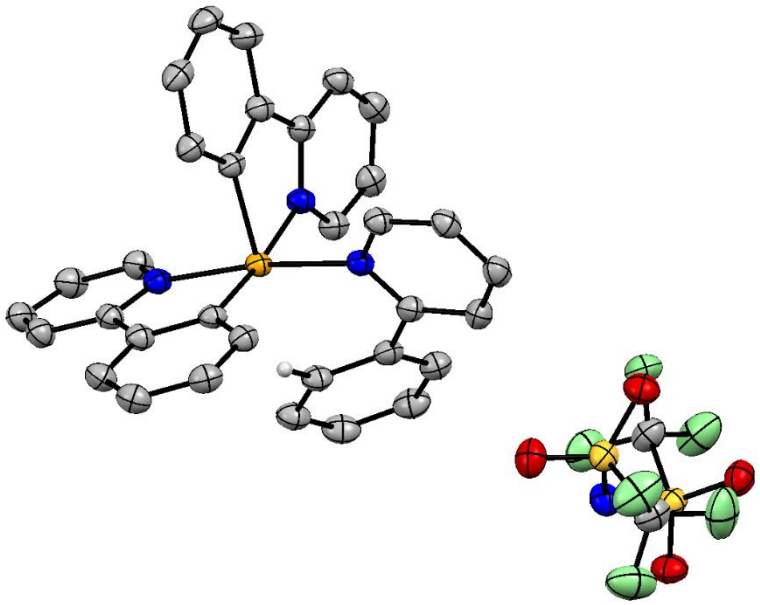

Figure S57. ORTEP view of **[Ir(ppy)$_2$(Hppy)](NTf$_2$)** at the 50% probability level. Most hydrogen atoms are omitted for clarity.

A clear intense yellow hexagonal-shaped crystal with dimensions 0.42×0.28×0.12 mm^3 was mounted. Data were collected using a SuperNova, Dual, Cu at home/near, Atlas diffractometer operating at T = 140.01(10) K.

Data were measured using ω scans using Cu$K\alpha$ radiation. The diffraction pattern was indexed and the total number of runs and images was based on the strategy calculation from the program CrysAlis^{Pro} 1.171.41.110a (CrysAlis^{Pro} Software System, Rigaku Oxford Diffraction, 2021).[15] The maximum resolution that was achieved was Θ = 76.610° (0.79 Å).

The unit cell was refined using CrysAlis^{Pro} 1.171.41.105a on 57568 reflections, 71% of the observed reflections.

Data reduction, scaling and absorption corrections were performed using CrysAlis^{Pro} 1.171.41.105a. The final completeness is 99.90% out to 76.610° in Θ. A gaussian absorption correction was performed using CrysAlis^{Pro} 1.171.41.105a. Numerical absorption correction based on gaussian integration over a multifaceted crystal model Empirical absorption correction using spherical harmonics, implemented in SCALE3 ABSPACK scaling algorithm. The absorption coefficient μ of this material is 9.913 mm^{-1} at this wavelength (λ = 1.54184 Å) and the minimum and maximum transmissions are 0.083 and 0.661.

The structure was solved and the space group $P2_1/c$ (# 14) was determined by the ShelXT 2018/2[16] structure solution program using dual methods and refined by full matrix least squares minimization on F^2 using version 2018/3 of ShelXL 2018/3.[17] All non-hydrogen atoms were refined anisotropically. Hydrogen atom positions were calculated geometrically and refined using the riding model.

The value of *Z'* is 2. This means that there are two independent molecules in the asymmetric unit.

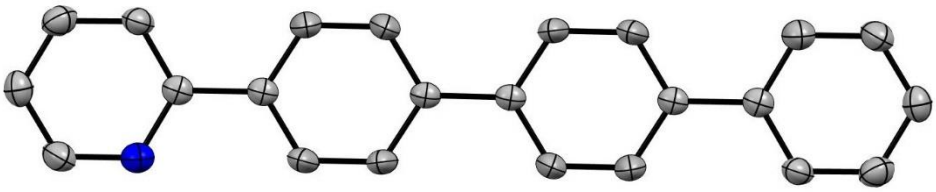

Figure S58. ORTEP view of **Htppy** at the 50% probability level.

A colorless plate-shaped crystal with dimensions 0.32×0.19×0.02 mm^3 was mounted. Data were collected using a SuperNova, Dual, Cu at home/near, Atlas diffractometer operating at T = 150.00(10) K.

Data were measured using ω scans using Cu$K\alpha$ radiation. The diffraction pattern was indexed and the total number of runs and images was based on the strategy calculation from the program CrysAlis^{Pro} 1.171.41.110a (CrysAlis^{Pro} Software System, Rigaku Oxford Diffraction, 2021).[15] The maximum resolution achieved was Θ = 73.999° (0.80 Å).

The unit cell was refined using CrysAlis^{Pro} 1.171.41.110a on 1539 reflections, 28% of the observed reflections.

Data reduction, scaling and absorption corrections were performed using CrysAlis^{Pro} 1.171.41.110a. The final completeness is 99.80 % out to 73.999° in Θ. A Gaussian absorption correction was performed using CrysAlis^{Pro} 1.171.41.110a. Numerical absorption correction based on Gaussian integration over a multifaceted crystal model. Empirical absorption correction using spherical harmonics as implemented in SCALE3 ABSPACK scaling algorithm. The absorption coefficient μ of this material is 0.585 mm^{-1} at this wavelength (λ = 1.54184 Å) and the minimum and maximum transmissions are 0.635 and 1.000.

The structure was solved and the space group $P2_1/c$ (# 14) was determined by the ShelXT 2018/2[16] structure solution program using dual methods and refined by full matrix least squares minimization on F^2 using version 2018/3 of ShelXL 2018/3.[17] All non-hydrogen atoms were refined anisotropically. Hydrogen atom positions were calculated geometrically and refined using the riding model. Due to the presence of inversion center in the structure, atoms C1 and N1 lie on the same positions with the s.o.f of half in the asymmetric unit.

The value of *Z'* is 0.5. This means that only half of the formula unit is present in the asymmetric unit, with the other half consisting of symmetry equivalent atoms.

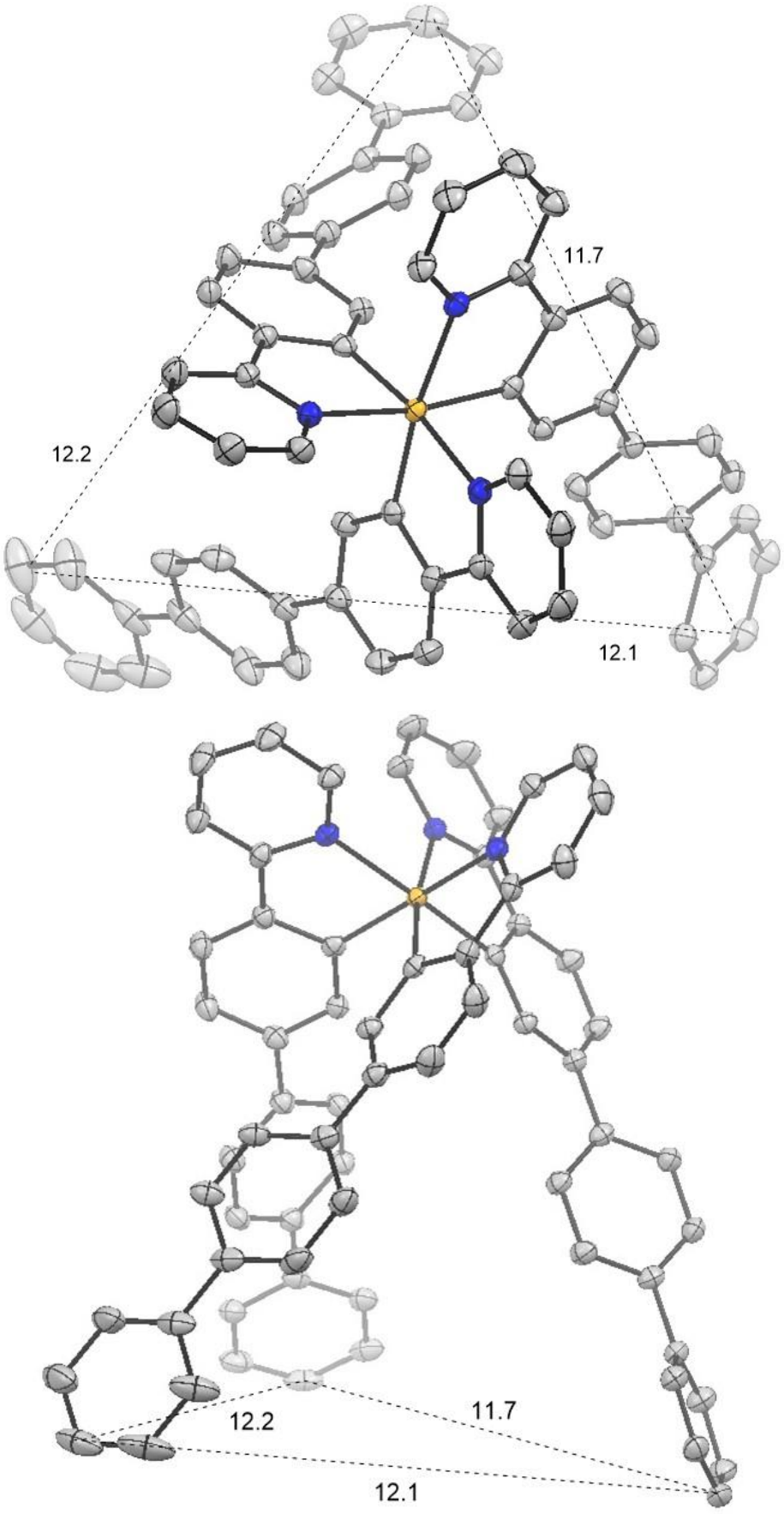

Figure S59. ORTEP views of ***fac*-Ir(tppy)$_3$** with depth cue (50% probability level). Hydrogen atoms are omitted for clarity.

A clear dark orange prism-shaped crystal with dimensions 0.26×0.17×0.04 mm^3 was mounted. Data were collected using a XtaLAB Synergy R, DW system, HyPix–Arc 150 diffractometer operating at T = 139.99(10) K.

Data were measured using ω scans using Cu$K\alpha$ radiation. The diffraction pattern was indexed and the total number of runs and images was based on the strategy calculation from the program CrysAlis^{Pro} 1.171.41.110a (CrysAlis^{Pro} Software System, Rigaku Oxford Diffraction, 2021).[15] The maximum resolution achieved was Θ = 76.166° (0.79 Å).

The unit cell was refined using CrysAlis^{Pro} 1.171.41.110a on 45783 reflections, 82% of the observed reflections.

Data reduction, scaling and absorption corrections were performed using CrysAlis^{Pro} 1.171.41.110a. The final completeness is 99.90 % out to 76.166° in Θ. A Gaussian absorption correction was performed using CrysAlis^{Pro} 1.171.41.110a. Numerical absorption correction based on Gaussian integration over a multifaceted crystal model. Empirical absorption correction using spherical harmonics as implemented in SCALE3 ABSPACK scaling algorithm. The absorption coefficient μ of this material is 6.173 mm^{-1} at this wavelength (λ = 1.54184 Å) and the minimum and maximum transmissions are 0.218 and 1.000.

The structure was solved and the space group $P\bar{1}$ (# 2) was determined by the ShelXT 2018/2[16] structure solution program using dual methods and refined by full matrix least squares minimization on F^2 using version 2018/3 of ShelXL 2018/3.[17] All non–hydrogen atoms were refined anisotropically. Hydrogen atom positions were calculated geometrically and refined using the riding model.

There is a single molecule in the asymmetric unit, which is represented by the reported sum formula. In other words: Z is 2 and Z' is 1.

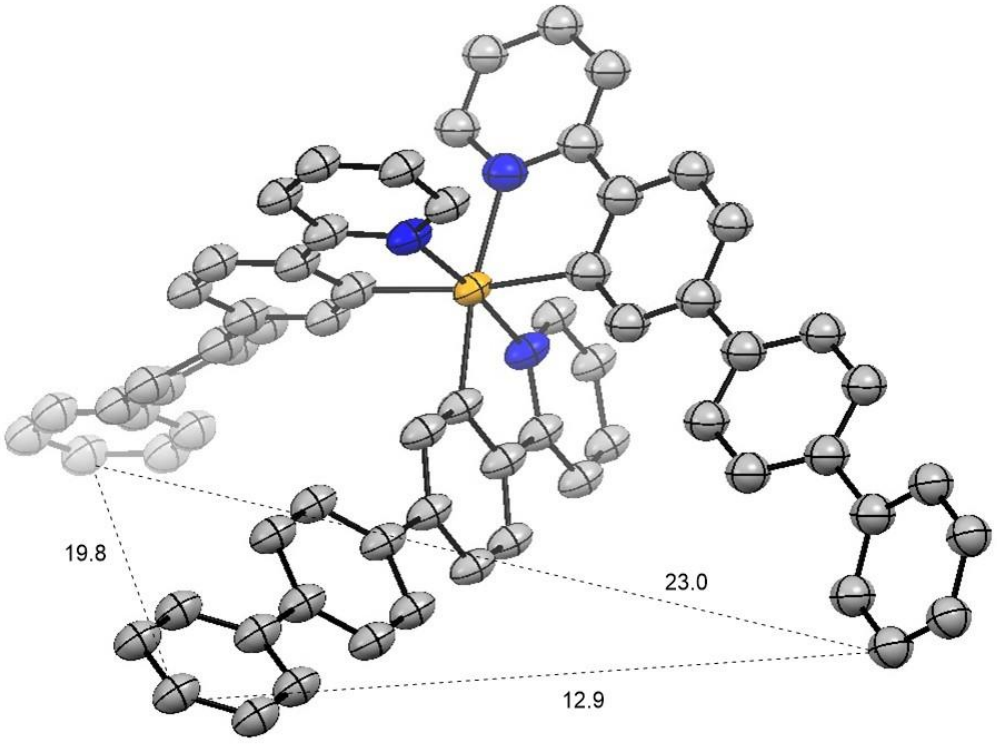

Figure S60. ORTEP view of ***mer*-Ir(tppy)$_3$** with depth cue (25% probability level). Hydrogen atoms are omitted for clarity.

A clear intense orange plate-shaped crystal with dimensions 0.18×0.06×0.01 mm^3 was mounted. Data were collected using a XtaLAB Synergy R, DW system, HyPix-Arc 150 diffractometer operating at T = 139.99(10) K.

Data were measured using ω scans using Cu$K\alpha$ radiation. The diffraction pattern was indexed and the total number of runs and images was based on the strategy calculation from the program CrysAlis^{Pro} 1.171.41.110a (CrysAlis^{Pro} Software System, Rigaku Oxford Diffraction, 2021).[15] The maximum resolution that was achieved was Θ = 75.272° (0.80 Å).

The unit cell was refined using CrysAlis^{Pro} 1.171.41.110a on 25613 reflections, 98% of the observed reflections.

Data reduction, scaling and absorption corrections were performed using CrysAlis^{Pro} 1.171.41.110a. The final completeness is 99.70% out to 75.272° in Θ. A Gaussian absorption correction was performed using CrysAlis^{Pro} 1.171.41.110a. Numerical absorption correction based on Gaussian integration over a multifaceted crystal model. Empirical absorption correction using spherical harmonics as implemented in SCALE3 ABSPACK scaling algorithm. The absorption coefficient μ of this material is 5.255 mm^{-1} at this wavelength (λ = 1.54184 Å) and the minimum and maximum transmissions are 0.425 and 1.000.

The structure was solved, and the space group $P\bar{1}$ (# 2) was determined by the ShelXT 2018/2[16] structure solution program using dual methods and refined by full matrix least squares minimization on F^2 using version 2018/3 of ShelXL 2018/3.[17] All non-hydrogen

atoms were refined anisotropically. Hydrogen atom positions were calculated geometrically and refined using the riding model.

This structure was *r*efined as a 2-component twin.

The value of *Z'* is 2. This means that there are two independent molecules in the asymmetric unit.

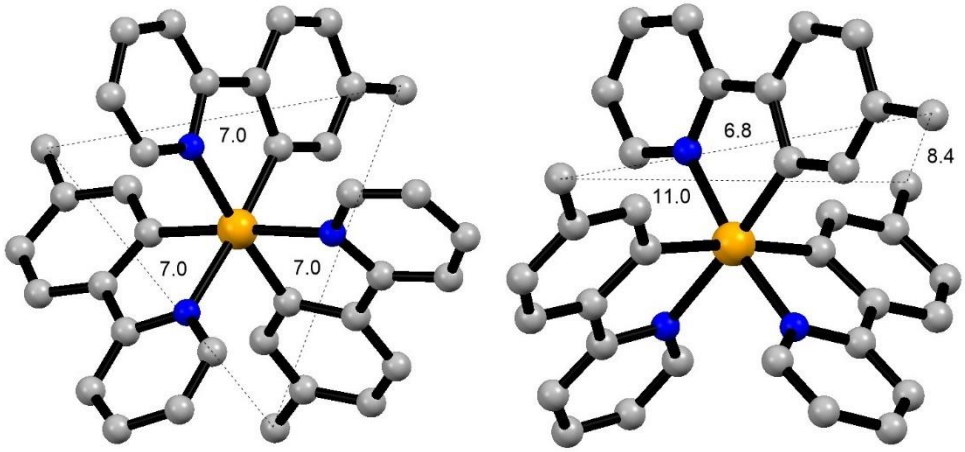

Figure S61. Crystal structures of ***fac*-Ir(tpy)$_3$** (CCDC 215418)[18] and ***mer*-Ir(tpy)$_3$** (CCDC 1290063).[3] Hydrogen atoms are not shown for clarity.

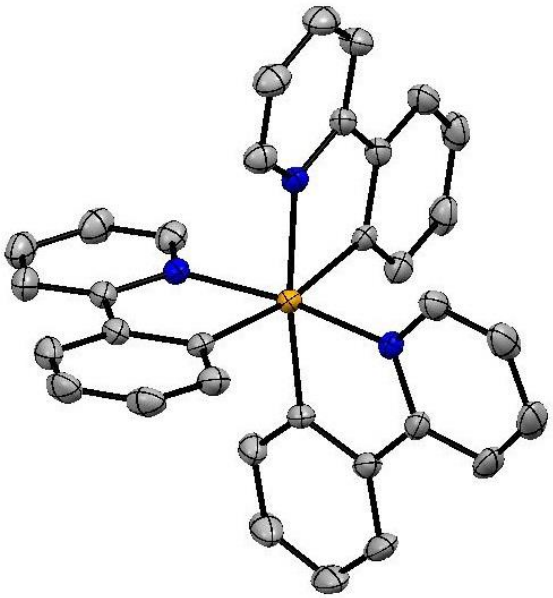

Figure S62. ORTEP view of ***Δ*-*mer*-Ir(ppy)$_3$** at the 50% probability level. Hydrogen atoms are omitted for clarity.

A clear intense orange plate-shaped crystal with dimensions 0.15×0.12×0.03 mm^3 was mounted. Data were collected using a XtaLAB Synergy R, DW system, HyPix-Arc 150 diffractometer operating at T = 140.00(10) K.

Data were measured using ω scans with Mo$K\alpha$ radiation. The diffraction pattern was indexed and the total number of runs and images was based on the strategy calculation from the program CrysAlis^{Pro} 1.171.41.118a (CrysAlis^{Pro} Software System,

Rigaku Oxford Diffraction, 2021).[15] The maximum resolution achieved was Θ = 41.261˚ (0.54 Å).

The unit cell was refined using CrysAlis^{Pro} 1.171.41.118a on 42711 reflections, 43% of the observed reflections.

Data reduction, scaling and absorption corrections were performed using CrysAlis^{Pro} 1.171.41.118a. The final completeness is 100.00 % out to 41.261˚ in Θ. A Gaussian absorption correction was performed using CrysAlis^{Pro} 1.171.41.118a. Numerical absorption correction based on Gaussian integration over a multifaceted crystal model. Empirical absorption correction using spherical harmonics as implemented in SCALE3 ABSPACK scaling algorithm. The absorption coefficient μ of this material is 4.643 mm^{-1} at this wavelength (λ = 0.71073Å) and the minimum and maximum transmissions are 0.593 and 1.000.

The structure was solved and the space group $P4_12_12$ (# 92) was determined by the ShelXT 2018/2[16] structure solution program using dual methods and refined by full matrix least squares minimization on $\boldsymbol{F^2}$ using version 2018/3 of **ShelXL** 2018/3.[17] All non-hydrogen atoms were refined anisotropically. Hydrogen atom positions were calculated geometrically and refined using the riding model.

This structure was *r*efined as a 2-component inversion twin.

The value of *Z'* is 0.5. This means that only half of the formula unit is present in the asymmetric unit, with the other half consisting of symmetry equivalent atoms.

The Flack parameter was refined to 0.070(11). Determination of absolute structure using Bayesian statistics on Bijvoet differences using the Olex2 results in Note.

Note: The Flack parameter is used to determine chirality of the crystal studied, the value should be near 0, a value of 1 means that the stereochemistry is wrong, and the model should be inverted. A value of 0.5 means that the crystal consists of a racemic mixture of the two enantiomers.

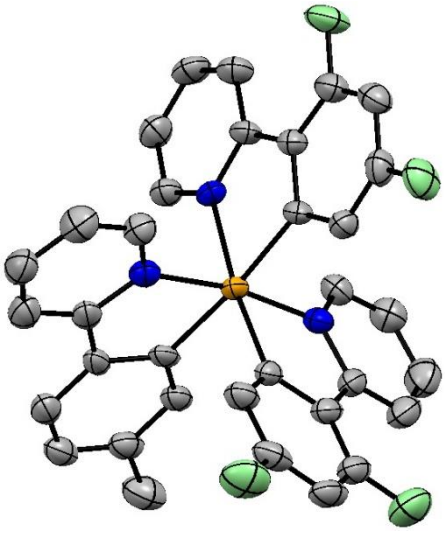

Figure S63. ORTEP view of ***mer*-Ir(dfppy)$_2$(tpy)** at the 50% probability level. Hydrogen atoms are omitted for clarity.

A clear intense yellow plate-shaped crystal with dimensions 0.16×0.15×0.01 mm^3 was mounted. Data were collected using a XtaLAB Synergy R, DW system, HyPix-Arc 150 diffractometer operating at T = 140.00(10) K.

Data were measured using ω scans with Cu$K\alpha$ radiation. The diffraction pattern was indexed and the total number of runs and images was based on the strategy calculation from the program CrysAlis^{Pro} 1.171.41.120a (CrysAlis^{Pro} Software System, Rigaku Oxford Diffraction, 2021).[15] The maximum resolution achieved was Θ = 75.533° (0.80 Å).

The unit cell was refined using CrysAlis^{Pro} 1.171.41.120a on 20871 reflections, 46% of the observed reflections.

Data reduction, scaling and absorption corrections were performed using CrysAlis^{Pro} 1.171.41.120a. The final completeness is 100.00 % out to 75.533° in Θ. A Gaussian absorption correction was performed using CrysAlis^{Pro} 1.171.41.120a. Numerical absorption correction based on Gaussian integration over a multifaceted crystal model. Empirical absorption correction using spherical harmonics as implemented in SCALE3 ABSPACK scaling algorithm. The absorption coefficient μ of this material is 10.238 mm^{-1} at this wavelength (λ = 1.54184 Å) and the minimum and maximum transmissions are 0.218 and 1.000.

The structure was solved, and the space group *C*2/*c* (# 15) was determined by the ShelXT 2018/2[16] structure solution program using dual methods and refined by full matrix least squares minimization on F^2 using version 2018/3 of ShelXL 2018/3.[17] All non-hydrogen atoms were refined anisotropically. Hydrogen atom positions were calculated geometrically and refined using the riding model.

There is a single molecule in the asymmetric unit, which is represented by the reported sum formula. In other words: *Z* is 8 and *Z'* is 1.

Table S4. Crystallographic data of the compounds.

Compound	**[Ir(ppy)$_2$(Hppy)](NTf$_2$)**	**Htppy**	***fac*-Ir(tppy)$_3$**
Formula	$C_{35.5}H_{26}ClF_6IrN_4O_4S_2$	$C_{23}H_{17}N$	$C_{70}H_{50}Cl_2IrN_3$
Formula Weight	978.37	307.38	1196.23
$D_{calc.}$, g cm^{-3}	1.858	1.327	1.501
μ, mm^{-1}	9.913	0.585	6.173
Colour	intense yellow	colorless	dark orange
Shape	hexagonal	plate	prism
Size, mm^3	0.42×0.28×0.12	0.32×0.19×0.02	0.26×0.17×0.04
T, K	140.01(10)	150.00(10)	139.99(10)
Crystal System	monoclinic	monoclinic	triclinic
Space Group	$P2_1/c$	$P2_1/c$	$P\bar{1}$
a, Å	27.8756(2)	17.7468(11)	13.85396(12)
b, Å	12.70840(9)	5.5397(4)	14.21567(12)
c, Å	20.40752(14)	7.8676(5)	14.60645(14)
α, °	90	90	100.2746(8)
β, °	104.6080(7)	95.986(6)	100.6552(8)
γ, °	90	90	105.2857(7)
V, Å^3	6995.75(9)	769.26(8)	2647.62(4)
Z	8	2	2
Z'	2	0.5	1
λ, Å	1.54184	1.54184	1.54184
Radiation type	Cu$K\alpha$	Cu$K\alpha$	Cu$K\alpha$
Θ_{min}, °	3.845	5.012	3.171
Θ_{max}, °	76.610	73.999	76.166
Measured Refl.	81444	5478	56071
Independent Refl.	14600	1527	10852
Refl. $I \geq 2\sigma(I)$	14192	1032	10760
R_{int}	0.0383	0.0430	0.0184
Parameters	964	109	704
Restraints	0	0	43
Largest Peak, e Å^{-3}	1.564	0.469	0.439
Deepest Hole, e Å^{-3}	–1.299	–0.213	–0.664
GooF	1.082	1.049	1.067
wR_2 (all data)	0.0761	0.2065	0.0402
wR_2	0.0754	0.1775	0.0401
R_1 (all data)	0.0299	0.0857	0.0163
R_1	0.0290	0.0612	0.0161
CCDC number	**2101920**	**2102440**	**2096259**

Compound	***mer*-Ir(tppy)$_3$**	***Δ*-*mer*-Ir(ppy)$_3$**	***mer*-Ir(dfppy)$_2$(tpy)**
Formula	$C_{69}H_{48}IrN_3$	$C_{33}H_{24}IrN_3$	$C_{34}H_{22}F_4IrN_3$
Formula Weight	1111.30	654.75	1.852
$D_{calc.}$, g cm^{-3}	1.402	1.504	10.238
μ, mm^{-1}	5.255	4.643	740.74
Colour	intense orange	intense orange	intense yellow
Shape	plate	plate	plate
Size, mm^3	0.18×0.06×0.01	0.15×0.12×0.03	0.16×0.15×0.01
T, K	139.99(10)	140.00(10)	140.00(10)
Crystal System	triclinic	tetragonal	monoclinic
Space Group	$P\bar{1}$	$P4_12_12$	$C2/c$
a, Å	18.0800(5)	9.72023(11)	33.9701(5)
b, Å	18.3585(7)	9.72023(11)	8.77822(19)
c, Å	19.0127(7)	30.5949(5)	18.0310(3)
α, °	68.335(3)	90	90
β, °	85.431(3)	90	98.8980(14)
γ, °	64.368(3)	90	90
V, Å^3	5263.6(3)	2890.70(8)	5312.07(16)
Z	4	4	8
Z'	2	0.5	1
λ, Å	1.54184	0.71073	1.54184
Radiation type	Cu$K\alpha$	Mo$K\alpha$	Cu$K\alpha$
Θ_{min}, °	2.512	2.198	2.633
Θ_{max}, °	75.272	41.261	75.533
Measured Refl.	26115	99418	45625
Independent Refl.	26115	8678	5386
Refl. $I \geq 2\sigma(I)$	15824	6667	4613
R_{int}	*n/a*	0.0786	0.0556
Parameters	1028	169	381
Restraints	2270	1	0
Largest Peak, e Å^{-3}	5.309	1.810	2.376
Deepest Hole, e Å^{-3}	–2.857	–2.757	-2.012
GooF	1.402	1.043	1.057
wR_2 (all data)	0.3936	0.0720	0.1133
wR_2	0.3576	0.0687	0.1092
R_1 (all data)	0.1771	0.0594	0.0503
R_1	0.1321	0.0357	0.0424
CCDC number	**2102439**	**2118152**	**2122690**
Flack parameter	–	0.070(11)	–

NMR spectra

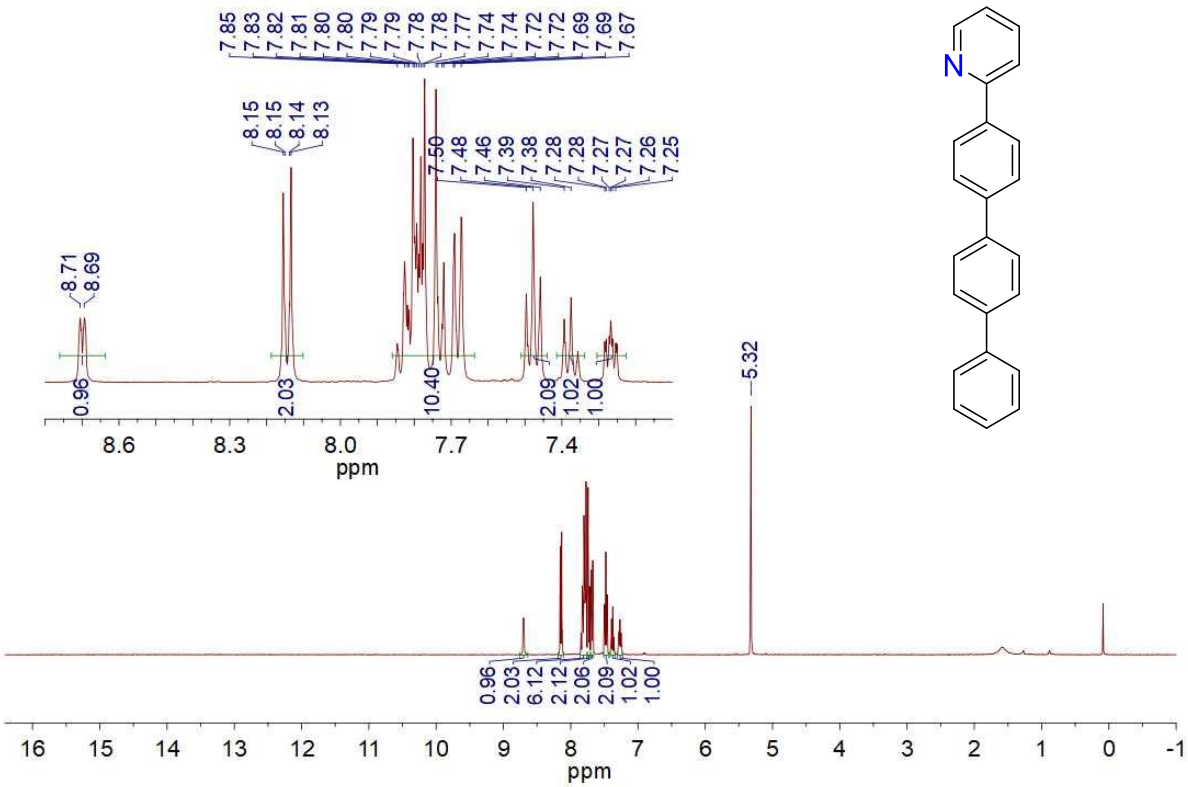

^{1}H NMR (400 MHz, CD_2Cl_2, 298 K) spectrum of **Htppy**

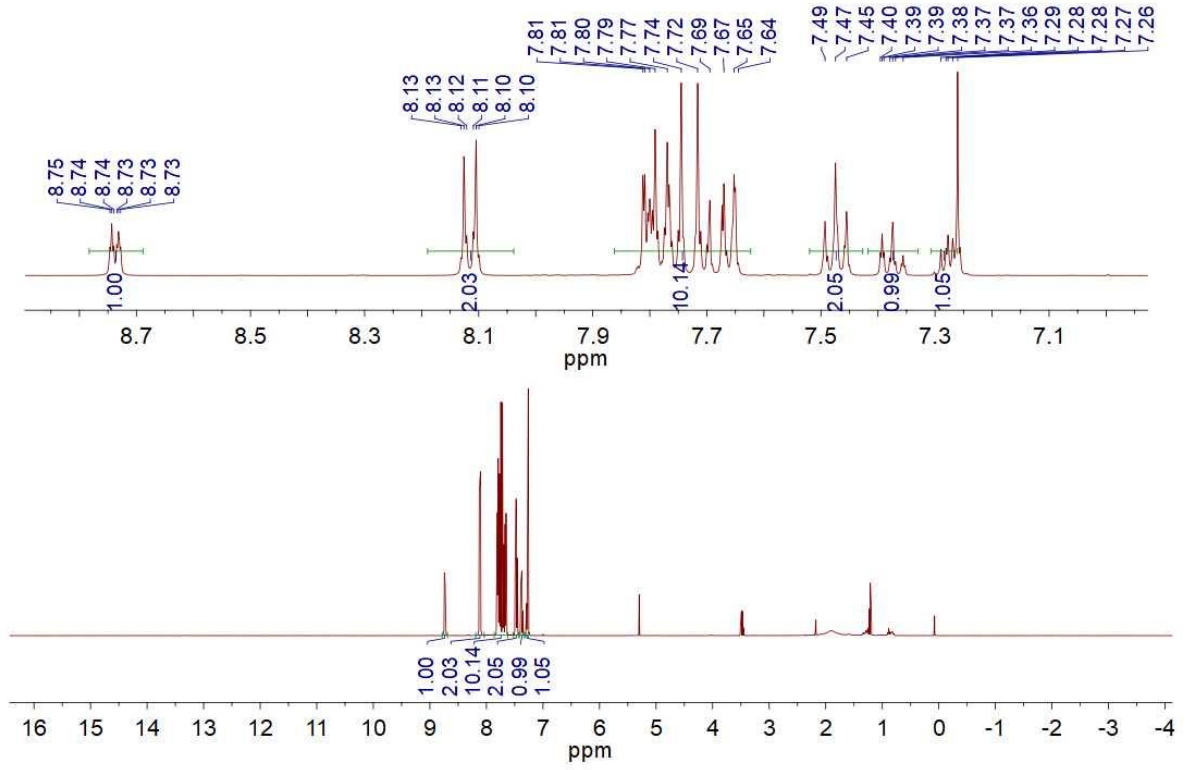

^{1}H NMR (400 MHz, $CDCl_3$, 298 K) spectrum of **Htppy**

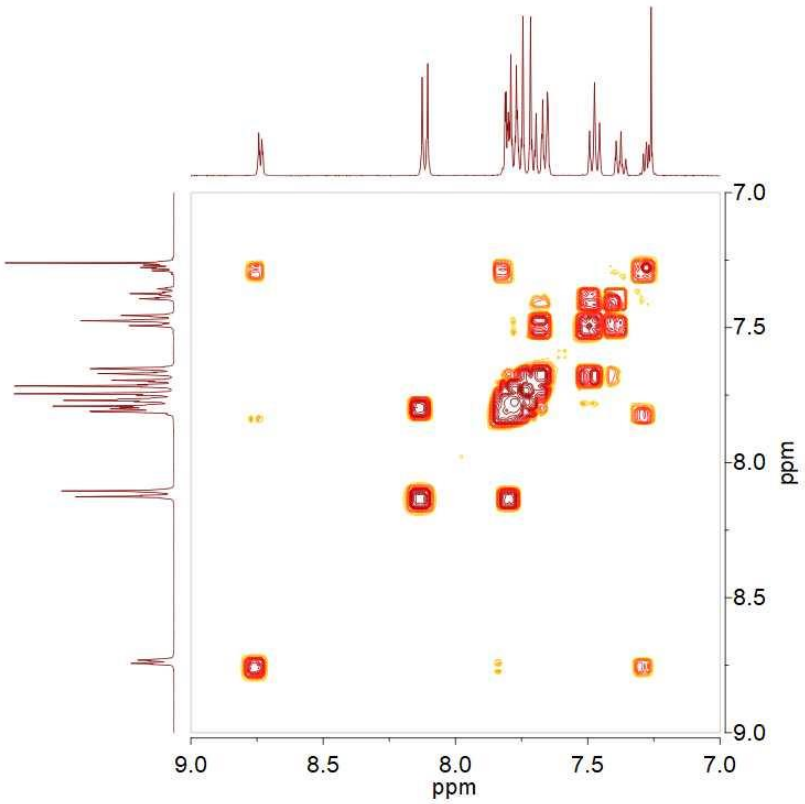

$^{1}H–^{1}H$ COSY NMR (400 MHz, $CDCl_3$, 298 K) spectrum of **Htppy**

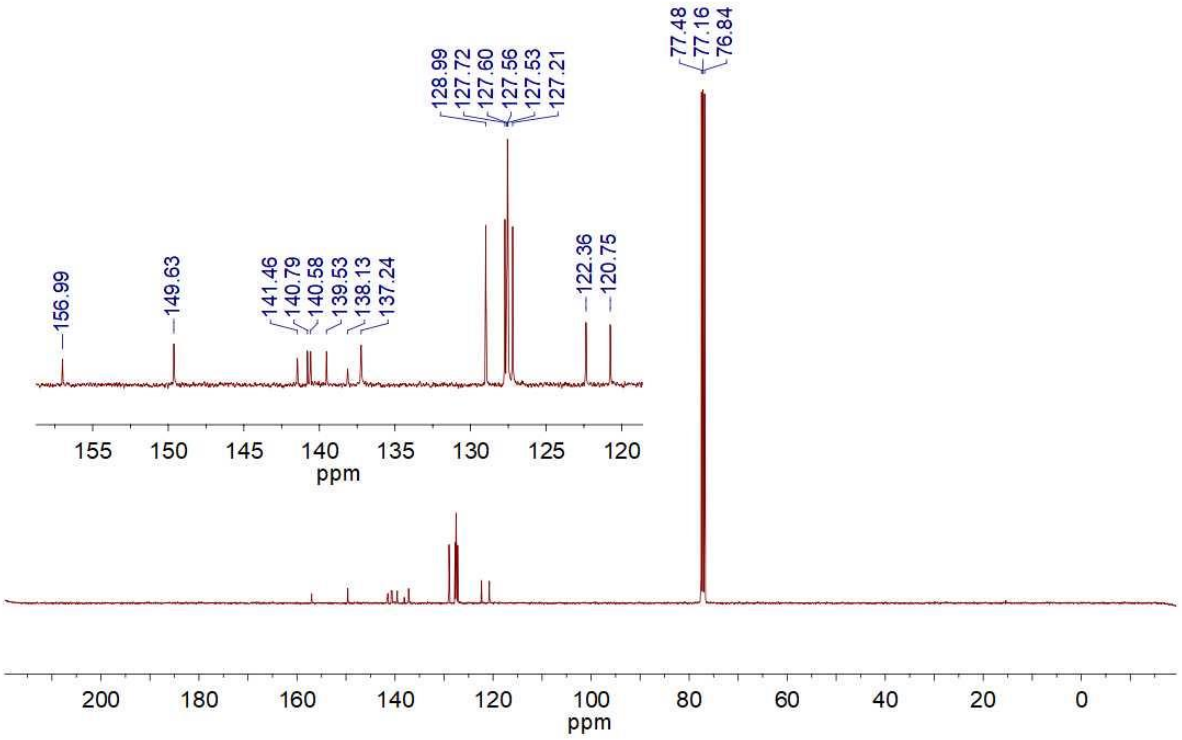

^{13}C NMR (101 MHz, $CDCl_3$, 298 K) spectrum of **Htppy**

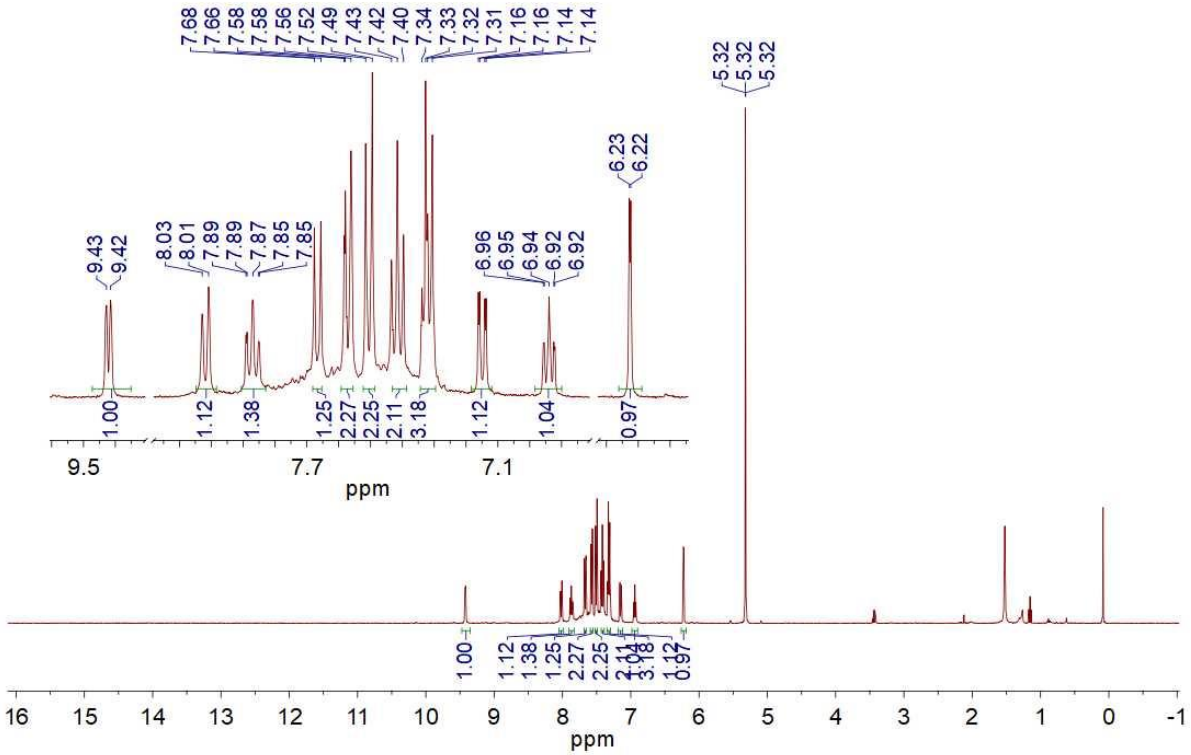

^{1}H NMR (400 MHz, CD_2Cl_2, 298 K) spectrum of **[Ir(tppy)$_2$(μ-Cl)]$_2$**

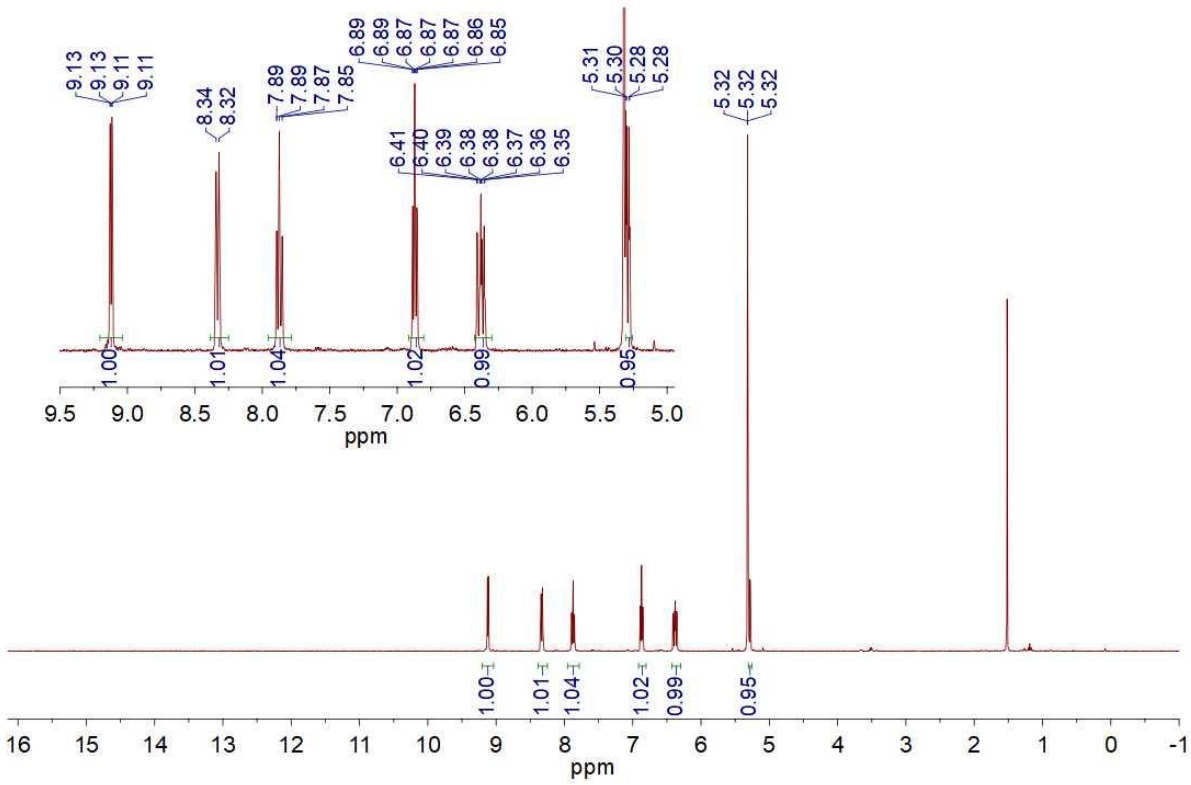

^{1}H NMR (400 MHz, CD_2Cl_2, 298 K) spectrum of **[Ir(dfppy)$_2$(μ-Cl)]$_2$**

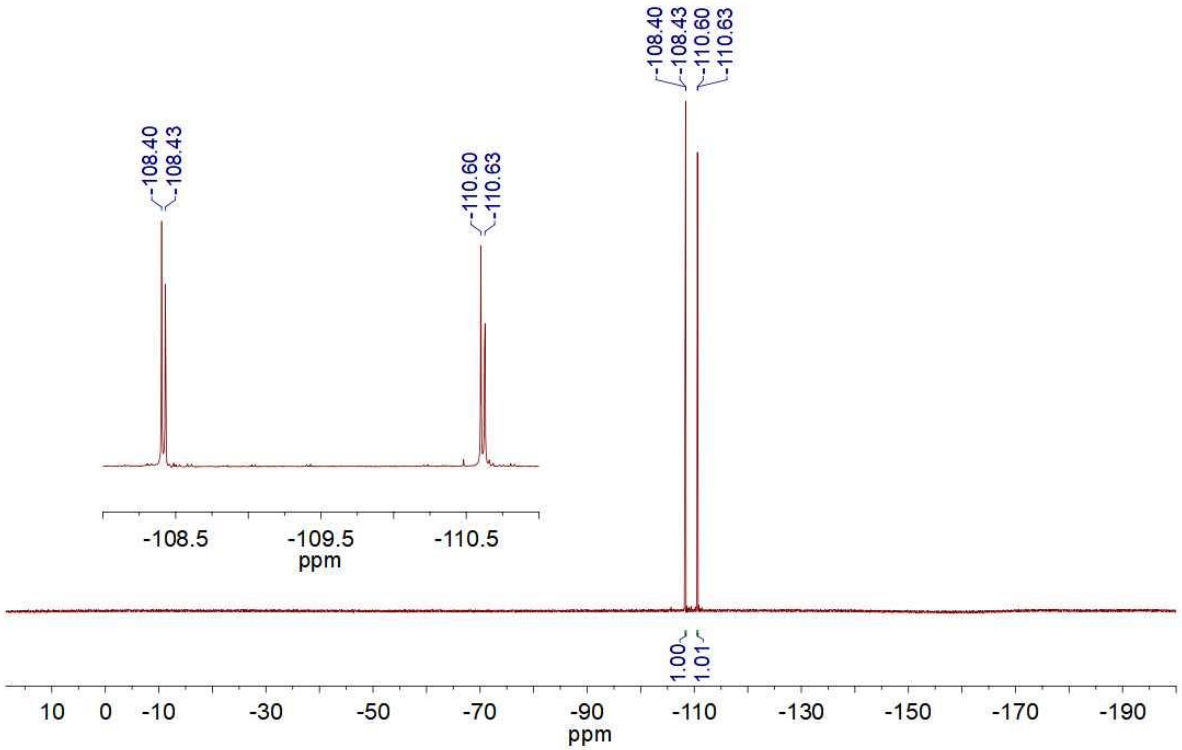

^{19}F NMR (376 MHz, CD_2Cl_2, 298 K) spectrum of **[Ir(dfppy)$_2$(μ-Cl)]$_2$**

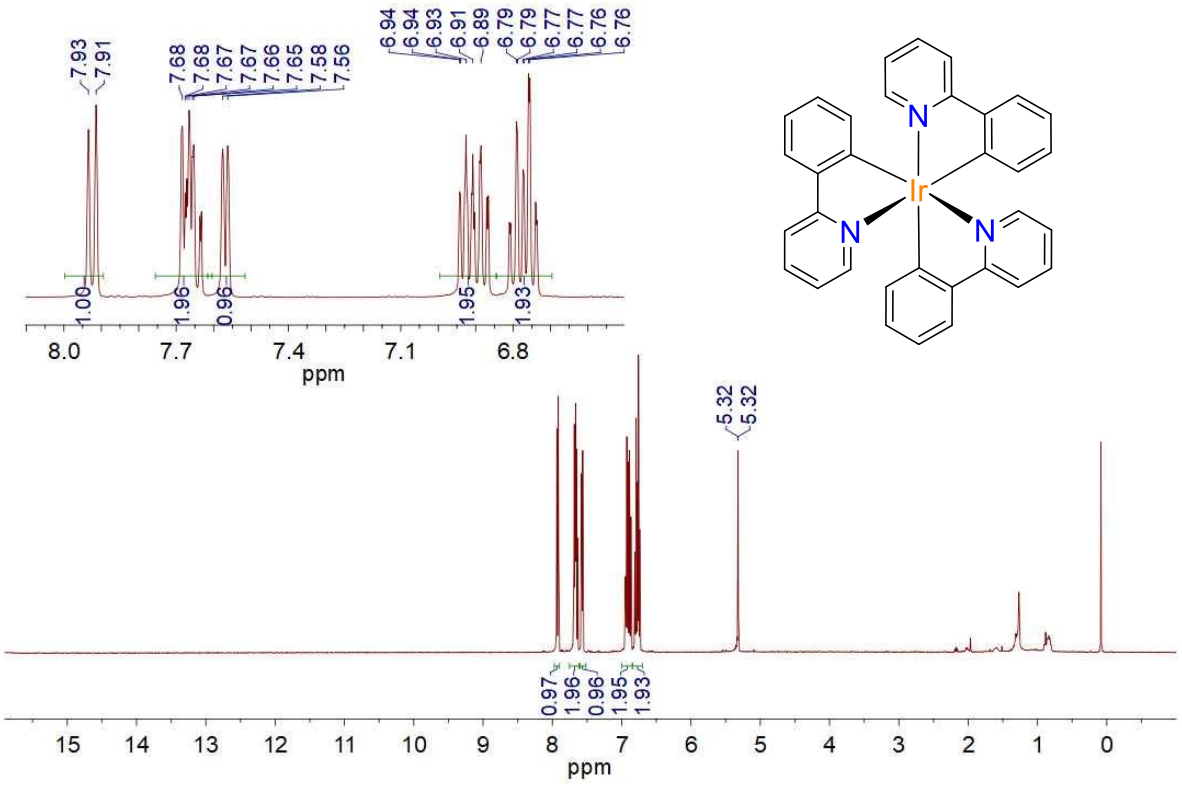

^{1}H NMR (400 MHz, CD_2Cl_2, 298 K) spectrum of ***fac*-Ir(ppy)$_3$**

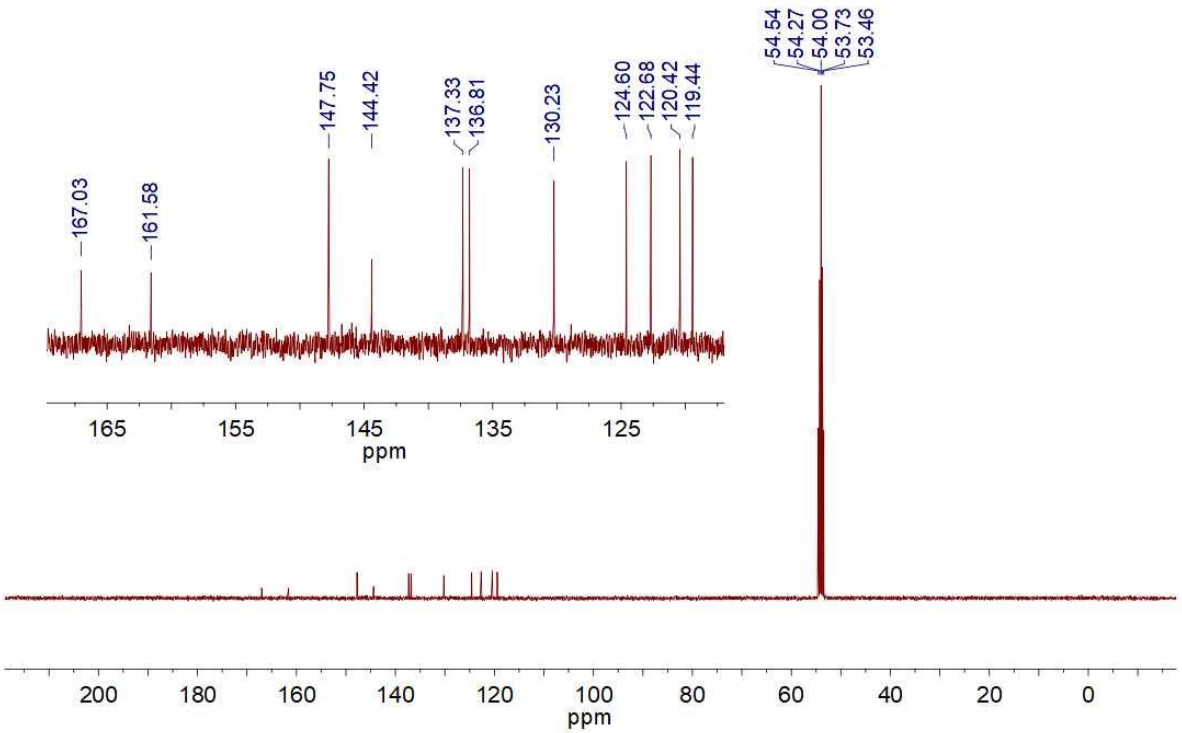

^{13}C NMR (101 MHz, CD_2Cl_2, 298 K) spectrum of ***fac*-Ir(ppy)$_3$**

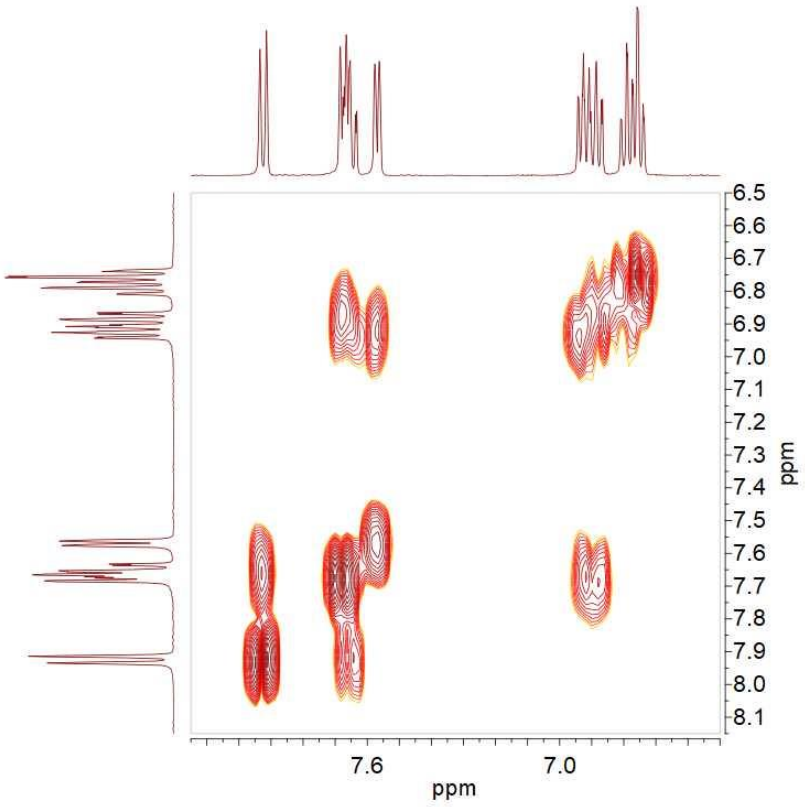

^{1}H–^{1}H COSY NMR (400 MHz, CD_2Cl_2, 298 K) spectrum of ***fac*-Ir(ppy)$_3$**

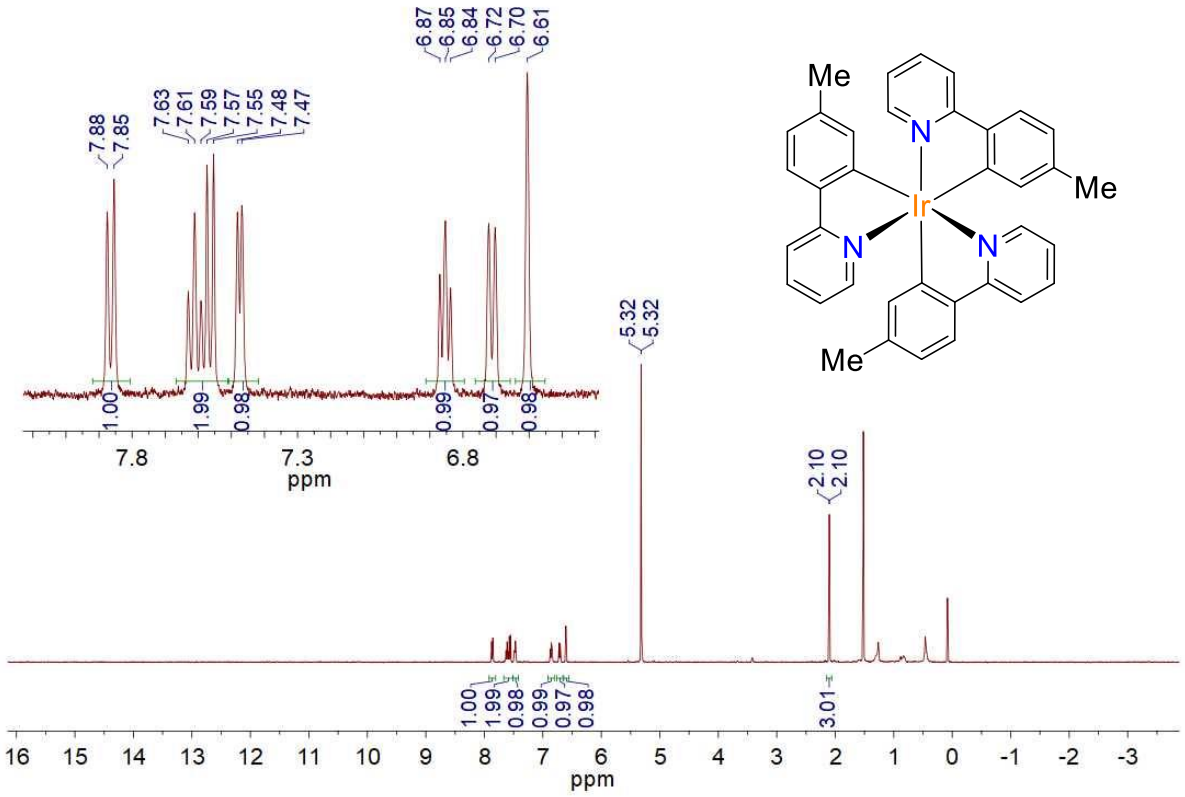

^{1}H NMR (400 MHz, CD_2Cl_2, 298 K) spectrum of ***fac*-Ir(tpy)$_3$**

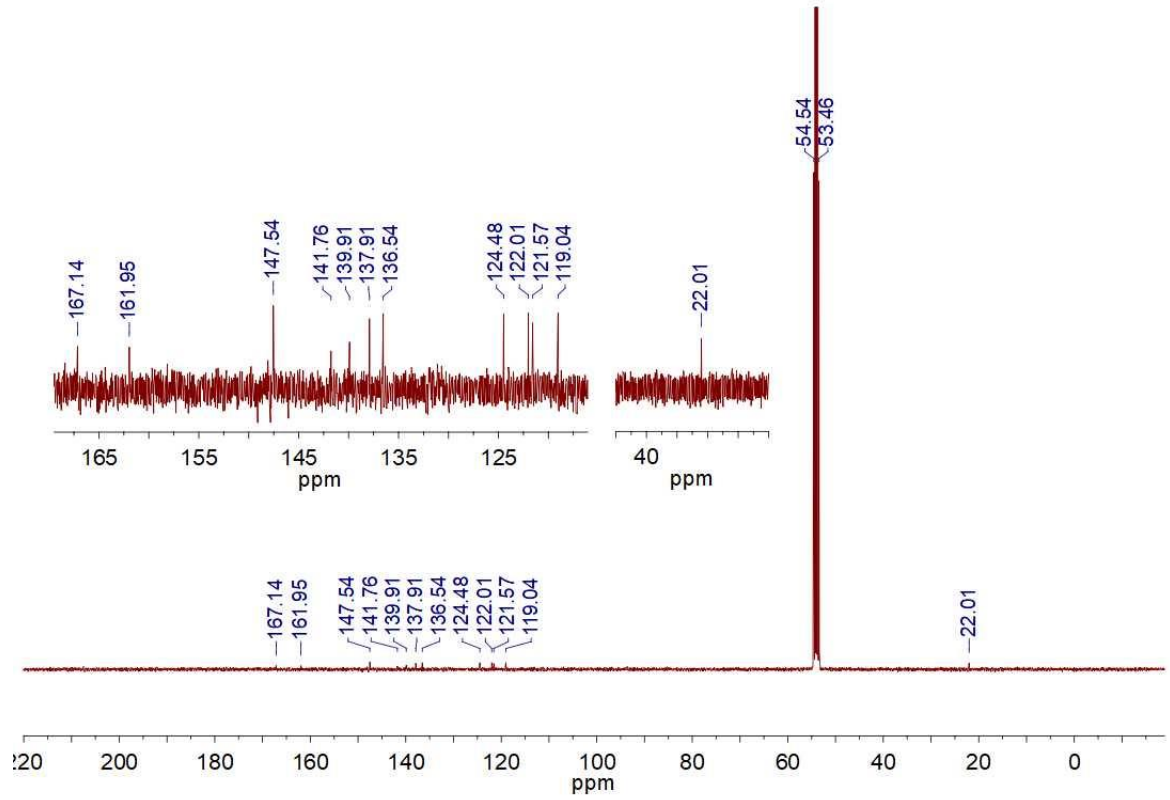

^{13}C NMR (101 MHz, CD_2Cl_2, 298 K) spectrum of ***fac*-Ir(tpy)$_3$**

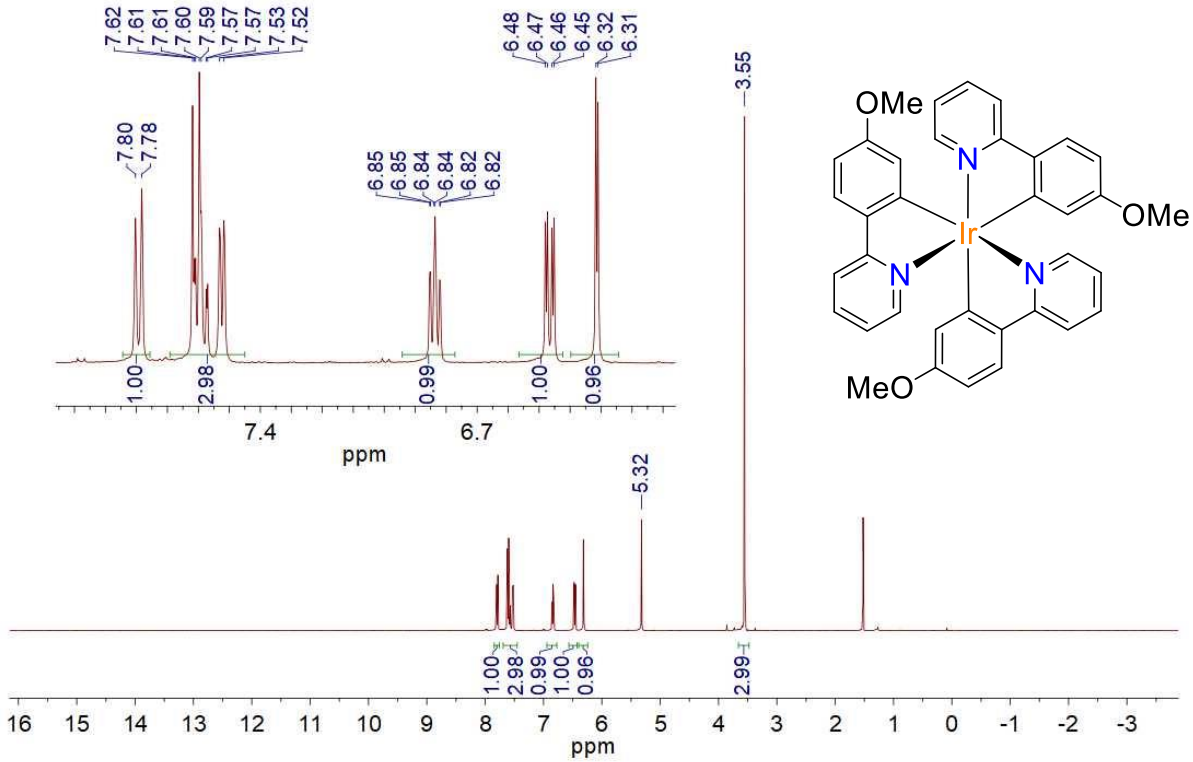

^{1}H NMR (400 MHz, CD_2Cl_2, 298 K) spectrum of ***fac*-Ir(meppy)$_3$**

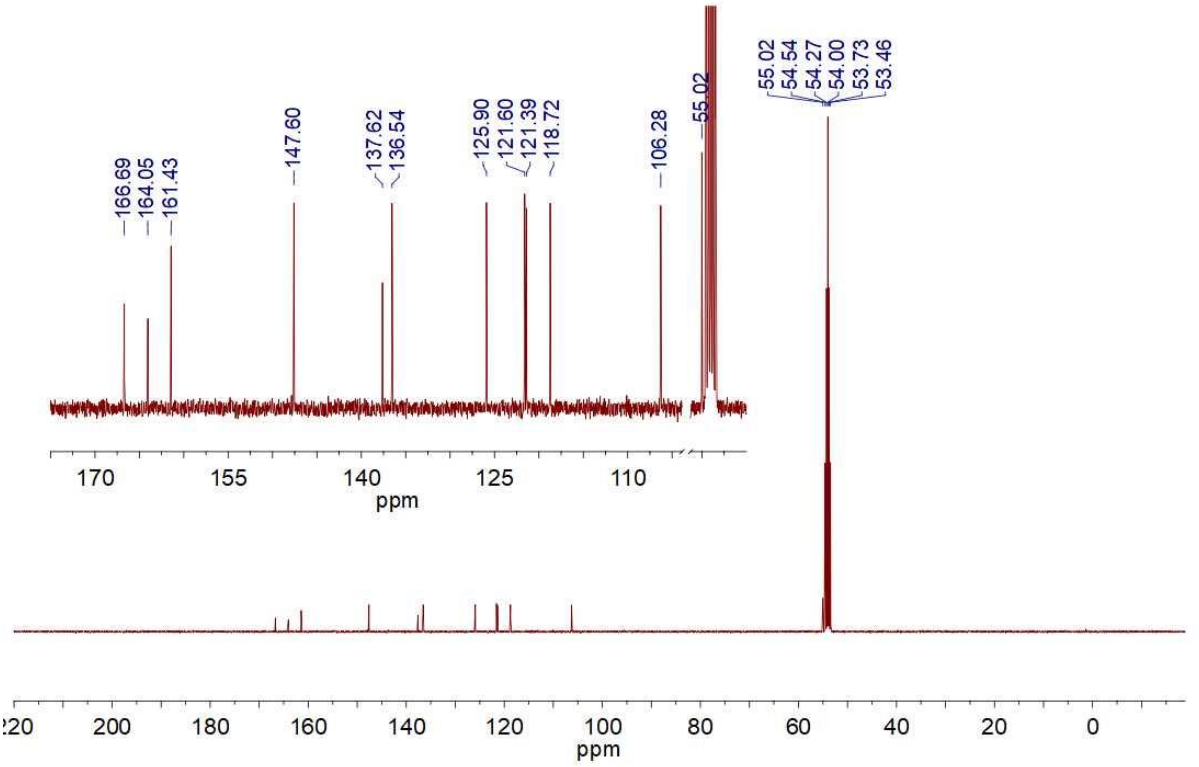

^{13}C NMR (101 MHz, CD_2Cl_2, 298 K) spectrum of ***fac*-Ir(meppy)$_3$**

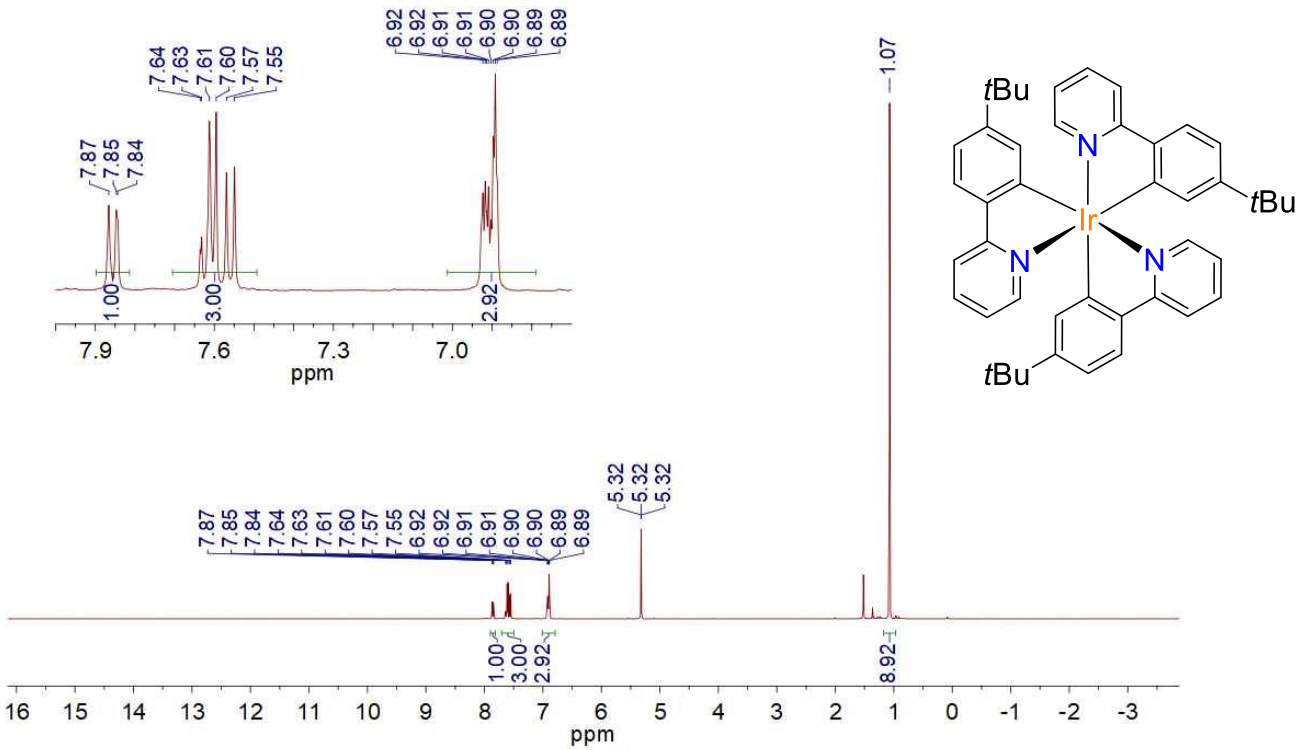

^{1}H NMR (400 MHz, CD_2Cl_2, 298 K) spectrum of ***fac*-Ir(buppy)$_3$**

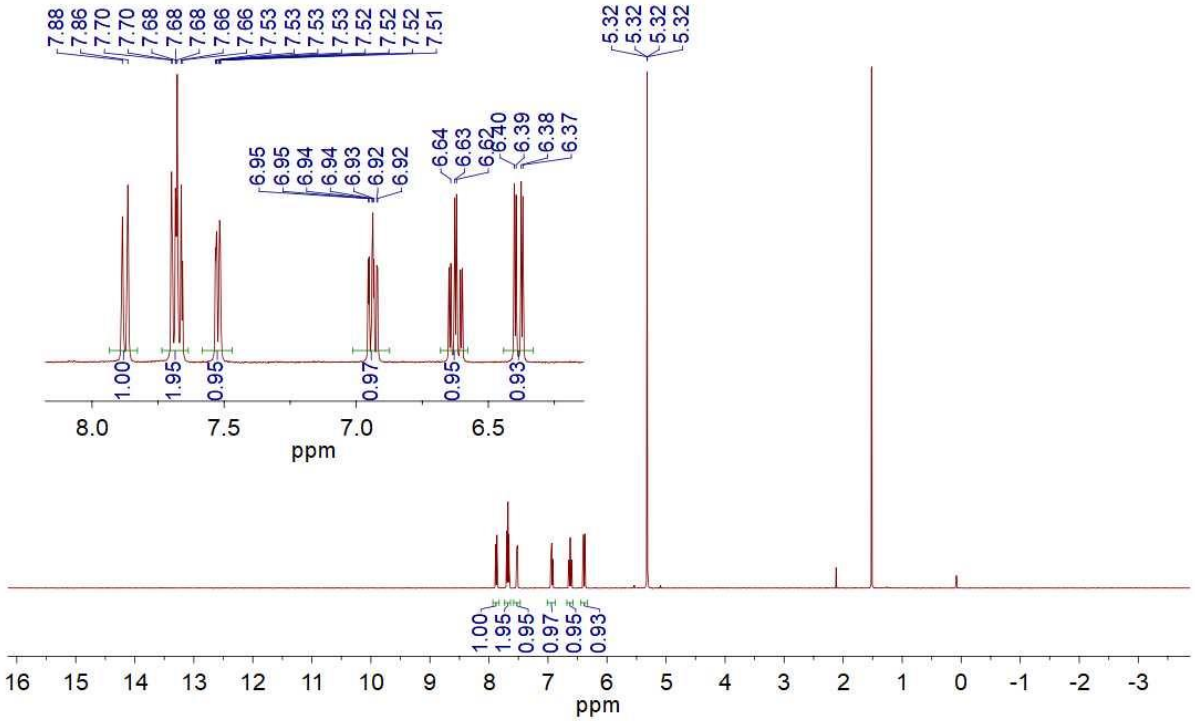

^{1}H NMR (400 MHz, CD_2Cl_2, 298 K) spectrum of ***fac*-Ir(fppy)$_3$**

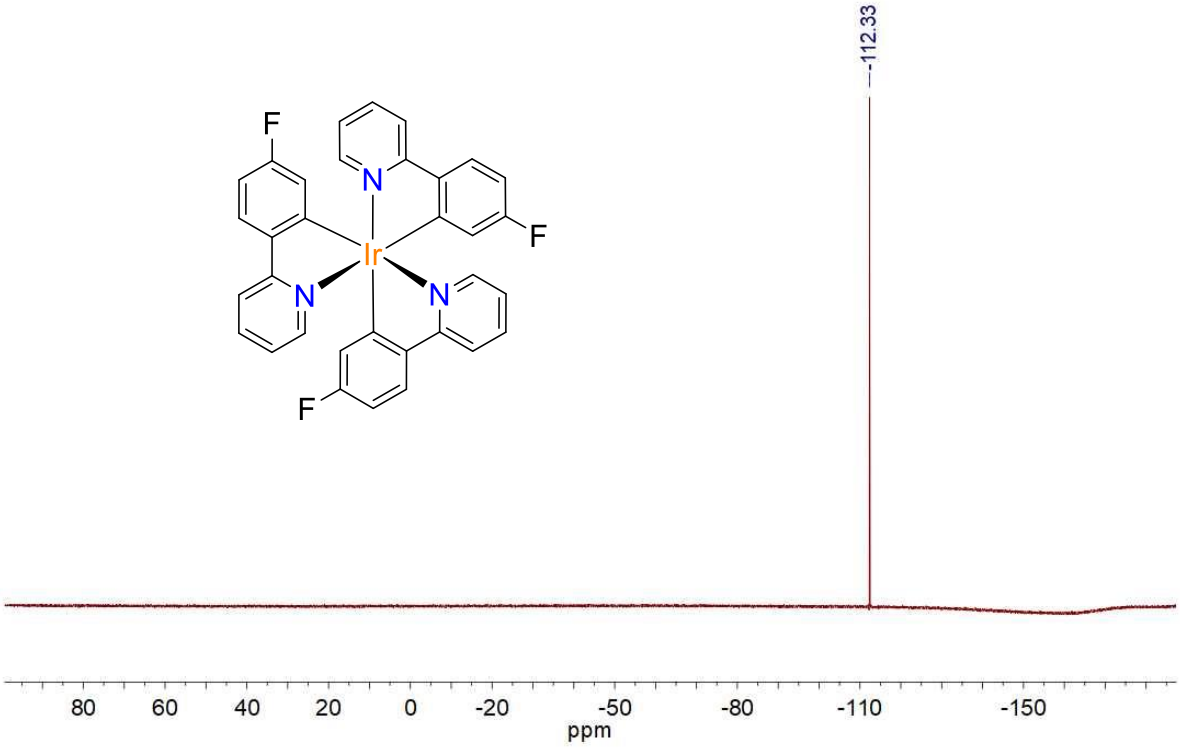

^{19}F NMR (376 MHz, CD_2Cl_2, 298 K) spectrum of ***fac*-Ir(fppy)$_3$**

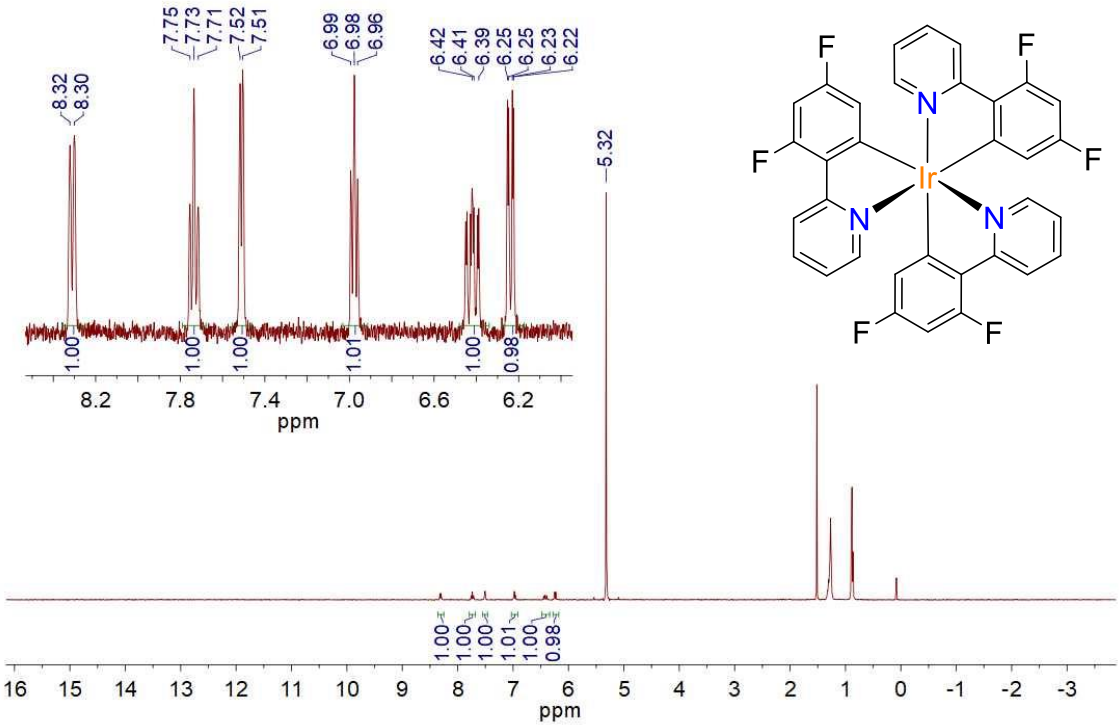

^{1}H NMR (400 MHz, CD_2Cl_2, 298 K) spectrum of ***fac*-Ir(dfppy)$_3$**

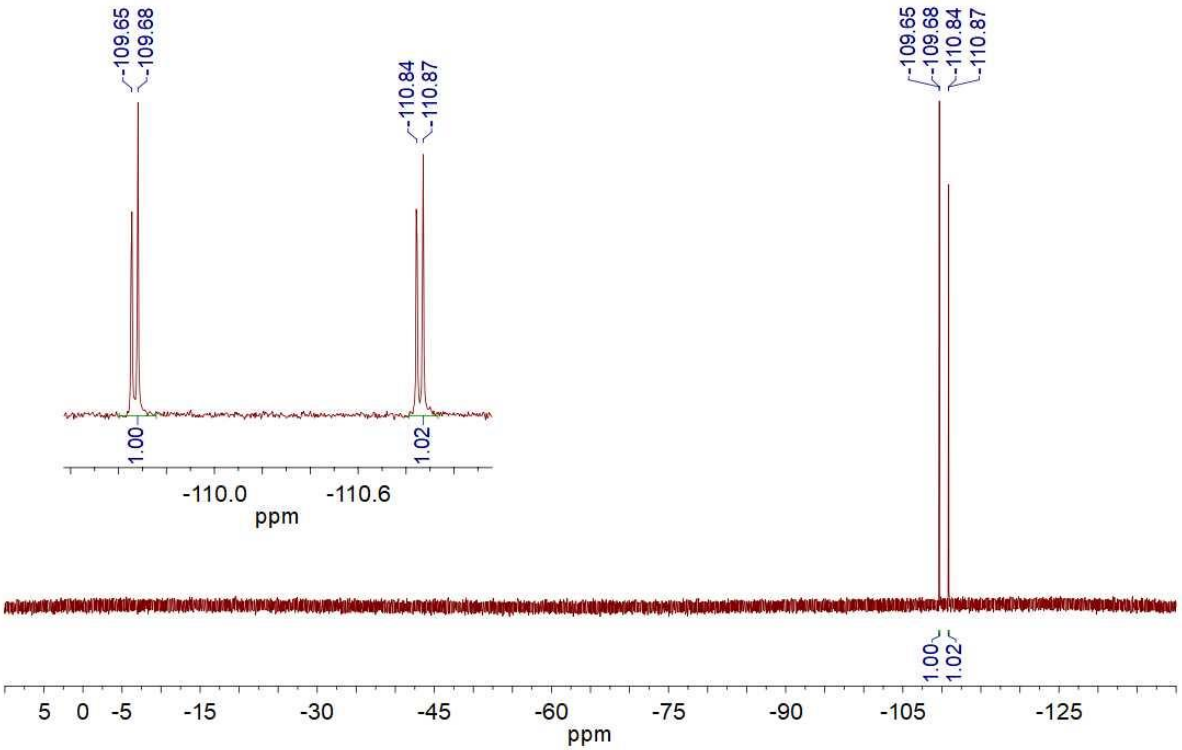

^{19}F NMR (376 MHz, CD_2Cl_2, 298 K) spectrum of ***fac*-Ir(dfppy)$_3$**

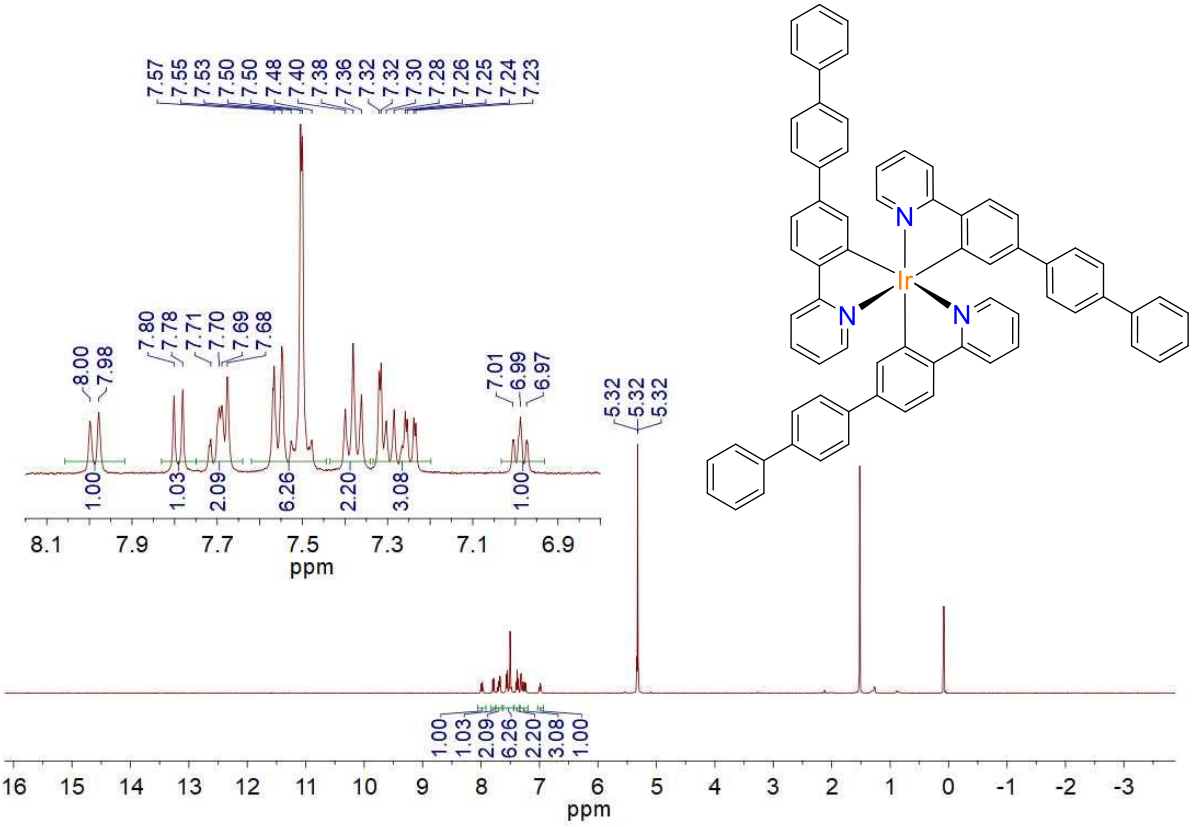

^{1}H NMR (400 MHz, CD_2Cl_2, 298 K) spectrum of ***fac*-Ir(tppy)$_3$**

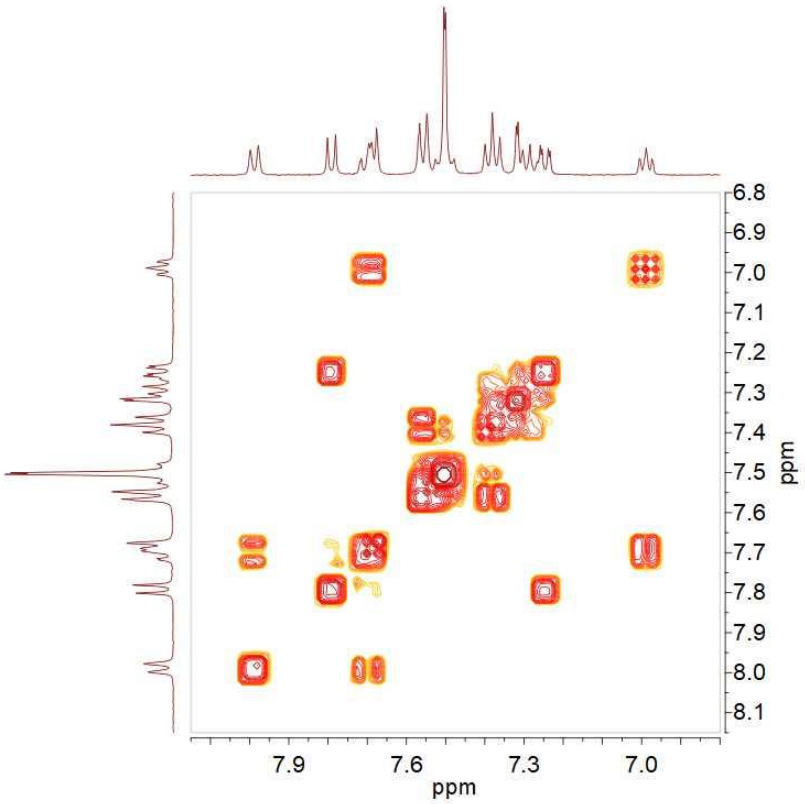

^{1}H–^{1}H COSY NMR (400 MHz, CD_2Cl_2, 298 K) spectrum of ***fac*-Ir(tppy)$_3$**

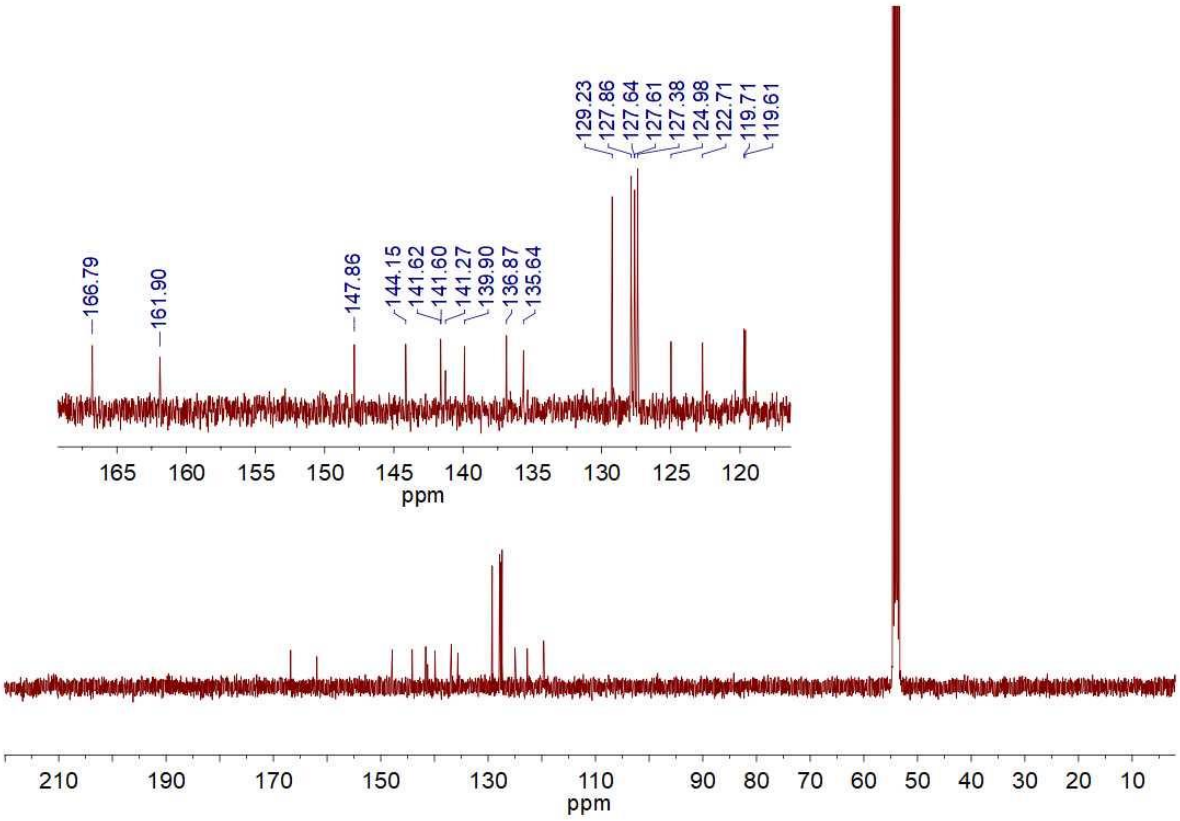

^{13}C NMR (101 MHz, CD_2Cl_2, 298 K) spectrum of ***fac*-Ir(tppy)$_3$**

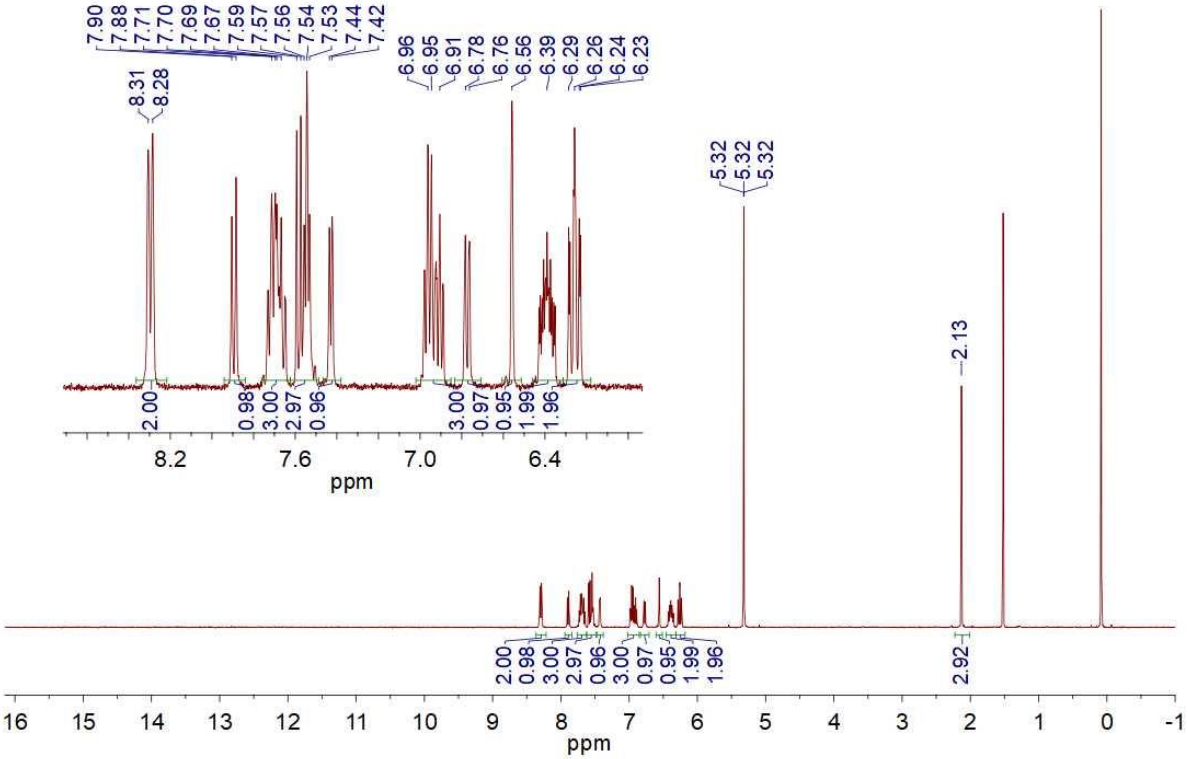

^{1}H NMR (400 MHz, CD_2Cl_2, 298 K) spectrum of ***fac*-Ir(dfppy)$_2$(tpy)**

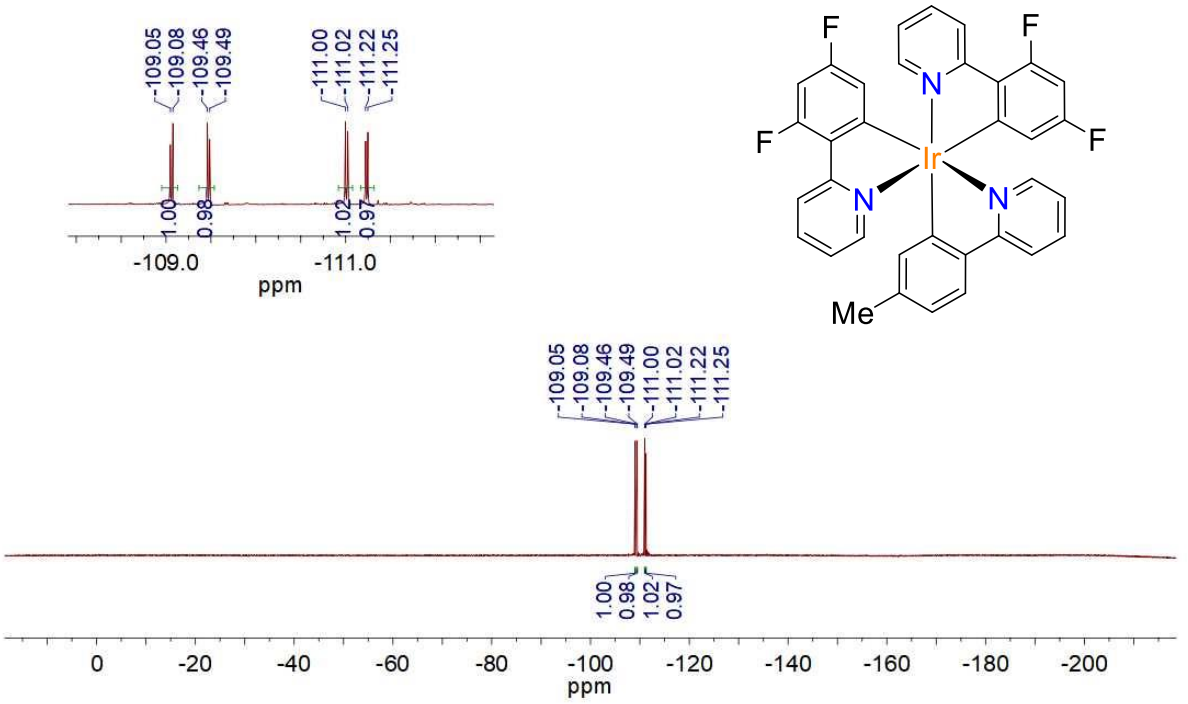

^{19}F NMR (376 MHz, CD_2Cl_2, 298 K) spectrum of ***fac*-Ir(dfppy)$_2$(tpy)**

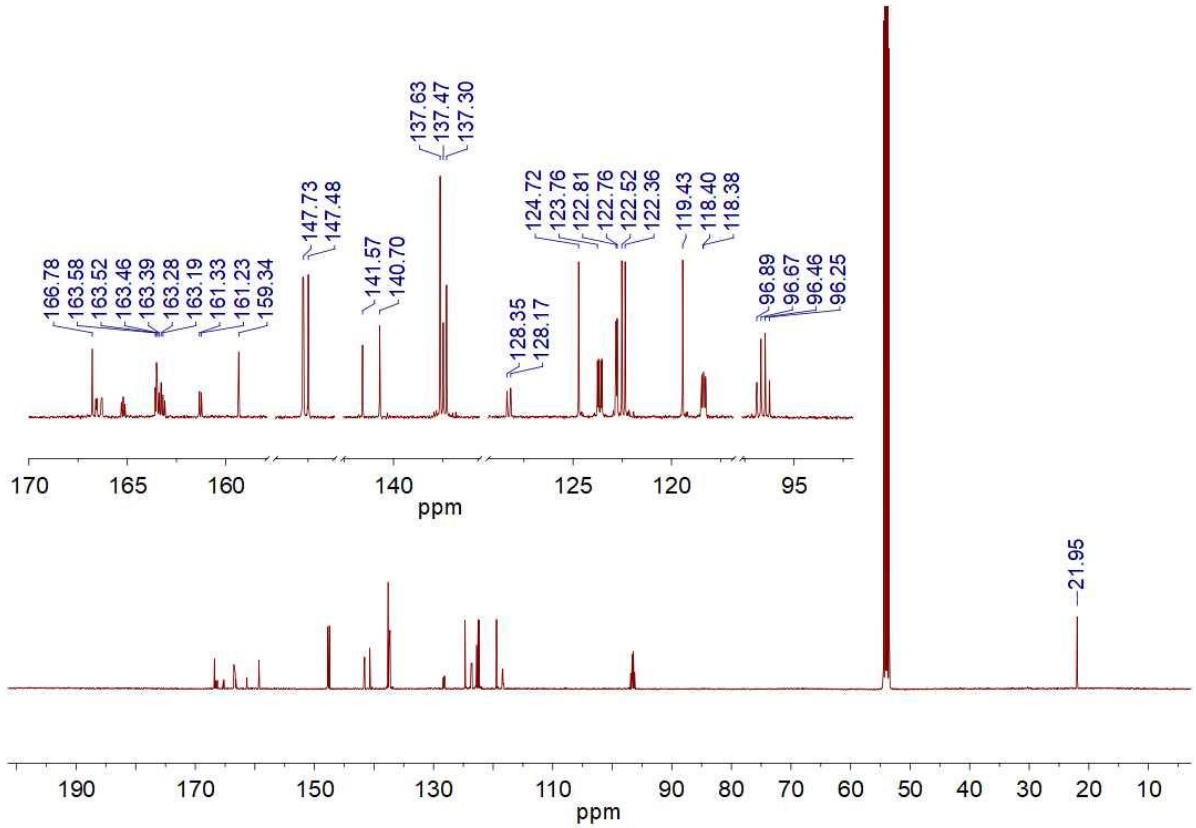

^{13}C NMR (126 MHz, CD_2Cl_2, 298 K) spectrum of ***fac*-Ir(dfppy)$_2$(tpy)**

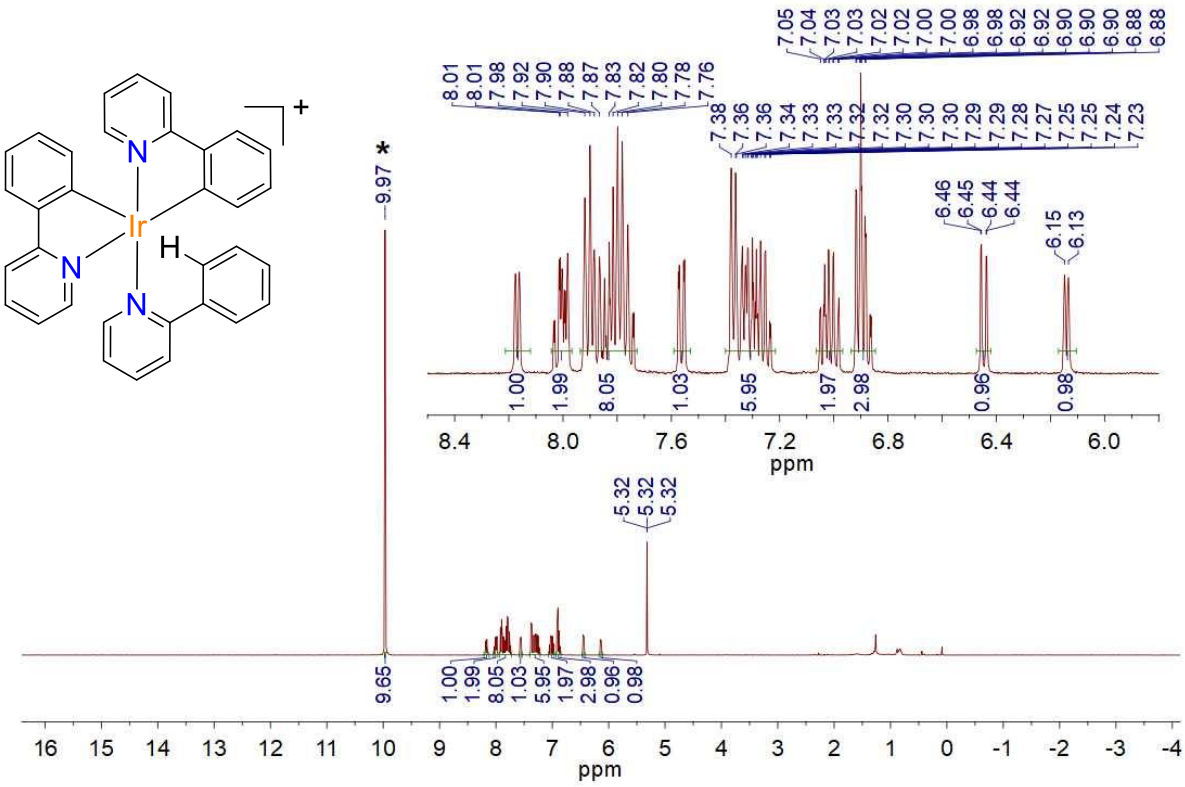

^{1}H NMR (400 MHz, CD_2Cl_2, 298 K) spectrum of **[Ir(ppy)$_2$(Hppy)](O$_2$CCF$_3$)** (the O_2CCF_3 anion is omitted for clarity). The TFA signal is marked by an asterisk.

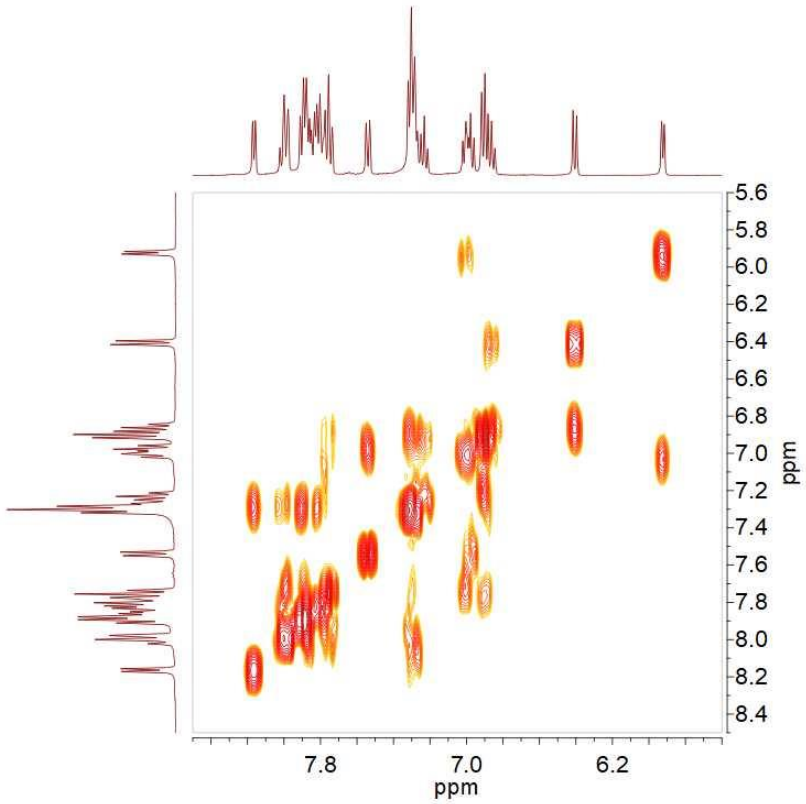

^{1}H–^{1}H COSY NMR (400 MHz, CD_2Cl_2, 253 K) spectrum of **[Ir(ppy)$_2$(Hppy)](O$_2$CCF$_3$)**

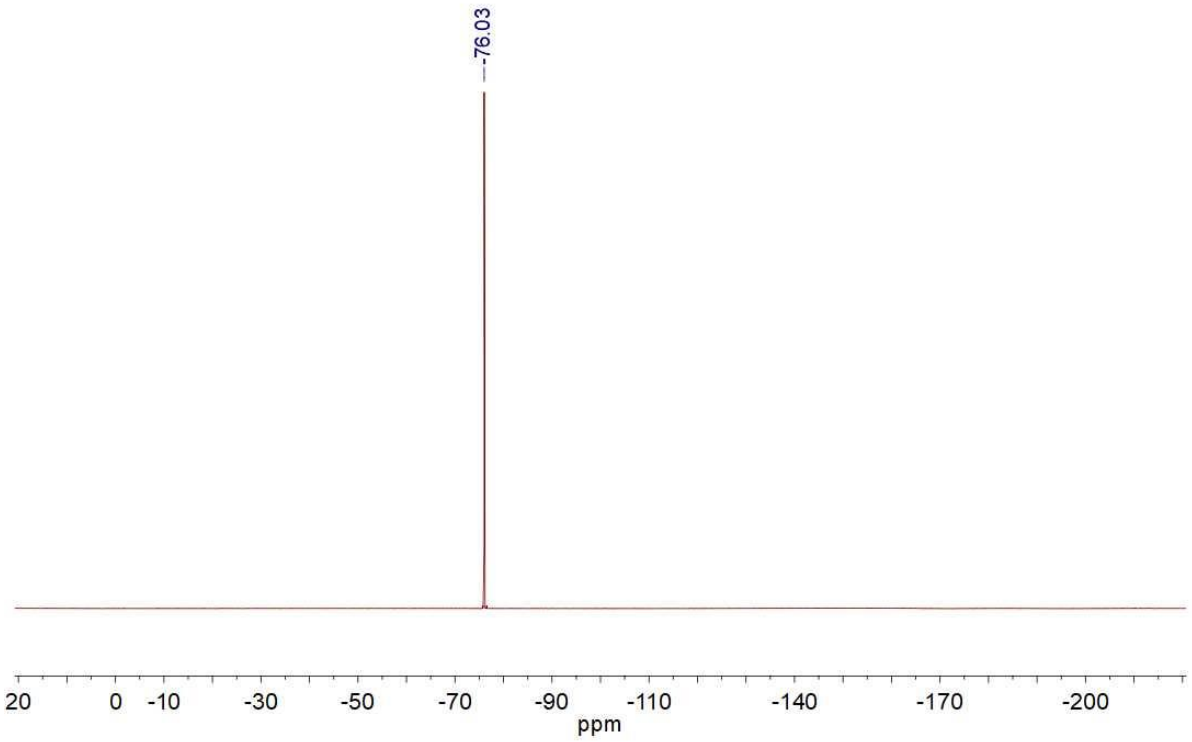

^{19}F NMR (376 MHz, CD_2Cl_2, 253 K) spectrum of **[Ir(ppy)$_2$(Hppy)](O$_2$CCF$_3$)**

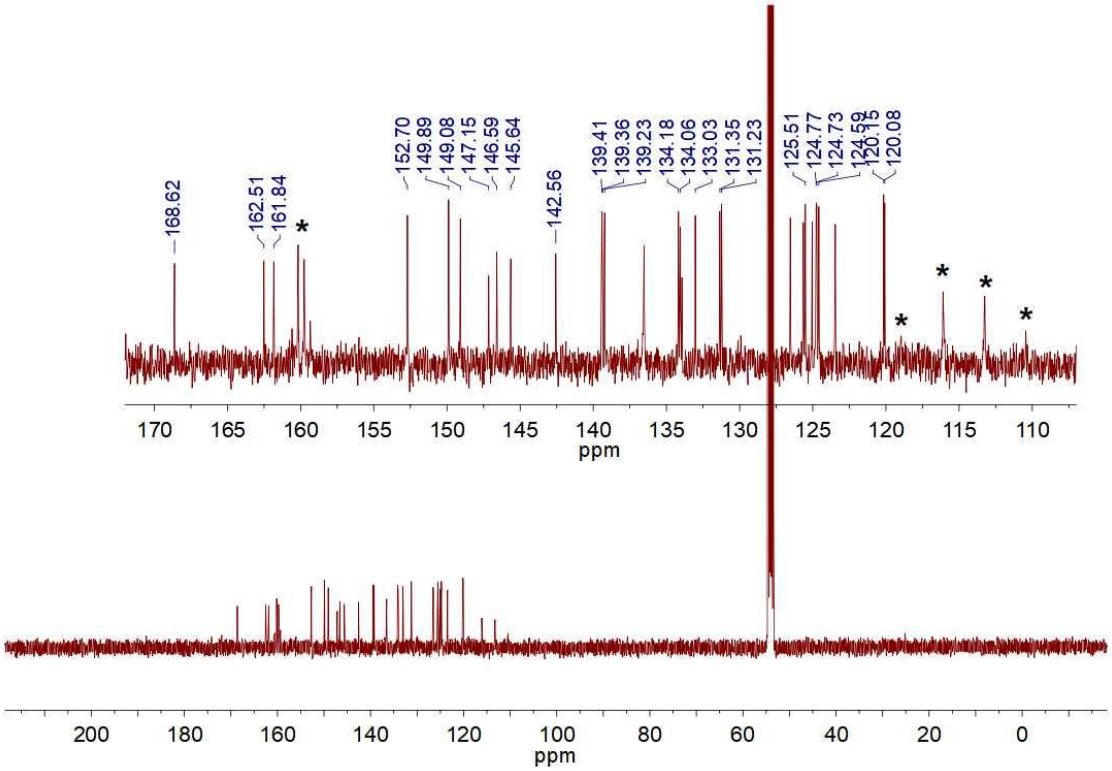

^{13}C NMR (101 MHz, CD_2Cl_2, 253 K) spectrum of **[Ir(ppy)$_2$(Hppy)](O$_2$CCF$_3$).** The TFA signals are marked by asterisks.

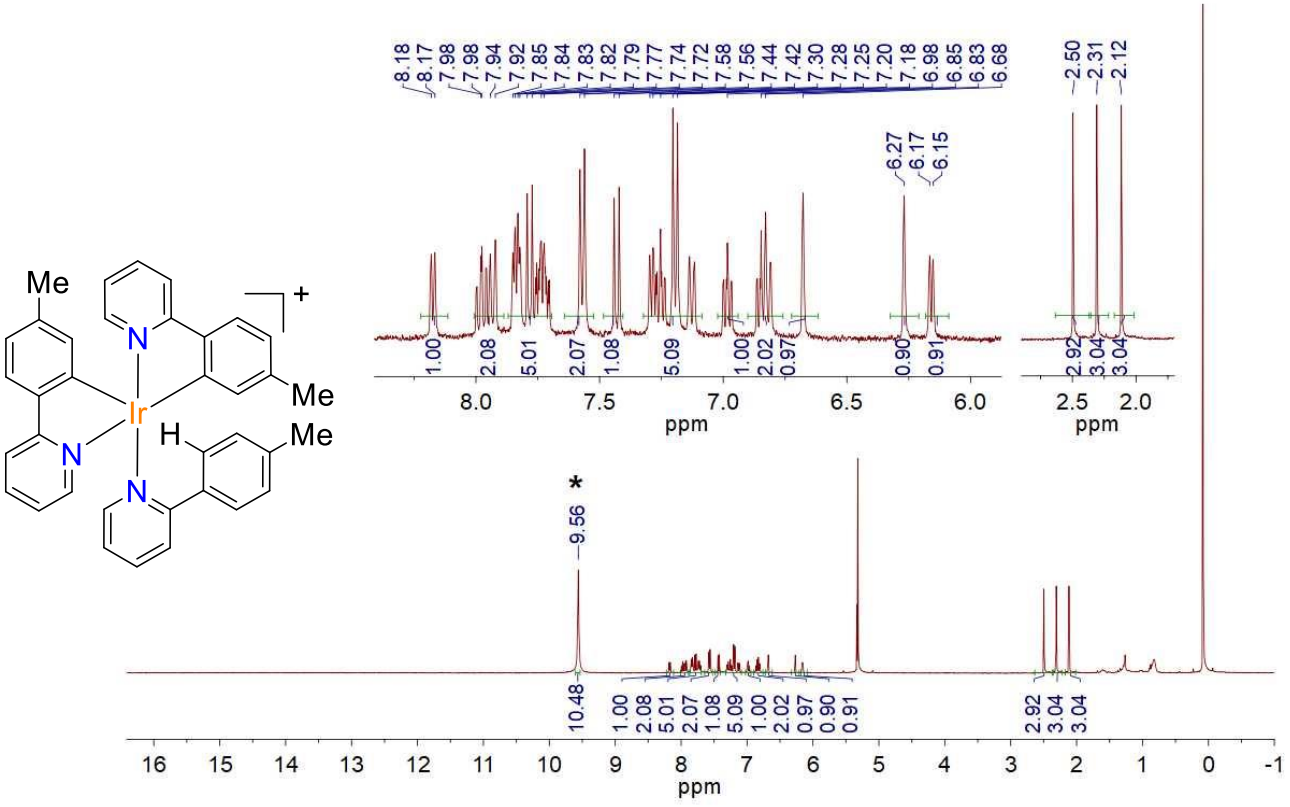

^{1}H NMR (400 MHz, CD_2Cl_2, 298 K) spectrum of **[Ir(tpy)$_2$(Htpy)](O$_2$CCF$_3$)** (the O_2CCF_3 anion is omitted for clarity). The TFA signal is marked by an asterisk.

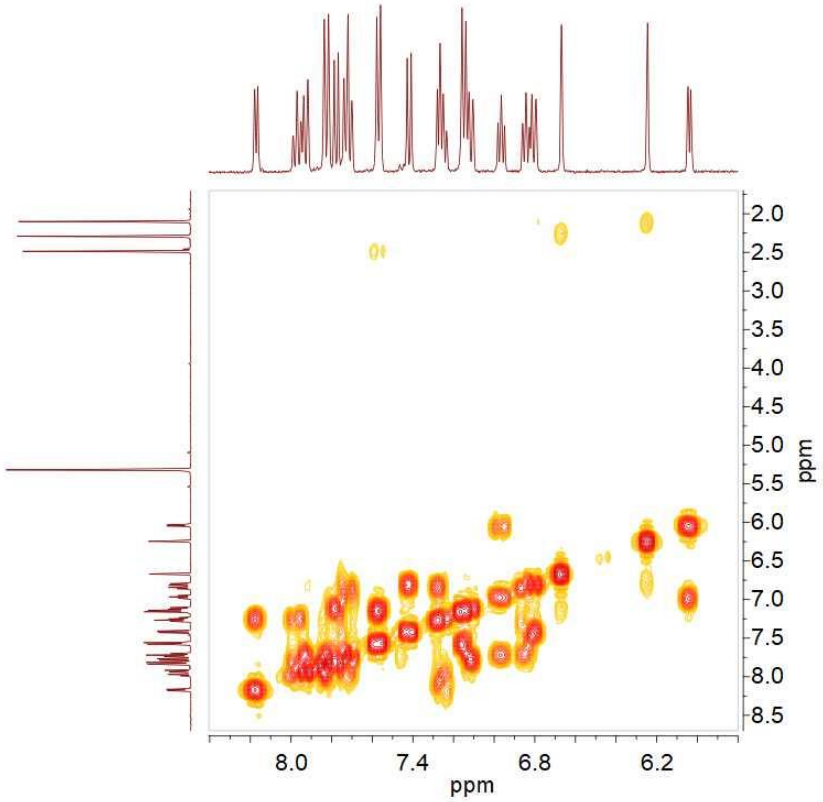

^{1}H–^{1}H COSY NMR (400 MHz, CD_2Cl_2, 273 K) spectrum of **[Ir(tpy)$_2$(Htpy)](O$_2$CCF$_3$)**

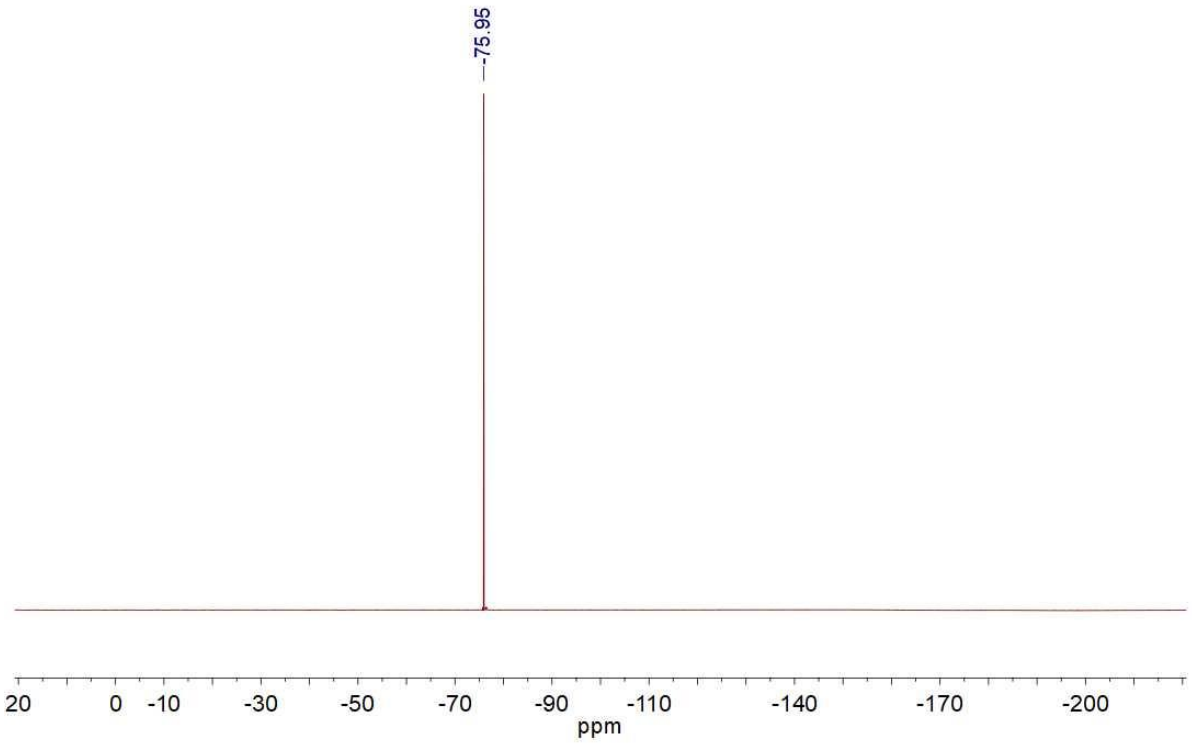

^{19}F NMR (376 MHz, CD_2Cl_2, 273 K) spectrum of **[Ir(tpy)$_2$(Htpy)](O$_2$CCF$_3$)**

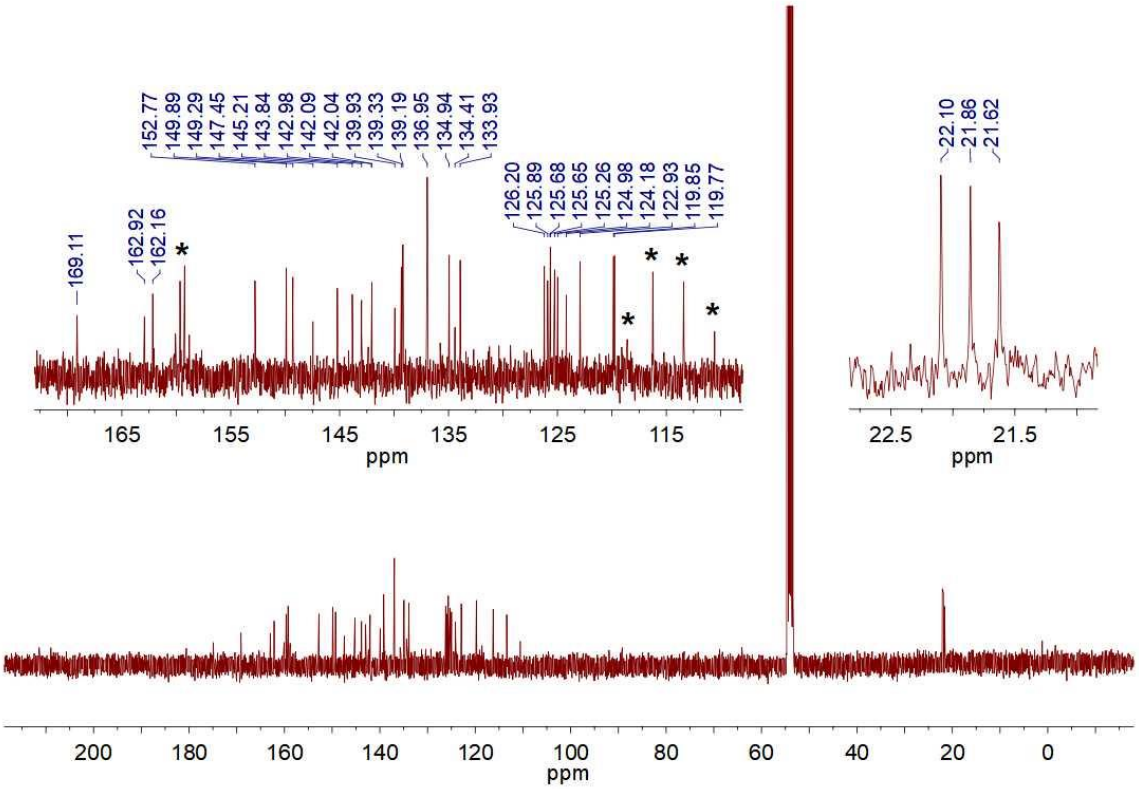

^{13}C NMR (101 MHz, CD_2Cl_2, 273 K) spectrum of **[Ir(tpy)$_2$(Htpy)](O$_2$CCF$_3$)**. TFA signals are marked by asterisks.

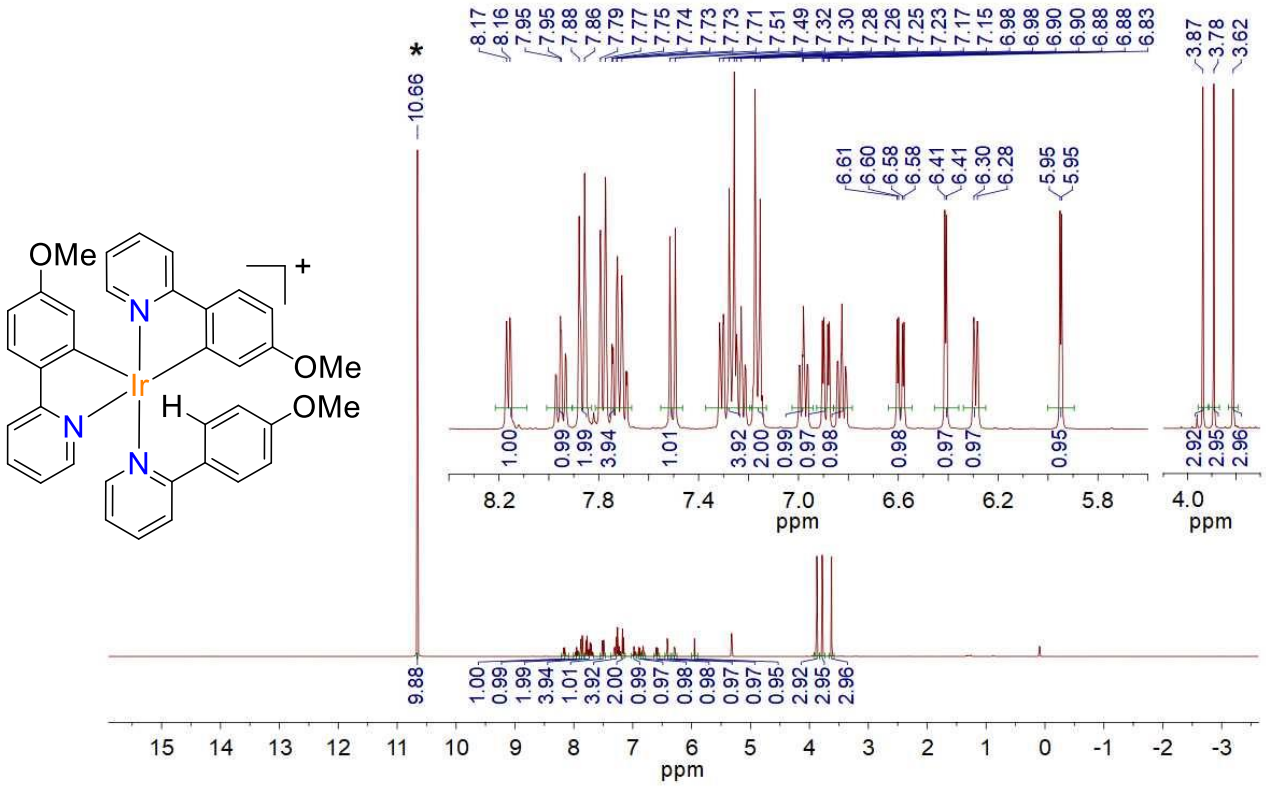

^{1}H NMR (400 MHz, CD_2Cl_2, 298 K) spectrum of **[Ir(meppy)$_2$(Hmeppy)](O$_2$CCF$_3$)** (the O_2CCF_3 anion is omitted for clarity). The TFA signal is marked by an asterisk.

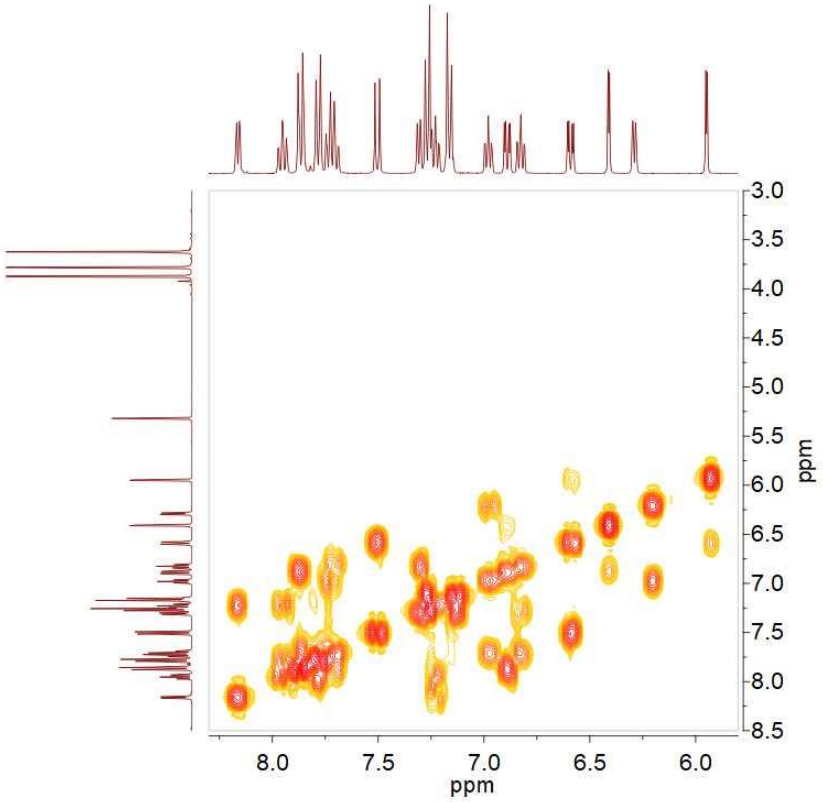

^{1}H–^{1}H COSY NMR (400 MHz, CD_2Cl_2, 273 K) spectrum of **[Ir(meppy)$_2$(Hmeppy)](O$_2$CCF$_3$)**

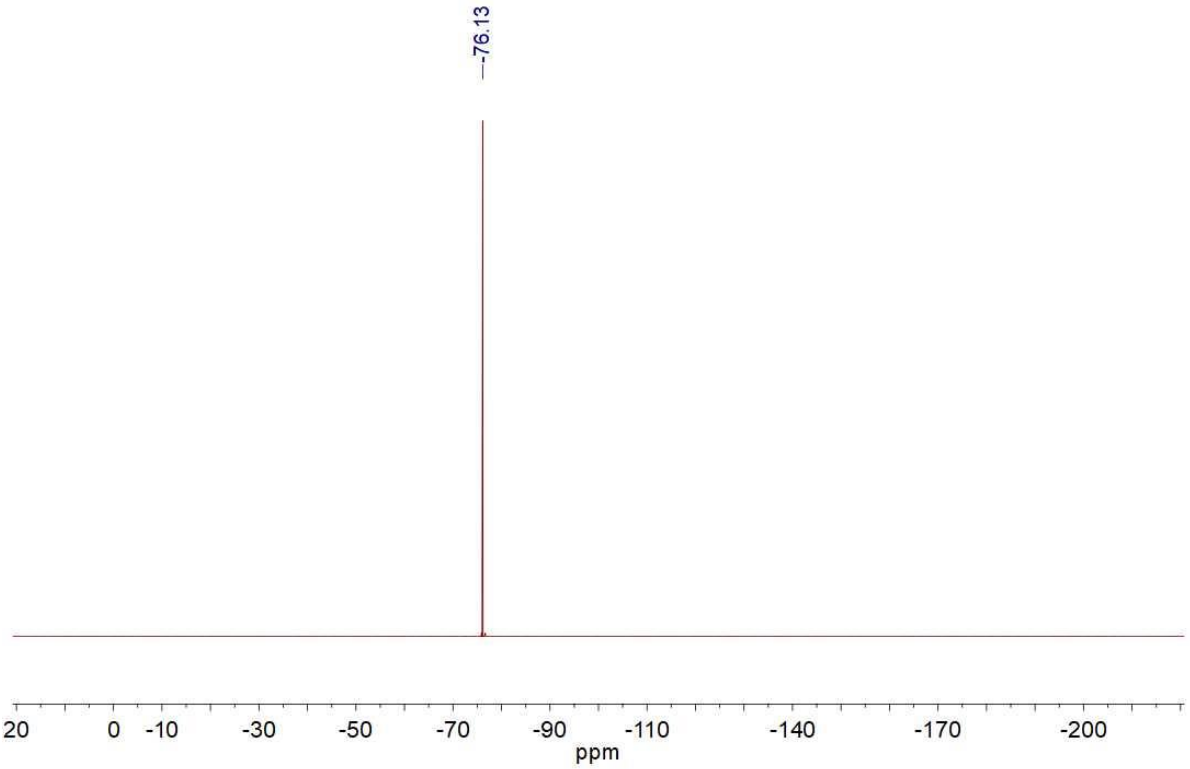

^{19}F NMR (376 MHz, CD_2Cl_2, 273 K) spectrum of **[Ir(meppy)$_2$(Hmeppy)](O$_2$CCF$_3$)**

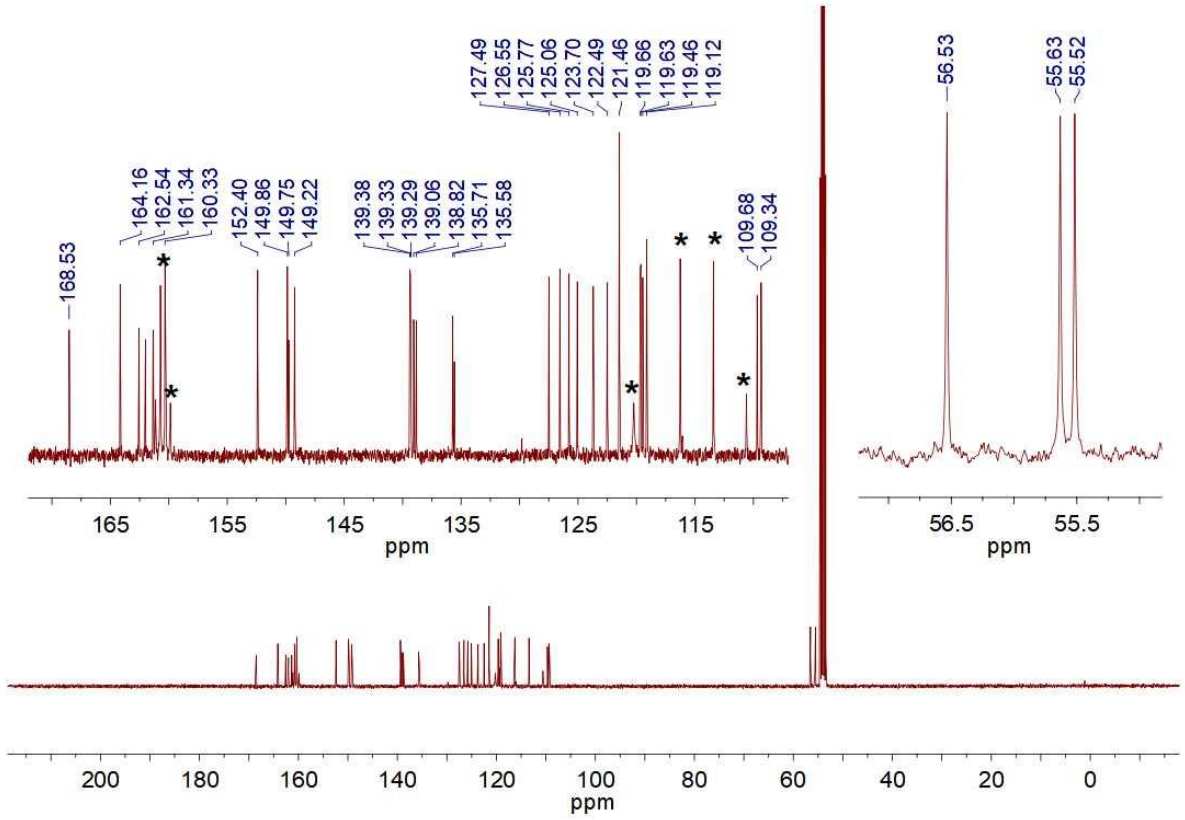

^{13}C NMR (101 MHz, CD_2Cl_2, 273 K) spectrum of **[Ir(meppy)$_2$(Hmeppy)](O$_2$CCF$_3$)**. TFA signals are marked by asterisks.

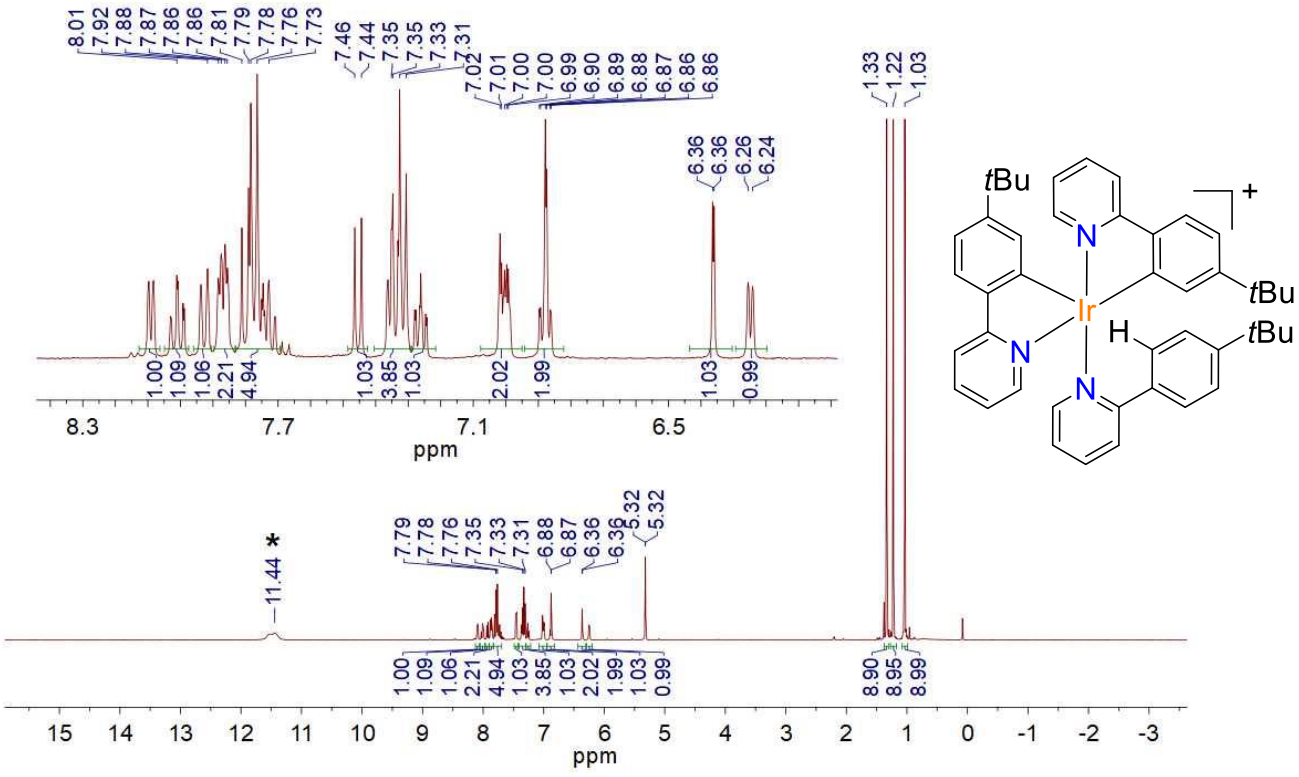

^{1}H NMR (400 MHz, CD_2Cl_2, 298 K) spectrum of **[Ir(buppy)$_2$(Hbuppy)](O$_2$CCF$_3$)** (the O_2CCF_3 anion is omitted for clarity). The TFA signal is marked by an asterisk.

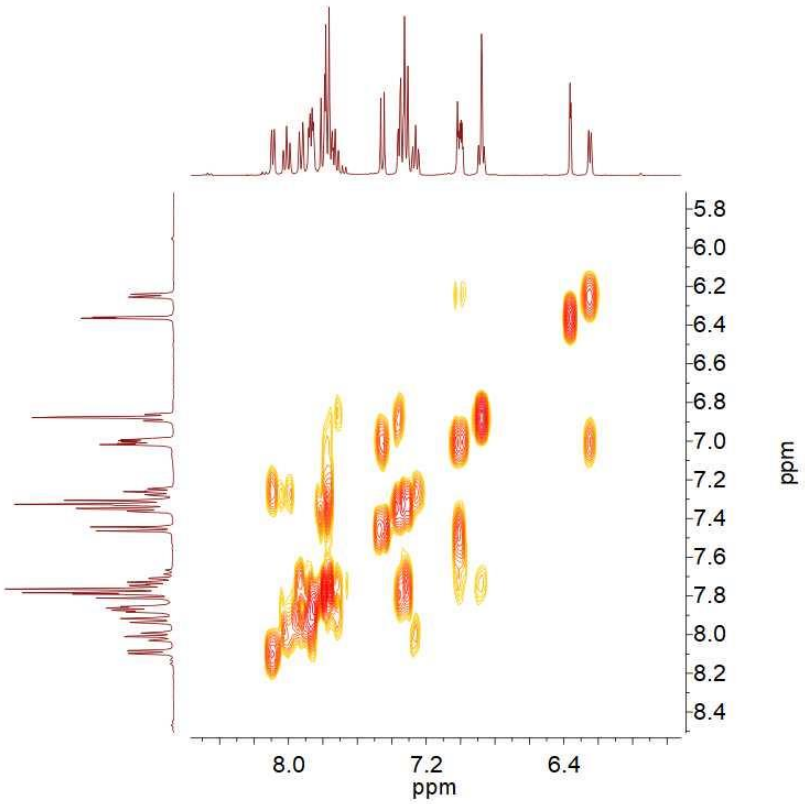

^{1}H–^{1}H COSY NMR (400 MHz, CD_2Cl_2, 273 K) spectrum of **[Ir(buppy)$_2$(Hbuppy)](O$_2$CCF$_3$)**

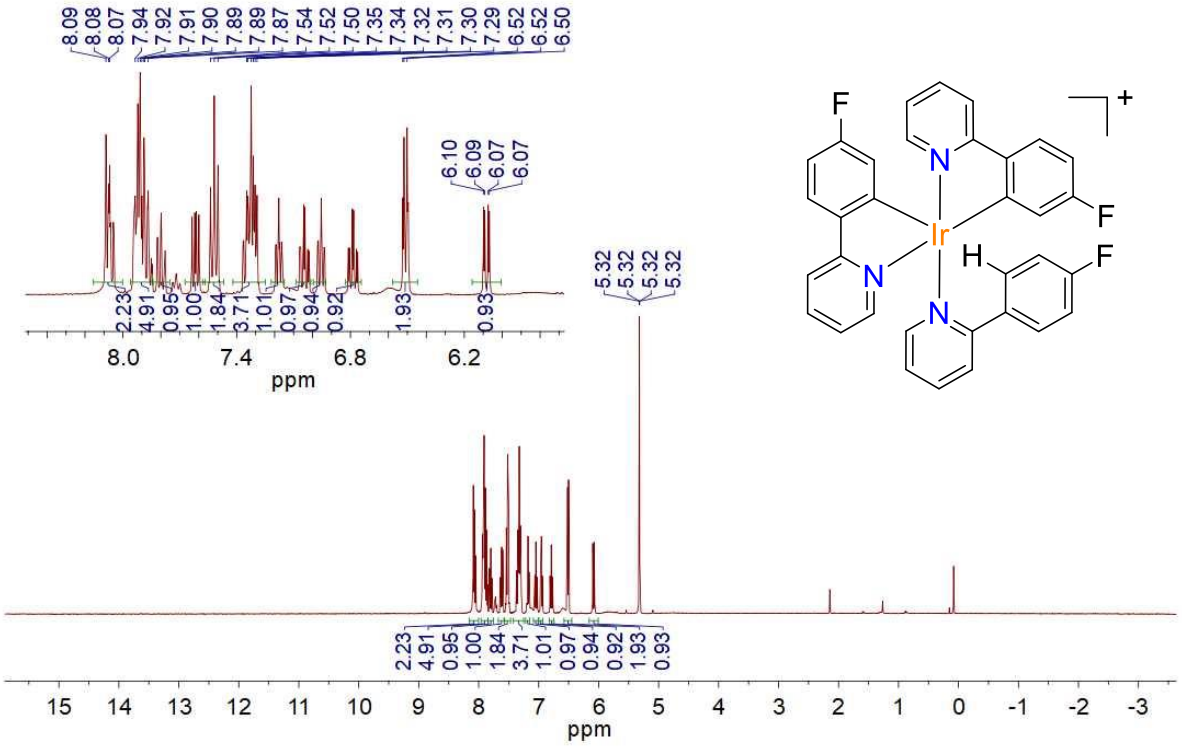

^{1}H NMR (400 MHz, CD_2Cl_2, 298 K) spectrum of **[Ir(fppy)$_2$(Hfppy)](NTf$_2$)** (the NTf_2 anion is omitted for clarity)

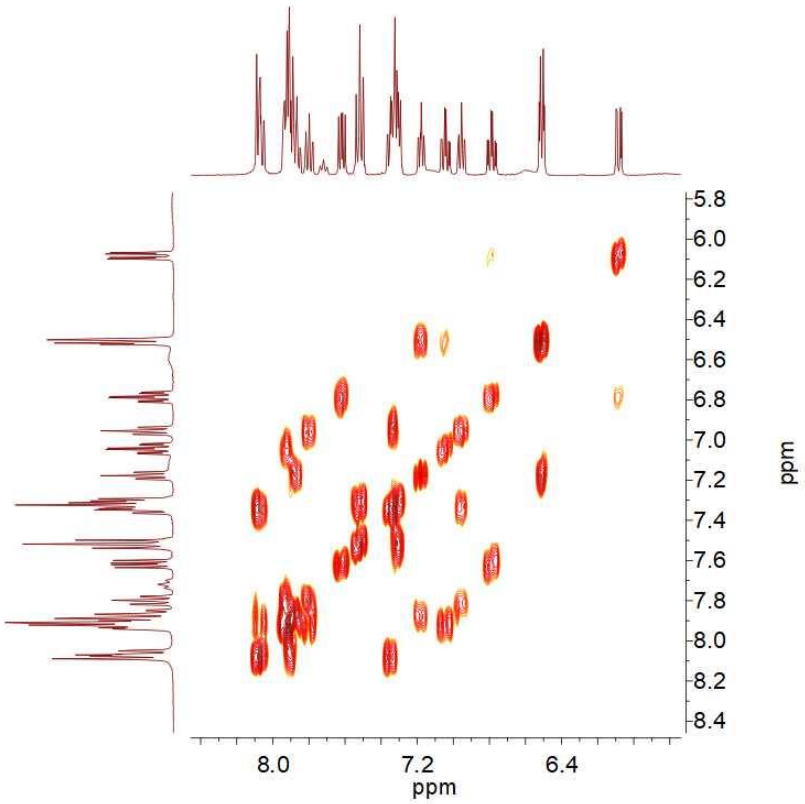

^{1}H–^{1}H COSY NMR (400 MHz, CD_2Cl_2, 273 K) spectrum of **[Ir(fppy)$_2$(Hfppy)](NTf$_2$)**

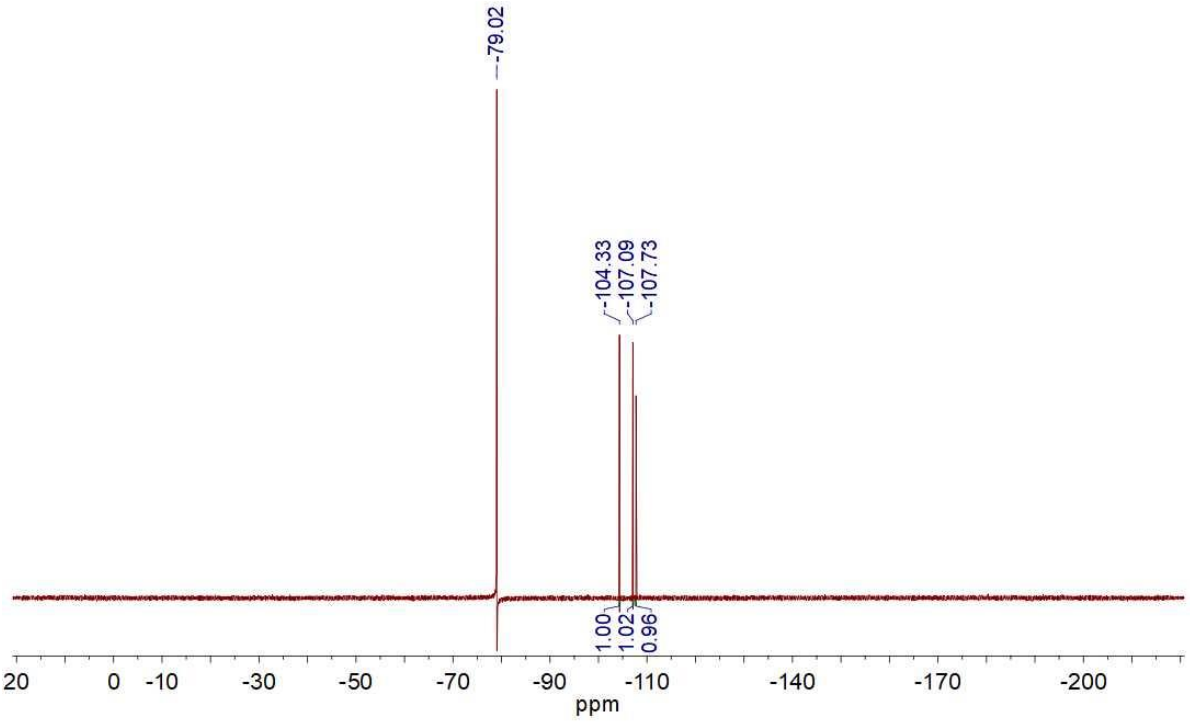

^{19}F NMR (376 MHz, CD_2Cl_2, 298 K) spectrum of **[Ir(fppy)$_2$(Hfppy)](NTf$_2$)**

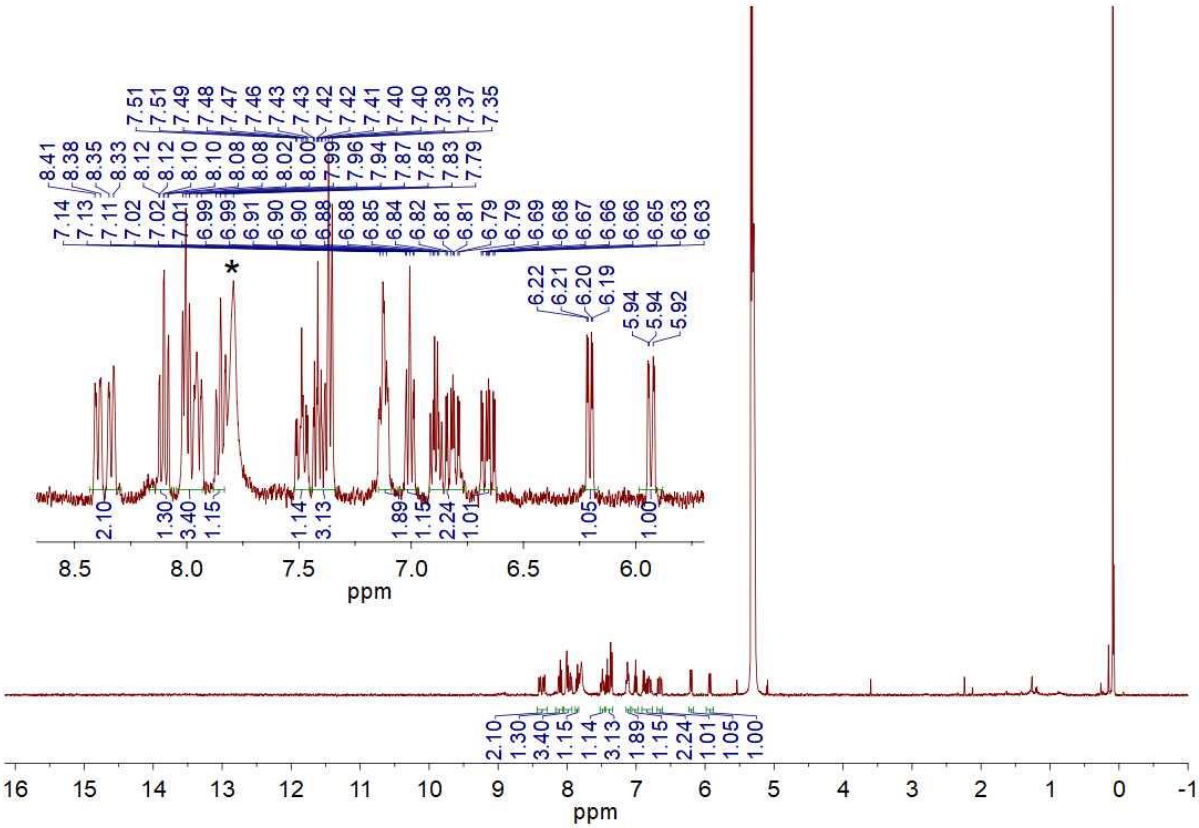

^{1}H NMR (400 MHz, CD_2Cl_2, 298 K) spectrum of **[Ir(dfppy)$_2$(Hdfppy)](NTf$_2$)**. The Tf_2NH signal is marked by an asterisk.

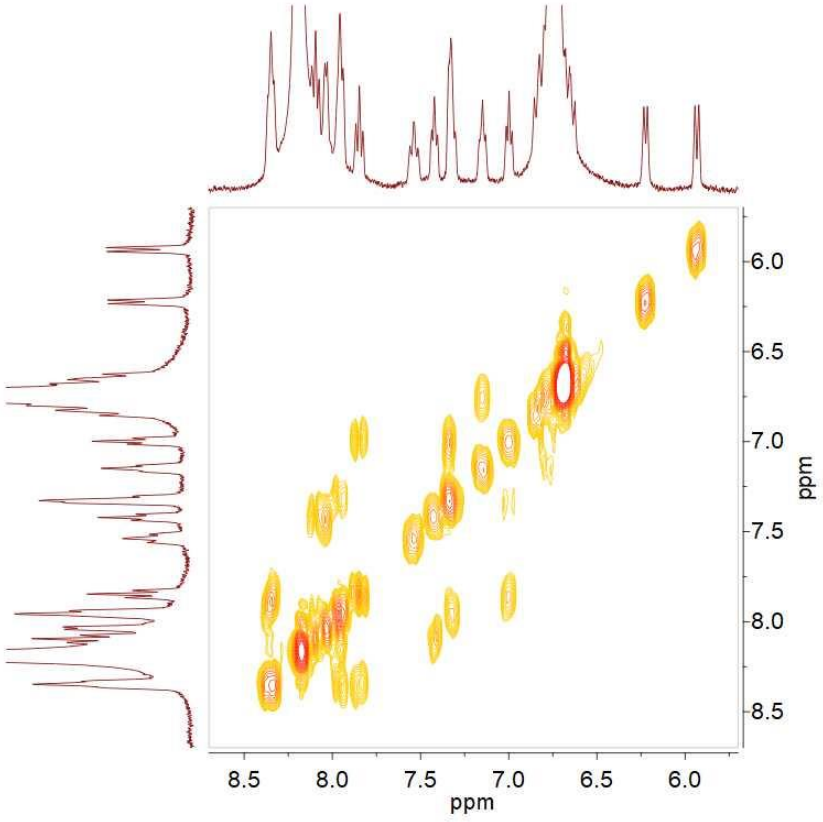

^{1}H–^{1}H COSY NMR (400 MHz, CD_2Cl_2, 273 K) spectrum of **[Ir(dfppy)$_2$(Hdfppy)](NTf$_2$)**

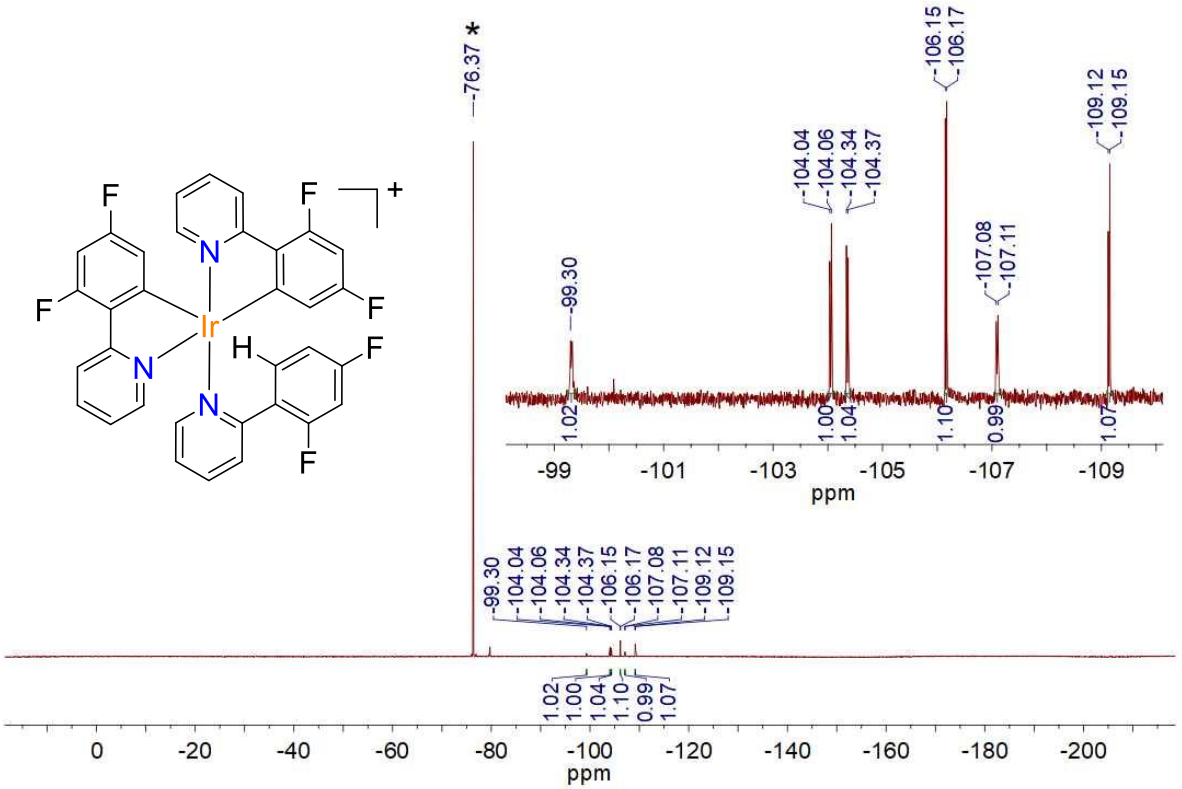

^{19}F NMR (376 MHz, CD_2Cl_2, 298 K) spectrum of **[Ir(dfppy)$_2$(Hdfppy)](NTf$_2$)** (the NTf_2 anion is omitted for clarity). The Tf_2NH signal is marked by an asterisk.

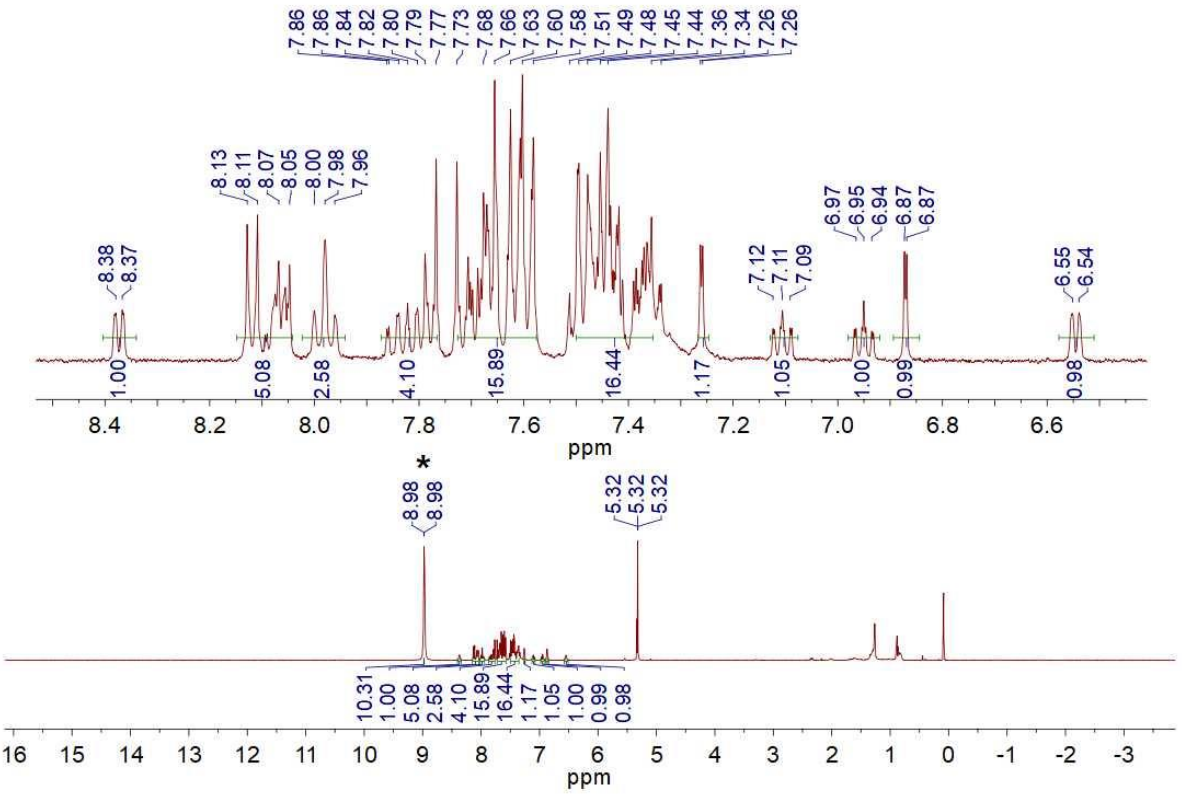

^{1}H NMR (400 MHz, CD_2Cl_2, 298 K) spectrum of **[Ir(tppy)$_2$(Htppy)](O$_2$CCF$_3$)**. The TFA signal is marked by asterisk.

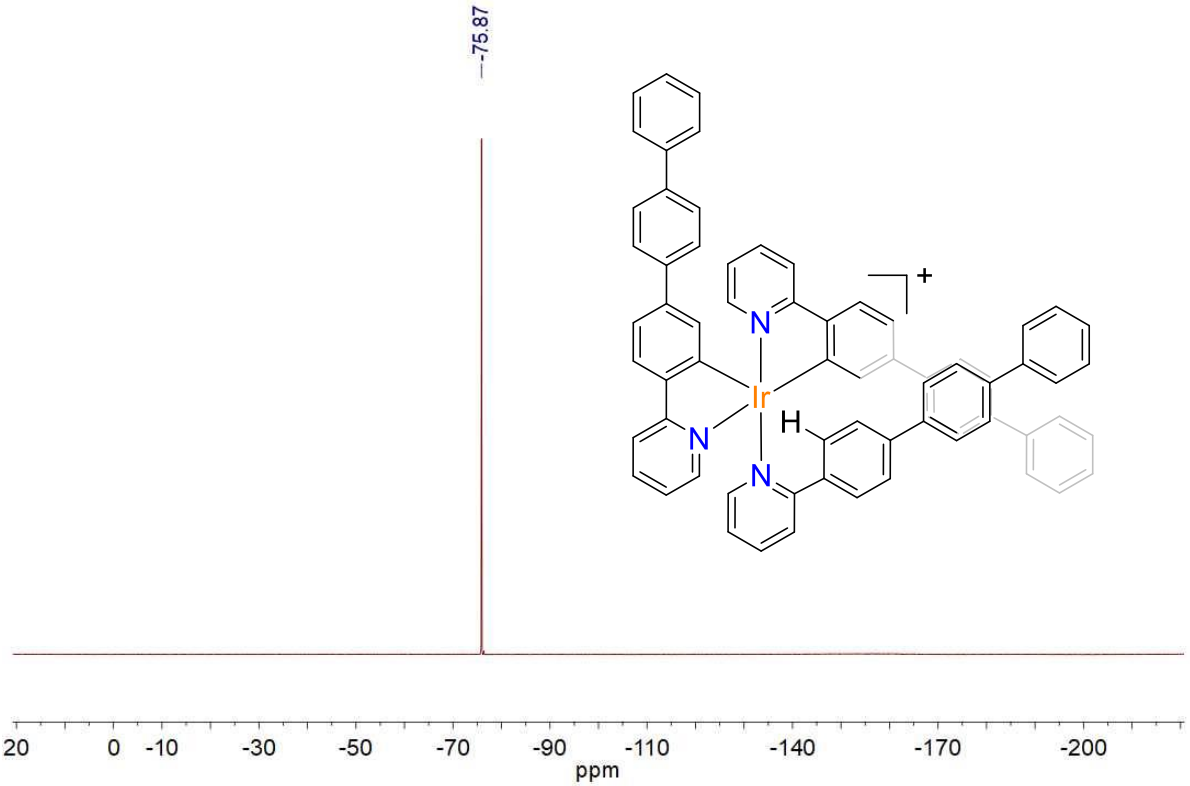

^{19}F NMR (376 MHz, CD_2Cl_2, 298 K) spectrum of **[Ir(tppy)$_2$(Htppy)](O$_2$CCF$_3$)** (the O_2CCF_3 anion is omitted for clarity)

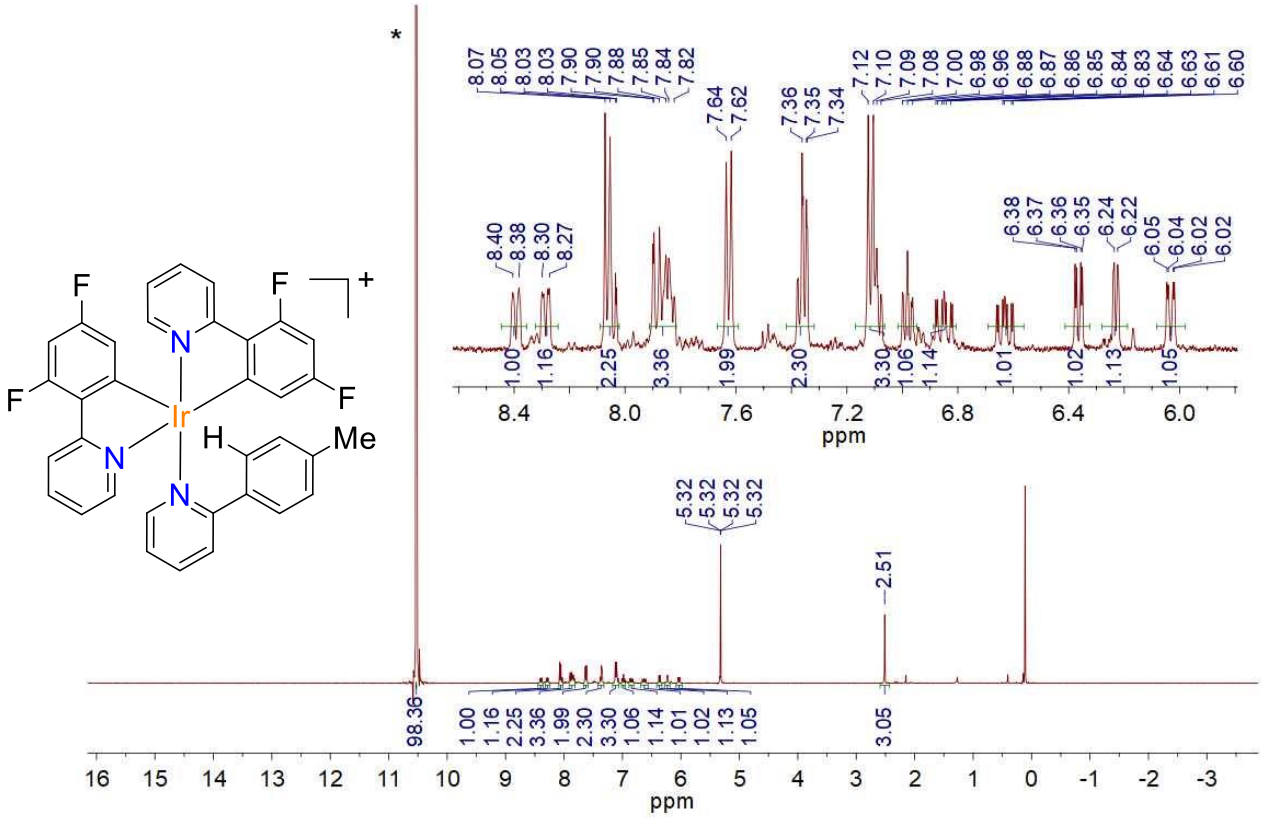

^{1}H NMR (400 MHz, CD_2Cl_2, 298 K) spectrum of **[Ir(dfppy)$_2$(Htpy)](O$_2$CCF$_3$)**. The TFA signal is marked by an asterisk.

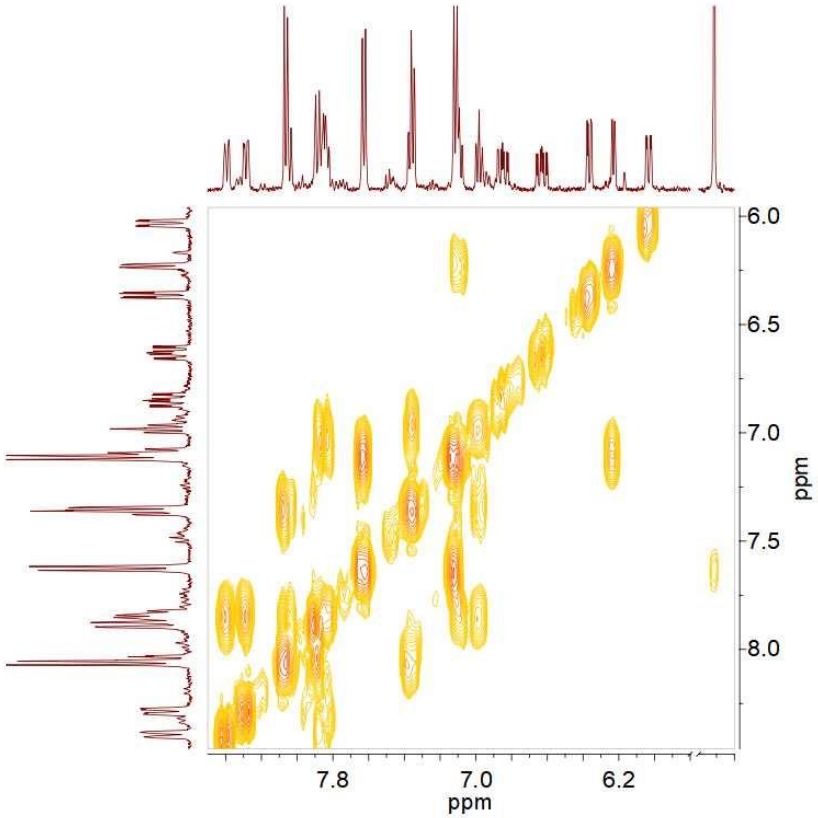

^{1}H–^{1}H COSY NMR (400 MHz, CD_2Cl_2, 273 K) spectrum of **[Ir(dfppy)$_2$(Htpy)](O$_2$CCF$_3$)**

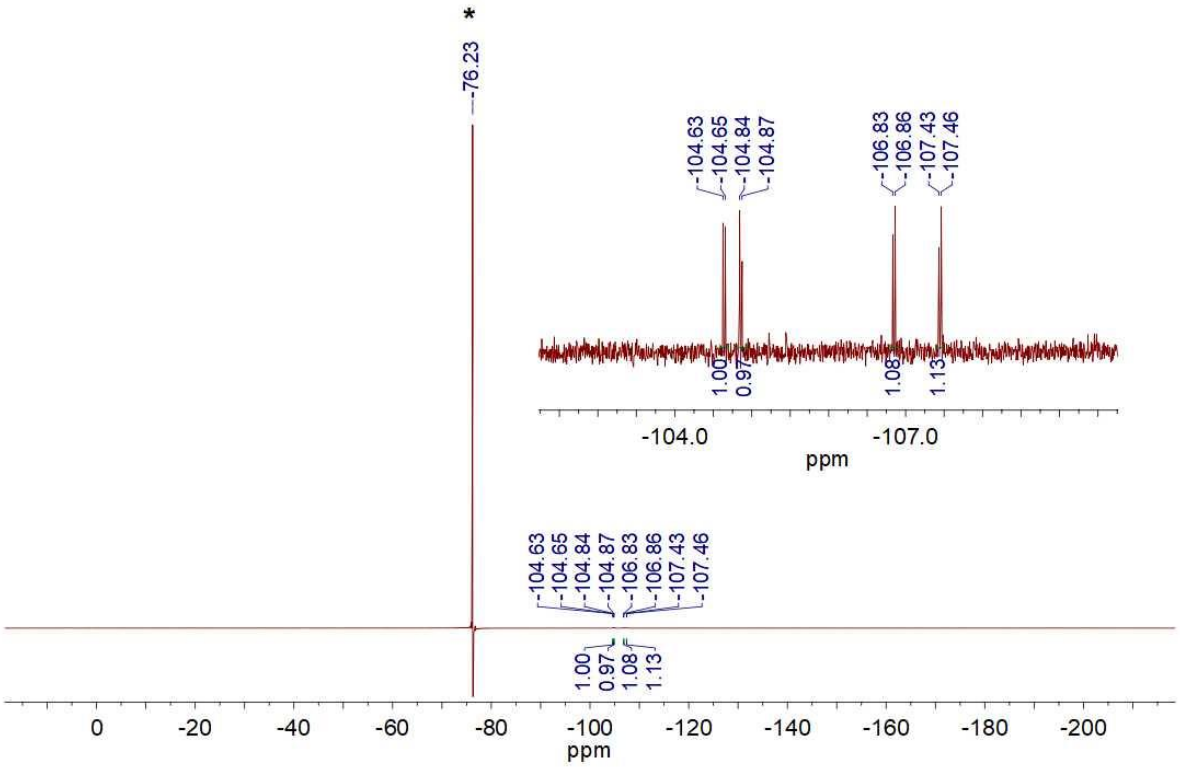

^{19}F NMR (376 MHz, CD_2Cl_2, 298 K) spectrum of **[Ir(dfppy)$_2$(Htpy)](O$_2$CCF$_3$)** (the O_2CCF_3 anion is omitted for clarity). The TFA signal is marked by an asterisk.

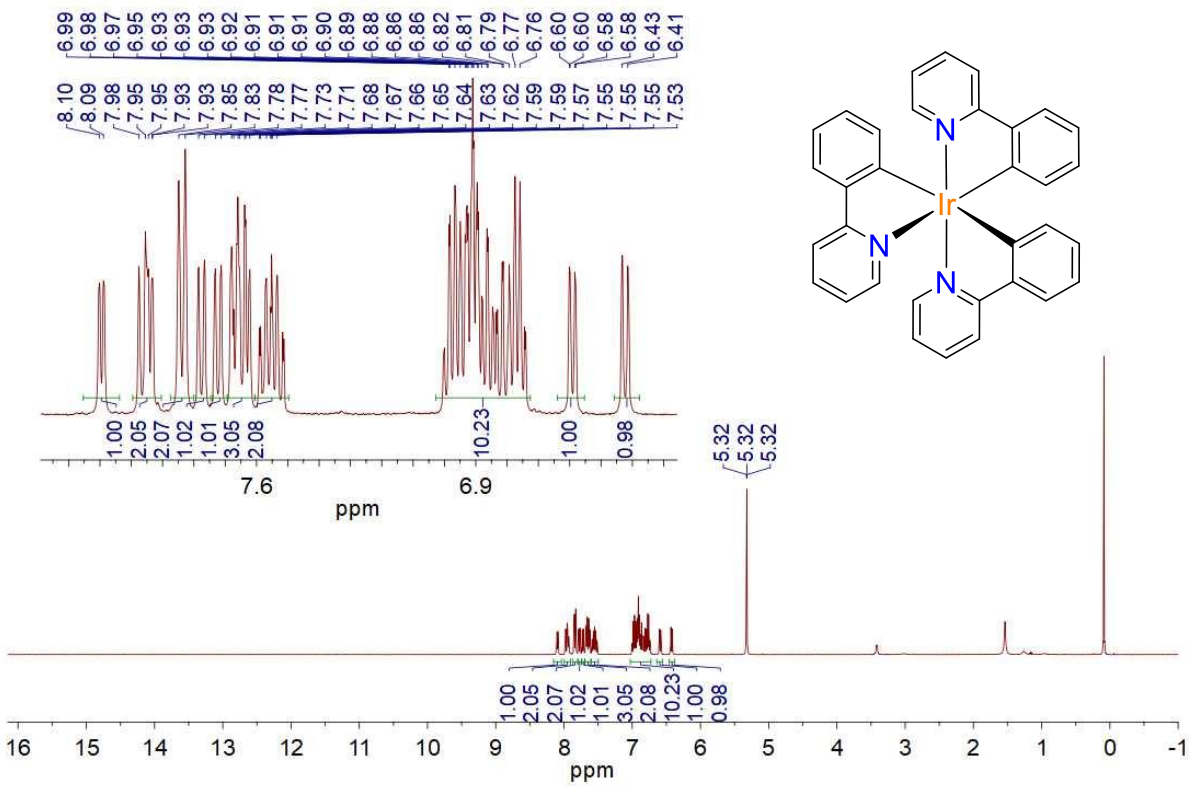

^{1}H NMR (400 MHz, CD_2Cl_2, 298 K) spectrum of ***mer*-Ir(ppy)$_3$** obtained in large-scale synthesis from ***fac*-Ir(ppy)$_3$**

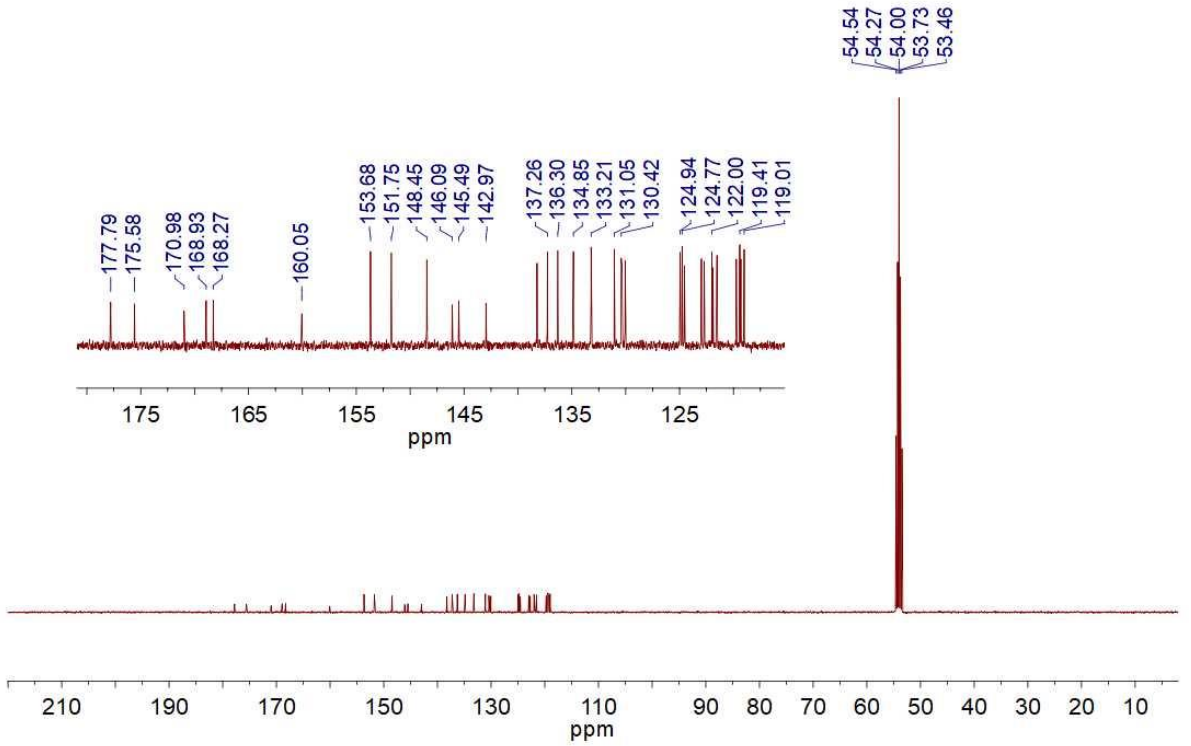

^{13}C NMR (101 MHz, CD_2Cl_2, 298 K) spectrum of ***mer*-Ir(ppy)$_3$** obtained in large-scale synthesis from ***fac*-Ir(ppy)$_3$**

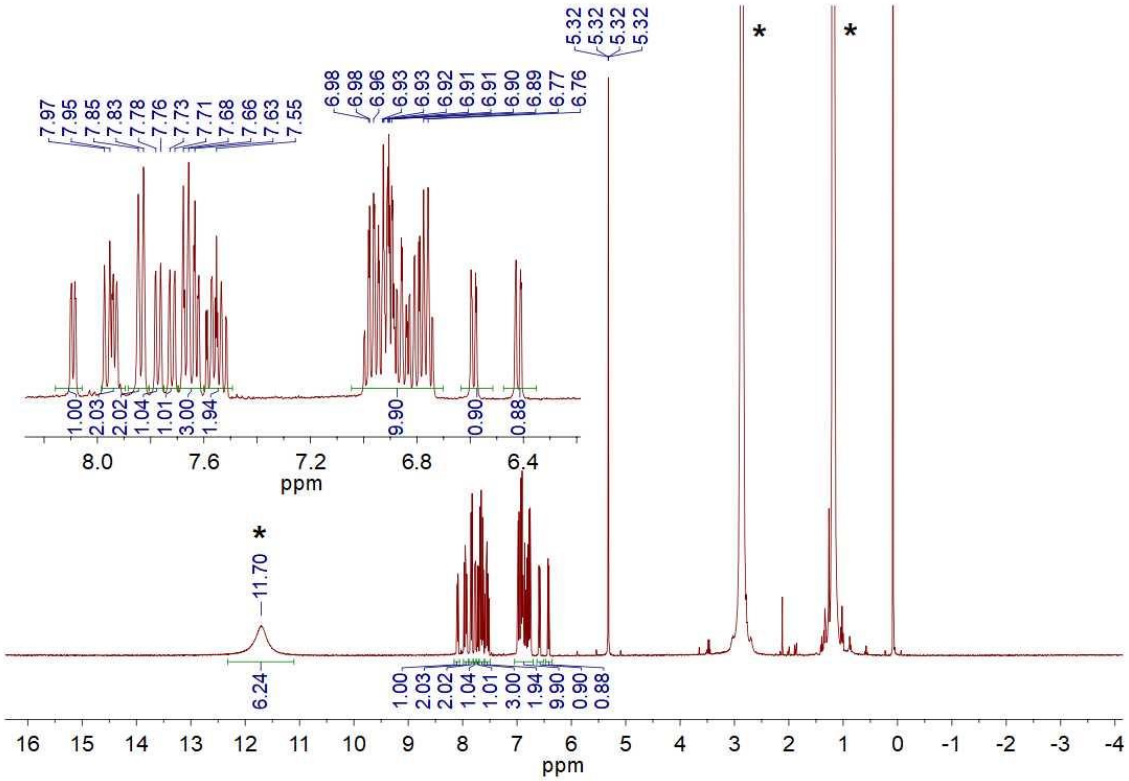

^{1}H NMR (400 MHz, CD_2Cl_2, 298 K) spectrum of ***mer*-Ir(ppy)$_3$** obtained from ***fac*-Ir(ppy)$_3$** using the General Procedure. The signals of $HNEt_3(O_2CCF_3)$ are marked by asterisks.

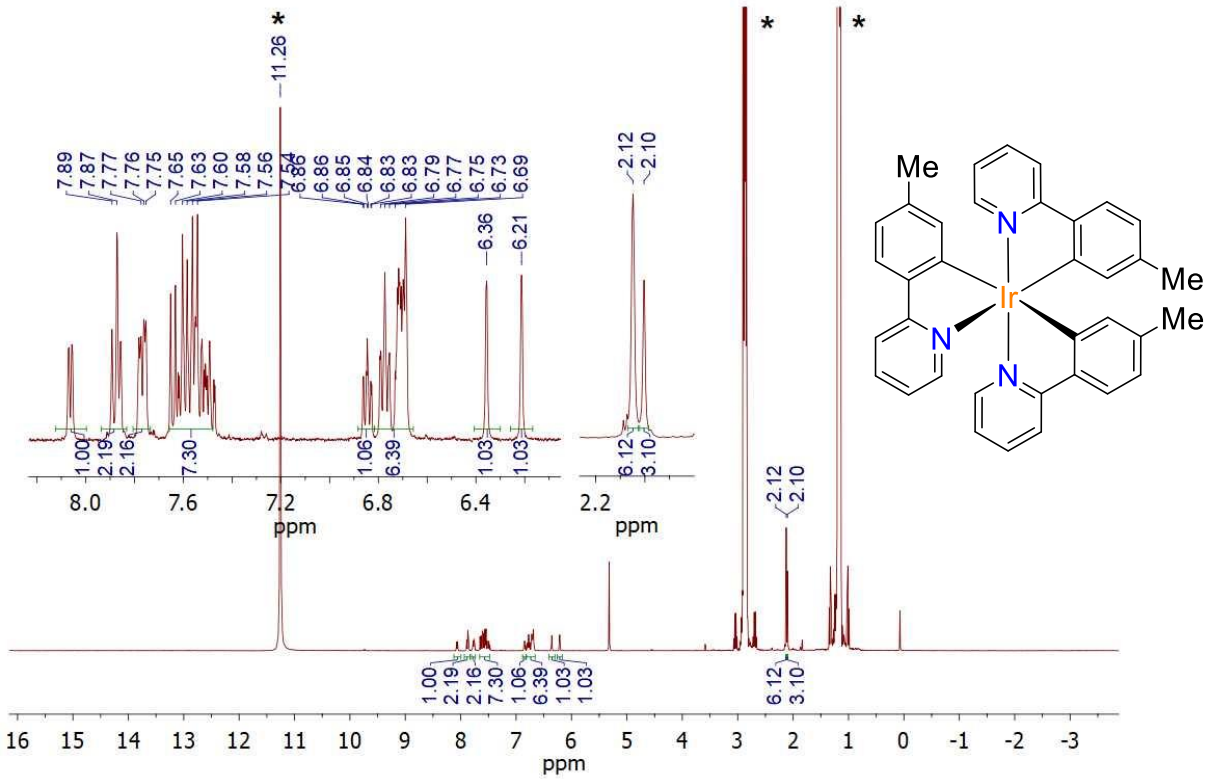

^{1}H NMR (400 MHz, CD_2Cl_2, 298 K) spectrum of ***mer*-Ir(tpy)$_3$** obtained from ***fac*-Ir(tpy)$_3$** using the General Procedure. The signals of $HNEt_3(O_2CCF_3)$ are marked by asterisks.

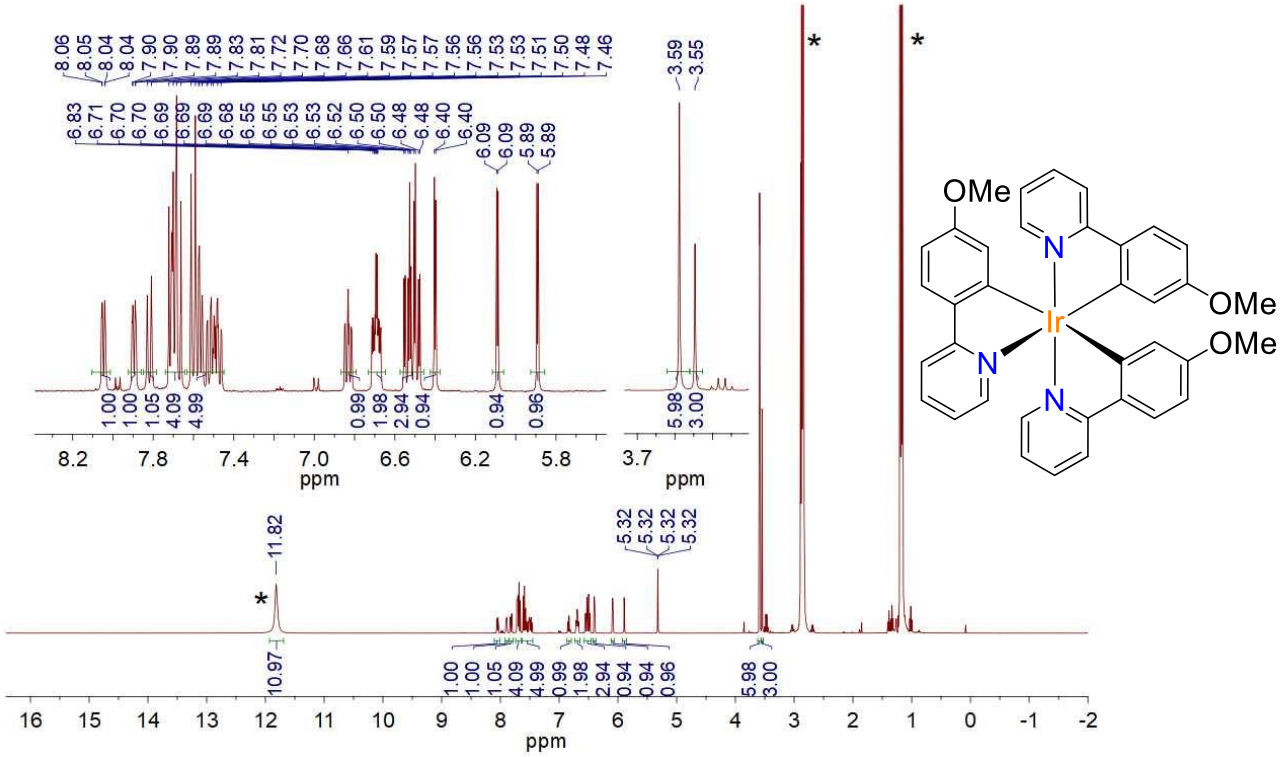

^{1}H NMR (400 MHz, CD_2Cl_2, 298 K) spectrum of ***mer*-Ir(meppy)$_3$** obtained from ***fac*-Ir(meppy)$_3$** using the General Procedure. The peaks of $HNEt_3(O_2CCF_3)$ are marked by asterisks.

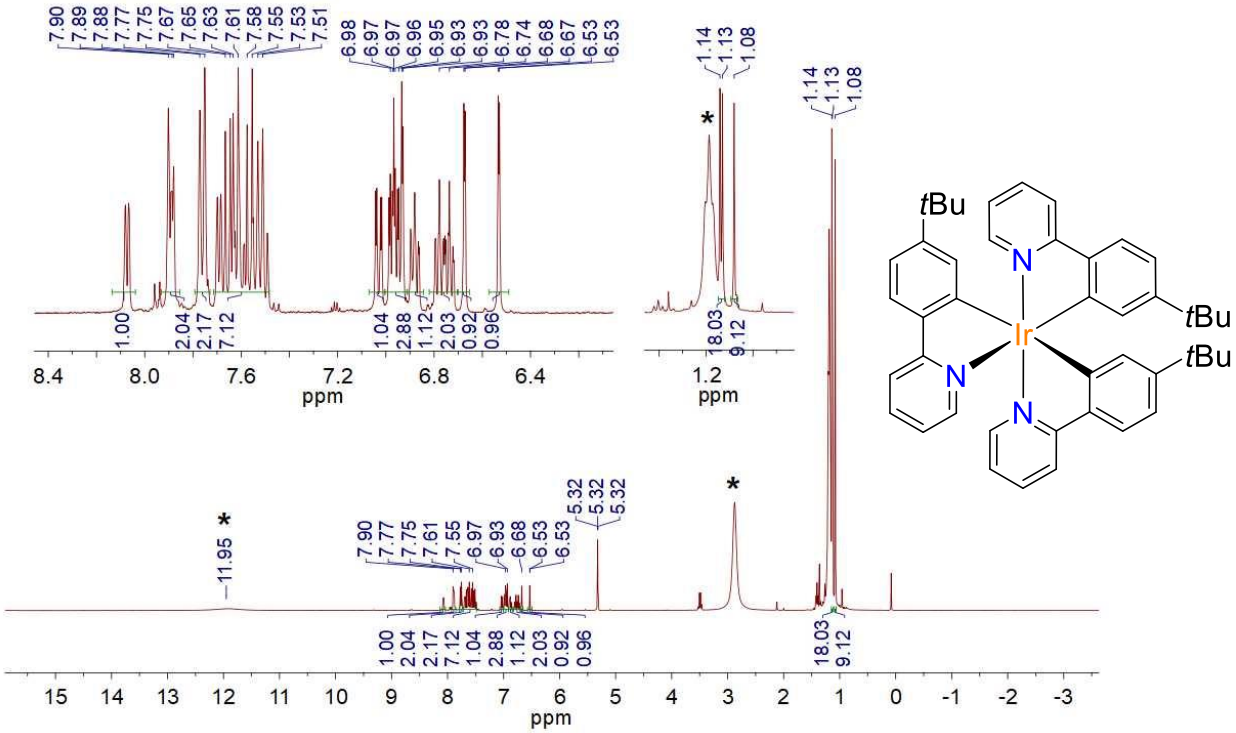

^{1}H NMR (400 MHz, CD_2Cl_2, 298 K) spectrum of ***mer*-Ir(buppy)$_3$** obtained from ***fac*-Ir(buppy)$_3$** using the General Procedure. The peaks of $HNEt_3(O_2CCF_3)$ are marked by asterisks.

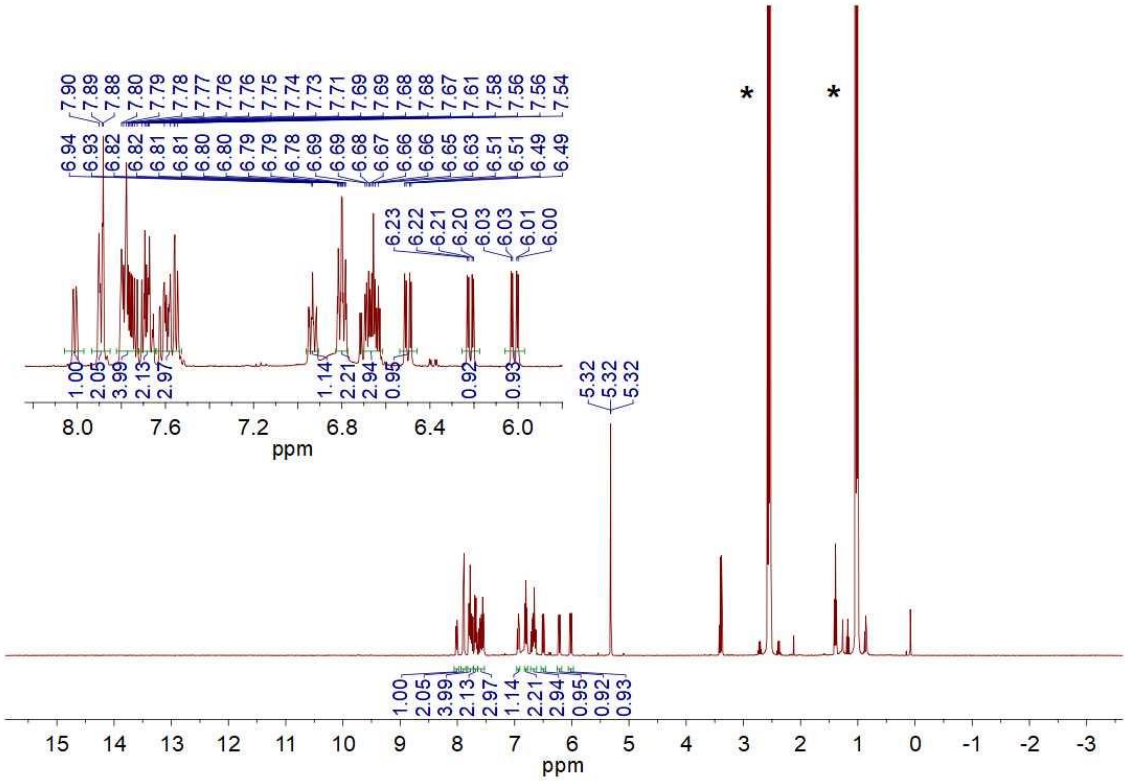

^{1}H NMR (400 MHz, CD_2Cl_2, 298 K) spectrum of ***mer*-Ir(fppy)$_3$** obtained from ***fac*-Ir(fppy)$_3$** using the General Procedure. The signals of NEt_3 excess are marked by asterisks.

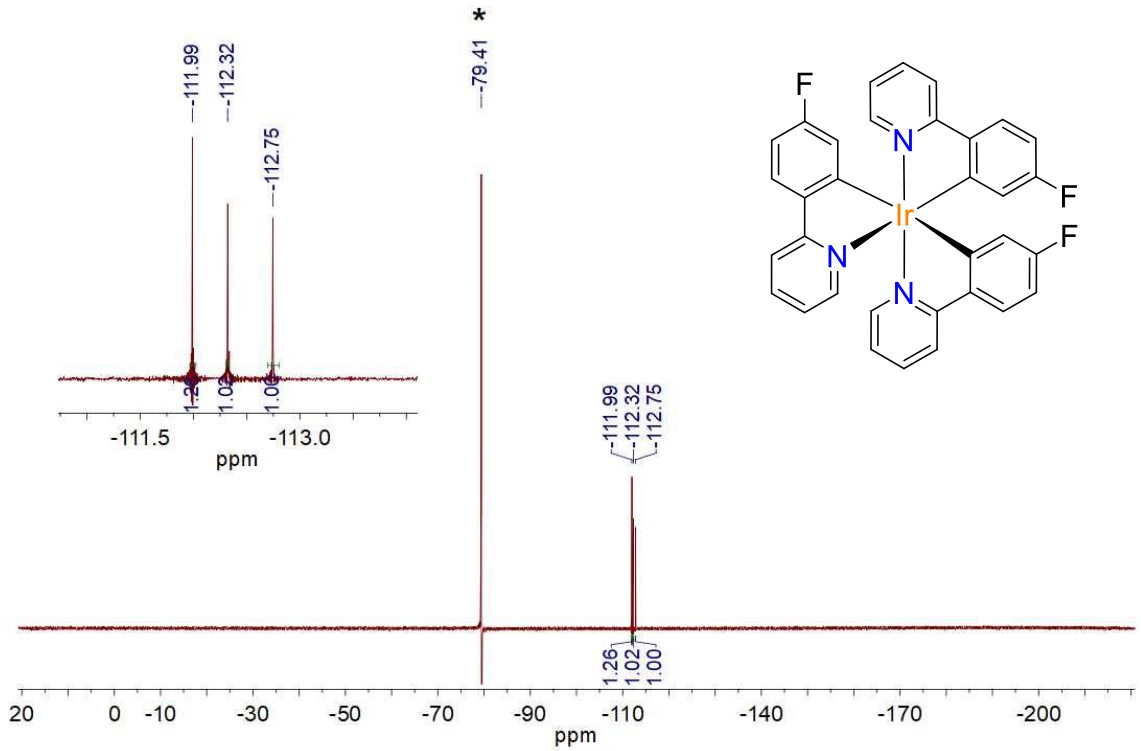

^{19}F NMR (376 MHz, CD_2Cl_2, 298 K) spectrum of ***mer*-Ir(fppy)$_3$** obtained from ***fac*-Ir(fppy)$_3$** using the General Procedure. The signal of $HNEt_3(NTf_2)$ is marked by an asterisk.

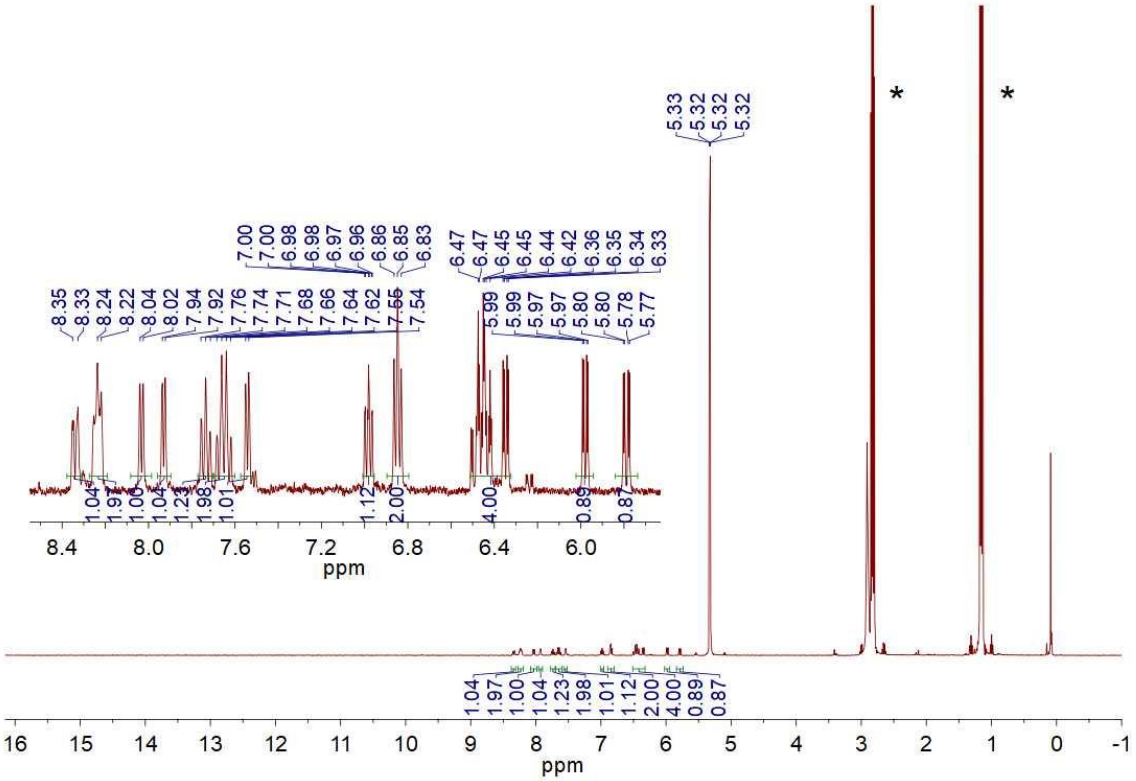

^{1}H NMR (400 MHz, CD_2Cl_2, 298 K) spectrum of ***mer*-Ir(dfppy)$_3$** obtained from ***fac*-Ir(dfppy)$_3$** using the General Procedure. The signals of $HNEt_3(NTf_2)$ are marked by asterisks.

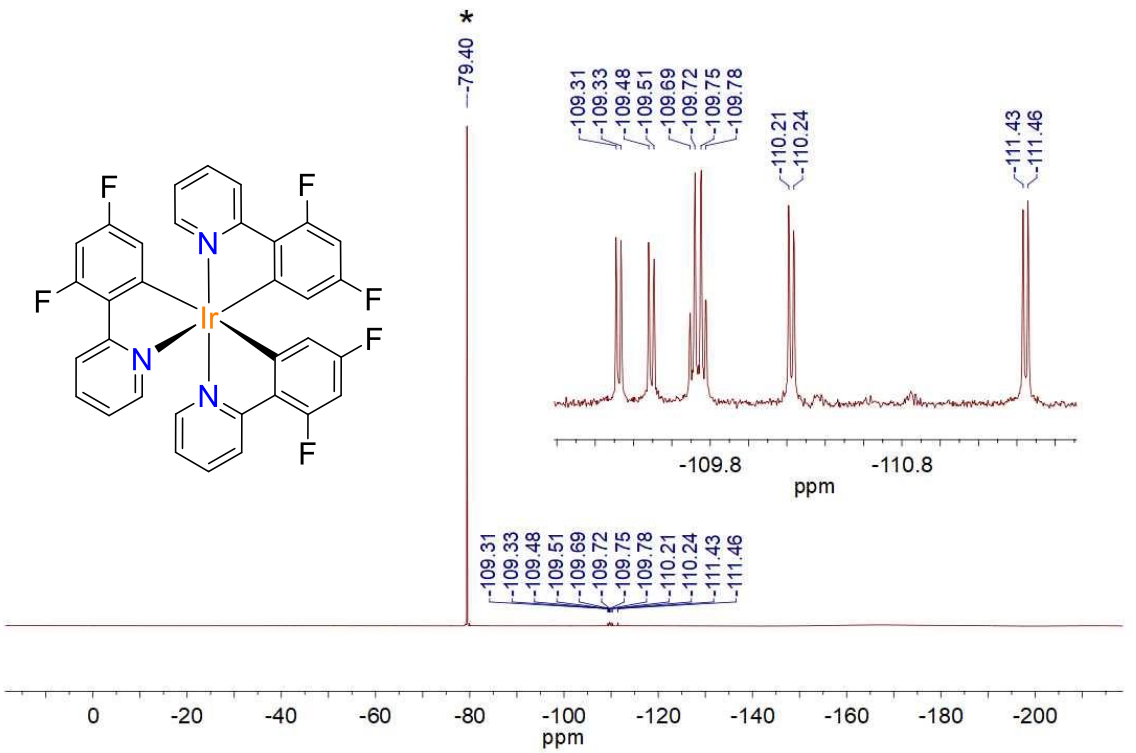

^{19}F NMR (376 MHz, CD_2Cl_2, 298 K) spectrum of ***mer*-Ir(dfppy)$_3$** obtained from ***fac*-Ir(dfppy)$_3$** using the General Procedure. The signal of $HNEt_3(NTf_2)$ is marked by an asterisk.

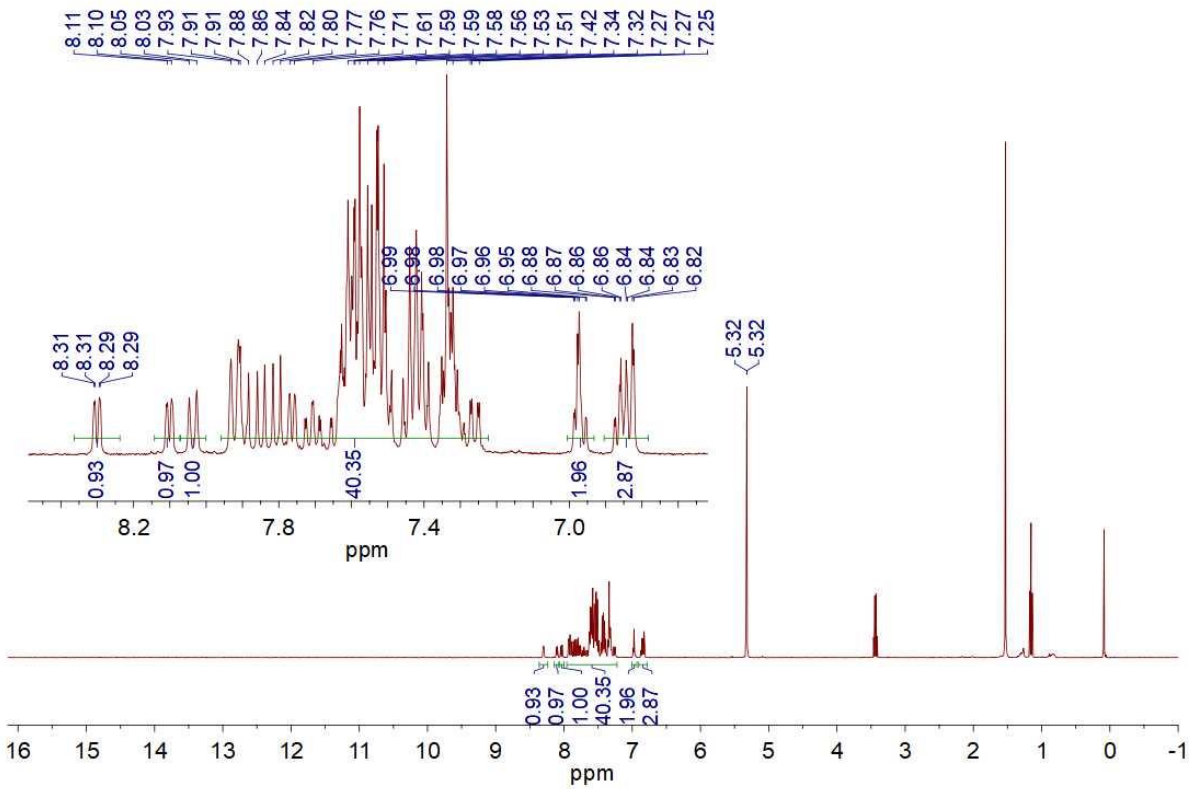

^{1}H NMR (400 MHz, CD_2Cl_2, 298 K) spectrum of ***mer*-Ir(tppy)$_3$** synthesized from **[Ir(tppy)$_2$(μ-Cl)]$_2$** and **Htppy**

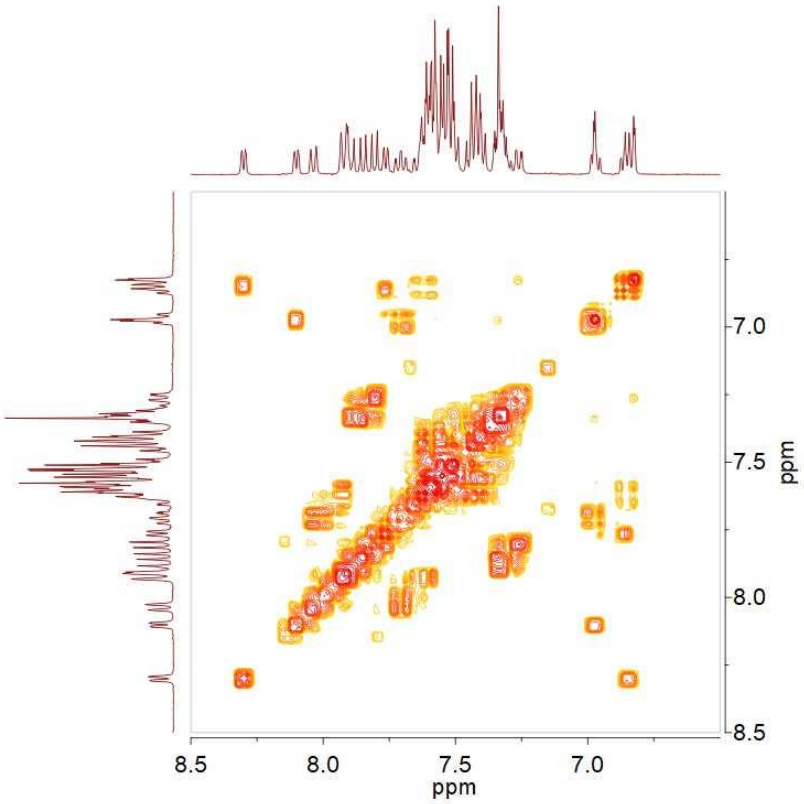

^{1}H–^{1}H COSY NMR (400 MHz, CD_2Cl_2, 273 K) spectrum of ***mer*-Ir(tppy)$_3$** synthesized from **[Ir(tppy)$_2$(μ-Cl)]$_2$** and **Htppy**

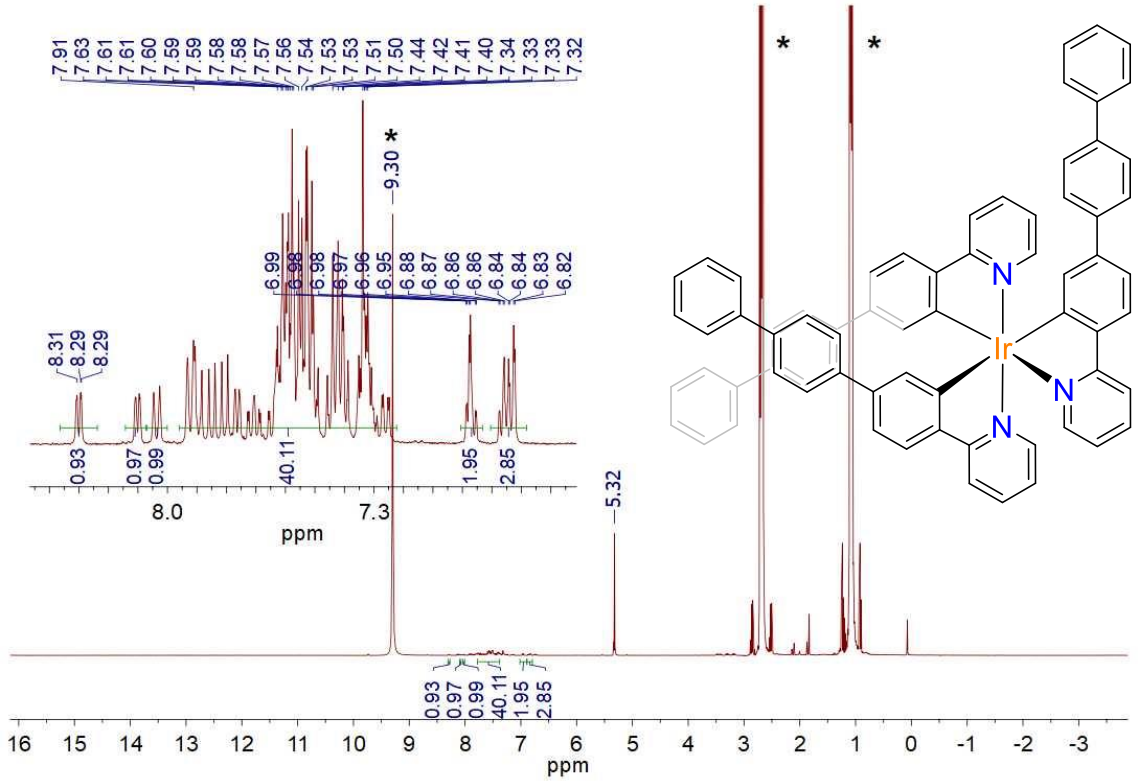

^{1}H NMR (400 MHz, CD_2Cl_2, 298 K) spectrum of ***mer*-Ir(tppy)$_3$** obtained from ***fac*-Ir(tppy)$_3$** using the General Procedure. The signals of $HNEt_3(O_2CCF_3)$ are marked by asterisks.

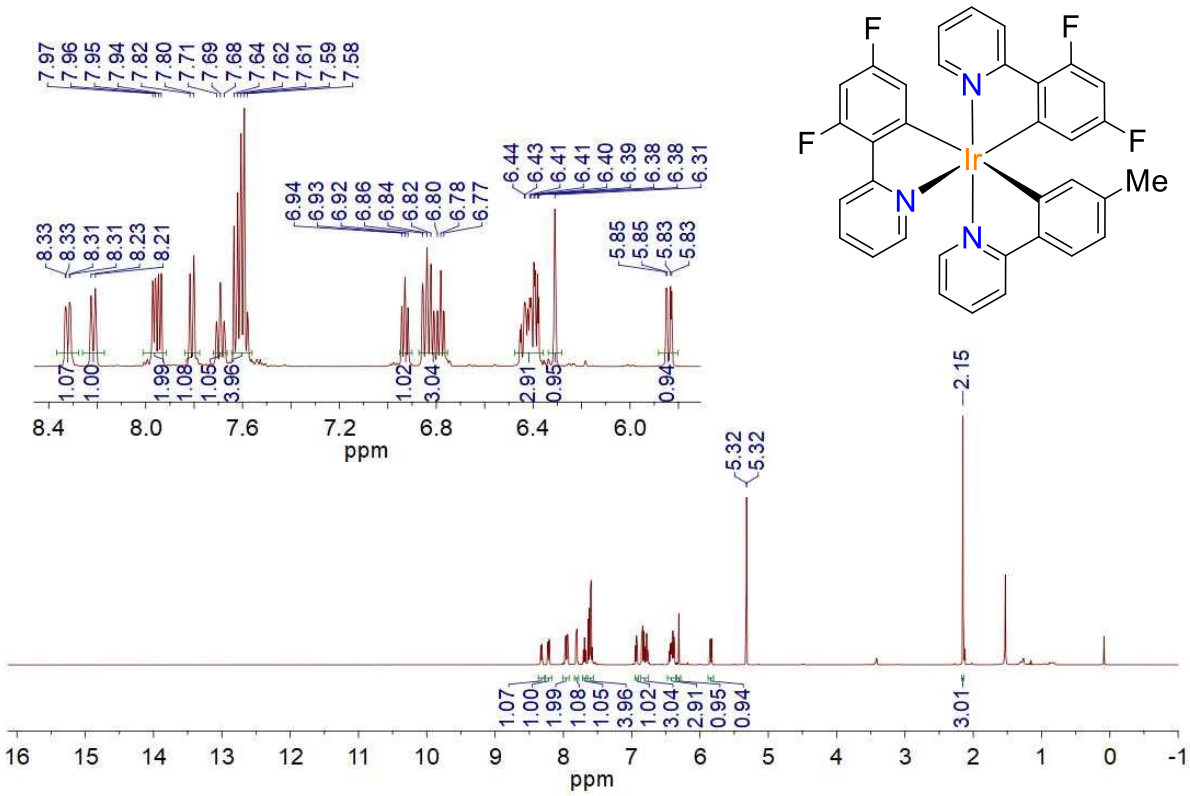

^{1}H NMR (500 MHz, CD_2Cl_2, 298 K) spectrum of ***mer*-Ir(dfppy)$_2$(tpy)** obtained in large-scale synthesis from ***fac*-Ir(dfppy)$_2$(tpy)**

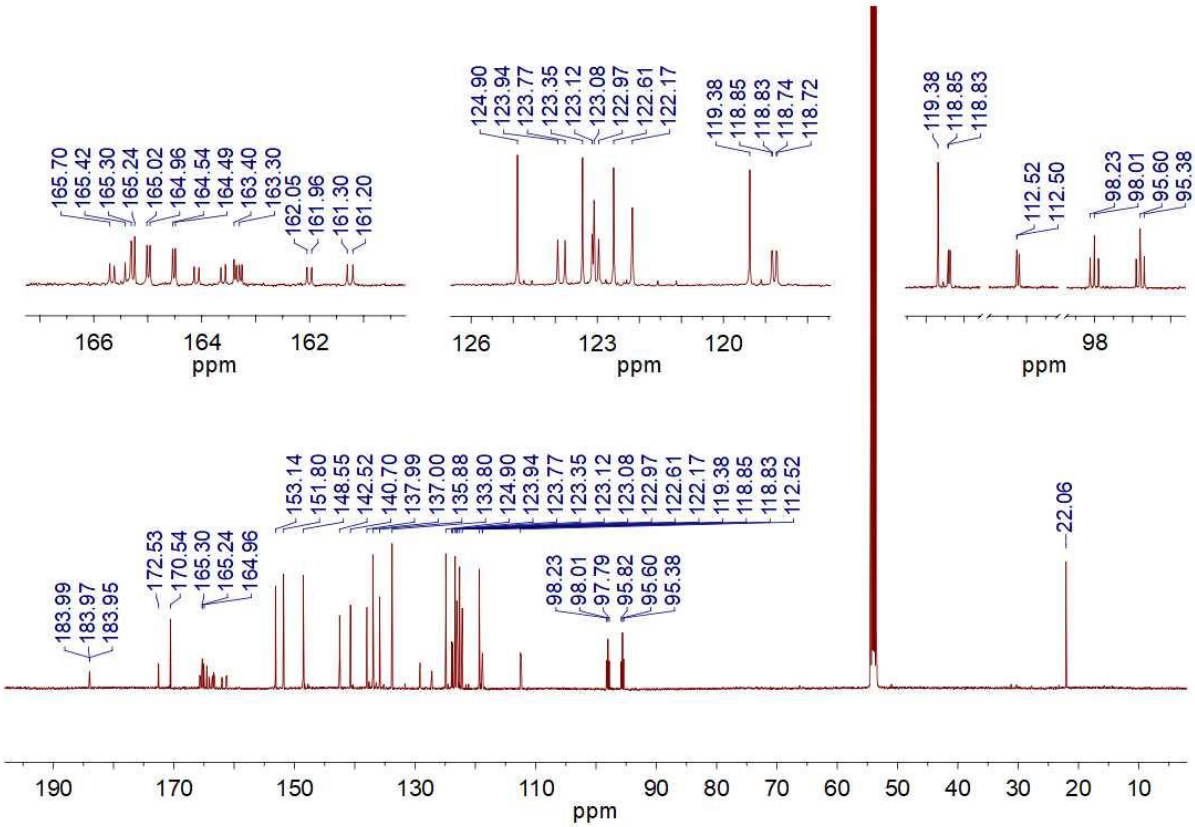

^{13}C NMR (126 MHz, CD_2Cl_2, 298 K) spectrum of ***mer*-Ir(dfppy)$_2$(tpy)** obtained in large-scale synthesis from ***fac*-Ir(dfppy)$_2$(tpy)**

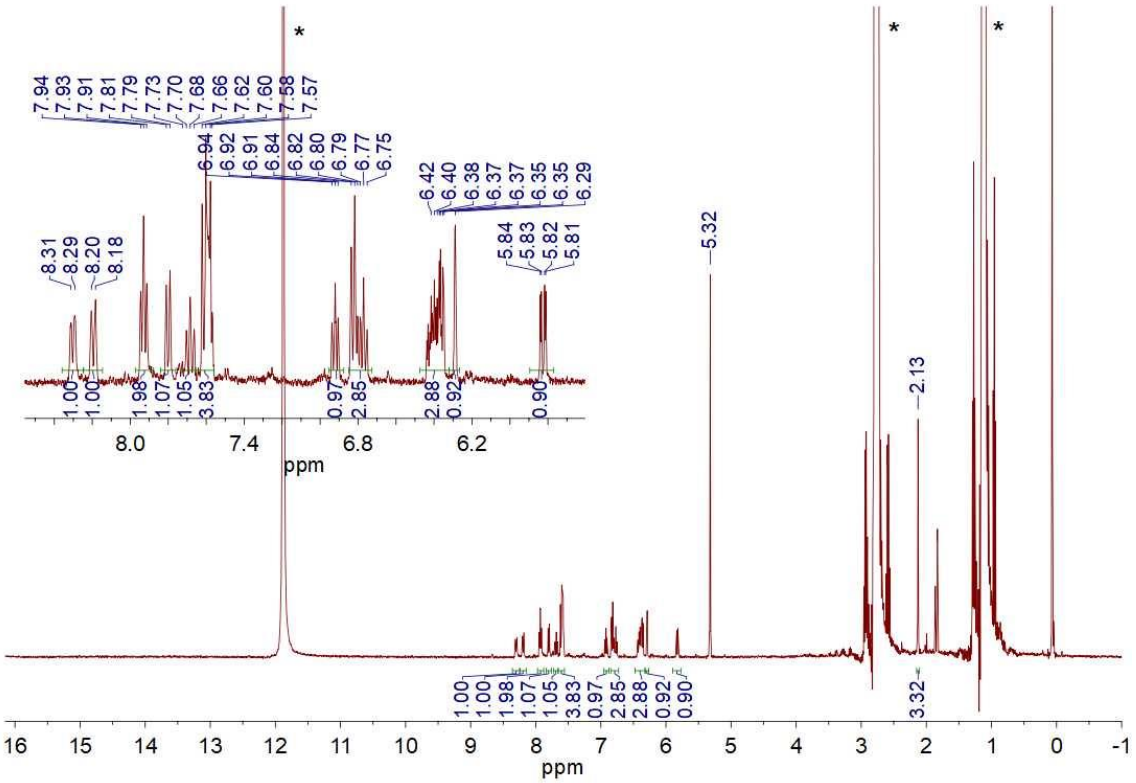

^{1}H NMR (400 MHz, CD_2Cl_2, 298 K) spectrum of ***mer*-Ir(dfppy)$_2$(tpy)** obtained from ***fac*-Ir(dfppy)$_2$(tpy)** using the General Procedure. The signals of $HNEt_3(O_2CCF_3)$ are marked by an asterisk.

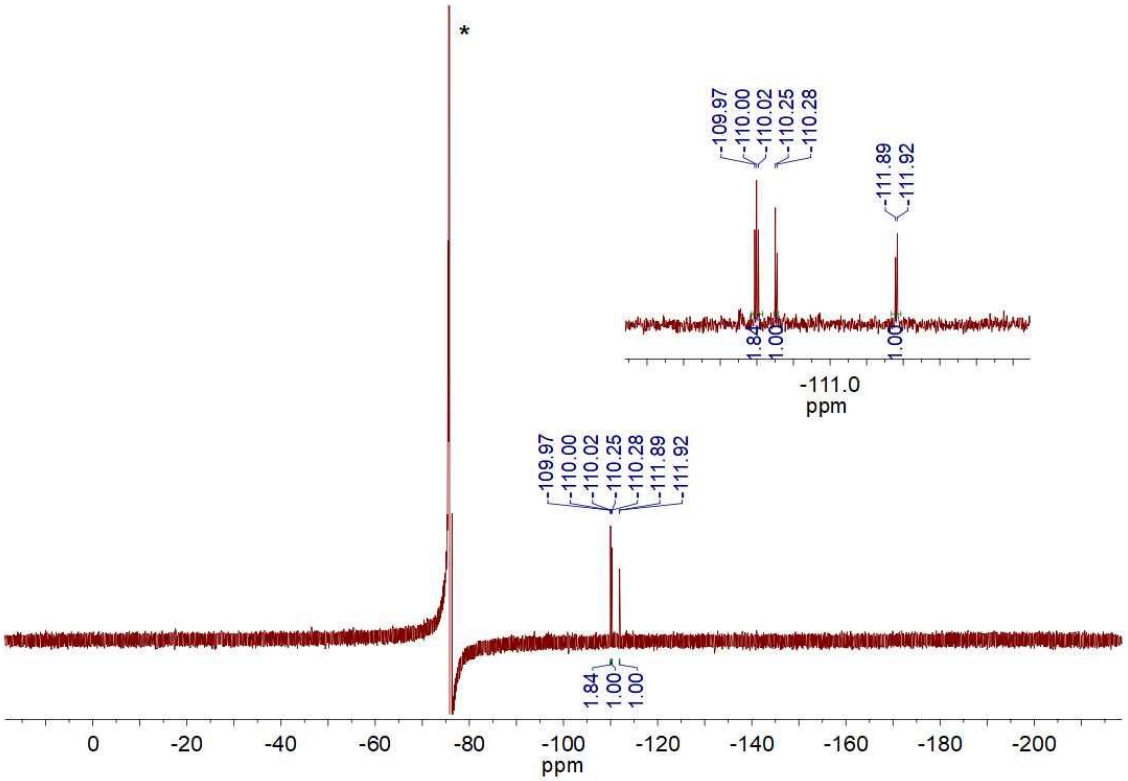

^{19}F NMR (376 MHz, CD_2Cl_2, 298 K) spectrum of ***mer*-Ir(dfppy)$_2$(tpy)** obtained from ***fac*-Ir(dfppy)$_2$(tpy)** using the General Procedure. The signals of $HNEt_3(O_2CCF_3)$ are marked by an asterisk.

Variable-temperature (VT) NMR spectra

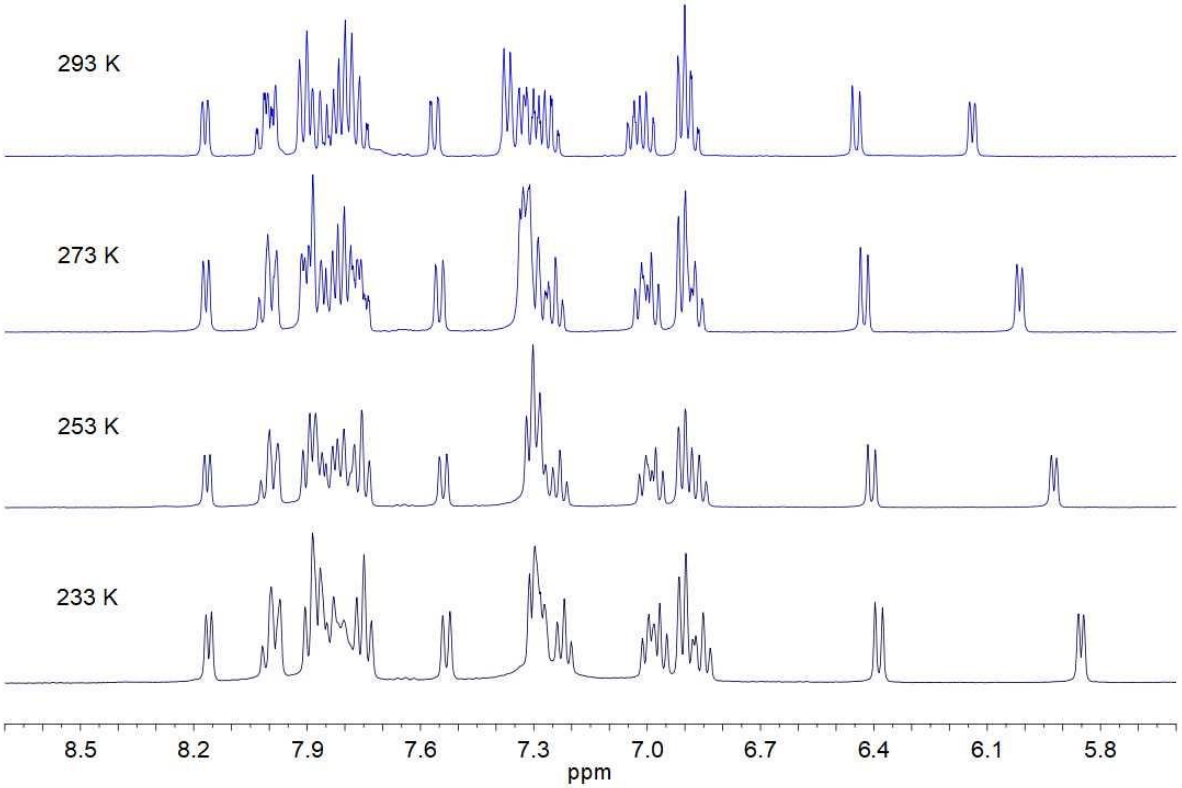

VT ^{1}H NMR (400 MHz, CD_2Cl_2) spectra of **[Ir(ppy)$_2$(Hppy)](O$_2$CCF$_3$)**

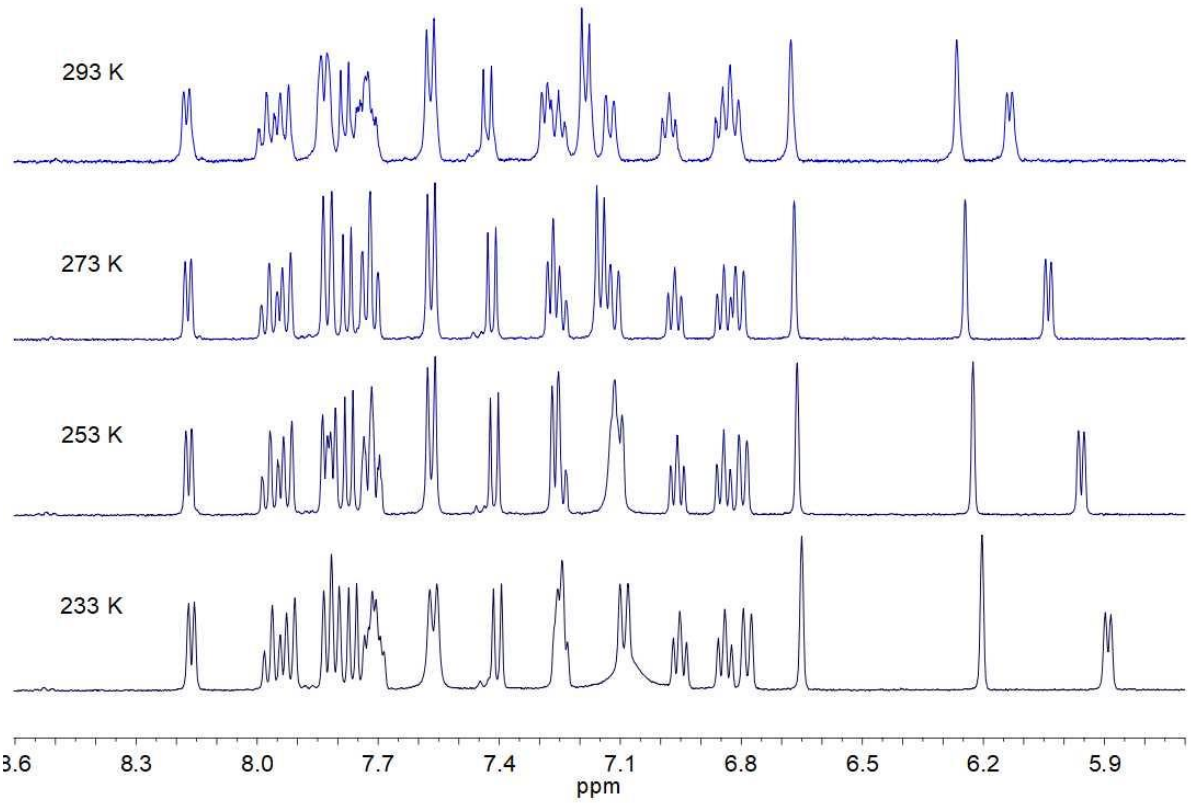

Aromatic region of VT ^{1}H NMR (400 MHz, CD_2Cl_2) spectra of **[Ir(tpy)$_2$(Htpy)](O$_2$CCF$_3$)**

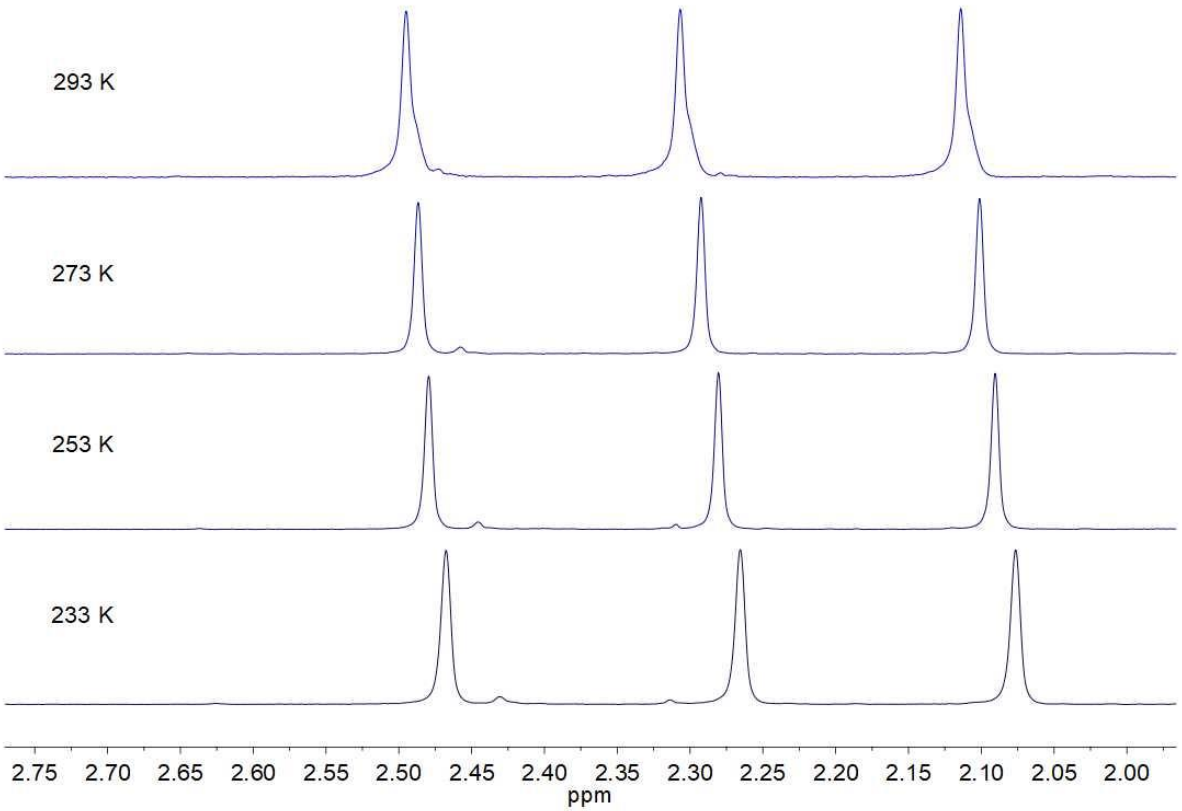

Aliphatic region of VT ^{1}H NMR (400 MHz, CD_2Cl_2) spectra of
[Ir(tpy)$_2$(Htpy)](O$_2$CCF$_3$)

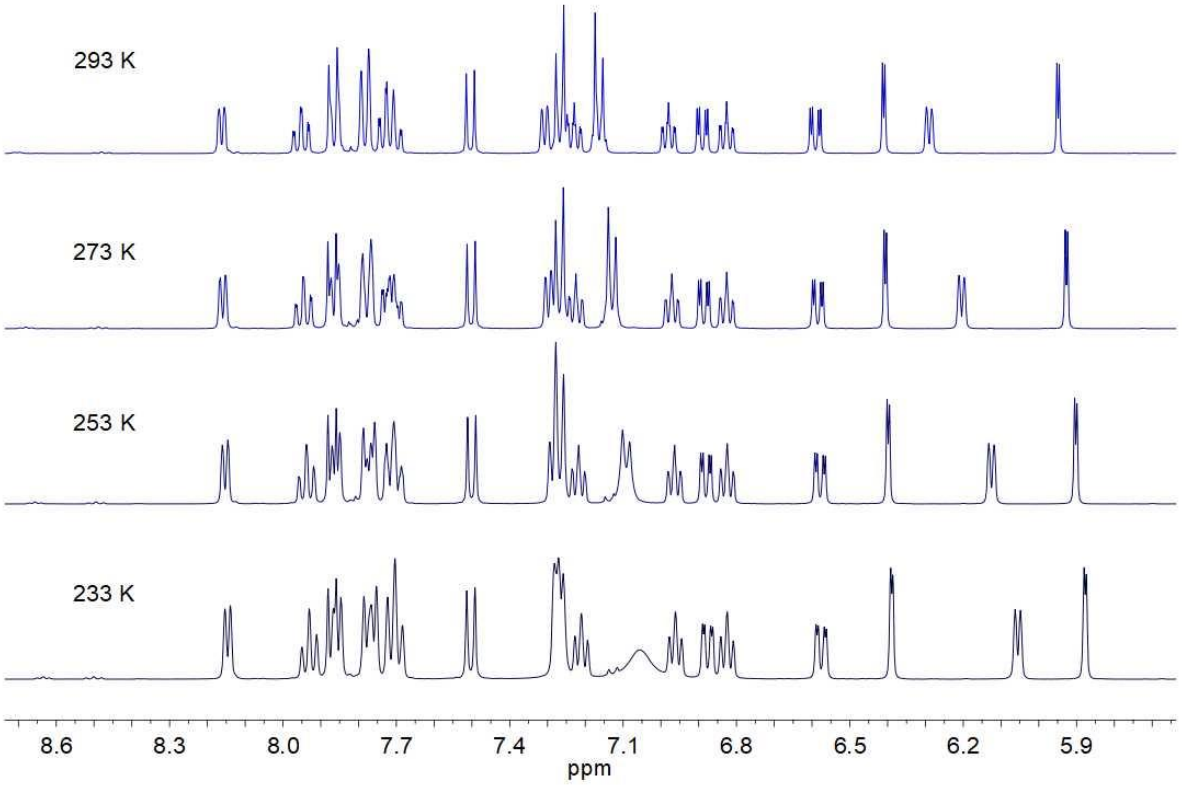

Aromatic region of VT ^{1}H NMR (400 MHz, CD_2Cl_2) spectra of
[Ir(meppy)$_2$(Hmeppy)](O$_2$CCF$_3$)

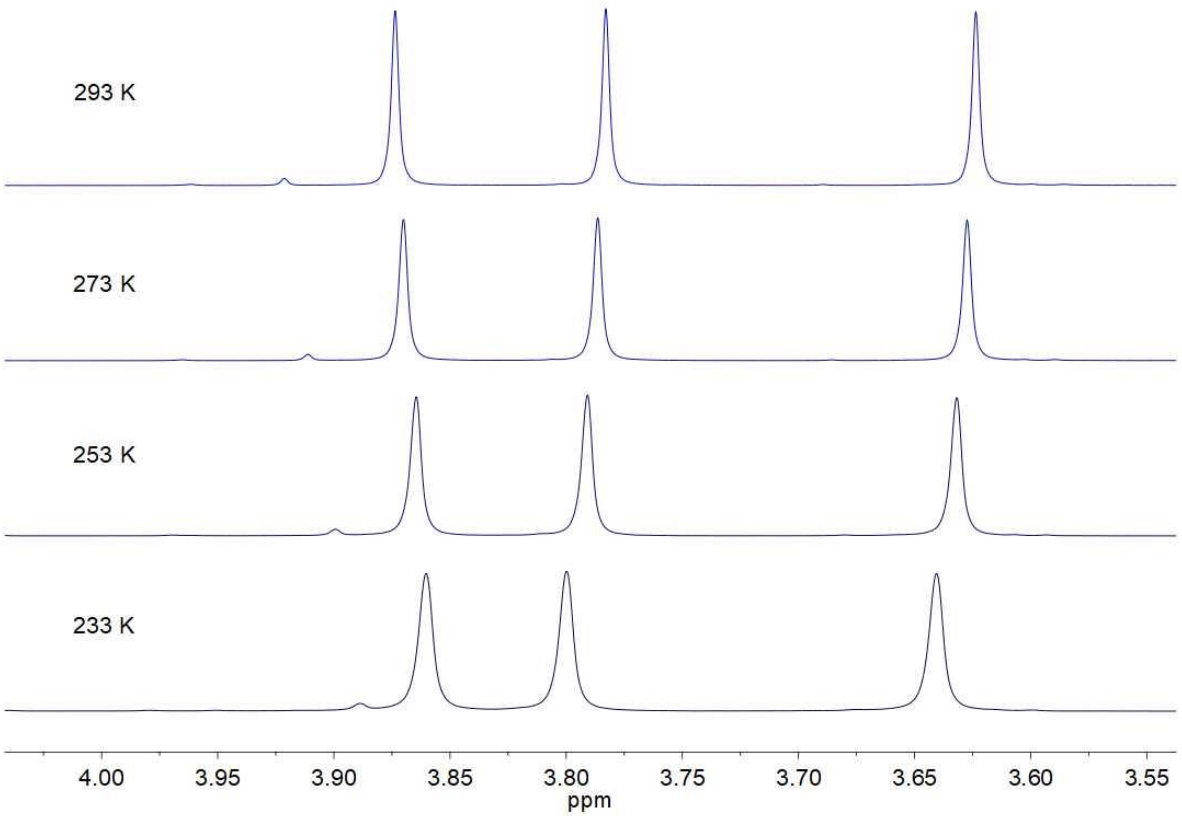

Aliphatic region of VT ^{1}H NMR (400 MHz, CD_2Cl_2) spectra of **[Ir(meppy)$_2$(Hmeppy)](O$_2$CCF$_3$)**

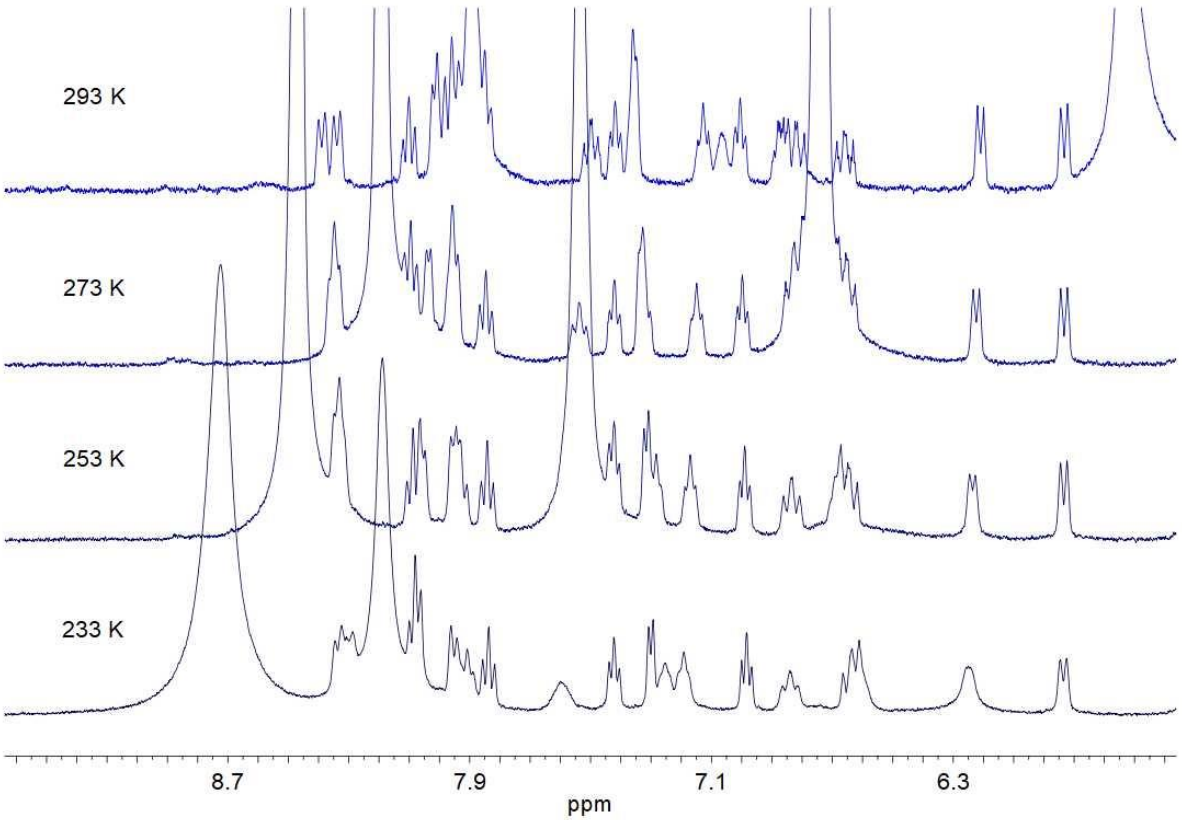

VT ^{1}H NMR (400 MHz, CD_2Cl_2) spectra of **[Ir(dfppy)$_2$(Hdfppy)](NTf$_2$)**

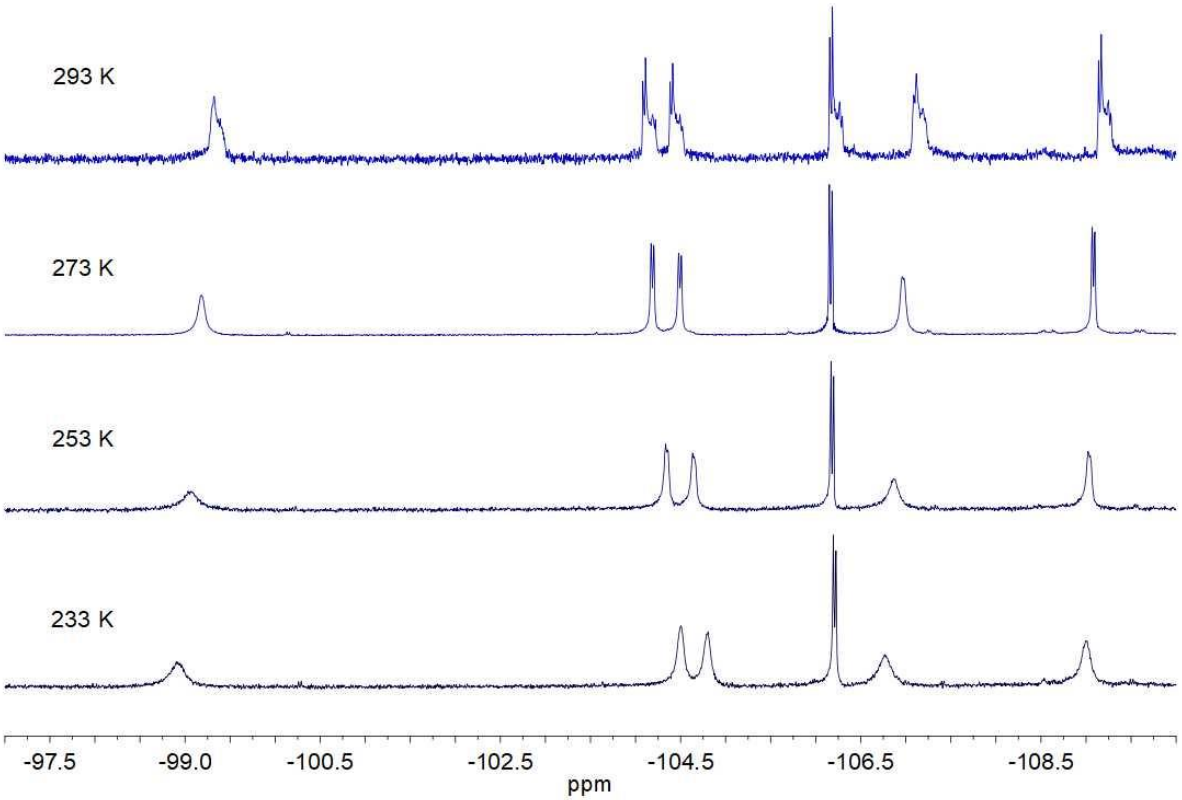

VT ^{19}F NMR (376 MHz, CD_2Cl_2) spectra of **[Ir(dfppy)$_2$(Hdfppy)](NTf$_2$)**

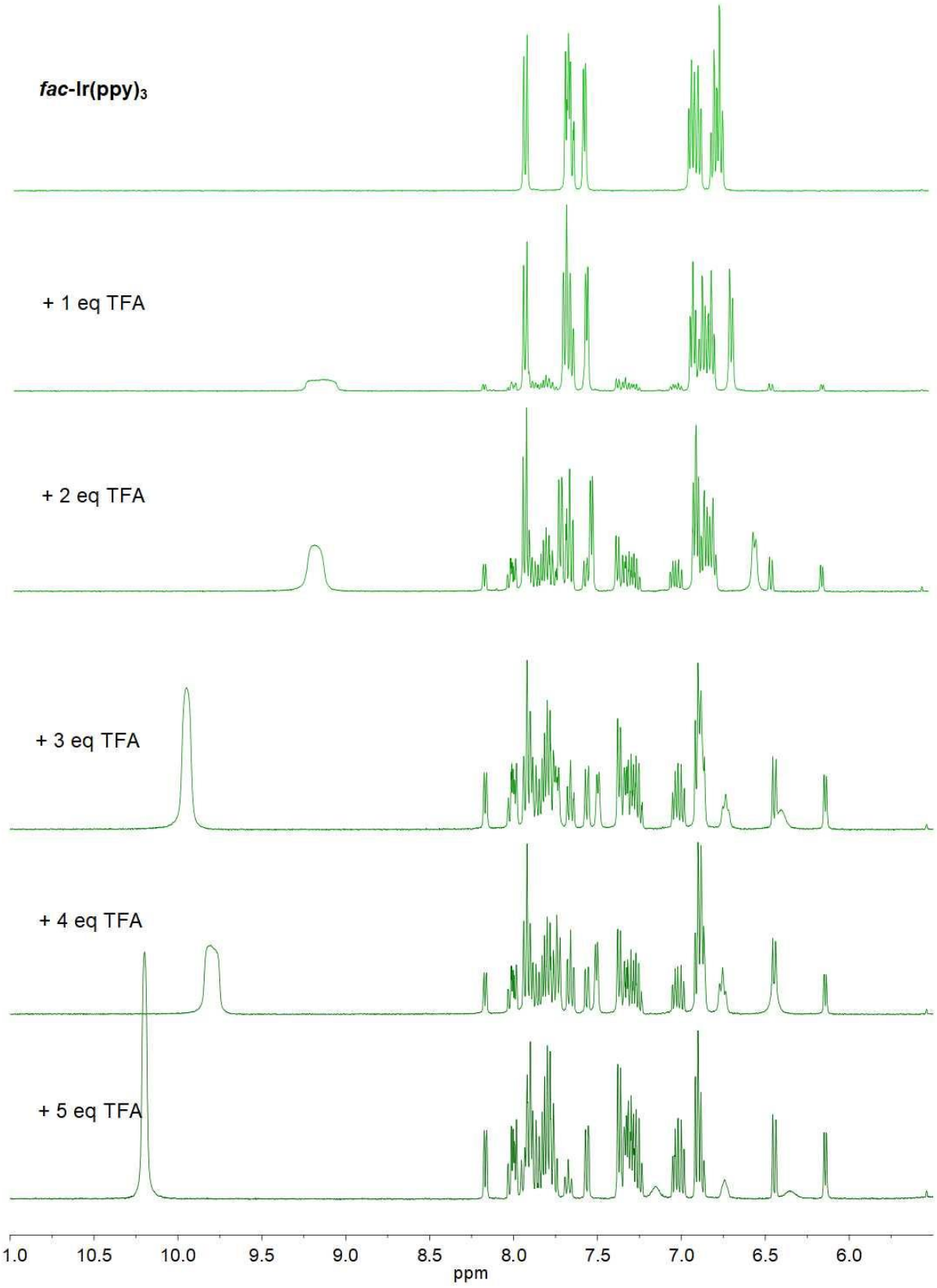
fac-Ir(ppy)$_3$
+ 1 eq TFA
+ 2 eq TFA
+ 3 eq TFA
+ 4 eq TFA
+ 5 eq TFA
1.0
10.5
10.0
9.5
9.0
8.5
8.0
7.5
7.0
6.5
6.0
ppm

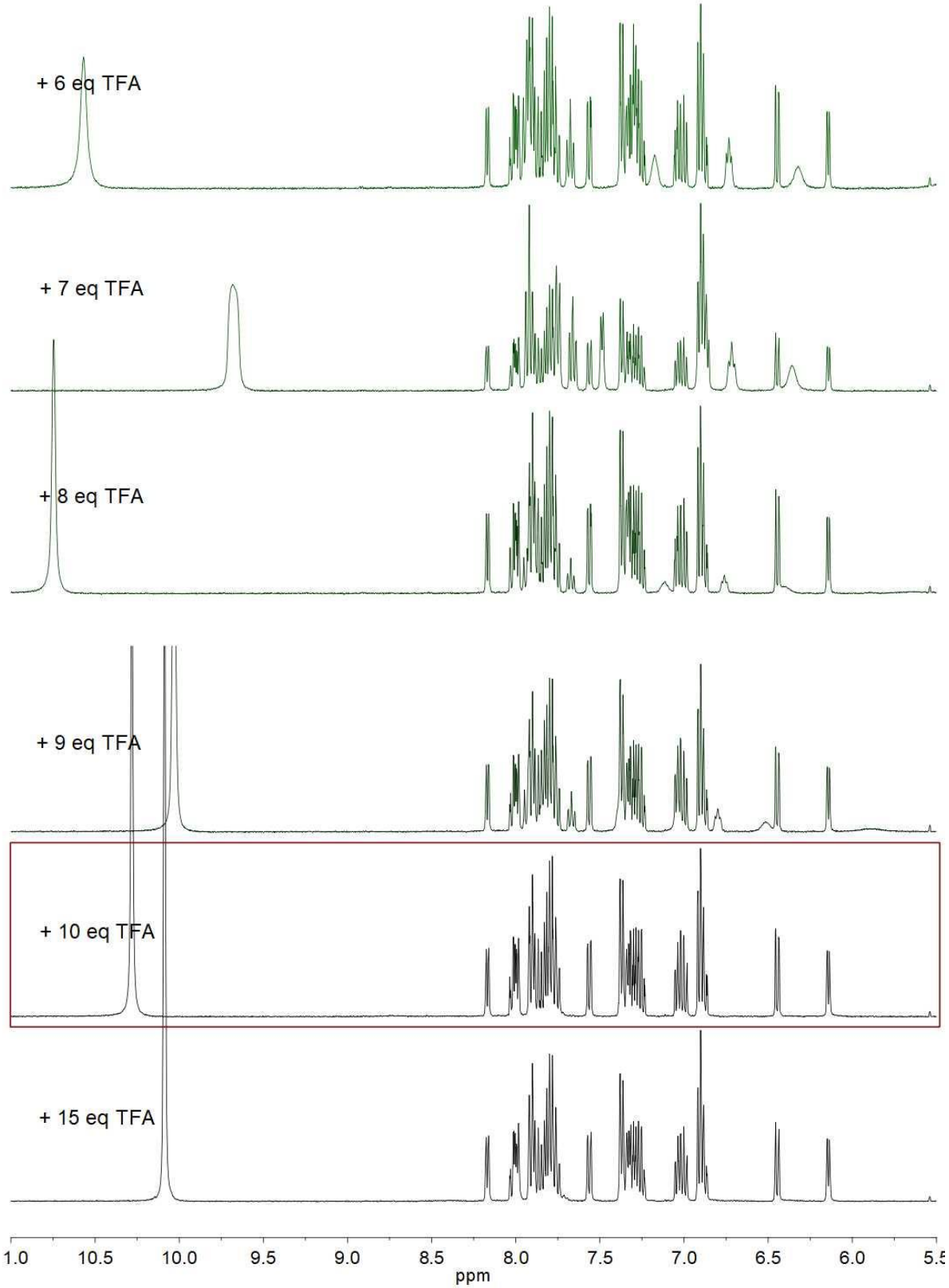

^{1}H NMR (400 MHz, CD_2Cl_2, 298 K) study of the influence of the TFA concentration on the reaction ***fac*-Ir(ppy)$_3$→[Ir(ppy)$_2$(Hppy)](O$_2$CCF$_3$)**. The spectra were measured after the addition of the indicated amount of TFA to a fresh sample of ***fac*-Ir(ppy)**. The conditions used for the General Procedure are highlighted by a red rectangle.

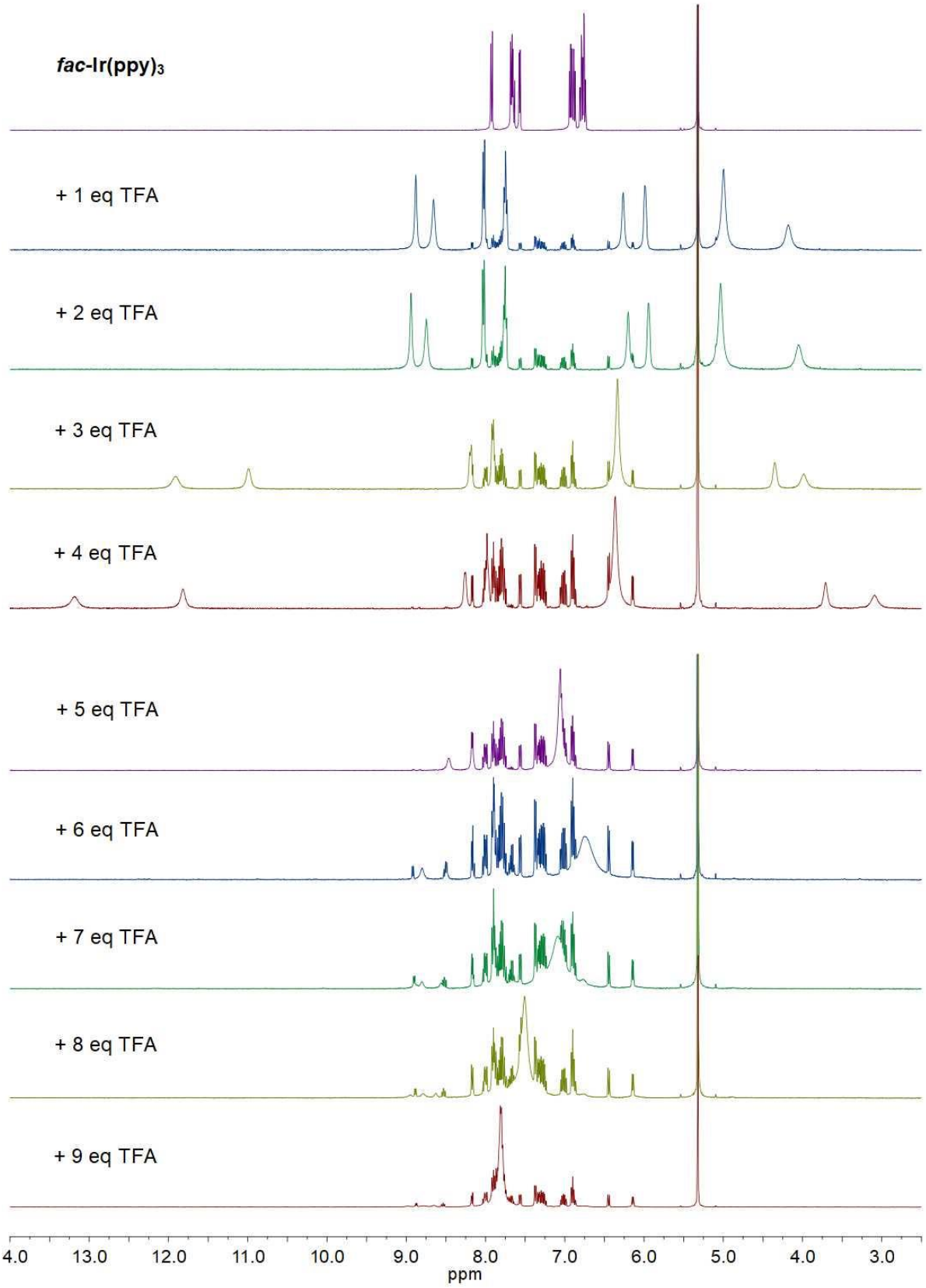

^{1}H NMR (400 MHz, CD_2Cl_2, 298 K) study of the influence of the TFA concentration on the reaction ***fac*-Ir(ppy)$_3$→[Ir(ppy)$_2$(Hppy)](O$_2$CCF$_3$)**. Increasing amounts of TFA were added to the same sample of ***fac*-Ir(ppy)$_3$**.

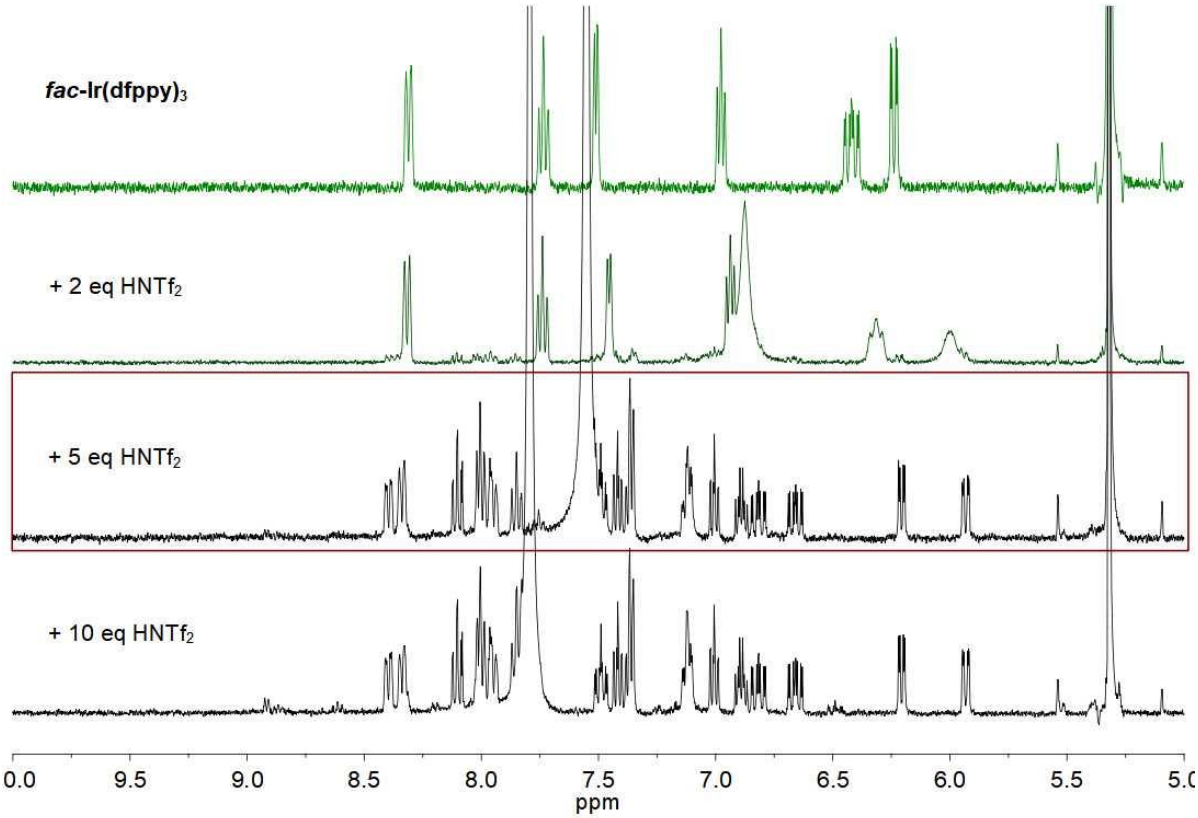

^{1}H NMR (400 MHz, CD_2Cl_2, 298 K) study of the influence of the $HNTf_2$ concentration on reaction ***fac*-Ir(dfppy)$_3$→[Ir(dfppy)$_2$(Hdfppy)](NTf$_2$)**. The spectra were measured after the addition of the indicated amount of $HNTf_2$ to a fresh sample of ***fac*-Ir(dfppy)**. The conditions used for the General Procedure are highlighted by a red rectangle.

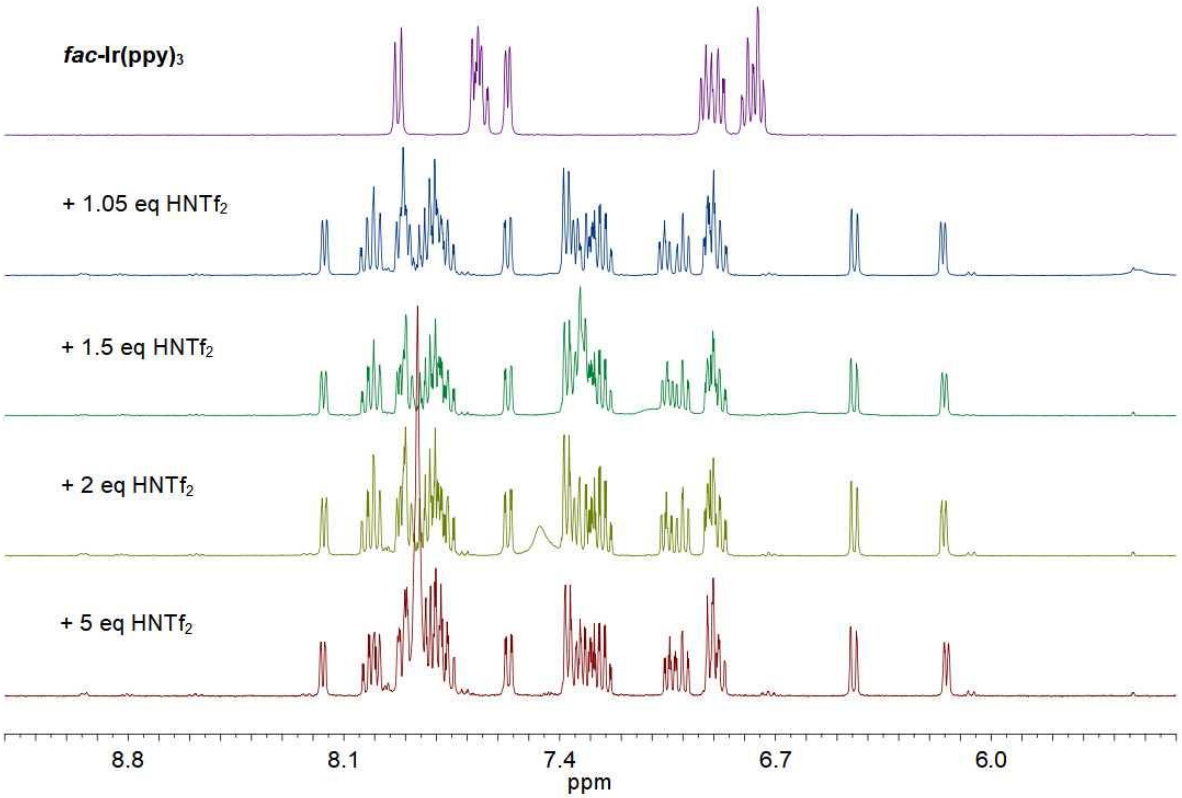

^{1}H NMR (400 MHz, CD_2Cl_2, 298 K) study of the influence of the $HNTf_2$ concentration on reaction ***fac*-Ir(ppy)$_3$→[Ir(ppy)$_2$(Hppy)](NTf$_2$)**. The spectra were measured after the addition of the indicated amount of $HNTf_2$ to a fresh sample of ***fac*-Ir(dfppy)**.

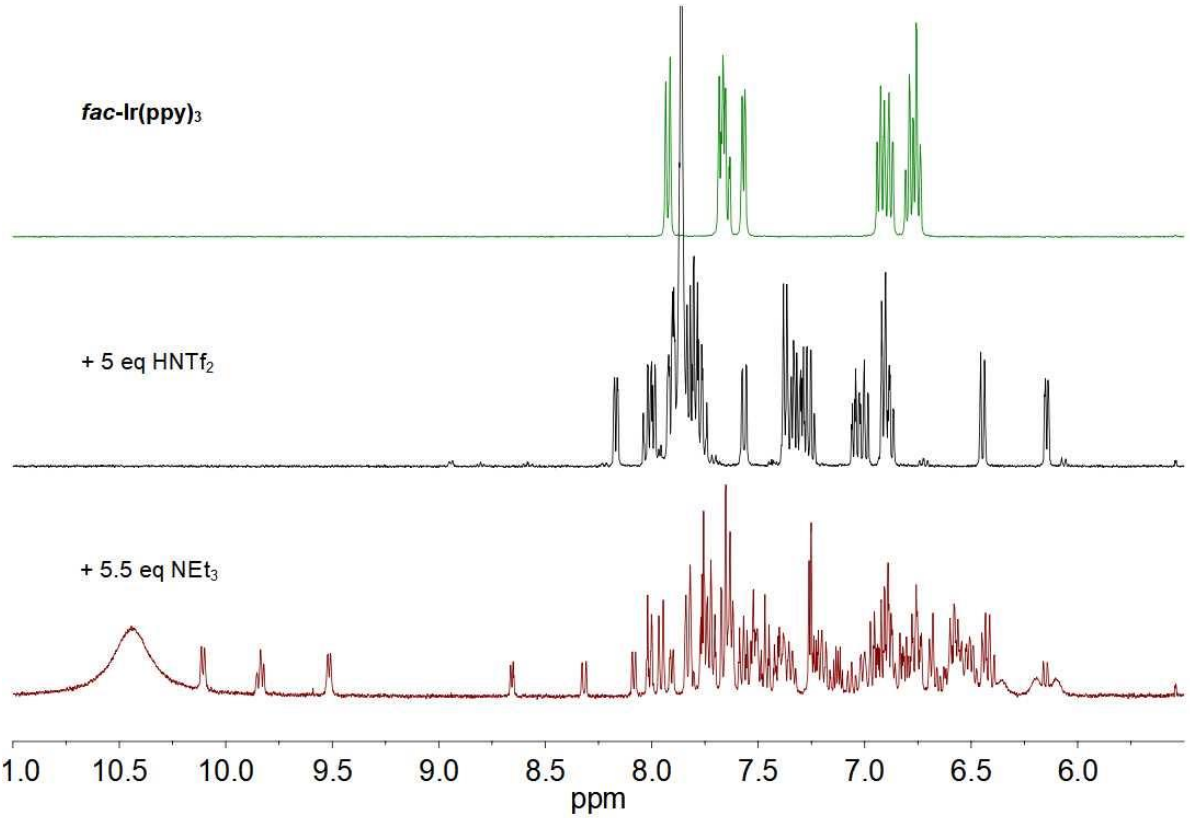

^{1}H NMR (400 MHz, CD_2Cl_2, 298 K) spectra of a solution of ***fac*-Ir(ppy)$_3$** upon addition of first $HNTf_2$ and then NEt_3.

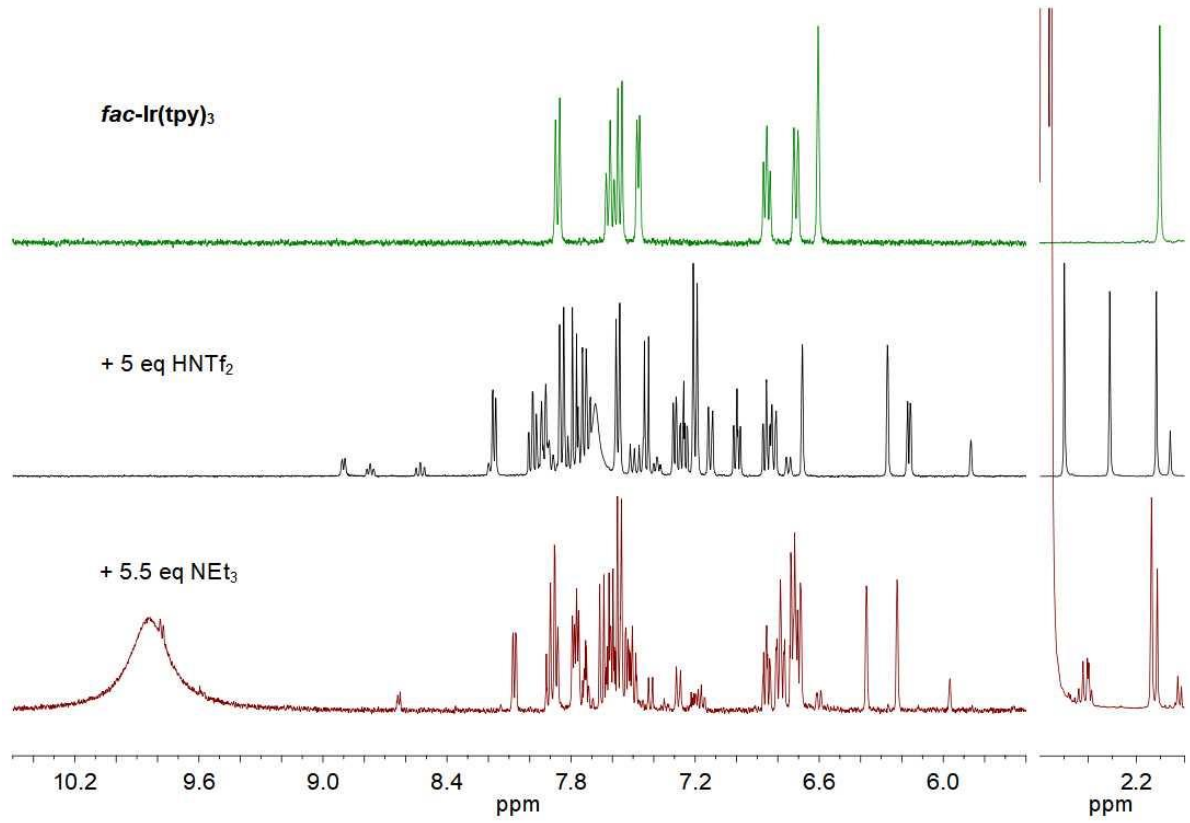

^{1}H NMR (400 MHz, CD_2Cl_2, 298 K) spectra of a solution of ***fac*-Ir(tpy)$_3$** upon addition of first $HNTf_2$ and then NEt_3.

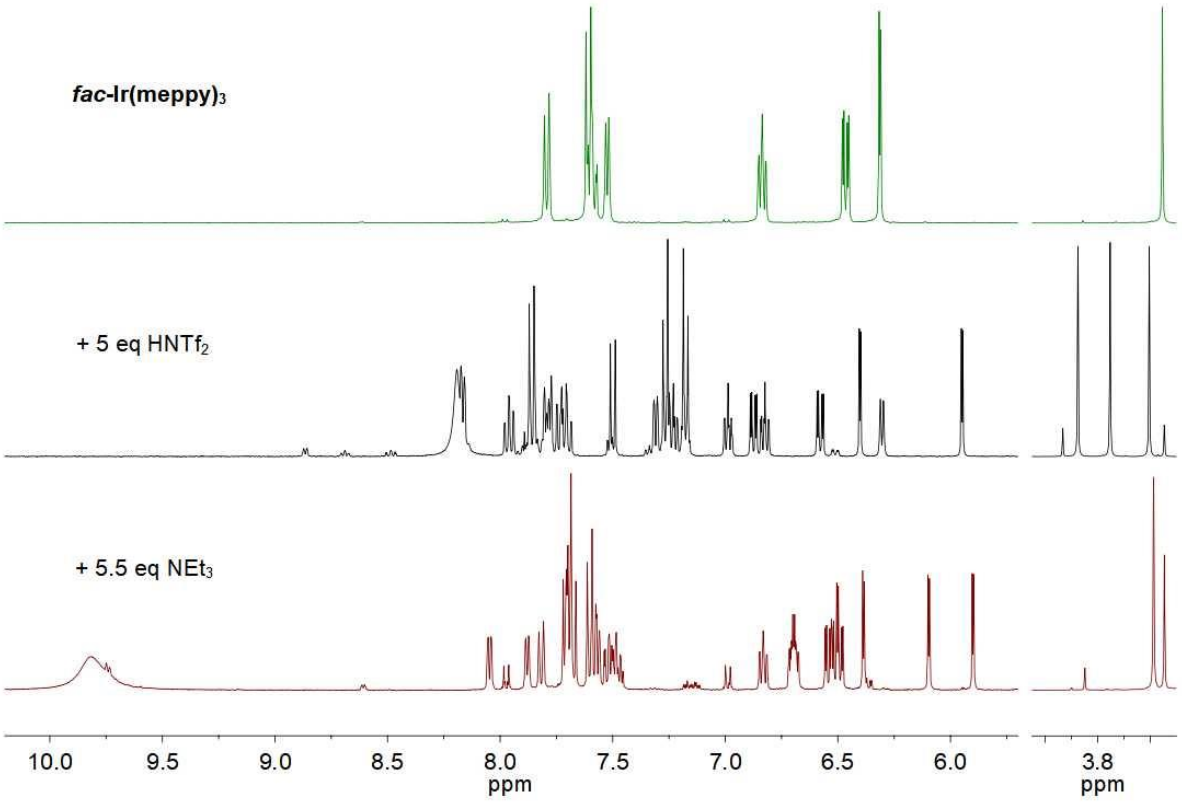

^{1}H NMR (400 MHz, CD_2Cl_2, 298 K) spectra of a solution of ***fac*-Ir(meppy)$_3$** upon addition of first $HNTf_2$ and then NEt_3.

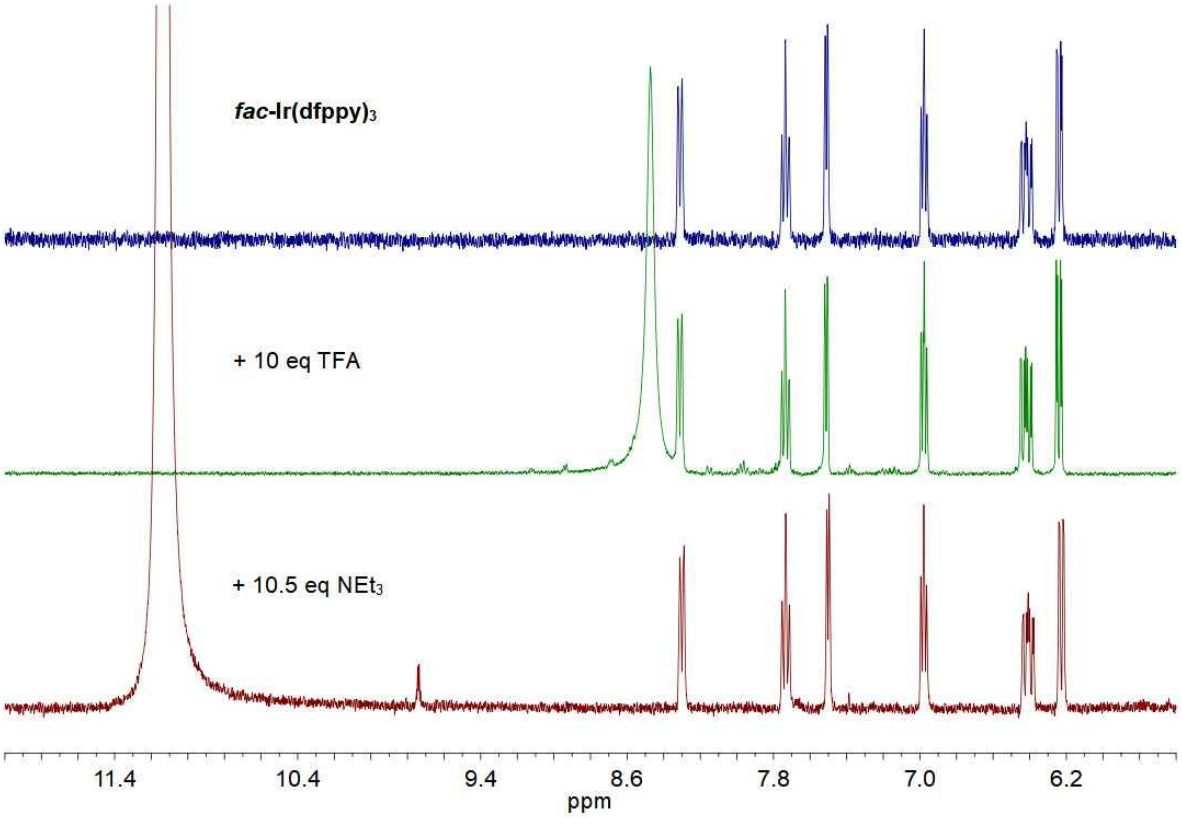

^{1}H NMR (400 MHz, CD_2Cl_2, 298 K) spectra of a solution of ***fac*-Ir(dfppy)$_3$** upon addition of first TFA and then NEt_3.

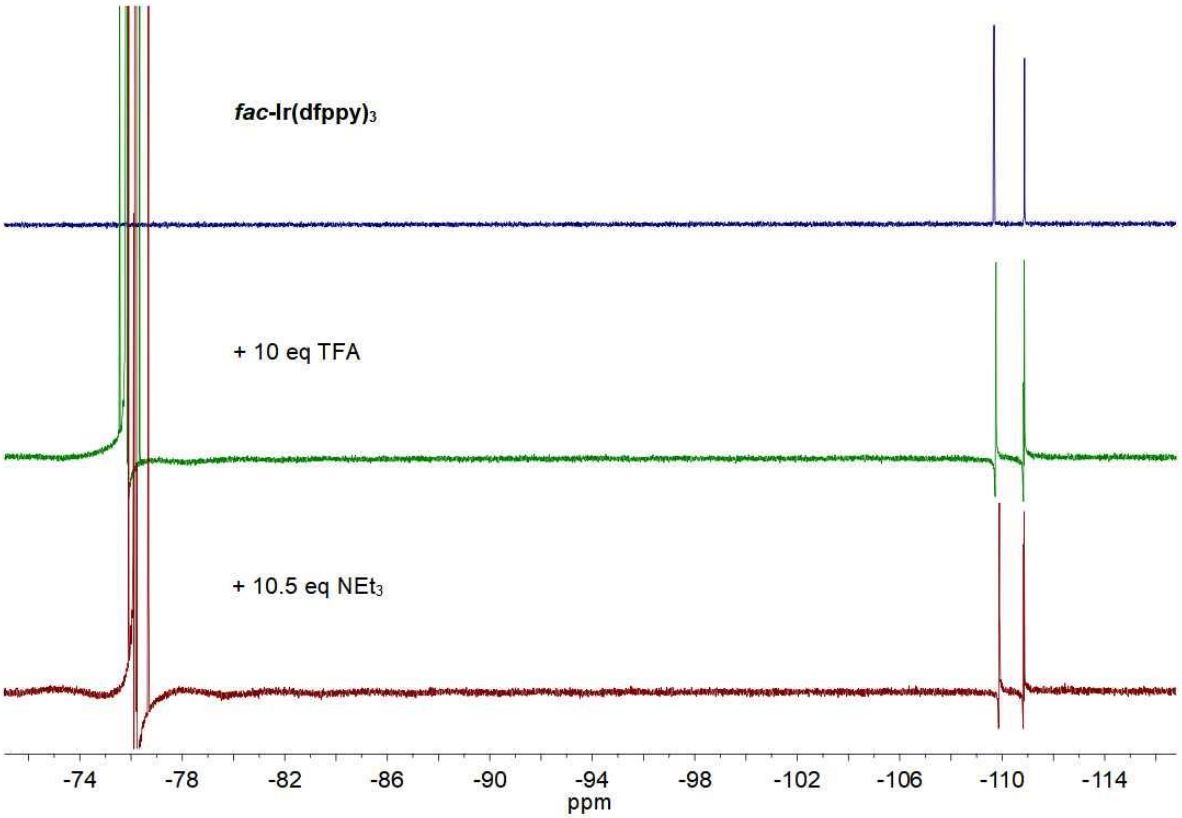

^{19}F NMR (376 MHz, CD_2Cl_2, 298 K) spectra of a solution of ***fac*-Ir(dfppy)$_3$** upon addition of first TFA and then NEt_3

References

1 G. R. Fulmer, A. J. M. Miller, N. H. Sherden, H. E. Gottlieb, A. Nudelman, B. M. Stoltz, J. E. Bercaw and K. I. Goldberg, *Organometallics*, 2010, **29**, 2176–2179.

2 H. Konno and Y. Sasaki, *Chem. Lett.*, 2003, **32**, 252–253.

3 A. B. Tamayo, B. D. Alleyne, P. I. Djurovich, S. Lamansky, I. Tsyba, N. N. Ho, R. Bau and M. E. Thompson, *J. Am. Chem. Soc.*, 2003, **125**, 7377–7387.

4 Y. Hisamatsu and S. Aoki, *Eur. J. Inorg. Chem.*, 2011, 5360–5369.

5 A. Singh, K. Teegardin, M. Kelly, K. S. Prasad, S. Krishnan and J. D. Weaver, *J. Organomet. Chem.*, 2015, **776**, 51–59.

6 R. H. Wiley, P. X. Callahan, C. H. Jarboe Jr., J. T. Nielsen and B. J. Wakefield, *J. Org. Chem.*, 1960, **25**, 366–371.

7 B. Orwat, M. J. Oh, M. Zaranek, M. Kubicki, R. Januszewski and I. Kownacki, *Inorg. Chem.*, 2020, **59**, 9163–9176.

8 A. R. Mcdonald, M. Lutz, L. S. von Chrzanowski, G. P. M. van Klink, A. L. Spek and G. van Koten, *Inorg. Chem.*, 2008, **47**, 6681–6691.

9 A. F. Henwood, A. K. Bansal, D. B. Cordes, A. M. Z. Slawin, I. D. W. Samuel and E. Zysman-Colman, *J. Mater. Chem. C*, 2016, 3726–3737.

10 A. Kazama, Y. Imai, Y. Okayasu, Y. Yamada, J. Yuasa and S. Aoki, *Inorg. Chem.*, 2020, **59**, 6905−6922.

11 J. Haribabu, Y. Tamura, K. Yokoi, C. Balachandran, M. Umezawa, K. Tsuchiya, Y. Yamada, R. Karvembu and S. Aoki, *Eur. J. Inorg. Chem.*, 2021, 1796–1814.

12 Y. Tamura, Y. Hisamatsu, S. Kumar, T. Itoh, K. Sato, R. Kuroda and S. Aoki, *Inorg. Chem.*, 2017, **56**, 812–833.

13 M. Montalti, A. Credi, L. Prodi and M. T. Gandolfi, *Handbook of Photochemistry*, CRC Press, 3rd ed., 2006.

14 X. Chen, Y. Okamoto, T. Yano and J. Otsuki, *J. Sep. Sci.*, 2007, **30**, 713–716.

15 Rigaku, 2021.

16 G. M. Sheldrick, *Acta Crystallogr. Sect. A*, 2015, **71**, 3–8.

17 G. M. Sheldrick, *Acta Crystallogr. Sect. C*, 2015, **71**, 3–8.

18 F. O. Garces, K. Dedeian, N. L. Keder and R. J. Watts, *Acta Crystallogr. Sect. C*, 1993, **49**, 1117–1120.